Mathematical Algorithms for Power Distribution Systems

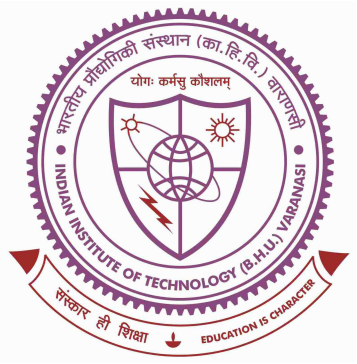

Thesis submitted in partial fulfillment
for the award of degree

Doctor of Philosophy

by

Abhishek Kumar

DEPARTMENT OF ELECTRICAL ENGINEERING
Indian Institute of Technology
(Banaras Hindu University)
Varanasi-221005
INDIA

Roll No: 13181003

2019

CERTIFICATE

It is certified that the work contained in the thesis titled **"Mathematical Algorithms for Power Distribution Systems"** by **"Abhishek Kumar"** has been carried out under our supervision and that this work has not been submitted elsewhere for a degree.

It is further certified that the student has fulfilled all the requirements of Comprehensive Examination, Candidacy and SOTA for the award of Ph.D. Degree.

Supervisor
Rakesh Kumar Misra
Professor
Dept. of Electrical Engg.
IIT(BHU), Varanasi

Co-supervisor
Devender Singh
Professor
Dept. of Electrical Engg.
IIT(BHU), Varanasi

DECLARATION

I, **Abhishek Kumar**, certify that the work embodied in this thesis is my own bona fide work and has been carried out by us under the supervision of **Dr. Rakesh Kumar Misra**, and **Dr. Devender Singh** from **July-2013** to **Sept-2019**, at the Departement of **Electrical Engineering**, **Indian Institute of Technology (Banaras Hindu University)**, **Varanasi (UP)**. The matter embodied in this thesis has not been submitted for the award of any other degree/diploma. I declare that I have faithfully acknowledged and given credits to the research workers wherever their works have been cited in my work in this thesis. I further declare that I have not wilfully copied any other's work, paragraphs, text, data, results, etc., reported in journals, books, magazines, reports dissertations, theses, etc., or available at websites and have not included them in this thesis and have not cited as my own work.

Date: **(Abhishek Kumar)**

Place: **Signature of the student**

CERTIFICATE BY THE SUPERVISOR

It is certified that the above statement made by the student is correct to the best of our knowledge.

Supervisor

Dr. Rakesh Kumar Misra

Co-supervisor

Dr. Devender Singh

Head of Department

Dr. Devender Singh

COPYRIGHT TRANSFER CERTIFICATE

Title of the Thesis: **"Mathematical Algorithms for Power Distribution Systems".**
Name of Student: **Abhishek Kumar**

Copyright Transfer

The undersigned hereby assigns to the Indian Institute of Technology (Banaras Hindu University) Varanasi all rights under copyright that may exist in and for the above thesis submitted for the award of the Doctor of Philosophy.

Date:

Place: **(Abhishek Kumar)**

Note: However, the author may reproduce or authorize others to reproduce material extracted verbatim from the thesis or derivative of the thesis for author's personal use provided that the source and the Institute's copyright notice are indicated.

To

The

Supreme Personality

Almighty God

My Supervisors

My Friends

and

My Beloved Family

Acknowledgments

Though, only my name appears on the cover of this dissertation, I owe my gratitude to all those people who have made this thesis possible and because of whom my experience as a research scholar has been one that i will cherish forever.

I take this opportunity to express my profound gratitude to my supervisors Dr. Rakesh K. Misra and Dr. Devender Singh, Professors, Department of Electrical Engineering, IIT(BHU), Varanasi for their exemplary guidance, mentoring and constant encouragement throughout the course of this dissertation.

I am obliged to the faculty members and staff members of Department of Electrical Engineering, IIT(BHU), Varanasi with special mention to Mr. A. K. Yadav and Mr. Satish Singh who have been patient to deal with challenges my candidature threw up.

In addition, I want to express my deepest gratitude to Mr. Sujeet Mishra who supported me throughout my experimental work. I am grateful to Mr. Bablesh Kumar Jha, who have provided me through technical, moral and emotional support during my research program.

A very special gratitude goes out to my colleagues and friends with special mention to Mr. Sachin Kumar, Mr. Tarun Maini, Mrs. Arpita Roy , Mr. Avneet Kumar, Mr. Amit Singh, and Mr. Basant Sethi.

Last but not the least, I thank specially to my parents, Mr. Chandeshwar Singh and Mrs. Meera Singh, my sister Mrs. Anuradha Singh, my brother Mr. Abhimanyu Kumar Singh and my sister-in-law Mrs. Swati Singh, for their constant support and encouragement, without which this assignment would have not been completed at all. I am grateful to my other family members who have supported me along the way.

Date: _____ Abhishek Kumar

Abstract

Distribution Power Flow analysis is one of the main features of power system studies and design. It is required for monitoring, contingency analysis, economic scheduling, planning, exchange of power between utilities, stability analysis, and expansion of Distribution Power System. Conventionally, the power flow problem is determined by numerical techniques such as Newton-Raphson (NR) and their variants Fast Decoupled Method. Such methods fail to provide the power flow solutions in some conditions, like ill-conditioned systems, distribution systems having large r/x ratio, islanded microgrids, etc. This thesis studies these aspects of Distribution Power Flow Analysis and investigates some new ideas and approaches to solve them in an effective and efficient ways.

This thesis thoroughly explores the distribution power flow problem and originates significant contributions. We investigate various numerical techniques and evolutionary algorithms in order to solve the different class of power flow problem of modern distribution systems. Using these approaches, we have been able to resolve some of the open issues regarding power flow of modern distribution systems, such as ill-conditioning, a high value of r/x ratio, issues related to islanding of distribution system. The thesis proposes 11 algorithms addressing the problem such as: (i) Ill-conditioned test systems, (ii) High r/x ratio of lines, (iii) Unbalanced test systems, (iv) Absence of slack bus in islanded microgrids, and (v) Variable system frequency in islanded microgrids.

In five algorithms, modifications is proposed in conventional power flow algorithms to overcome the above said problems. In addition, six nature-inspired optimization technique are proposed to solve power flow problems.

In grid connected distribution, systems are usually ill-conditioned and conventional algorithms poorly performs or even diverges. This thesis introduces a novel Current Injection based Newton-Raphson (CINR) power flow algorithm with new PV bus representation for improving the convergence characteristics. Moreover, an algorithm based

on fourth-order Levenberg-Marquardt algorithm with a non-monotone line search is introduced for solving power flow problem of ill-conditioned unbalanced and balanced grid-connected systems. We also propose a fourth-order Runge-Kutta algorithm in order to solve ill-conditioned grid-connected systems. The proposed approaches are validated for several ill- and well-conditioned cases. Results show that the proposed approaches have better efficiency than the conventional load flow algorithms.

In this work, a new optimization algorithm called Spherical Search (SS) is proposed to solve the bound-constrained non-linear global optimization problems. In addition, an extension of a newly proposed optimization technique, Butterfly Optimizer (BO) for constrained optimization problems (called as Butterfly Constrained Optimizer (BCO)) has been proposed to solve load flow problem. Results show that the BCO and SS perform competitively and more effectively with respect to well-known algorithms.

The existing methods of power flow problem are intricate and hard to realize due to the absence of reference bus (slack bus) in the islanded microgrids. To address this issue, an iterative power flow based technique is proposed to obtain the operating point of Droop Controlled Islanded Microgrid (DCIMG). To solve these set of equations, a nested-iterative Newton-Rapshon based algorithm is proposed. A modified version of well-known Backward/Forward Sweep (BFS) algorithm is also proposed to solve the load flow problem for droop-regulated AC microgrids operated in islanded mode. To solve this problem, a novel formulation as a constrained optimization problem is proposed. Two global optimization algorithm, Differential Evolution with Gauss-Newton based mutation (ϵDE-GN) and Matrix Adaptation Evolution Strategy (MAES), are utilized to solve this optimization problem. The performance of the proposed algorithms is compared with the Newton-trust, Interior-point and time domain methods. The proposed algorithms are employed on several test systems and results are compared with that obtained from other Jacobian-free based, Jacobian based algorithms and time-domain simulator PSCAD/EMTDC. The proposed algorithms for droop-regulated AC microgrid exhibit faster convergence, simple, accurate and easy to realize.

Effective Butterfly Optimizer with Covariance Matrix Adapted Retreat Phase (EBOwith-CMAR) is a self-adaptive Butterfly Optimizer which uses covariance matrix to generate a new solution and thus improves the local search capability of EBO. Optimal Power Flow (OPF) of grid-connected microgrids is a highly non-linear complex optimization problem.

This work utilizes EBOwithCMAR as an optimization algorithm and CINR as a power flow tool to solve the OPF of grid-connected microgrids effectively and efficiently. The proposed approach has been validated on the standard test systems for several OPF objectives. Simulation outcomes have been compared and analyzed with the recent studies.

In this thesis, an optimization approach to determine the optimal droop settings of Droop-Controlled Islanded Microgrid (DCIMG) is proposed. The objective functions are minimization of system losses in DCIMG while meeting all the power flow constraints. Therefore, this approach requires a powerful power flow tool to determine objective function values. The resultant single-objective optimization problem is solved using a powerful variant of Differential Evolution, named as ESHADE. The proposed approach is tested on a several DCIMG test system. The obtained outcomes show the superior performance of the proposed algorithm.

Contents

Page

Abstract **v**

Contents **ix**

List of Tables **xv**

List of Figures **xxiii**

List of Abbreviations **xxv**

1 Introduction **1**

1.1 General 1

1.2 Existing Algorithms used in Power Flow Analysis 2

1.2.1 Deterministic Power Flow Methods 2

1.2.2 Probabilistic Power Flow Methods 3

1.2.3 Power Flow Methods based on Slack Bus 4

1.2.4 Power Flow Methods for Droop Controlled Islanded Microgrids . . 7

1.2.5 Power Flow Methods based on Evolutionary Algorithm 9

1.3 Objectives of the Thesis 11

1.4 Outline of the Thesis 12

2 Power Flow Algorithms for Ill-conditioned Unbalanced Distribution Systems **15**

2.1 Introduction 15

2.2 Problem Formulation 18

2.2.1 Formulation based on Power Injection 18

2.2.2 Formulation based on Current Injection 20

2.3 Proposed Algorithms . . . 25
2.3.1 Modified Newton-Raphson Method . . . 26
2.3.2 Fourth-order Levenberg-Marquardt Method . . . 27
2.3.3 Modified Runge-Kutta Method . . . 28
2.4 Results and Discussion . . . 30
2.4.1 Test Systems . . . 30
2.4.2 Parameter Settings of Algorithms . . . 32
2.4.3 Validation of Proposed Algorithms . . . 32
2.4.4 Comparison of Algorithms . . . 37
2.5 Summary . . . 44

3 Spherical Search and Butterfly Constrained Optimizer for Power Flow of Unbalanced Distribution System 45

3.1 Introduction . . . 45
3.2 Power Flow Formulation as a Constrained Optimization Problem . . . 48
3.2.1 Formulation based on Power Injection. . . . 48
3.2.2 Formulation as a Constrained Optimization Problem . . . 49
3.3 Spherical Search . . . 49
3.3.1 Initialization of Population . . . 50
3.3.2 Spherical Surface and Trial Solutions . . . 51
3.3.3 Selection of New Population for Next Iteration . . . 54
3.3.4 Stopping Criteria . . . 54
3.3.5 Steps of Spherical Search Algorithm . . . 54
3.3.6 Validation of Spherical Search on Benchmark Problems . . . 56
3.3.7 Application of SS Algorithm for Initial Seed for Power Flow . . . 60
3.4 Butterfly Constrained Optimizer . . . 66
3.4.1 Dual-population of BCO . . . 66
3.4.2 Perching . . . 68
3.4.3 Patrolling . . . 70
3.4.4 Selection of Perching and Patrolling Operator . . . 70
3.4.5 Selection of Maximum Attractive Butterfly, $maxuv_i$ . . . 71
3.4.6 Controlling of the υ-level . . . 71

3.4.7 Reflecting Back and Cutting-off . . . 72
3.4.8 Validation of Butterfly Constrained Optimizer on Benchmark Problems . . . 72
3.4.9 BCO based Power Flow for Loadability Evaluation . . . 83
3.5 Summary . . . 85

4 Power Flow Algorithms for Islanded Microgrids 89
4.1 Introduction . . . 89
4.2 Modeling of Distributed Generations and Different Loads . . . 91
4.2.1 Modeling of Distributed Generation . . . 91
4.2.2 Load Modelling . . . 93
4.3 Current Injection Newton-Raphson Algorithm for DCIMG . . . 95
4.3.1 Classification of Bus-Types . . . 96
4.3.2 Current-injection based Power Flow Formulation . . . 96
4.3.3 Update of the System Frequency and AR Bus Voltage . . . 98
4.3.4 Validation of CINR . . . 100
4.3.5 Performance Analysis of CINR . . . 101
4.4 Nested Backward/Forward Sweep Algorithm for DCIMG . . . 104
4.4.1 Initialization . . . 104
4.4.2 Modified Backward Sweep . . . 104
4.4.3 Modified Forward Sweep . . . 105
4.4.4 Calculation of **BIBC** and **BCBV** . . . 106
4.4.5 Frequency and AR Bus Voltage Update . . . 107
4.4.6 Validation of NBFS . . . 108
4.4.7 Performance Analysis of NBFS . . . 110
4.5 Application of Proposed Approach for DG Modeling and Frequency Update in NTR and MNR . . . 121
4.5.1 Significance of Proposed DG Model in NTR . . . 121
4.5.2 Significance of Proposed Frequency Update Procedure in NTR and MNR . . . 122
4.6 Summary . . . 123

5 Differential Evolution and MAES for Power Flow Problem of Droop Controlled Islanded Microgrids 125

5.1 Introduction . . . 125
5.2 Modelling of Droop Controlled Microgrid . . . 128
5.2.1 Modeling of Frequency and Voltage Dependent Loads . . . 128
5.2.2 Modeling of Lines in Islanded MGs . . . 129
5.2.3 Modeling of DGs in Islanded MGs . . . 129
5.3 Power Flow Formulation . . . 130
5.3.1 Modeling of Droop Bus . . . 130
5.3.2 Modeling of PQ Bus . . . 132
5.3.3 Modeling of PV bus . . . 132
5.3.4 Objective Function . . . 132
5.4 Differential Evolution with Gauss-Newton based Mutation . . . 134
5.4.1 Differential Evolution . . . 134
5.4.2 Gauss-Newton Mutation . . . 135
5.4.3 ϵ-Constrained Handling Technique . . . 135
5.4.4 The Algorithm: ϵDE-GN . . . 136
5.5 Matrix Adaptation Evolution Strategy . . . 137
5.5.1 υ-level Modification in Constraints . . . 138
5.5.2 Broyden-based Mutation . . . 144
5.5.3 Proposed Algorithm: υMA-ESbm . . . 146
5.6 Performance of Proposed Algorithm . . . 149
5.7 Case Studies . . . 151
5.8 Summary . . . 158

6 EBOwithCMAR in Optimization of Grid-connected Microgrids 163

6.1 Introduction . . . 163
6.2 Problem Formulation . . . 165
6.3 Proposed Methodology . . . 167
6.3.1 EBOwithCMAR . . . 167
6.3.2 Evaluation of Objective Function . . . 178
6.3.3 Proposed Algorithm . . . 178

6.4 Results and Discussion . . . 179
6.4.1 Parameter Settings . . . 180
6.4.2 Case Studies . . . 180
6.4.3 24-hour loading scenario . . . 183
6.5 Summary . . . 188

7 ESHADE in Optimization of Islanded Microgrids 191
7.1 Introduction . . . 191
7.2 Problem Formulation . . . 192
7.3 Proposed Methodology . . . 194
7.3.1 ESHADE . . . 194
7.3.2 Evaluation of Objective Function . . . 199
7.3.3 Proposed Algorithm . . . 200
7.4 Results and Discussion . . . 200
7.4.1 Parameter Setting . . . 201
7.4.2 Case Studies . . . 201
7.5 Summary . . . 202

8 Conclusions and Future Scope 205
8.1 Conclusions . . . 205
8.2 Future Scope . . . 206

Appendix I 209

Appendix II 219

Appendix III 229

Appendix IV 237

References 255

References 255

List of Publication 281

List of Tables

Chapter 2

2.1 Power Flow (PF) solution of ill-conditioned version of CASE13 system using CINR 34

2.2 PF solution of ill-conditioned version of CASE13 test system using LMPF 35

2.3 PF solution of ill-conditioned version of CASE13 system using RK4PF . . 35

2.4 PF solution of ill-conditioned version of CASE28 test system using CINR . 37

2.5 PF solution of ill-conditioned version of CASE28 test system using LMPF 38

2.6 PF solution of ill-conditioned version of CASE28 test system using RK4PF 39

2.7 Obtained results of CINR, LMPF, RK4PF, BFS, TCIM, and iTCIM over several test systems. (NC: Not Converged) 41

2.8 Obtained results of CINR, LMPF, RK4PF, BFS, TCIM, and iTCIM over large test systems. (NC: Not Converged) 41

2.9 Execuation time (in sec) of CINR, LMPF, RK4PF, BFS, TCIM, and iTCIM. (NC: Not Converged) 41

2.10 Total Number of iterations required for different PF algorithms in heavily loaded ill-conditioned systems.(LF: Loading Factor, NC: Not Converged) . 42

2.11 Total Number of iterations required for different PF algorithms in ill-conditioned systems with high r/x ratios.(NC: Not Converged) 43

3.1 Mean and SD of best error value obtained by algorthms on 30-D CEC2014 problem suite. 55

3.2 Mean and SD of best error value obtained by algorithms on 30-D CEC2014 problem suite. 57

3.3 Mean and SD of best error value obtained by algorithms on 30-D CEC2014 problem suite. 59

3.4 Mean and SD of best error value obtained by algorithms on 30-D CEC2014 problem suite. 61
3.5 Initial seed obtained by SS for CASE25 test system 62
3.6 Power Flow solution obtained using SSTCIM for CASE25 test system . . . 63
3.7 Total Number of iterations required for different Power Flow algorithms. . 64
3.8 Total Number of iterations required for different Power Flow algorithms. . 65
3.9 Mean and SD of best error value obtained by algorithms on 30-D CEC2014 problem suite. 67
3.10 Ranking of Algorithm according to Friedman ranking 68
3.11 Properties of benchmark problems given in CEC 2006. 74
3.12 Error Values achieved when FEs are 5000, 50000, and 500000 for test function $g01 - g06$ 75
3.13 Error Values achieved when FEs are 5000, 50000, and 500000 for test function $g07 - g12$ 75
3.14 Error Values achieved when FEs are 5000, 50000, and 500000 for test function $g13 - g18$ 76
3.15 Error Values achieved when FEs are 5000, 50000, and 500000 for test function $g19 - g24$ 76
3.16 Best, Median, worst, mean, and standard deviation of NFES to achieve the fixed accuarcy level. 77
3.17 Mean NFES to schieve the accuracy level and SR on the CEC 2006 78
3.18 Ranking based on the SP of all algorithm on the CEC 2006. 79
3.19 Average ranking of the Friedman test 80
3.20 Multiple solution obtained using BCO for ill-conditioned CASE13 82

Chapter 4

4.1 Component modelling of microgrid in Power Flow algorithm 92
4.2 Representation of elements of Jacobian Matrix 97
4.3 Data required for modeling of the six bus test system in time-domain . . . 100
4.4 Validation of results obtained for six-bus test system. 101

4.5 Computation time required by different algorithms to solve power flow for different cases . . . 102
4.6 Validation of obtained result of the six-bus test system . . . 110
4.7 NBFS algorithm versus DBFS, MBFS, and PSCAD/EMTDC results for CASE33 system. . . . 111
4.8 Droop gains, nominal values and operative mode of DGs and Q_{max} limit for the 22-bus, 38-bus, and 69-bus test system. . . . 116
4.9 Computation time required by algorithms to solve power flow for 22-bus, 38-bus, and 69-bus systems. . . . 116
4.10 computation time required by algorithms to solve power flow problem of CASE160 test system. . . . 118
4.11 Number of iteration and computation time (in second) required to solve power flow problem of CASE38 test system for different value of λ. . . . 120
4.12 Computation time required by algorithms to solve power flow for different cases. . . . 122
4.13 Computational effort of different algorithms for solving different test cases. 123

Chapter 5

5.1 Default value of parameters of MA-ES [1] . . . 148
5.2 Validation of obtained result of the six-bus test system . . . 150
5.3 Comparison of results on 33-bus system . . . 150
5.4 Droop control settings of DGs in CASE6 test system. . . . 151
5.5 Outcomes of proposed load flow algorithm for a CASE6 test system compared with other methods. . . . 153
5.6 Droop control settings of DGs in CASE69 test system. . . . 154
5.7 Voltage profile obtained from ϵDE-GN for CASE69 distribution system operated as an islanded microgrid. . . . 154
5.8 Voltage profile obtained from υMAESbm for CASE69 distribution system operated as an islanded microgrid. . . . 155
5.9 Droop control settings of DGs in CASE33 system. . . . 157
5.10 Load exponents of different loads . . . 157

5.11 Voltage profile obtained by ϵDE-GN for CASE33 distribution system operated as an islanded microgrid. 157
5.12 Voltage profile obtained by υMAESbm for CASE33 distribution system operated as an islanded microgrid. 158
5.13 Droop control settings of DGs in CASE25 test system. 158
5.14 Power flow result obtained by ϵDE-GN for CASE25 unbalanced distribution system operated as an islanded microgrid. 160
5.15 Power flow result obtained by υMAESbm for CASE25 unbalanced distribution system operated as an islanded microgrid. 161

Chapter 6

6.1 The detail of experimental setup 180
6.2 Simulation results for CASE13 test system. 181
6.3 Results for CASE13 for scenario-4 181
6.4 Value of main parameters of system for different cases of CASE13 181
6.5 Simulation results for CASE25 test system for scenario-4 182
6.6 Obtained results for CASE25 183
6.7 Value of main parameters of system for different cases of CASE25 183
6.8 Simulation results for CASE37 test system of scenario-4 184
6.9 Obtained results for CASE37 184
6.10 Value of main parameters of system for different cases of CASE37 184

Chapter 7

7.1 Results of optimal power flow problem of CASE6 201
7.2 Results of optimal power flow problem of CASE22 202
7.3 Results of optimal power flow problem of CASE38 203

Appendix I

I.1 General Data of CASE13 209
I.2 Topology of CASE13 209

I.3 Line Parameter of CASE13 . . . 210
I.4 Load Data of CASE13 . . . 210
I.5 Load Data of ill-conditioned CASE13 . . . 211
I.6 General Data of CASE25 . . . 211
I.7 Topology of CASE25 . . . 212
I.8 Line Parameters of CASE25 . . . 212
I.9 Load Data of CASE25 . . . 213
I.10 General Data of CASE37 . . . 213
I.11 Tolology of CASE37 . . . 214
I.12 Line Parameters of CASE37 . . . 215
I.13 Load Data of CASE37 . . . 216
I.14 General Data of CASE28 . . . 216
I.15 Topology of CASE28 . . . 217
I.16 Line Parameters of CASE28 . . . 217
I.17 Load Data of CASE28 . . . 218
I.18 Load and Voltage Data of CASE28 . . . 218

Appendix II

II.1 Line Data of CASE6 . . . 219
II.2 Active Load Data of CASE6 . . . 219
II.3 Reactive Load Data of CASE6 . . . 219
II.4 DG's Data of CASE6 . . . 220
II.5 Line Data of CASE22 . . . 220
II.6 Active Load Data of CASE22 . . . 221
II.7 Reactive Load Data of CASE22 . . . 222
II.8 DG's Data of CASE22 . . . 222
II.9 Line Data of CASE38 . . . 223
II.10 Active Load Data of CASE38 . . . 224
II.11 Reactive Load Data of CASE38 . . . 225
II.12 DG's Data of CASE38 . . . 226
II.13 Line Data of CASE33 . . . 226
II.14 Active Load Data of CASE33 . . . 227

II.15 Reactive Load Data of CASE33 228
II.16 DG's Data of CASE33 228

Appendix III

III.1 Experimental Results of ϵDE-GN on CEC-2006 Benchmark Suite. 229
III.2 Comparison of algorithms on CEC-2006 benchmark problems 230
III.3 Experimental results of υMA-ESbm over 25 independent run on 18 test problems with 10D of IEEE CEC 2010. 231
III.4 Experimental results of υMA-ESbm over 25 independent run on 18 test problems with 30D of IEEE CEC 2010. 232
III.5 Experimental results of algorithms on 18 test problems with $10D$ of IEEE CEC 2010 233
III.6 Experimental results of algorithms on 18 test problems with $30D$ of IEEE CEC 2010 234
III.7 number of trials of ESHADE in a run of 50 that found correct digits . . . 235
III.8 Score achieved by HSES, EBOwithCMAR and ESHADE for problem suite of 100-Digit Challenge. 236

Appendix IV

IV.1 Power Flow solution of CASE22 test system operating in conventional droop.237
IV.2 Power Flow solution of CASE22 test system operating in inverse droop. . 238
IV.3 Power Flow solution of CASE22 test system operating in mixed droop. . . 238
IV.4 Power Flow solution of CASE22 test system operating in isochronous mode.239
IV.5 Power Flow solution of CASE38 test system operating in conventional mode.239
IV.6 Power Flow solution of CASE38 test system operating in inverse mode. . . 240
IV.7 Power Flow solution of CASE38 test system operating in mixed mode. . . 241
IV.8 Power Flow solution of CASE38 test system operating in isochronous mode.242
IV.9 Power Flow solution of CASE69 test system operating in conventional mode.243
IV.10 Power Flow solution of CASE69 test system operating in inverse mode. . . 244
IV.11 Power Flow solution of CASE69 test system operating in mixed mode. . . 245
IV.12 Power Flow solution of CASE69 test system operating in isochronous mode.246
IV.13 Power Flow solution of CASE6 test system operating in islanded mode. . . 247

IV.14 Power Flow solution of CASE22 test system in case of without optimization condition. 247
IV.15 Power Flow solution of CASE22 test system in case of minimization of $\mathbf{P}_{loss}$. 248
IV.16 Power Flow solution of CASE22 test system in case of minimization of $\mathbf{Q}_{loss}$. 249
IV.17 Power Flow solution of CASE22 test system in case of minimization of $(0.5 * \mathbf{P}_{loss} + 0.5 * \mathbf{Q}_{loss})$. 249
IV.18 Power Flow solution of CASE38 test system in without optimization condition. 250
IV.19 Power Flow solution of CASE38 test system in case of minimization of $\mathbf{P}_{loss}$. 251
IV.20 Power Flow solution of CASE38 test system in case of minimization of $\mathbf{Q}_{loss}$. 252
IV.21 Power Flow solution of CASE38 test system in case of minimization of $(0.5 * \mathbf{P}_{loss} + 0.5 * \mathbf{Q}_{loss})$. 253

List of Figures

2.1 Nose curve (PV curve) of bus 7c, 8c, 9c, and 10c. 34

Chapter 2

2.2 Convergence characteristics of CASE13(ill-conditioned case) using CINR, LMPF, and RK4PF. 36
2.3 Convergence characteristics of CASE28 (ill-conditioned case) using CINR, LMPF, and RK4PF. 40

Chapter 3

3.1 Voltage profile of Bus 7c, 8c, 9c, and 10c of CASE13 for different loading condition. 84
3.2 Voltage profile of Bus 7a, 9a, 10a, 11c, 12a and 14c of CASE25 for different loading condition. 86
3.3 Voltage profile of Bus 13a, 15a, 16a, and 17a of CASE25 for different loading condition. 87

4.1 Flow chart of CINR 99

Chapter 4

4.2 r/x ratio vs computation time (sec) for CASE38 test systems. 103
4.3 Loading factor vs computation time (sec) for CASE38 test systems. 104
4.4 Flow chart of NBFS 109
4.5 6-bus MG [2]. 109
4.6 Convergence of the solution with respect to computation time for CASE33 system 110
4.7 Divergence of MBFS for 33-bus test system 113

4.8 Divergence of DBFS for 33-bus test system 114
4.9 Convergence of NBFS for 33-bus test system 115
4.10 Effect of the value of β on the convergence of voltage magnitude of bus 35 of CASE38 test system in the case of $\lambda = 4$. 119

Chapter 5

5.1 Sharing of active power among DGs using droop based controller 131
5.2 Sharing of reactive power among DGs using droop based controller 131
5.3 Graphical representation of main feature of υ-level modification. 140
5.4 Topology of CASE6 test system operated as an islanded microgrid. 152
5.5 Topology of CASE69 test system operated as an islanded microgrid. . . . 153
5.6 Topology of CASE33 system operating in islanded mode. 156
5.7 Topology of CASE25 test system operated as an islanded microgrid. . . . 159

Chapter 6

6.1 Hourly positive-, zero-, negative-sequence currents without and with SPDGs.185
6.2 Hourly phase currents without and with SPDGs. 186
6.3 Bus voltages without and with SPDGs. 187
6.4 Minimum of the all bus Voltages without SPDGs and with SPDGs for 24 hour. 188
6.5 Total active and reactive power line loses for 24-hours. 189
6.6 Phase Utilization Index at main feeder for 24 hours. 190

List of Abbreviations

AA	Analytical Approach
AR	Angle Reference
BBM	Broyden-based Mutation
BCO	Butterfly Constrained Optimizer
BFS	Backward/Forward Sweep
CINR	Current Injection based Newton-Raphson
CMAR	Covariance Matrix Adapted Retreat Phase
CN	Continuous variant of Newton-Raphson
COP	Constrained Optimization Problem
DBFS	Direct Backward/Forward Sweep
DCIMGs	Droop Controlled Islanded Microgrids
DE	Differential Evolution
DGs	Distributed Generations
EAs	Evolutionary Algorithms
EBO	Effective Butterfly Optimizer
EBOwithCMAR	Effective Butterfly Optimizer with Covariance Matrix Adapted Retreat Phase
ESHADE	Enhanced Success-History based Adpated Differential Evolution
FR	Feasible Rate
FT	Friedman Test
GA	Genetic Algorithm

GN	Gauss-Newton
HOLM	High-Order Levenberg-Marquardt
HV	High Voltage
LM	Levenberg-Marquardt
LMPF	Levenberg-Marquardt based Power Flow
MAES	Matrix Adaptation Evolution Strategy
MBFS	Modified Backward/Forward Sweep
MGs	Microgrids
MGCC	Microgrid Central Controller
MODE	Multi-operator based Differential Evolution
MNR	Modified Newton-Raphson
NBFS	Nested Backward/Forward Sweep
NR	Newton-Raphson
NTR	Newton-Trust Region
OPF	Optimal Power Flow
PF	Power Flow
PHEVs	Plug-in Hybrid Electric Vehicles
PSO	Particle Swarm Optimization
RK4	Fourth-order Runge-Kutte
RK4PF	Fourth-order Runge-Kutta based Power Flow
SP	Success Performance
SR	Success Rate
SPDGs	Single-Phase Distributed Generators
SS	Spherical Search
SSTCIM	Spherical Search with Three Phase Current Injection Method
Ybus	Admittance Matrix

Chapter 1

Introduction

1.1 General

The current electric utilities include central power generation units connected to High Voltage (HV) lines. At the central generation units, electric power is generated and transferred to the distribution centers through HV lines. The transferred electric power is then distribution to the consumers through medium and low voltage lines. Generally, the distribution network is supplied power unidirectionally, as the structure of the distribution network is radial. Power conservation has been the major issue in the distribution networks. In the distribution system, minimization of power loss improves the efficiency and effectiveness of the power distribution. Generally, as compared to HV lines, distribution system power loss is higher because of the high r/x ratio in the distribution lines and due to low voltage operations of the systems.

The electric utility industry has been developing rapidly after creation of competitive market for power supply. In the current scenario, the most important concern of utilities is to address the increased demand for electricity without disturbing the existing networks. Besides, the profile of bus voltages needs to be maintained within a prescribed limit. Under the deregulated environment, the Optimal Power Flow (OPF) and Power Flow (PF) in general play an important role in power system planning and operation. PF analysis is essential before power system planning and operation can be taken up. The main objective of PF analysis is to minimize the power mismatches at all the system buses. The results from PF analysis provide solution for steady-state conditions. The major aim of OPF is minimizing the operating cost of the power utility while meeting the load demand by

satisfying all the security constraints for the power networks. For the last two decades, research has been carried out to propose different kinds of numerical techniques to solve the PF and OPF problems of power networks. A detailed description of three-phase modeling of the network components for PF analysis have been provided in [3–7].

Several non-conventional and conventional techniques have been employed to solve these problems of PF because these problems are non-linear and/or non-convex. Due to the non-convexity of the PF and OPF problems, conventional optimization algorithms may be stuck on a local minimum. To address this issue, many population-based meta-heuristics have been utilized in the area of PF and OPF tool.

1.2 Existing Algorithms used in Power Flow Analysis

In [8], numerous challenges of modern power system analysis have been discussed. One of such challenges is that the current flow becomes bi-directional in many branches due to the inclusion of Distributed Generations (DGs) and sometimes applied PF techniques of distribution systems may diverge as a result of high penetrations of DGs. The new challenges have also evolved due to change in the system topology as a result of islanded Microgrids (MGs) and network reconfiguration [9]. Conventional PF techniques experience convergence issues when applied to a distribution system. The main reason behind this issue is the radial or weakly meshed structure of the distribution network with a high r/x ratio which leads to ill-conditioning of system of non-linear equations of PF problems [10, 11]. Consequently, algorithms such as Gauss-Seidel, Newton-Raphson (NR) or fixed-point-type algorithms have poor convergence. For such cases, a robust and efficient PF algorithms is required. Algorithms used to solve the PF problem of distribution systems can be categorized into three classes: Deterministic, Probabilistic, and Evolutionary power flow methods.

1.2.1 Deterministic Power Flow Methods

Backward/forward sweep methods

For distribution PF analysis, backward/forward sweep based algorithms are the most popular tool to obtain the steady-state solution of distribution networks. The first variant

of this class of algorithm was introduced in [12], where only PQ nodes were considered in the radial structure of the network. Since this version, numerous improved versions have been proposed to solve weakly meshed distribution networks [13, 14], networks with DGs [15], three-phase distribution network [16, 17], and voltage-dependent loads [18]. A detailed review and comparison of this class of algorithms are presented in [19].

Newton-Raphson type methods

In [20], one of the first attempts to address the convergence issues of conventional NR for ill-conditioned test systems is proposed in an optimal sizing problem of capacitors. In [21], three algorithms based on work discussed in [20] were proposed to solve the PF problem of ill-conditioned systems. Based on the nodal current injection, a PF method, called the current injection method, is proposed for balanced and unbalanced distribution systems with voltage-dependent loads in [22–24], respectively. A detailed comparison between the backward/forward sweep algorithm and the current injection method is reported in [25].

Fixed-Point type methods (or Gauss-Seidel)

Some algorithms based on Gauss-Seidel technique are proposed to solve three-phase distribution systems in [26–28]. Some other algorithms based on the above-mentioned Gauss-like approach are proposed in [29] in which loop frame of reference and Grid Lab-D are utilized.

1.2.2 Probabilistic Power Flow Methods

Deterministic models cannot consider uncertainties of the different aspects of power systems. Therefore, different numerical approaches are need in existing systems for considering uncertainties. The first algorithm of this class, probabilistic PF, was proposed in 1974 and thereafter many improved algorithms have been proposed and utilized in the steady-state analysis of power system [30–35]. In [35, 36], an extensive review on probabilistic PF is presented. The probabilistic PF algorithms are usually classified into analytical approaches and numerical approaches. In numerical solution approaches, probabilistic PF uses deterministic PF to solve nonlinear equations for numerous times with different combinations of inputs [34]. The different combination of inputs are generated as per

the requirement of probabilistic parameter considered. Results obtained from probabilistic PF are considered as a reference solution to investigate the accuracy of the other probabilistic PF solutions [37]. The primary purpose of the analytical technique is to determine the density functions of the random variables applying the density functions of random inputs and by dealing with arithmetic computations. Two difficulties usually occur in dealing with probabilistic PF equations. The first one is the high non-linearity of equations and the second one is that of correlation between output and input power variables. To address these difficulties, some simplifications have been suggested to determine probabilistic PF by an analytical technique. The simplest approach is to implement probabilistic PF by linearizing the PF equations employing first-order Taylor series expansion around the predicted mean of the PF variables [30]. Besides this technique, the density function of load and generation can be assumed as a normal distribution for simplicity. Different approaches have been established to deal with the linearization error introduced in PF equations by utilizing quadratic probabilistic PF in [31, 32]. The utilization of point estimation method in probabilistic PF was initiated in [34]. Thereafter, several works based on the point estimation method to overcome the issues of probabilistic PF have been suggested in [38, 39].

In [33], a merger of Gram-Charlier and cumulants expansion theory is introduced to increase the capability of a probabilistic PF method. Similarly, in [40], the Cornish-Fisher expansion is recommended as a substitute for different distribution than the normal distribution to reduce convergence issues.

1.2.3 Power Flow Methods based on Slack Bus

Several algorithms have been proposed to solve non-linear simultaneous equations which are based on numerical computation. PF problem is also a type of non-linear simultaneous equation. Therefore, several numerical techniques have utilized to solve the PF problem. In this thesis, those algorithms which uses the conventional numerical computation approach to solve PF is referred as numerical PF methods. A numerical technique is introduced to determine the PF solution in [41]. Another numerical technique based approach to deal with the PF problems is suggested in [42]. Some of these approaches are based on the NR approach to solve non-linear simultaneous equations [23, 43], while other alternatives are based on the Gauss-Seidel approach [26, 28]. To enhance the con-

vergence aspects of the Gauss-Siedel method for ill-conditions and large systems, some techniques based on iterative design have been established [44, 45]. Several decoupled versions of NR have also been introduced to improve the computing time and speed of convergence [46–48]. Among all the proposed numerical techniques, NR based techniques have became the de facto industry models due to its simplicity and higher speed of convergence.

PF algorithms based on NR and its decoupled versions fail to provide solutions for the PF problems of Distribution Systems and microgrids due to the presence of high value of r/x in lines [49, 50].

In [51], an iterative method based on primitive electric circuit rules is presented for solving the PF problems in radial distribution systems. Using the NR-based technique, an optimal multiplier based technique for solving for PF problem is designed in [52]. A revised algorithm, named backward/forward sweep algorithm, is proposed in [52]. An implicit Z-Bus algorithm is designed in [27] to deal with the PF equations by using a superposition rule where only one source is considered at a time.

In [28], an implicit Z-Bus method integrated with the Gauss-Siedel approach is introduced to cut down the computational burden of the PF study. A three-phase PF algorithm based on the backward/forward method is proposed in [53] that is suitable only for a system with one power source. Consequently, this method does not provide solutions for the PF problem of distribution systems with DGs or droop control based islanded microgrids.

The quadratic equations of the PF equations are used to solve for the voltage magnitude in [54, 55]. However, the voltage angle is ignored in the calculation process of the PF solution to reduce computational time. In [56], a three-phase PF analysis is proposed addressing characteristics of islanded microgrids with decentralized droop controlled distributed generations.

In [57], a second-order PF algorithm has been presented using current injection equations represented in rectangular form instead of classical polar form.In [58], an iterative procedure is proposed to solve the PF problem that improves the computation complexity (number of iterations and CPU time). In this approach, or impedance matrix is utilized in place of the admittance matrix.

To solve the PF problem, high-order NR algorithms have been proposed in [59]. The

foremost advantages of these algorithms as compared to NR are their simple structures, faster and significant reduction of CPU time.

Iwamoto *et al.* proposed a NR-based algorithm for ill-conditioned PF solution [60]. In this approach, an optimal multiplier is calculated at each iteration to minimize the power mismatches ($\triangle P$ and $\triangle Q$). In literature, several algorithms have been proposed to address the PF problem of ill-conditioned power systems [10,61–66]. In [67], concavity theory is utilized to calculate an optimal multiplier at each iteration and polar coordinates are used instead of rectangular coordinates. In [68], the quadratic discriminant index is employed to improve the performance of optimal multiplier based PF techniques for evaluating solutions at the maximum loading conditions.

In [69], the Levenberg-Marquardt (LM) algorithm is proposed to solve the PF problem in ill-conditioned systems. In such cases, this approach is a reliable and efficient technique. In [70], a Continuous variant of Newton-Raphson (CN) method is developed to solve the PF problem in ill-conditioned systems. Additionally, several algorithms based on LM and CN have been proposed in [71, 72]. In large-scale test systems, algorithms based on CN provide fast convergence and are more robust than other numerical techniques.

Authors of [73] have presented a variant of LM to solve the PF problem in case of ill-conditioned as well as well-conditioned power systems. However, LM-based algorithms have several issues such as dependence of convergence rate on λ, and inaccuracy in final solution. To address this issue, the authors of [74] have proposed High-Order Levenberg-Marquardt (HOLM). In this approach, good performance is obtained in the case of ill-conditioned test systems.

Authors of [70] have proposed a Fourth-order Runge-Kutte (RK4) algorithm to solve the PF problem. However, RK4 requires four matrix inversions of the Jacobian matrix at each iteration. Moreover, the number of required iterations to solve the problem is also higher than NR-based algorithms. Nevertheless, the performance of RK4 is better than NR-based algorithms in case of ill-conditioned power systems [70].

1.2.4 Power Flow Methods for Droop Controlled Islanded Microgrids

In [2, 75–82], few PF tools have been introduced to deal with the PF problem of an islanded microgrids with decentralized droop controlled DGs and the shortcomings of the traditional PF tools have also been discussed. The concept of droop controlled DGs has been applied to control the power distribution among the DGs without employing the inter-communication among them. The decentralized droop control approach gives way to centrally controlled microgrids having low costs, low complexity, expandability, and enhanced reliability. Thus, such an arrangement can waive the need of inter-communication networks and cut down the investment costs [83–93].

To determine the PF solution for DCIMG, new algorithms have been introduced. These techniques have considered linear equations of the droop characteristics of DGs. In [94], a new PF method that employs particle swarm optimizer is introduced to solve the PF problem of Droop Controlled Islanded Microgrids (DCIMGs).

A revised technique based on the traditional NR approach is presented in [2] for PF evaluation in the presence of decentralized droop controlled DGs. However, this method does not consider unbalanced systems. The power-sharing among the DGs has been examined in [78] but, the voltage angles are not evaluated in this approach. Also the approach, does not consider the PV and PQ models of DGs in their study.

In [95,96], NR based PF study has been introduced that employs virtual impedance in the model of droop controlled DGs. Limited case studies have been conducted in this work where voltage-dependent and frequency-dependent loads are not modeled. Consequently, dependance of the bus admittance matrix on the frequency is ignored in the computation process. A PF analysis of balanced islanded microgrids is performed in [97] by employing power injection equations in polar form. Nevertheless, droop equations and islanded operations for DGs units have not been studied.

References [98], [99] and [100] address the PF problem of a DCIMG. However, these PF techniques cannot be applied to the PF problem of DCIMG because a DG unit is considered as a slack bus. These algorithms assume this DG unit as an infinite bus, but this assumption cannot work for the DCIMG system. In [98], a direct backward-forward sweep technique is proposed to solve the PF problem of DCIMGs. In [101], a

new methodology based on Nested-iterative NR is proposed for DCIMGs. However, this approach does not provide convergence for a system having high r/x ratio and thus is not applicable for distribution systems having high r/x ratio.

In [100], to solve the three-phase PF problem, a model based on sequence components is introduced for voltage source inverter and synchronous generators. This model is improved in [102] by considering constraint of DGs and operational limits. However, the model discussed in [102] does not consider the behavior of DCIMGs.

The Newton-Trust Region (NTR) method has been proposed [56] to solve equations obtained after consolidating (i) linear droop bus equations, and (ii) power-flow equation. To solve this optimization problem using NTR algorithm, gradient and Hessian of the objective function are required in the optimization procedure. Therefore, as concluded in [103], the solution of such a transformed problem is not acceptable as the solution is non-trivial.

In NR-based PF algorithm, there is requirement of calculation of the Jacobian matrix at each iteration. System frequency has been considered as a PF variable in Modified Newton-Raphson (MNR) and NTR. Therefore, elements of Jacobian matrix contain derivatives of bus admittance matrix with respect to system frequency. To calculate the gradient of the admittance matrix, the coupling of line parameters have not been considered [2]. Therefore, the gradient of the admittance matrix cannot be accurate in the case of coupling of lines. In the case of coupling of lines, the gradient of the bus admittance matrix cannot be calculated directly. Therefore, a finite difference approximation of the gradient of the bus admittance matrix has been done in [56]. Use of finite difference approximate Jacobian matrix in place of analytic Jacobian matrix affects the convergence property of NR-based algorithms [100]. In addition, finite difference approximation of gradient of the bus admittance matrix increases the time and space complexity of the algorithm. In present thesis, this issue of MNR and NTR has been fixed in the algorithm proposed in this thesis where the gradient of the bus admittance matrix is not required in the PF process.

In [104, 105], three types of droop characteristic are reported on the basis of output impedance of the DG. The NTR algorithm can accommodate only inductive droop characteristics. On the other hand, MNR can perform PF incorporating any particular droop characteristics out of three options but is not able to perform PF for a system

having a mix of droop characteristics. This issue is also addressed in present thesis and the algorithm proposed in this thesis is able to perform PF for a system having a mix of droop characteristics.

1.2.5 Power Flow Methods based on Evolutionary Algorithm

During the last three decades, comprehensive research works have been published and a substantial number of numerical techniques have been developed. Since PF analysis has been used in range of applications, several types of approaches have been proposed. In few situations, PF equations must be solved with their non-linearity. Similarly, in other situations, PF equations may be solved by using their linearized models with different levels of approximations. PF solutions have been established for unbalanced as well as balanced power systems. PF algorithms have also been proposed for low voltage radial systems.

Conventional PF algorithms encounter bottlenecks in dealing with systems having lines with high r/x ratios or when the loading condition approach maximum loadability limit of the system. PF problems have multiple solutions i.e. total $2^N - 1$ for a N-bus test system. However, among all possible solutions, only one is the operating point solution which is generally calculated by iterative numerical techniques. The main reason behind the use of iterative numerical techniques is the local search capability around the starting point solution of system. In general, 1 p.u. is considered as the initial seed for bus voltages because the power system is operated close to predefined rated voltage levels. Solutions other than operating point solution are low voltage solutions which have little physical significance in many applications. However, they may provide information related to the voltage stability study of the system. Hence, the determination of such solutions are also required in the power system analysis. To address this issue, the PF problem has been formulated as an optimization problem and solved by using special search procedures to find multiple solutions.

In such circumstances, PF analysis can also be expressed as an optimization problem in which active and reactive power mismatches and voltage mismatches at buses are to be minimized. Several conventional optimization algorithms have been utilized to solve the PF problem and the maximum loadability problem in the literature. However, most of the non-linear programming techniques may converge to local optimum solutions. The opti-

mization algorithm (especially search based) inherently have high chance of convergence due to their formulations and techniques. The above advantages though were obvious at all times, however their practical implementation were subject to contemporary computational advancements. In the present times the computational resources have improved quite significantly (or exponentially increased). This has lead to several successful implementations of computationally demanding algorithms as apparent from literature. Thus it is imperative to revisit and explore the performance of algorithms vis-a-vis contemporary computational resource scenario.

Nature-Inspired algorithms are prevalent for solving non-smooth/non-convex optimization problems from different engineering fields. The algorithms such as Genetic Algorithm (GA), Particle Swarm Optimization (PSO), and Differential Evolution (DE) have been introduced as a PF solver for balanced power systems and for computing maximum loadability limit for a system.

DE is a simple yet powerful technique for the global optimization problem. It provides better convergence property and it requires only a few parameters to be tuned. Similar to other evolutionary algorithms, it involves three basic operators, i.e., mutation, crossover, and selection.

GA was first proposed in [106]. It is a population-based search algorithm based on the Darwinian theory of evolution which contains three basic operators such as mutation, recombination, and selection. The initial population of solutions is initialized randomly throughout the search-space. These solutions are called chromosomes which are updated iteratively by using the above-mentioned operators. The fitness of the individuals is evaluated on the basis of their objective function value. The fittest chromosomes are selected as parents to generate offsprings for the next generation. Generations of offspring comprises of recombination and mutation operations. The maximum number of function evaluations is considered as a termination criterion for the optimization process.

Besides the above-mentioned numerical models, numerous studies that analyze PF analysis based on nature-inspired optimization algorithms have been approached in the literature. The best feature of these algorithms is that they are independent of the initial seed of the decision variables. Elrayyah et al., [94] introduced a method based on PSO algorithm to solve the PF problem of DCIMGs. In this method, PSO is employed to calculate the optimum droop parameters for sharing the reactive power. However, this

method did not consider the sharing of active power among the DGs. An algorithm based on PSO solves the PF problem for DCIMGs in [107]. In this method, PSO is utilized to find the droop parameters to optimize the reactive power sharing among the DGs. However, this algorithm does not achieve optimized active power sharing among DGs. GA has also been used as an optimization tool to minimize the voltage and power mismatches at the buses [108, 109].

A GA based PF technique is proposed in [108]. This method includes a voltage differential technique and a gradient technique. In [109], a hybrid of PSO and GA based algorithm is proposed to solve the PF problem of islanded microgrids. In this algorithm, two different steps of GA and PSO are employed to find unknown parameters. To solve the optimal PF problem, an algorithm based on DE is proposed in [110]. However, the main drawback of this method is that solution quality is dependent on initial population.

1.3 Objectives of the Thesis

PF evaluation of distribution systems is a prerequisite for any kind of investigation and analysis of the system. However under certain circumstances PF of a distribution system may not be possible due to following reasons.

1. Due to high r/x ratio and unbalanced loading in distribution system, the ill-conditioning of PF equations may appears. Conventional algorithms either cannot provide solution or poorly converge in such situations. In order to resolve this issue, topology based algorithms have been proposed, but these algorithms perform poorly in case of multi-source distribution systems. Thus, it is required to introduce new robust algorithms which perform effectively in case of ill-conditioned distribution systems.

2. Presence of PV buses in a distribution system can be considered as a problem of modern system due to adoption of renewable generations at distribution level. The renewable generations are power converter based interconnection to distribution systems which have a capability to provide voltage control at the interconnection behaving as PV buses. Thus, it is required to revisit the PF algorithms which were developed with PQ buses only so that modifications and improvements can be incorporated in the PF algorithms.

3. Nowadays, MGs have come up as a reality which may be operated either in an autonomous mode or in a grid connected mode. Further, the autonomous MGs can also get into arrangements of power sharing among them. In MGs, unlike transmission system or distribution system, there is no concept of swing bus or root node, respectively.

4. Also, in autonomously operated MGs, the excursion in frequency can be tolerated which may lead to wide variations in frequency dependent loads and line impedance apart from voltage dependency of loads. Thus, the above scenario of MGs requires a fresh approach and perceptive in relation to PF solutions of MG systems.

The problem statement of this thesis is as follows. Development and formulation of new algorithms to solve PF and optimal PF problems efficiently, accurately and in robust manner for distribution system having ill-conditioned equations, large number of PV buses and autonomous/islanded and grid connected microgrid mode of operations.

The main objectives of the thesis are as follows.

1. To develop new robust and efficient algorithms to solve the PF problem for grid-connected and islanded microgrids.

2. To investigate the performance of evolutionary algorithms in solving the above-mentioned PF problems.

3. To determine the maximum loadability limit of power system using evolutionary algorithm.

4. To formulate an optimization problem to solve the optimal PF problem of grid-connected and islanded microgrids.

1.4 Outline of the Thesis

- **Chapter 1:** This chapter describes the background and motivation for the thesis and provides an overview of the research work and objectives of the thesis.

- **Chapter 2:** This chapter presents robust and efficient PF algorithms to obtain fast and accurate PF solution for ill-conditioned unbalanced distribution systems or grid-connected microgrids.

- **Chapter 3:** This chapter discusses evolutionary algorithm based approaches to find out the maximum loadability limit of unbalanced distribution systems or grid-connected microgrids.

- **Chapter 4:** This chapter describes and proposes new robust and efficient numerical algorithms to solve the PF problem for decentralized droop controlled islanded microgrids.

- **Chapter 5:** This chapter presents an evolutionary algorithm based approach to solve the PF problem for decentralized droop controlled islanded microgrids.

- **Chapter 6:** This chapter describes application of different PF tools to find the optimum value of power system variables for operating robustly with minimum cost.

- **Chapter 7:** This chapter proposes an approach to minimize the system losses by calculating optimal setting of droop using evolutionary computation.

- **Chapter 8:** This chapter concludes the works done in this thesis and also proposes future scope of work.

Chapter 2

Power Flow Algorithms for Ill-conditioned Unbalanced Distribution Systems

2.1 Introduction

Most of the power systems are well-conditioned and their PF problem can be easily evaluated using NR-based algorithms. Nevertheless, in certain circumstances, the conditions of the system may become ill-conditioned. Consequently, the aforementioned algorithms can diverge or have poor convergence characteristics. This chapter addresses the issue of solving PF for ill-conditioned distribution system and proposes some numerical techniques to solve these kind of problems.

For the steady-state analysis, solving the PF problem has been one of the major area of investigation in the power systems since mid 1950s [111]. Different methods have been proposed to solve the PF problem in the literature. Different metrics are utilized to compare these algorithms on the basis of basic requirements of PF calculations. These metrics are as follows: (i) The memory requirements and CPU time (computing efficiency). (ii) The reliability and flexibility of algorithms. (iii) The convergence characteristics of algorithms.

In a power system, determining the voltage magnitude and phase of each bus, as well as the flow of active and reactive power through each bus, are the main objectives of the PF problem. In some circumstances, the Jacobian matrix may get near singular or may

become singular during the evaluation process when using NR-like algorithms [59]. When the Jacobian matrix is non-singular during the evaluation of solutions, the PF solution can be obtained using a flat initial start. This system is said to be well-conditioned and PF solution can be easily evaluated using conventional NR-based algorithms within a small number of iterations [59]. In some cases, the PF solution of the system exists, but conventional NR-based algorithms cannot provide the solution due to the near-singularity or singularity of the Jacobian matrix. In this situation, the power system is termed as ill-conditioned or bad-conditioned [112, 113]. In ill-conditioned power systems, the PF solution is very sensitive to small variations of the elements of the Jacobian matrix [70,114]. There are several reasons which may lead to deterioration of the condition of the system to ill-condition such as, high ratio of r/x, installation of some types of equipment, and location of the swing bus, etc. To solve the PF problem, one of the most popular numerical methods is the NR algorithm. Some of the popular algorithms are second-order NR-based algorithms which are utilized to solve ill-conditioned test systems. In [115], a fast-decoupled version was proposed to solve the PF problem of systems with high r/x ratio lines. In [57], a second-order PF algorithm has been proposed to deal with PF problem of distribution systems. Iwamoto *et.al.* propose a most popular NR-based algorithm for ill-conditioned PF solution [60]. In literature, several algorithms have been proposed to address the PF problem of ill-conditioned power systems [10, 61–66]. In [69], the LM algorithm has been proposed to solve the PF problem in ill-conditioned systems. In [70], a CN method is developed to solve the PF problem in ill-conditioned systems. Additionally, several algorithms based on LM and CN have been proposed in [71, 72]. Authors of [73] have presented a variant of LM to solve the PF problem in case of ill-conditioned as well as well-conditioned power systems. Authors of [70] have proposed a RK4 algorithm to solve the PF problem. To solve the PF problem, high-order NR-based algorithms have been proposed in [59].

The above-mentioned works have been studied on the transmission system which is ill-conditioned due to high loading conditions. However, in the distribution system, some features that are distinct from the transmission system make the system ill-conditioned [15]. There features are (i) weakly meshed or radial topology, (ii) having high r/x ratio, and (iii) having unbalanced system load. To address these issues, topology based algorithms have been proposed but these algorithms are only applicable to single source

systems.

Due to the increase of penetration of DGs in the distribution systems, many algorithms have been proposed to solve the PF problem of distribution system having DGs. Authors of [116, 117] have proposed different models of various equipment of distribution system (i.e. DGs and voltage regulators) to solve the distribution PF problem. In these approaches, DGs can be modeled as PV bus or as PQ bus. In [118], three different mathematical models of DGs have been proposed and these models are (1) constant voltage model, (2) variable reactive power model, and (3) constant power factor model.

Earlier, the PV buses were rare in the distribution system, but in the modern distribution systems, substantial number of PV buses can be present. Regular PF routines based on NR have limitations of convergence when applied to distribution systems due to large number of PV buses which makes the system ill-conditioned. The development of backward/forward sweep method mitigated this problem of convergence. However, forward/backward methods have limitations in handling PV buses.

In this chapter, simplified, generalized and efficient algorithms are proposed to solve the PF problem of the ill-conditioned unbalanced three-phase distribution system. Different models of DGs are also incorporated in this algorithms. These algorithms are based on LM and CN which are simple because these approaches depend mainly on the Jacobian matrix similar to NR-based algorithms. A strategy to control the step-size or the acceleration factor of LM and CN has been proposed to avoid ill-conditioning of the Jacobian. Further the problem of determining the step-size has been considered as an optimization sub-problem within the framework of CN and LM algorithm. The proposed modifications provide good convergence rate in different operating conditions. Moreover, they are generalized because they incorporate more accurate load modeling, unbalanced loads, three-phase modeling of feeders and different DG modeling. These algorithms are benchmarked on several unbalanced radial distribution systems (some of them are available in [119]). Different case studies have been performed to demonstrate the robustness and efficiency of these algorithms.

The outline of this chapter is as follows. In Section 2.2, PF formulations based on current injection and power injection are discussed with the calculation procedure of the Jacobian matrix. Section 2.3 presents the procedure of proposed algorithms for solving the PF problems. In Section 2.4, different numerical examples are performed to demonstrate

the robustness and validity of the proposed algorithm on different operating cases.

2.2 Problem Formulation

In this section, the PF formulation based on power injection and current injection is briefly discussed. Moreover, the calculation procedure of the Jacobian matrix is also included.

2.2.1 Formulation based on Power Injection

The PF problem can be represented by the power balance equation at each bus. Reactive and active powers are specified at each PQ buses (load buses) and only active power is specified at PV buses (generator buses). These active and reactive power can also be calculated using bus voltages and system Admittance Matrix (Ybus), which are termed as calculated power. The solution to PF problem is bus voltages (magnitude and phase angle) where the difference of specified power and calculated power at each bus become zero or within the specified tolerance limit. Consequently, the main objective of PF is to calculate the voltage magnitude and angles of the system buses that equals the specified power and the calculated power at each bus of the system. Hence, the PF problem can be treated as a system of non-linear equations.

In polar co-ordinates, the power balance equation at k-th bus can be represented by the following equations.

$$P_k - \sum_{i=1}^{N} |V_k||V_i||Y_{ki}|cos(\delta_k - \delta_i - \theta_{ki}) = 0, \tag{2.1}$$

$$Q_k - \sum_{i=1}^{N} |V_k||V_i||Y_{ki}|sin(\delta_k - \delta_i - \theta_{ki}) = 0, \tag{2.2}$$

where $P_k (= P_{g,k} - P_{l,k})$ and $Q_k (= Q_{g,k} - Q_{l,k})$ are total active and reactive power injected at the k-th bus, respectively, $V_k (|V_k| \angle \delta_k)$ represents the bus voltage at the k-th bus, and $Y_{ki} (|Y_{ki}| \angle \theta_{ki})$ represents the ij-th element of admittance matrix. Here, $P_{g,k}$ and $Q_{g,k}$ are total generated active and reactive power at the k-th bus, respectively, $P_{l,k}$ and $Q_{l,k}$ represent total required active and reactive load at the k-th bus.

Formation of Jacobian matrix:

To derive the elements of the Jacobian matrix,

$$P_k - \sum_{i=1}^{N} |V_k||V_i||Y_{ki}|cos(\delta_k - \delta_i - \theta_{ki}) = P_k - |V_k|^2 G_{kk} - \sum_{i=1, i\neq k}^{N} |V_k||V_i||Y_{ki}|cos(\delta_k - \delta_i - \theta_{ki}) = 0, \tag{2.3}$$

$$Q_k - \sum_{i=1}^{N} |V_k||V_i||Y_{ki}|sin(\delta_k - \delta_i - \theta_{ki}) = Q_k - |V_k|^2 B_{kk} - \sum_{i=1, i\neq k}^{N} |V_k||V_i||Y_{ki}|sin(\delta_k - \delta_i - \theta_{ki}) = 0, \tag{2.4}$$

where $G_{kk} = |Y_{kk}|cos(\theta_{kk})$ and $B_{kk} = |Y_{kk}|sin(\theta_{kk})$.

The elements of Jacobian matrix can be calculated as follows.

$$\frac{\partial P_i}{\partial \delta_j} = - \sum_{k=1, k\neq i}^{N} |V_i||V_k||Y_{ik}|sin(\delta_i - \delta_k - \theta_{ik}); j = i, \tag{2.5}$$

$$\frac{\partial P_i}{\partial \delta_j} = |V_i||V_j||Y_{ij}|sin(\delta_i - \delta_j - \theta_{ij}); j \neq i, \tag{2.6}$$

$$\frac{\partial P_i}{\partial |V_j|} = 2|V_i|G_{ii} + \sum_{k=1, k\neq i}^{N} |V_k||Y_{ik}|cos(\delta_i - \delta_k - \theta_{ik}); j = i, \tag{2.7}$$

$$\frac{\partial P_i}{\partial |V_i|} = |V_i||Y_{ij}|cos(\delta_i - \delta_j - \theta_{ij}); j \neq i, \tag{2.8}$$

$$\frac{\partial Q_i}{\partial \delta_j} = \sum_{k=1, k\neq i}^{N} |V_i||V_k||Y_{ik}|cos(\delta_i - \delta_k - \theta_{ik}); j = i, \tag{2.9}$$

$$\frac{\partial Q_i}{\partial \delta_j} = -2V_i B_{ii} + \sum_{k=1, k\neq i}^{N} |V_k||Y_{ik}|sin(\delta_i - \delta_k - \theta_{ik}); j = i, \text{and} \tag{2.10}$$

$$\frac{\partial Q_i}{\partial |V_j|} = |V_i||Y_{ij}|sin(\delta_i - \delta_j - \theta_{ij}); j \neq i \tag{2.11}$$

Taylor's expansion of Equations 2.3 and 2.4 can be written as follows in compact form.

$$\begin{bmatrix} \frac{\partial P_2}{\partial \delta_2} & :: & \frac{\partial P_2}{\partial \delta_N} & \frac{\partial P_2}{V_2} & :: & \frac{\partial P_2}{\partial V_N} \\ :: & :: & :: & :: & :: & :: \\ \frac{\partial P_N}{\partial \delta_2} & :: & \frac{\partial P_N}{\partial \delta_N} & \frac{\partial P_N}{V_2} & :: & \frac{\partial P_N}{\partial V_N} \\ \frac{\partial Q_2}{\partial \delta_2} & :: & \frac{\partial Q_2}{\partial \delta_N} & \frac{\partial Q_2}{V_2} & :: & \frac{\partial Q_2}{\partial V_N} \\ :: & :: & :: & :: & :: & :: \\ \frac{\partial Q_N}{\partial \delta_2} & :: & \frac{\partial Q_N}{\partial \delta_N} & \frac{\partial Q_N}{V_2} & :: & \frac{\partial Q_N}{\partial V_N} \end{bmatrix} \begin{bmatrix} \triangle\delta_2 \\ :: \\ \triangle\delta_N \\ \triangle V_2 \\ :: \\ \triangle V_N \end{bmatrix} = \begin{bmatrix} P_2^{sp} - P_2(\boldsymbol{\delta}^{(0)}, \boldsymbol{V}^{(0)}) \\ :: \\ P_N^{sp} - P_N(\boldsymbol{\delta}^{(0)}, \boldsymbol{V}^{(0)}) \\ Q_2^{sp} - Q_2(\boldsymbol{\delta}^{(0)}, \boldsymbol{V}^{(0)}) \\ :: \\ Q_N^{sp} - Q_N(\boldsymbol{\delta}^{(0)}, \boldsymbol{V}^{(0)}) \end{bmatrix} \tag{2.12}$$

where $P_i(\boldsymbol{\delta}^{(0)}, \boldsymbol{V}^{(0)})$ and $Q_i(\boldsymbol{\delta}^{(0)}, \boldsymbol{V}^{(0)})$ are the calculated injected active and reactive power, respectively, at i-th bus. With new notation, the Equation 2.12 can be written as

$$\begin{bmatrix} \boldsymbol{J1} & \boldsymbol{J2} \\ \boldsymbol{J3} & \boldsymbol{J4} \end{bmatrix} \begin{bmatrix} \triangle\boldsymbol{\delta} \\ \triangle\boldsymbol{V} \end{bmatrix} = \begin{bmatrix} \triangle\boldsymbol{P} \\ \triangle\boldsymbol{Q} \end{bmatrix} \tag{2.13}$$

where,

$$\boldsymbol{J1} = \frac{\partial \boldsymbol{P}}{\partial \boldsymbol{\delta}} = \begin{bmatrix} \frac{\partial P_2}{\partial \delta_2} & :: & \frac{\partial P_2}{\partial \delta_N} \\ :: & :: & :: \\ \frac{\partial P_N}{\partial \delta_2} & :: & \frac{\partial P_N}{\partial \delta_N} \end{bmatrix}, \tag{2.14}$$

$$\boldsymbol{J2} = \frac{\partial \boldsymbol{P}}{\partial \boldsymbol{V}} = \begin{bmatrix} \frac{\partial P_2}{\partial V_2} & :: & \frac{\partial P_2}{\partial V_N} \\ :: & :: & :: \\ \frac{\partial P_N}{\partial V_2} & :: & \frac{\partial P_N}{\partial V_N} \end{bmatrix}, \tag{2.15}$$

$$\boldsymbol{J3} = \frac{\partial \boldsymbol{Q}}{\partial \boldsymbol{\delta}} = \begin{bmatrix} \frac{\partial Q_2}{\partial \delta_2} & :: & \frac{\partial Q_2}{\partial \delta_N} \\ :: & :: & :: \\ \frac{\partial Q_N}{\partial \delta_2} & :: & \frac{\partial Q_N}{\partial \delta_N} \end{bmatrix}, \text{ and} \tag{2.16}$$

$$\boldsymbol{J4} = \frac{\partial \boldsymbol{Q}}{\partial \boldsymbol{V}} = \begin{bmatrix} \frac{\partial Q_2}{\partial V_2} & :: & \frac{\partial Q_2}{\partial V_N} \\ :: & :: & :: \\ \frac{\partial Q_N}{\partial V_2} & :: & \frac{\partial Q_N}{\partial V_N} \end{bmatrix}. \tag{2.17}$$

Equation 2.13 creates a basis for the NR-based algorithms. In this work, two power injection based algorithm are proposed which utilize the Jacobian matrix (explained in Equation 2.13) for updating the solution.

2.2.2 Formulation based on Current Injection

Power injection based PF formulation has been dealth in the above section. In this subsection, the current injection based PF formulation for power systems is proposed which is more accurate than the conventional power injection based formulation. Conventional power injection based formulation does not account for the voltage dependency of the loads which should not be ignored in distribution systems. The PF equation are expressed in rectangular coordinates i.e, elements of nodal admittance matrix, bus voltages, injected powers, and current injections are represented in rectangular coordinates.

The active and reactive current mismatch, for a given bus k, is given by the following relation.

$$\Delta I_{rk} = \sum_{i=1}^{n}(G_{ki}V_{ri} - B_{ki}V_{mi}) - \frac{P_k V_{rk} + Q_k V_{mk}}{(V_{rk})^2 + (V_{mk})^2}, \tag{2.18}$$

$$\Delta I_{mk} = \sum_{i=1}^{n}(B_{ki}V_{ri} + G_{ki}V_{mi}) - \frac{P_k V_{mk} - Q_k V_{rk}}{(V_{rk})^2 + (V_{mk})^2}. \tag{2.19}$$

Total injected active and reactive powers can be calculated by following equations.

$$P_k = P_{g,k} - P_{l,k}, \tag{2.20}$$

$$Q_k = Q_{g,k} - Q_{l,k}. \tag{2.21}$$

The voltage dependency of loads are represented by the following polynomial equations.

$$P_{lk} = P_{0k}\{\alpha_p + \beta_p V_k + \gamma_p {V_k}^2\}, \tag{2.22}$$

$$Q_{lk} = Q_{0k}\{\alpha_q + \beta_q V_k + \gamma_q {V_k}^2\}. \tag{2.23}$$

Where,

$$\alpha_p + \beta_p + \gamma_p = 1$$

and,

$$V_k = (V_{rk}^2 + V_{mk}^2)^{\frac{1}{2}}.$$

Similarly,

$$\alpha_q + \beta_q + \gamma_q = 1.$$

Taylor's series expansion of equations (2.18) and (2.19) after neglecting the higher order terms, gives the following equations.

$$\begin{aligned}\begin{bmatrix}\Delta I_{rk}\\ \Delta I_{mk}\end{bmatrix} = &\sum_{\substack{i=1,\\ i\neq k}}^{n}\begin{bmatrix}G_{ki} & -B_{ki}\\ B_{ki} & G_{ki}\end{bmatrix}\begin{bmatrix}\Delta V_{ri}\\ \Delta V_{mi}\end{bmatrix}\\ &+\begin{bmatrix}G'_{kk} & B'_{kk}\\ B''_{kk} & G''_{kk}\end{bmatrix}\begin{bmatrix}\Delta V_{rk}\\ \Delta V_{mk}\end{bmatrix}\\ &-\frac{1}{V_k^2}\begin{bmatrix}V_{rk} & V_{mk}\\ V_{mk} & -V_{rk}\end{bmatrix}\begin{bmatrix}\Delta P_k\\ \Delta Q_k\end{bmatrix}.\end{aligned} \tag{2.24}$$

Where, the values of G'_{kk}, B'_{kk}, G''_{kk} and B''_{kk} depend on the type of k^{th} bus (PQ/PV).

Representation of PQ buses:

In case of PQ buses, injected real and reactive powers are specified on the buses, i.e. $P_k = P_k^{sp}$ and $Q_k = Q_k^{sp}$, where 'k' is the PQ bus.

$G_{kk}^{'}$, $B_{kk}^{'}$, $G_{kk}^{''}$ and $B_{kk}^{''}$ can be expressed as follows.

$$G_{kk}^{'} = G_{kk} - \frac{1}{V_k^4}\{(V_{mk}^2 - V_{rk}^2)P_k^{sp} - 2V_{mk}V_{rk}Q_k^{sp}\}, \tag{2.25}$$

$$B_{kk}^{'} = -B_{kk} - \frac{1}{V_k^4}\{(V_{rk}^2 - V_{mk}^2)Q_k^{sp} - 2V_{mk}V_{rk}P_k^{sp}\}, \tag{2.26}$$

$$B_{kk}^{''} = B_{kk} - \frac{1}{V_k^4}\{(V_{rk}^2 - V_{mk}^2)Q_k^{sp} - 2V_{mk}V_{rk}P_k^{sp}\}, \tag{2.27}$$

$$G_{kk}^{''} = G_{kk} + \frac{1}{V_k^4}\{(V_{mk}^2 - V_{rk}^2)P_k^{sp} - 2V_{mk}V_{rk}Q_k^{sp}\}. \tag{2.28}$$

Where,

$$P_k^{sp} = P_g - P_{0k}\{\alpha_p + \beta_p V_k + \gamma_p {V_k}^2\},$$

$$Q_k^{sp} = Q_g - Q_{0k}\{\alpha_q + \beta_q V_k + \gamma_q {V_k}^2\}.$$

The values of ΔP_k and ΔQ_k are calculated as follows.

$$\Delta P_k = \Delta P_g - P_{0k}\beta_p \Delta V_k - 2V_k\gamma_p \Delta V_k. \tag{2.29}$$

Similarly,

$$\Delta Q_k = \Delta Q_g - Q_{0k}\beta_q \Delta V_k - 2V_k\gamma_q \Delta V_k. \tag{2.30}$$

Substituting $\Delta P_g = 0$ and $\Delta Q_g = 0$ at PQ buses,

$$\Delta P_k = -P_{0k}\left(\beta_p + 2V_k\gamma_p\right)\Delta V_k,$$

$$\Delta Q_k = -Q_{0k}\left(\beta_q + 2V_k\gamma_q\right)\Delta V_k$$

and,

$$\Delta V_k = \frac{1}{V_k}\left(V_{rk}\Delta V_{rk} + V_{mk}\Delta V_{mk}\right). \tag{2.31}$$

This yields,

$$\Delta P_k = -\frac{P_{ok}}{V_k}\left(\beta_p + 2V_k\gamma_p\right)\left(V_{rk}\Delta V_{rk} + V_{mk}\Delta V_{mk}\right),$$

$$\Delta Q_k = -\frac{Q_{ok}}{V_k}\left(\beta_q + 2V_k\gamma_q\right)\left(V_{rk}\Delta V_{rk} + V_{mk}\Delta V_{mk}\right).$$

Substituting the expressions of ΔP_k and ΔQ_k in equation (2.24), yields,

$$\begin{aligned}\begin{bmatrix}\Delta I_{rk}\\ \Delta I_{mk}\end{bmatrix} &= \sum_{\substack{i=1,\\ i\neq k}}^{n}\begin{bmatrix}G_{ki} & -B_{ki}\\ B_{ki} & G_{ki}\end{bmatrix}\begin{bmatrix}\Delta V_{ri}\\ \Delta V_{mi}\end{bmatrix}\\ &+\begin{bmatrix}G^{'}_{kk} & B^{'}_{kk}\\ B^{"}_{kk} & G^{"}_{kk}\end{bmatrix}\begin{bmatrix}\Delta V_{rk}\\ \Delta V_{mk}\end{bmatrix}\\ &-\begin{bmatrix}A & B\\ C & D\end{bmatrix}\begin{bmatrix}\Delta V_{rk}\\ \Delta V_{mk}\end{bmatrix}.\end{aligned} \tag{2.32}$$

Where,

$$A = \frac{-P_{0k}V_{rk}^2\left(\beta_p + 2\gamma_p V_k\right) - Q_{0k}V_{rk}V_{mk}\left(\beta_q + 2\gamma_q V_k\right)}{V_k^3},$$

$$B = \frac{-P_{0k}V_{rk}V_{mk}\left(\beta_p + 2\gamma_p V_k\right) - Q_{0k}V_{mk}^2\left(\beta_q + 2\gamma_q V_k\right)}{V_k^3},$$

$$C = \frac{-P_{0k}V_{rk}V_{mk}\left(\beta_p + 2\gamma_p V_k\right) + Q_{0k}V_{rk}^2\left(\beta_q + 2\gamma_q V_k\right)}{V_k^3},$$

$$D = \frac{-P_{0k}V_{mk}^2\left(\beta_p + 2\gamma_p V_k\right) + Q_{0k}V_{rk}V_{mk}\left(\beta_q + 2\gamma_q V_k\right)}{V_k^3}.$$

Representation of PV bus:

In case of PV bus 'k', Q_k is not specified. For a PV bus, Q_k is calculated in every iteration by using the following equation.

$$Q_k = V_{mk}I_{rk}^{cal} - V_{rk}I_{mk}^{cal}. \tag{2.33}$$

Substituting the values of Q_k in equation (2.25), (2.26), (2.27) and (2.28) following expressions of $G^{'}_{kk}$, $B^{'}_{kk}$, $G^{''}_{kk}$ and $B^{''}_{kk}$ are obtained.

$$\begin{aligned}G^{'}_{kk} =& G_{kk} - \frac{1}{V_k^4}(V_{mk}^2\{P_k^{sp} - 2V_{rk}I_{rk}^{cal}\} - V_{rk}^2\{P_k^{sp} +\\ & 2V_{mk}I_{mk}^{cal}\}),\end{aligned} \tag{2.34}$$

$$\begin{aligned}B^{'}_{kk} =& -B_{kk} - \frac{1}{V_k^4}(V_{mk}\{(V_{rk}^2 - V_{mk}^2)I_{rk}^{cal} - V_{rk}P_k^{sp}\}\\ & - V_{rk}\{(V_{rk}^2 - V_{mk}^2)I_{mk}^{cal} - V_{mk}P_k^{sp}\}),\end{aligned} \tag{2.35}$$

$$\begin{aligned}B^{''}_{kk} =& B_{kk} - \frac{1}{V_k^4}(V_{mk}\{(V_{rk}^2 - V_{mk}^2)I_{rk}^{cal} - V_{rk}P_k^{sp}\}\\ & - V_{rk}\{(V_{rk}^2 - V_{mk}^2)I_{mk}^{cal} - V_{mk}P_k^{sp}\}),\end{aligned} \tag{2.36}$$

$$G_{kk}^{''} = G_{kk} + \frac{1}{V_k^4}(V_{mk}^2(P_k^{sp} - 2V_{rk}I_{rk}^{cal}) - V_{rk}^2(P_k^{sp} + 2V_{mk}I_{mk}^{cal})). \tag{2.37}$$

Since, for a PV bus, ΔP_g and $\Delta V_k = 0$, equations (2.29) and (7.18) get reduced as follows,

$$\Delta P_k = \Delta P_g = 0,$$

$$\Delta Q_k = \Delta Q_{gk}.$$

Substituting $\Delta V_k = 0$ in equation (2.31) yields,

$$\Delta V_{rk} = -\frac{V_{mk}}{V_{rk}}\Delta V_{mk}.$$

Substituting expressions of ΔQ_k and ΔV_{rk} in equation (2.24) yields following expressions.

$$\begin{bmatrix} \Delta I_{rk} \\ \Delta I_{mk} \end{bmatrix} = \sum_{\substack{i=1,\\ i\neq k}}^{n} \begin{bmatrix} G_{ki} & -B_{ki} \\ B_{ki} & G_{ki} \end{bmatrix} \begin{bmatrix} \Delta V_{ri} \\ \Delta V_{mi} \end{bmatrix} + \begin{bmatrix} G'_{kk} & B'_{kk} \\ G^{"}_{kk} & B^{"}_{kk} \end{bmatrix} \begin{bmatrix} -\frac{V_{mk}}{V_{rk}}\Delta V_{mk} \\ \Delta V_{mk} \end{bmatrix} - \frac{1}{V_k^2} \begin{bmatrix} V_{rk} & V_{mk} \\ V_{mk} & -V_{rk} \end{bmatrix} \begin{bmatrix} 0 \\ \Delta Q_g \end{bmatrix}. \tag{2.38}$$

Simplification of equation (2.38) yields,

$$\begin{bmatrix} \Delta I_{rk} \\ \Delta I_{mk} \end{bmatrix} = \sum_{\substack{i=1,\\ i\neq k}}^{n} \begin{bmatrix} G_{ki} & -B_{ki} \\ B_{ki} & G_{ki} \end{bmatrix} \begin{bmatrix} \Delta V_{ri} \\ \Delta V_{mi} \end{bmatrix} + \begin{bmatrix} B'_{kk} - \frac{V_{mk}}{V_{rk}}G'_{kk} & -\frac{V_{mk}}{V_k^2} \\ G^{"}_{kk} - \frac{V_{mk}}{V_{rk}}B^{"}_{kk} & \frac{V_{rk}}{V_k^2} \end{bmatrix} \begin{bmatrix} \Delta V_{mk} \\ \Delta Q_g \end{bmatrix}. \tag{2.39}$$

After simplifying the equation (2.39), expressions for B'_{kk}, G'_{kk}, B''_{kk}, and G''_{kk} becomes as follows.

$$B'_{kk} = -B_{kk} - \frac{V_{mk}I_{rk}^{calc} - V_{rk}I_{mk}^{calc}}{V_k^2}, \tag{2.40}$$

$$G'_{kk} = G_{kk} - \frac{P_k^{sp}}{V_k^2}, \tag{2.41}$$

$$G''_{kk} = G_{kk} + \frac{P_k^{sp}}{V_k^2}, \tag{2.42}$$

$$B''_{kk} = B_{kk} - \frac{V_{mk}I_{rk}^{calc} - V_{rk}I_{mk}^{calc}}{V_k^2}. \tag{2.43}$$

Jacobian structure:

The proposed current injection based NR PF equation can be compactly expressed as,

$$\begin{bmatrix} \Delta I_{rm}^{pq} \\ \Delta I_{rm}^{pv} \end{bmatrix} = \begin{bmatrix} J_{pq-pq} & J_{pq-pv} \\ J_{pv-pq} & J_{pv-pv} \end{bmatrix} \begin{bmatrix} \Delta V_{rm}^{pq} \\ \Delta V_{mQ}^{pv} \end{bmatrix}. \tag{2.44}$$

Where,

$$\Delta I_{rm}^{pq} = \Big[\Delta I_{r1}, \Delta I_{r2}, \ldots, \Delta I_{rn}, \Delta I_{m1}, \Delta I_{m2}, \ldots, \Delta I_{mn}\Big]^T,$$

$$\Delta I_{rm}^{pv} = \Big[\Delta I_{r(n+1)}, \Delta I_{r(n+2)}, \ldots, \Delta I_{rN}, \Delta I_{m(n+1)}, \Delta I_{m(n+2)}, \ldots, \Delta I_{mN}\Big]^T,$$

$$\Delta V_{rm}^{pq} = \Big[\Delta V_{r1}, \Delta V_{r2}, \ldots, \Delta V_{rn}, \Delta V_{m1}, \Delta V_{m2}, \ldots, \Delta V_{mn}\Big]^T,$$

$$\Delta V_{mQ}^{pv} = \Big[\Delta V_{m(n+1)}, \Delta V_{m(n+2)}, \ldots, \Delta V_{mN}, \Delta Q_{(n+1)}, \Delta Q_{(n+2)}, \ldots, \Delta Q_N\Big]^T,$$

$$J_{pq-pq} = \left[\begin{array}{c|c} \mathbf{G}' & \mathbf{B}' \\ \hline \mathbf{B}'' & \mathbf{G}'' \end{array}\right],$$

$$J_{pq-pv} = \left[\begin{array}{c|c} -\mathbf{B} - \frac{V_m}{V_r}\mathbf{G} & 0 \\ \hline \mathbf{G} - \frac{V_m}{V_r}\mathbf{B} & 0 \end{array}\right],$$

$$J_{pv-pv} = \left[\begin{array}{c|c} \mathbf{B}^{*\prime} - \frac{V_m}{V_r}\mathbf{G}^{*\prime} & -\frac{V_m}{V^2} \\ \hline \mathbf{G}^{*\prime\prime} - \frac{V_m}{V_r}\mathbf{B}^{*\prime\prime} & \frac{V_r}{V^2} \end{array}\right] \text{ and,}$$

$$J_{pv-pq} = \left[\begin{array}{c|c} \mathbf{G} & -\mathbf{B} \\ \hline \mathbf{B} & \mathbf{G} \end{array}\right].$$

The above-described formulation of PF is more accurate for the distribution systems because it gives more accurate modeling of PV buses as compared to model suggested in [57] . Modeling of voltage dependency is incorporated with other models of components.

2.3 Proposed Algorithms

Three different PF algorithms are described in this section. These techniques are based on the system of non-linear equations and ordinary differential equations. This section is divided into three subsections: algorithms based on Conventional NR technique, algorithms based on the LM technique, and algorithms based on the Runge-Kutte technique.

2.3.1 Modified Newton-Raphson Method

Let us assume a nonlinear equation, $f(x) = 0$, where x represents a variable. If x_0 be an initial predicated solution, then $f(x)$ can be extended around x_0 using Taylor series.

$$\begin{aligned} &f(x) = 0, \text{ and } f(x) \\ &\quad = f(x_0) + f'(x_0)(x - x_0) + \frac{1}{2!}f''(x_0)(x - x_0)^2 + ... + \frac{1}{n!}f^n(x_0)(x - x_0)^n + ..., \end{aligned} \tag{2.45}$$

where, $f^n(x_0)$ is $n-$th derivative of $f(x)$ at $x = x_0$.

By neglecting the higher order derivatives (second and higher order) of $f(x)$ from Equation 2.45 yields

$$f(x) \simeq f(x_0) + f'(x_0)(x - x_0) = 0 \tag{2.46}$$

From Equation 2.46, x^* can be calculated as follows.

$$x^* = x_0 - \frac{f(x_0)}{f'(x_0)}, \tag{2.47}$$

where x^* is a predicated value of x.

Therefore, at $k-$th iteration, the predicated value of x, x^{k+1}, can be calculated by following equation.

$$x^{k+1} = x^k - \triangle x^k, \tag{2.48}$$

where,

$$\triangle x^k = \frac{f(x^k)}{f'(x^k)} \tag{2.49}$$

Equations 2.48 and 2.49 can be generalized for system of non-linear equations by following Equations.

$$\triangle \mathbf{x}^k = \mathbf{J_x}(\mathbf{x}^k)^{-1}\mathbf{F}(\mathbf{x}^k), \tag{2.50}$$

$$\mathbf{x}^{k+1} = \mathbf{x}^k - \triangle \mathbf{x}^k, \tag{2.51}$$

where $\mathbf{x}^k = [x_1^k, x_2^k, ..., x_n^k]^t$, $\mathbf{F}(\mathbf{x}^k) = [f_1(\mathbf{x}^k), f_2(\mathbf{x}^k), ..., f_n(\mathbf{x}^k)]^t$, and $\mathbf{J_x}$ represents the Jacobian matrix at $\mathbf{x}^k$.

The main steps of Newton's method are summarized in Algorithm 1.

In this work, one algorithm, named CINR, based on Algorithm 1 is proposed where the current injection based PF formulation are employed in NR method. In CINR, the Jacobian matrix is calculated by using Equation 2.44. To deal with the ill-conditioning of the system, an optimal multiplier is calculated in each iterations using following equation.

$$m^* \leftarrow \text{minimize}(||\mathbf{F}_{\mathbf{x}-m\triangle\mathbf{x}}||), \tag{2.52}$$

Algorithm 1: Newton's Method

Data: $\mathbf{x}^0 \leftarrow$ initial predicated solution

Result: $\mathbf{x}^*$

$\mathbf{F_x} \leftarrow \mathbf{F}(\mathbf{x}^0)$;

$TolF \leftarrow ||\mathbf{F_x}||$;

$\mathbf{J} \leftarrow \mathbf{J_x}(\mathbf{x}^0)$;

$k \leftarrow 0$;

while $TolF \leq 10^{-06}$ **do**

  $\triangle \mathbf{x}^k \leftarrow \mathbf{J}^{-1}\mathbf{F_x}$;

  $\mathbf{x}^{k+1} \leftarrow \mathbf{x}^{k+} - \triangle \mathbf{x}^k$;

  $\mathbf{F_x} \leftarrow \mathbf{F}(\mathbf{x}^{k+1})$;

  $TolF \leftarrow ||\mathbf{F_x}||$;

  $\mathbf{J} \leftarrow \mathbf{J_x}(\mathbf{x}^{k+1})$;

  $k \leftarrow k + 1$;

end

$\mathbf{x}^* \leftarrow \mathbf{x}^k$

where

$$\triangle \mathbf{x}^k = \mathbf{J}^{-1}\mathbf{F_x}. \tag{2.53}$$

Then, the solution is updated using following equation.

$$\mathbf{x}^{k+1} = \mathbf{x}^k - m^* \triangle \mathbf{x}. \tag{2.54}$$

Thus, the above modifications relate to finding the optimal value of step-size, m, such that the mismatch vector $F(x)$ is minimized.

2.3.2 Fourth-order Levenberg-Marquardt Method

The LM algorithm belongs to the class of conventional methods that solves the ill-conditioned system of nonlinear equations. At $k-$th iteration, the solution x^k can be estimated using LM algorithm by following Equations.

$$\triangle \mathbf{x}^k = (\mathbf{J_x}(\mathbf{x}^k)^t \mathbf{J_x}(\mathbf{x}^k) + \lambda_k \mathbf{I})^{-1} \mathbf{F}(\mathbf{x}^k), \tag{2.55}$$

$$\mathbf{x}^{k+1} = \mathbf{x}^k - \triangle \mathbf{x}^k, \tag{2.56}$$

where $\mathbf{I}$ represents identity matrix and λ_k can be calculated by Equation (2.57).

$$\lambda_k = \mu||\mathbf{F}(\mathbf{x}^k)||^\sigma, \tag{2.57}$$

where μ and σ are parameters used in LM. A suitable parameter setting is needed to achieve the convergence.

Bi-quadratic Levenberg-Marquardt

High order LM techniques are proficient in lessening the number of Jacobian calculations with better convergence rate as compared to LM. A bi-quadratic LM is introduced in [120]. The steps of bi-quadratic LM are shown in Algorithm 2. A PF algorithm based on Algorithm 2, named LMPF, is proposed in this chapter.

2.3.3 Modified Runge-Kutta Method

In this section, Runge-Kutta algorithm is briefly described. Formulation of system of non-linear equations problem based on conventional NR is discussed in the following paragraph.

Conventional Newton-Raphson

A set of ordinary differential equations can be presented by following equations.

$$\dot{\mathbf{x}} = \mathbf{f}(\mathbf{x}) \tag{2.58}$$

The following steps are used in explicit Euler method to integrate the Equation 2.58.

$$\triangle\mathbf{x}^k = \triangle t\mathbf{f}(\mathbf{x}^k), \tag{2.59}$$

$$\mathbf{x}^{k+1} = \mathbf{x}^k + \triangle\mathbf{x}^k, \tag{2.60}$$

where $\triangle t$ represents the time step.

An analogy between system of non-linear equations and ordinary differential equations can be easily established using Equations 2.50, 2.51, 2.59, and 2.60 by defining following relation.

$$\mathbf{f}(\mathbf{x}^k) = \mathbf{J}_\mathbf{x}(\mathbf{x}^k)^{-1}\mathbf{F}(\mathbf{x}^k), \text{ at } \triangle t = 1 \tag{2.61}$$

From above relation, it can be established that any numerical technique, used to solve ordinary differential equations, can be applied on the system of non-linear equations [70].

Algorithm 2: Bi-quadratic LM Method

Data: $\mathbf{x}^0 \leftarrow$ initial predicated solution;

Initial parameter for μ and σ

Result: $\mathbf{x}^*$

$\mathbf{F_x} \leftarrow \mathbf{F}(\mathbf{x}^0)$;

$TolF \leftarrow ||\mathbf{F_x}||$;

$\mathbf{J} \leftarrow \mathbf{J_x}(\mathbf{x}^0)$;

$k \leftarrow 0$;

while $TolF \leq 10^{-06}$ **do**

  $\lambda_k \leftarrow \mu_k ||\mathbf{F_x}||^{\sigma}$;

  $\mathbf{d}^k \leftarrow -(\mathbf{J}^t\mathbf{J} + \lambda_k\mathbf{I})^{-1}\mathbf{J}^t\mathbf{F_x}$;

  $\mathbf{y}^k \leftarrow \mathbf{x}^k + \mathbf{d}^k$;

  $\mathbf{F_y} \leftarrow \mathbf{F}(\mathbf{y}^k)$;

  $\mathbf{dd}^k \leftarrow -(\mathbf{J}^t\mathbf{J} + \lambda_k\mathbf{I})^{-1}\mathbf{J}^t\mathbf{F_y}$;

  $\mathbf{z}^k \leftarrow \mathbf{y}^{k+} + \mathbf{dd}^k$;

  $\mathbf{F_z} \leftarrow \mathbf{F}(\mathbf{z}^k)$;

  $\mathbf{ddd}^k \leftarrow -(\mathbf{J}^t\mathbf{J} + \lambda_k\mathbf{I})^{-1}\mathbf{J}^t\mathbf{F_z}$;

  $Ared^k \leftarrow ||\mathbf{F_x}||^2 - ||\mathbf{F}(\mathbf{x}^k + \mathbf{d}^k + \mathbf{dd}^k + \mathbf{ddd}^k)||^2$;

  $Pred^k \leftarrow$

  $||\mathbf{F_x}||^2 - ||\mathbf{F_x}|| + \mathbf{J}(\mathbf{d}^k)^2 + ||\mathbf{F_y}||^2 - ||\mathbf{F_y}|| + \mathbf{J}(\mathbf{dd}^k)^2 + ||\mathbf{F_z}||^2 - ||\mathbf{F_z}|| + \mathbf{J}(\mathbf{ddd}^k)^2$;

  $r^k \leftarrow \frac{Ared^k}{Pred^k}$;

  if $r^k \geq p_0$ **then**

    $\mathbf{x}^{k+1} \leftarrow \mathbf{x}^k + \mathbf{d}^k + \mathbf{dd}^k + \mathbf{ddd}^k$;

    $\mathbf{F}_x \leftarrow \mathbf{F}(\mathbf{x}^{k+1})$;

    $TolF \leftarrow ||\mathbf{F_x}||$;

    $\mathbf{J} \leftarrow \mathbf{J_x}(\mathbf{x}^{k+1})$;

  end

  $k \leftarrow k + 1$;

end

$\mathbf{x}^* \leftarrow \mathbf{x}^k$

Fourth-order Runge-Kutta method

In this work, the RK4 algorithm is adopted to solve the PF problem of the ill-conditioned three-phase power system. The main steps of the Runge-Kutta algorithm are depicted in Algorithm 3.

A PF algorithm based on Algorithm 3, named RK4PF, is used here to solve PF problem of ill-conditioned unbalanced distribution systems. In algorithm 3, steps at statement numbers, $20 - 25$, are the modifications in the existing Runge-kutta method towards adjustment of h, the step-size.

2.4 Results and Discussion

In this section of the chapter, the four proposed PF techniques are validated over the small, medium, large and very large test cases.

2.4.1 Test Systems

The following test systems are utilized to demonstrate the performance of proposed algorithms.

- **CASE13 test system**: This system is radial unbalanced type with 9 branches and 12 PQ buses.
- **CASE25 test system**: This system is radial unbalanced type with 24 branches and 24 PQ buses.
- **CASE37 test system**: This system is radial unbalanced type with 34 branches and 34 PQ buses.
- **CASE28 test system**: This system is radial unbalanced type with 27 branches, 24 PQ buses, and 3 PV buses.
- **CASE56 test system**: This system is radial unbalanced type with 55 branches, 49 PQ buses, and 6 PV buses.
- **CASE84 test system**: This system is radial unbalanced type with 83 branches, 74 PQ buses, and 9 PV buses.

Algorithm 3: RK4PF algorithm

Data: $\mathbf{x}^0 \leftarrow$ initial predicated solution; $h \leftarrow 1$

Result: $\mathbf{x}^*$

$\mathbf{F_x} \leftarrow \mathbf{F}(\mathbf{x}^0)$;

$TolF \leftarrow ||\mathbf{F_x}||$;

$\mathbf{J_x} \leftarrow \mathbf{J_x}(\mathbf{x}^0)$;

$k \leftarrow 0$;

while $TolF \leq 10^{-06}$ **do**

  $\mathbf{k_1}^k \leftarrow -(\mathbf{J_x})^{-1}\mathbf{F_x}$;

  $\mathbf{y}^k \leftarrow \mathbf{x}^k + \frac{h}{2}\mathbf{k_1}^k$;

  $\mathbf{F_y} \leftarrow \mathbf{F}(\mathbf{y}^k)$;

  $\mathbf{k_2}^k \leftarrow -(\mathbf{J_x}(\mathbf{y}^k))^{-1}\mathbf{F_y}$;

  $\mathbf{z}^k \leftarrow \mathbf{x}^{k+} + \frac{h}{2}\mathbf{k_2}^k$;

  $\mathbf{F_z} \leftarrow \mathbf{F}(\mathbf{z}^k)$;

  $\mathbf{k_3}^k \leftarrow -(\mathbf{J_x}(\mathbf{z}^k))^{-1}\mathbf{F_z}$;

  $\mathbf{u}^k \leftarrow \mathbf{x}^k + h\mathbf{k_3}^k$;

  $\mathbf{F_u} \leftarrow \mathbf{F}\mathbf{u}^k$;

  $\mathbf{k_4}^k \leftarrow -(\mathbf{J_x}(\mathbf{u}^k))^{-1}\mathbf{F_u}$;

  $\mathbf{x}^{k+1} \leftarrow \mathbf{x}^k + \frac{h}{6}(\mathbf{k_1}^k + 2\mathbf{k_2}^k + 2\mathbf{k_3}^k + \mathbf{k_4})$;

  $\mathbf{F}_x \leftarrow \mathbf{F}(\mathbf{x}^{k+1})$;

  $TolF \leftarrow ||\mathbf{F_x}||$;

  $\mathbf{J} \leftarrow \mathbf{J_x}(\mathbf{x}^{k+1})$;

  $\chi \leftarrow ||\mathbf{k_2}^k - \mathbf{x}^{k+1}||_\infty$;

  if $\chi \geq 001$ **then**

    $h \leftarrow \max\{0.985h, 0.75\}$;

  else

    $h \leftarrow \max\{1.015h, 0.75\}$;

  end

  $k \leftarrow k + 1$;

end

$\mathbf{x}^* \leftarrow \mathbf{x}^k$

- **CASE112 test system**: This system is radial unbalanced type with 111 branches, 99 PQ buses, and 12 PV buses.
- **CASE392 test system**: This system is radial unbalanced type with 391 branches, 349 PQ buses, and 42 PV buses.
- **CASE784 test system**: This system is radial unbalanced type with 783 branches, 699 PQ buses, and 84 PV buses.
- **CASE1176 test system**: This system is radial unbalanced type with 1175 branches, 1049 PQ buses, and 126 PV buses.

The above-mentioned test systems are well-conditioned at normal operating point. Since the performance of algorithms are to be analyzed on ill-conditioned systems, the condition of the test systems are deteriorated by increasing the loading levels at the PQ buses and r/x ratios of the branches. In addition, the flat initial start is applied in each algorithm to solve the PF problem of these test cases. The details of the above test cases and their modification are described in Appendix-I.

2.4.2 Parameter Settings of Algorithms

In this work, three robust PF techniques, named CINR, LMPF, and RK4PF, are proposed to solve the PF problem of ill-conditioned distribution test systems. The following parameter setting is adopted in the algorithms.

- **CINR**: $TolF = 10^{-06}$, $m0 = 1$, and $Max\_iter = 100$.
- **LMPF**: $TolF = 10^{-06}$, $\mu = 1.3$, $\sigma = 1$, $\rho_0 = 0.5$, and $Max\_iter = 100$.
- **RK4PF**: $TolF = 10^{-06}$, $h = 1$, and $Max\_iter = 300$.

All algorithms have been tested out on PC Intel Core i7-7700 3.60 GHz using MATLAB R2017b.

2.4.3 Validation of Proposed Algorithms

In this section, the accuracy of the proposed algorithms are validated on ill-conditioned version of CASE13 and CASE28 test systems. These test systems cannot be solved by

using conventional algorithms, TCIM, iTCIM, and BFS due to their ill-conditioning. Very few works based on the Newton-Raphson algorithm have been done on power flow problem of ill-conditioned distribution systems. The backward-forward sweep algorithm is a popular algorithm for the distribution system, but this algorithm do not converge on true solution of the power flow problem. Hence, there is no solution obtained which can be compared with our converged solution. Therefore, candidate could not validate the result of proposed algorithms with the result of other algorithms from the literature. However, the power flow problem of power system is a type of system of non-linear equations, where power flow equations are treated as system and solution of this system is power flow solution. As far as validation of power flow methods are concerned, they get validated when the solution of non-linear equations get solved accurately.

The precise idea behind taking the scenario of heavily loaded and ill-conditioned system was to investigate whether the proposed method can handle such scenarios. It is obvious that in the said scenarios, the system may have low system voltages. The load flow is planning tool which computes system voltages under full spectrum of loading to plan the operational strategies. A similar approach for investigating the unbalanced load scenario was also adopted. The severe system situations were deliberately adopted to show the enhanced capability of the proposed methods and approaches in terms of convergence and accuracy.

CASE13 test system

The structure of this test system is similar to the standard CASE13 test system. The PF solution of this test system is worked out using proposed algorithms and is depicted in Tables 2.1, 2.2, and 2.3. From these Tables, it can be concluded that the PF solution obtained from all the solutions is similar to each other with minor variations. Note that the optimal values of the step-size in case of CINR are calculated as 0.9811, 1.2457, and 0.5734. The system used here is an unbalanced test system. When we increase the loads on all buses such that the system operates in an ill-conditioned zone, the loads will be more unbalanced in the system. Therefore, in this case voltages are expected to be low at buses 7, 8, 9, and 10 in respective phases. Nose curve of case13 has been drawn in Figure 2.1. From Figure 2.1, it is verified that the obtained voltages for the given loading condition are quite low as expected. However, they are not intended as operational voltages for a

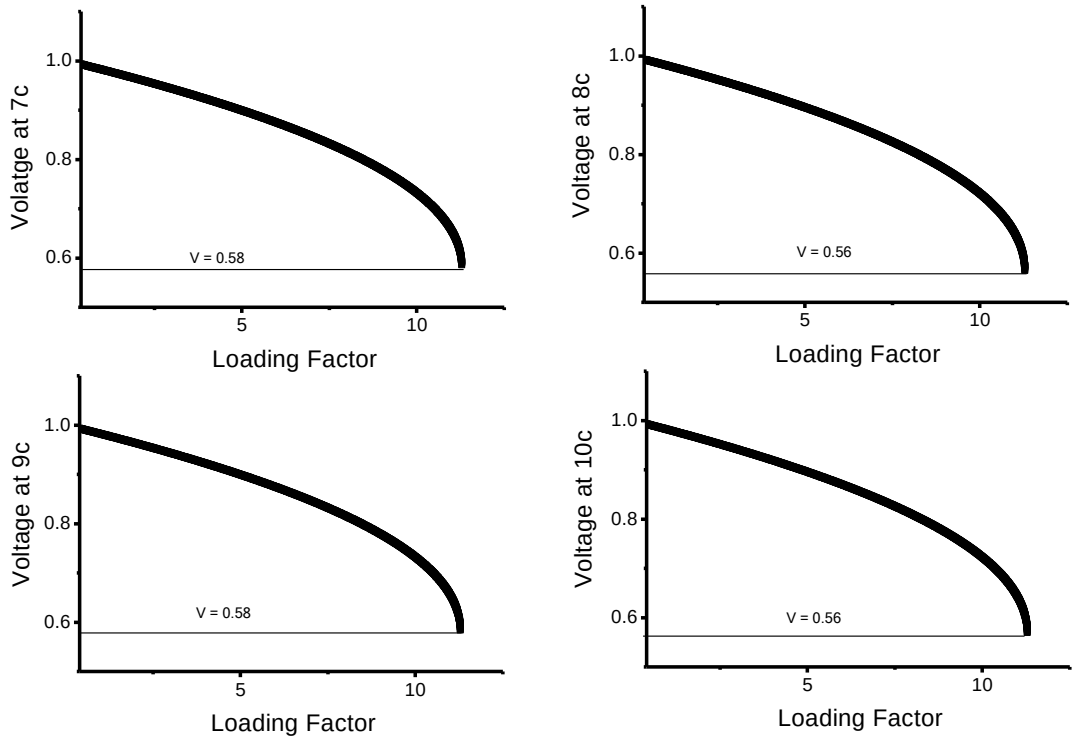

Figure 2.1: Nose curve (PV curve) of bus 7c, 8c, 9c, and 10c.

system. These are in fact the solutions obtained in planning scenario.

Table 2.1: PF solution of ill-conditioned version of CASE13 system using CINR

CINR						
Bus No.	$\|V_a\|$	$\angle_a$	$\|V_b\|$	$\angle_b$	$\|V_c\|$	$\angle_c$
1	1.00	0.00	1.00	-120.00	1.00	120.00
2	0.99	-0.22	0.99	-120.16	0.99	119.98
3	–	–	–	–	0.55	99.10
4	–	–	0.95	-120.65	1.01	119.63
5	–	–	0.93	-120.94	1.02	119.52
6	0.96	-13.42	–	–	–	–
7	0.98	-13.57	1.04	-117.21	0.58	101.56
8	0.97	-14.67	1.05	-117.44	0.56	101.05
9	0.98	-13.57	1.04	-117.21	0.58	101.56
10	0.98	-13.69	–	–	0.57	100.49

The convergence characteristics of all proposed algorithms on CASE13 ill-conditioned test system are depicted in Figure 2.2. From this figure, it can be concluded that the convergence characteristics of the proposed algorithm are different from each other. In the case of CINR, the convergence rate is faster than the other algorithms. RK4PF

Table 2.2: PF solution of ill-conditioned version of CASE13 test system using LMPF

LMPF						
Bus No.	$\|V_a\|$	$\angle_a$	$\|V_b\|$	$\angle_b$	$\|V_c\|$	$\angle_c$
1	1.00	0.00	1.00	-120.00	1.00	120.00
2	0.99	-0.22	0.99	-120.16	0.99	119.98
3	–	–	–	–	0.55	99.10
4	–	–	0.95	-120.65	1.01	119.63
5	–	–	0.93	-120.94	1.02	119.52
6	0.96	-13.43	–	–	–	–
7	0.98	-13.59	1.04	-117.24	0.58	101.56
8	0.96	-14.70	1.05	-117.47	0.56	101.04
9	0.98	-13.58	1.04	-117.26	0.58	101.58
10	0.98	-13.70	–	–	0.57	100.49

Table 2.3: PF solution of ill-conditioned version of CASE13 system using RK4PF

RK4PF						
Bus No.	$\|V_a\|$	$\angle_a$	$\|V_b\|$	$\angle_b$	$\|V_c\|$	$\angle_c$
1	1.00	0.00	1.00	-120.00	1.00	120.00
2	0.99	-0.22	0.99	-120.16	0.99	119.98
3	–	–	–	–	0.55	99.10
4	–	–	0.95	-120.65	1.01	119.63
5	–	–	0.93	-120.93	1.02	119.52
6	0.96	-13.47	–	–	–	–
7	0.99	-13.61	1.04	-117.13	0.58	101.55
8	0.97	-14.72	1.05	-117.36	0.56	101.05
9	0.99	-13.61	1.04	-117.13	0.58	101.55
10	0.98	-13.74	–	–	0.56	100.49

algorithm has a low convergence rate. Furthermore, the value of tolerance is least in the case of LMPF.

The above discussion concludes that the all the proposed algorithms are robust PF tool for ill-conditioned unbalanced test systems. CINR is a faster algorithm than others and LMPF has provided most accurate PF solution than other algorithms.

CASE28 test system

To explore the acceptance of the proposed algorithms for multi-source three-phase unbalanced radial networks, proposed algorithms are tested on an ill-conditioned CASE28 test system.

CASE28 represents an ill-conditioned unbalanced distribution system which includes 28-buses with four power sources (1-slack and 3-PV bus). This system can serve

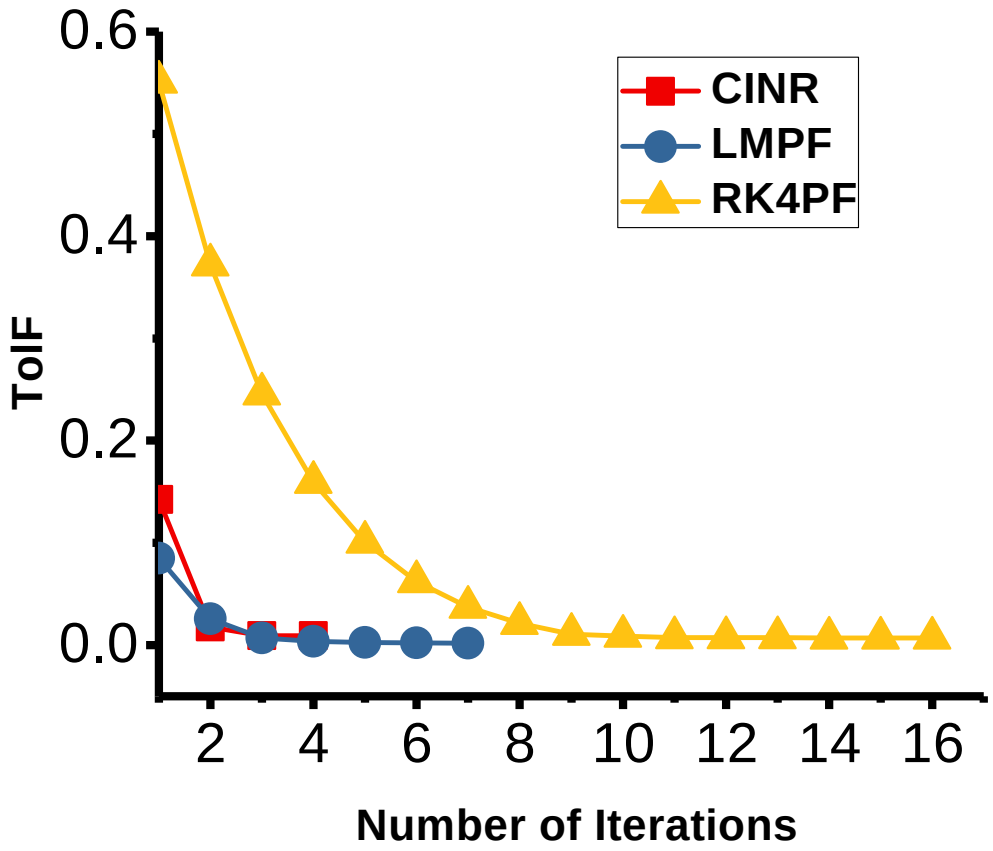

Figure 2.2: Convergence characteristics of CASE13(ill-conditioned case) using CINR, LMPF, and RK4PF.

as a benchmark test system to investigate the robustness of the algorithm over the ill-conditioned system because conventional methods fail to converge on the PF solution.

PF solution obtained from all proposed algorithms are reported in Tables 2.4, 2.5, and 2.6. These tables show that all the algorithms provide a similar solution with minor variations because all the algorithm stop solving at different accuracy level after fulfilling the specified tolerance.

To show the convergence characteristics of these algorithms, convergence curve of these algorithms is depicted in Figure 2.3. On the contrary to accuracy, the convergence characteristics of these algorithms are different from each other. CINR has the fastest convergence speed among all algorithms, but initially the convergence is slower than LMPF and RK4PF because of linear convergence rate. RK4PF has shown the least convergence speed among all of them. LMPF has provided the most accurate results with moderate convergence speed.

Table 2.4: PF solution of ill-conditioned version of CASE28 test system using CINR

CINR						
Bus No.	$\|V_a\|$	$\angle_a$	$\|V_b\|$	$\angle_b$	$\|V_c\|$	$\angle_c$
1	1.00	0.00	1.00	-120.00	1.00	120.00
2	0.93	-15.53	0.95	-129.59	0.97	111.49
3	0.93	-18.67	0.95	-131.78	0.97	109.68
4	0.94	-20.22	0.95	-132.86	0.97	108.84
5	0.93	-20.21	0.95	-132.84	0.96	108.83
6	0.85	-24.03	0.90	-134.42	0.92	106.97
7	0.81	-33.81	0.87	-139.71	0.89	102.09
8	0.84	-24.01	0.89	-134.39	0.91	106.96
9	0.77	-33.82	0.83	-139.67	0.86	102.05
10	0.73	-33.82	0.80	-139.65	0.84	102.02
11	0.72	-33.83	0.79	-139.65	0.83	102.02
12	0.71	-33.82	0.78	-139.64	0.82	102.05
13	0.71	-33.82	0.78	-139.65	0.82	102.03
14	0.84	-43.69	0.89	-145.10	0.91	97.17
15	0.83	-43.67	0.88	-145.09	0.90	97.16
16	0.80	-33.80	0.86	-139.70	0.89	102.08
17	0.83	-43.67	0.89	-145.09	0.90	97.18
18	0.93	-21.38	0.94	-133.78	0.95	108.03
19	0.93	-24.05	0.94	-135.82	0.95	106.47
20	0.94	-24.08	0.95	-135.83	0.96	106.41
21	0.91	-21.34	0.92	-133.74	0.93	108.10
22	0.90	-21.32	0.91	-133.71	0.92	108.15
23	0.92	-20.21	0.94	-132.86	0.95	108.81
24	0.91	-20.21	0.93	-132.88	0.94	108.80
25	0.89	-20.17	0.92	-132.93	0.93	108.82
26	0.99	-22.47	0.99	-134.24	0.99	107.98
27	0.98	-50.96	0.98	-148.59	0.99	94.21
28	0.99	-26.17	0.99	-137.27	0.99	105.46

2.4.4 Comparison of Algorithms

The proposed algorithms are compared with the following standard PF technique of distribution systems:

- TCIM [24]: NR-based three phase PF algorithm using current injection equations.
- iTCIM [57]: A second order NR-based three phase PF algorithm using current injection equations.
- BFS [121]: A three phase PF algorithm based on backward/forward sweep algorithm.

Table 2.5: PF solution of ill-conditioned version of CASE28 test system using LMPF

LMPF						
Bus No.	$\lvert V_a \rvert$	$\angle_a$	$\lvert V_b \rvert$	$\angle_b$	$\lvert V_c \rvert$	$\angle_c$
1	1.00	0.00	1.00	-120.00	1.00	120.00
2	0.93	-15.64	0.95	-129.67	0.97	111.33
3	0.93	-18.83	0.95	-131.88	0.97	109.49
4	0.94	-20.40	0.95	-132.98	0.97	108.64
5	0.93	-20.39	0.95	-132.96	0.96	108.63
6	0.85	-24.18	0.90	-134.52	0.92	106.72
7	0.81	-34.02	0.87	-139.84	0.89	101.73
8	0.83	-24.16	0.89	-134.49	0.91	106.71
9	0.76	-33.99	0.83	-139.78	0.86	101.69
10	0.73	-33.97	0.80	-139.75	0.83	101.65
11	0.72	-33.96	0.79	-139.74	0.82	101.65
12	0.71	-33.95	0.78	-139.72	0.82	101.69
13	0.71	-33.95	0.78	-139.73	0.82	101.67
14	0.84	-44.04	0.89	-145.30	0.91	96.71
15	0.82	-44.01	0.88	-145.29	0.90	96.69
16	0.80	-34.01	0.86	-139.83	0.89	101.73
17	0.83	-44.01	0.88	-145.29	0.90	96.72
18	0.93	-21.58	0.94	-133.91	0.95	107.82
19	0.93	-24.28	0.94	-135.99	0.95	106.23
20	0.94	-24.32	0.95	-135.99	0.96	106.17
21	0.91	-21.53	0.92	-133.87	0.93	107.88
22	0.89	-21.51	0.91	-133.84	0.92	107.93
23	0.92	-20.39	0.94	-132.98	0.95	108.61
24	0.91	-20.38	0.93	-133.00	0.94	108.60
25	0.89	-20.35	0.92	-133.05	0.93	108.62
26	0.99	-22.67	0.99	-134.41	0.99	107.78
27	0.98	-51.22	0.98	-148.94	0.99	93.93
28	0.99	-26.42	0.99	-137.49	0.99	105.23

The above-mentioned algorithms have been implemented on MATLAB environment to perform the experiments.

Well-conditioned Systems

The PF analysis of well-conditioned test systems is performed by applying proposed algorithms and other popular conventional techniques: TCIM, iTCIM, and BFS. For this investigation, the following test systems are considered: CASE13, CASE25, CASE37, CASE28, CASE56, CASE84, CASE112, CASE140, CASE168, and CASE196. The system data of these test systems is available at `https://github.com/abhisheka456`.

The total number of iterations of all algorithms for converging on all these test

Table 2.6: PF solution of ill-conditioned version of CASE28 test system using RK4PF

RK4PF						
Bus No.	$\|V_a\|$	$\angle_a$	$\|V_b\|$	$\angle_b$	$\|V_c\|$	$\angle_c$
1	1.00	0.00	1.00	-120.00	1.00	120.00
2	0.93	-15.57	0.95	-129.68	0.97	111.40
3	0.93	-18.73	0.95	-131.88	0.97	109.58
4	0.94	-20.30	0.95	-132.97	0.97	108.74
5	0.93	-20.29	0.95	-132.96	0.96	108.73
6	0.85	-24.07	0.90	-134.55	0.92	106.81
7	0.81	-33.88	0.87	-139.90	0.89	101.84
8	0.84	-24.05	0.89	-134.53	0.91	106.80
9	0.76	-33.87	0.83	-139.86	0.86	101.81
10	0.73	-33.86	0.80	-139.84	0.84	101.78
11	0.72	-33.86	0.79	-139.84	0.82	101.78
12	0.71	-33.84	0.78	-139.82	0.82	101.82
13	0.71	-33.84	0.78	-139.84	0.82	101.80
14	0.84	-43.83	0.89	-145.35	0.91	96.83
15	0.82	-43.81	0.88	-145.34	0.90	96.82
16	0.80	-33.87	0.86	-139.89	0.89	101.84
17	0.83	-43.81	0.88	-145.35	0.90	96.85
18	0.93	-21.46	0.94	-133.90	0.95	107.93
19	0.93	-24.15	0.94	-135.96	0.95	106.35
20	0.94	-24.19	0.95	-135.97	0.96	106.29
21	0.91	-21.42	0.92	-133.86	0.93	107.99
22	0.89	-21.40	0.91	-133.83	0.92	108.04
23	0.92	-20.29	0.94	-132.97	0.95	108.71
24	0.91	-20.28	0.93	-132.99	0.94	108.70
25	0.89	-20.24	0.92	-133.04	0.93	108.72
26	0.99	-22.56	0.99	-134.39	0.99	107.89
27	0.98	-50.97	0.98	-148.94	0.99	94.05
28	0.99	-26.28	0.99	-137.45	0.99	105.37

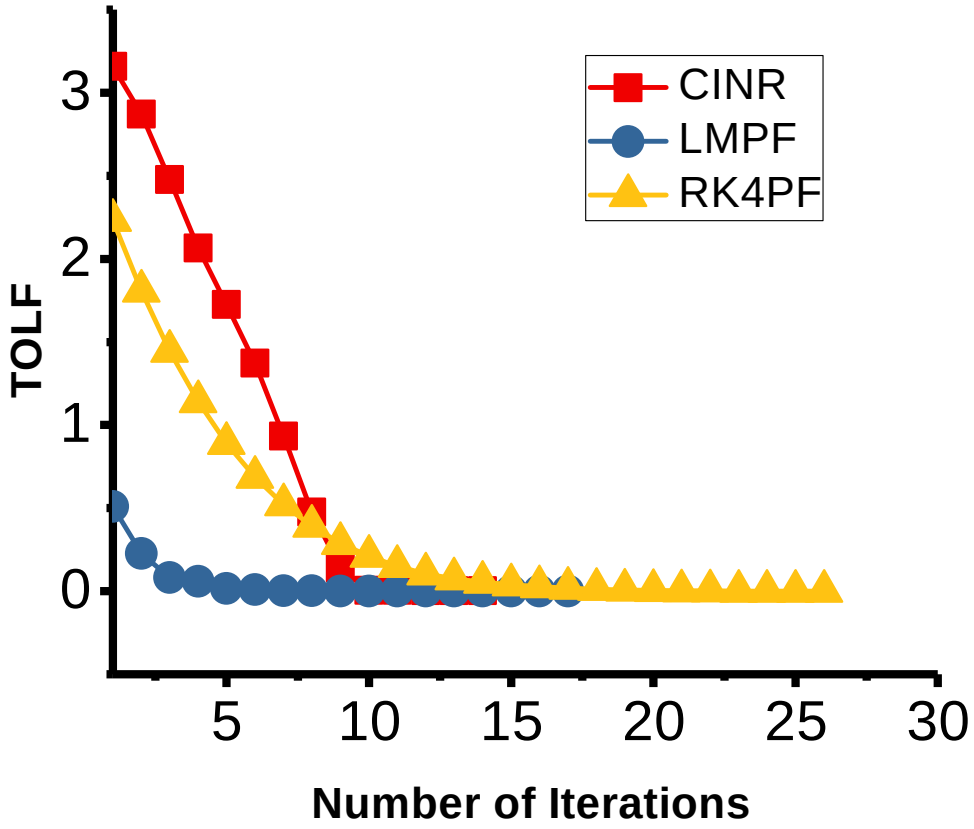

Figure 2.3: Convergence characteristics of CASE28 (ill-conditioned case) using CINR, LMPF, and RK4PF.

systems are illustrated in Table 2.7. It can be observed from Table 2.7 that the proposed algorithm NICR and LMPF have presented the fastest convergence rate among all the methods considered, in all the test cases and RK4PF has yielded the least convergence rate. BFS does not converge on multi-source test cases.

The performance of the proposed algorithms is further examined on multi-source large test systems: CASE392, CASE784, and CASE1176. The system data of these test systems is available at `https://github.com/abhisheka456`. The obtained outcomes are presented in Table 2.8. From Table 2.8, it can be observed that the proposed algorithms are more robust than other algorithms on large test systems. In addition, CINR and LMP exhibit the fastest convergence speed among all algorithms while RK4PF shows the least convergence speed. Moreover, the execution time consumed by all algorithms is also calculated and reported in Table 2.9. From Table 2.9, CINR is the most efficient algorithm while RK4PF is consuming more time than the other algorithms. However, the

robustness of RK4PF is better than the other algorithms.

From the above evaluation, it can be concluded that the proposed algorithms, CINR and LMPF are the fastest algorithms among all the methods considered, on well-conditioned test systems. However, the RK4PF demands a large number of iterations for convergence.

Table 2.7: Obtained results of CINR, LMPF, RK4PF, BFS, TCIM, and iTCIM over several test systems. (NC: Not Converged)

Test System	CINR	LMPF	RK4PF	BFS	TCIM	iTCIM
CASE13	2	2	17	6	3	3
CASE25	1	2	15	7	3	3
CASE37	1	2	15	9	2	2
CASE28	2	2	25	NC	3	3
CASE56	3	2	26	NC	6	4
CASE84	3	2	26	NC	6	4
CASE112	3	3	26	NC	6	4
CASE140	3	3	26	NC	6	4
CASE168	3	3	26	NC	7	4
CASE196	3	3	26	NC	7	4

Table 2.8: Obtained results of CINR, LMPF, RK4PF, BFS, TCIM, and iTCIM over large test systems. (NC: Not Converged)

Test System	CINR	LMPF	RK4PF	BFS	TCIM	iTCIM
CASE392	4	4	30	NC	19	5
CASE784	5	5	30	NC	NC	5
CASE1176	5	5	30	NC	NC	5

Table 2.9: Execuation time (in sec) of CINR, LMPF, RK4PF, BFS, TCIM, and iTCIM. (NC: Not Converged)

Test System	CINR	LMPF	RK4PF	BFS	TCIM	iTCIM
CASE13	0.0628	0.1790	0.3313	0.1032	0.0815	0.1048
CASE25	0.0997	0.2691	0.4235	0.1882	0.1206	0.1483
CASE37	0.1392	0.3530	0.4509	0.2610	0.2021	0.2615

Ill-conditioned systems

In section 2.4.3, two ill-conditioned test systems were already utilized to validate the robustness and accuracy of the proposed algorithms. Furthermore, the proposed algorithms

are evaluated on the test systems with high loading conditions and a high r/x ratio. These conditions make the PF equations of the test systems ill-conditioned. Conventional NR algorithms and conventional techniques may diverge on test systems with these conditions or take large number of iterations to converge.

Table 2.10: Total Number of iterations required for different PF algorithms in heavily loaded ill-conditioned systems.(LF: Loading Factor, NC: Not Converged)

CASE37						
LF(%)	CINR	LMPF	RK4PF	BFS	TCIM	iTCIM
200	2	3	16	6	3	3
600	2	3	17	7	3	3
1000	2	3	18	8	3	3
1400	3	4	18	9	4	4
1800	4	21	59	NC	NC	NC
2200	4	24	87	NC	NC	NC
2400	NC	26	88	NC	NC	NC
2500	NC	37	91	NC	NC	NC

CASE84						
LF(%)	CINR	LMPF	RK4PF	BFS	TCIM	iTCIM
100	3	2	26	NC	6	4
200	4	4	28	NC	13	7
300	6	5	29	NC	20	9
400	9	6	29	NC	33	11
500	17	9	29	NC	69	15
600	NC	40	43	NC	NC	NC
700	99	38	63	NC	NC	NC
800	31	35	87	NC	NC	NC

Test systems with high loading conditions

In this section, the stability of proposed algorithms is evaluated on various test systems with different loading conditions. The loading level at the buses of the different test systems is gradually increased to their maximum loading limit. Two test systems, CASE37 and CASE84, are considered for this analysis. Total number of iterations required by different algorithms for CASE37 and CASE84 are reported in Table 2.10.

It is observed from this table that the performance of proposed algorithms is better than the other conventional algorithms. In CASE37, CINR is the most robust algorithm among the other algorithms while LMPF is more efficient in CASE84. However, the RK4PF algorithm requires a high number of iterations to converge but the robustness of this algorithm is better than CINR.

Table 2.11: Total Number of iterations required for different PF algorithms in ill-conditioned systems with high r/x ratios.(NC: Not Converged)

CASE37						
r/x	CINR	LMPF	RK4PF	BFS	TCIM	iTCIM
2	2	3	15	6	3	3
6	2	4	15	7	3	3
10	2	5	15	8	3	3
14	3	6	15	9	4	4
18	3	18	50	NC	NC	NC
22	3	29	77	NC	NC	NC
24	4	22	78	NC	NC	NC
25	8	38	77	NC	NC	NC

CASE84						
r/x	CINR	LMPF	RK4PF	BFS	TCIM	iTCIM
1	3	2	26	NC	6	4
4	4	4	28	NC	14	6
7	5	5	27	NC	26	8
10	6	7	27	NC	48	10
13	16	16	27	NC	NC	20
14	21	43	59	NC	NC	NC
15	21	57	87	NC	NC	NC
16	21	39	94	NC	NC	NC

Test systems with high r/x ratio

The sensitivity of proposed algorithms is validated over different r/x ratios of the lines of test systems and the performance of proposed algorithms is compared with other algorithms. In this study, CASE37 and CASE84 are considered with different r/x ratios.

Number of iterations required to converge by the proposed algorithms with other algorithms are reported in Table 2.11. It can be observed that the proposed algorithms outperform the other conventional algorithms. CINR and LMPF are more efficient than RK4PF and other conventional algorithms.

2.5 Summary

In this chapter, the PF problem of the well and the ill-conditioned unbalanced distribution systems have been solved using the proposed algorithms. Three algorithms using different strategies are proposed. The first algorithm, CINR, is based on conventional NR method with optimal calculation of step-size, m. Other two algorithm, LMPF and RK4PF, consider PF problem as least-square optimization problem and ordinary differential equations problem, respectively. The step-size of these algorithms are adapted to improve their efficiency and robustness. These proposed algorithms are robust and efficient as compared to conventional PF algorithms. The proposed algorithms have been validated over several small, medium and large ill-conditioned unbalanced distribution test systems. The obtained outcomes reveal the superiority and effectiveness of the proposed PF methodology as compared to conventional techniques.

The maximum loadability limit of an unbalanced distribution system is also required to study the power system stability. Proposed algorithms can also be utilized to find the maximum loadability limit. However, the robustness of the algorithms is deteriorated as the system reaches the maximum loadability. In order to address these issues, the application of evolutionary algorithms is analyzeds in the next chapter.

Chapter 3

Spherical Search and Butterfly Constrained Optimizer for Power Flow of Unbalanced Distribution System

3.1 Introduction

In this chapter, general-purpose PF tools are developed which are handy and robust for all possible applications of power system analysis. Recently, evolutionary algorithms have emerged as robust optimization tools because of their potentials and versatile qualities. These search techniques are adequate to deal with a large collection of problems of various characteristics because they do not constrain the variable types and search-space.

In the traditional Jacobian based methods of PF, the solution proceeds as per the direction gradient (Jacobian or partial derivative). This direction gradient is a kind of static formulation to decide the step direction and step size. In this gradient direction procedure, the step direction and the step size can not be decided as per quality of solution achieved so far. In fact, during the iterations, we do not evaluate any metric related to the quality of solution.

In any optimization based formulation, this is not the case. In general, in an optimization based formulation, step direction and step size are decided based on the quality of the solution. There are two broad classifications of optimization: Conventional Opti-

mization, and Evolutionary (population based) optimization. Conventional optimization proceeds with one solution whereas evolutionaly optimization proceeds, iteration by iteration, with multiple solutions. This population of solution enhances the procedure of evaluation of the quality of solutions and consequently step direction and step size in a better way. This results in a dynamic formulation to decide the step direction and step size. Due to the above fundamental difference in the procedure to evaluate solutions, evolutionary optimization based PF formulation does not succumb to the ill-conditioning of the Jacobian matrix and is able to keep sailing in the search of solution and ultimately provides PF solution.

Traditional Jacobian based correction of solution does not consider the quality of solution in terms of present solution and solution expected in the next iteration. Whereas, conventional optimization based correction of solution considers the quality of solution in terms of present solution and the solution expected in the next iteration considering active and reactive power mismatch as objective function.

Almost all conventional (Jacobian and optimization based) PF algorithms reported in the literature utilize the following structure. The first iteration starts with the initial seed, and mismatches in reactive and active power at all buses are evaluated. Power injection equations or current injection equations at buses with their derivatives are used to calculate a correction for the variables to update the system variables. PF algorithms diverge when the required corrections are determined incorrectly. Thus, the cause of divergence exists in the procedures of an algorithm applied to determine the solutions. To address this issue, two robust algorithms are developed in this chapter. In these algorithms, rather than determining the corrections vectors, a population of solutions is perturbed around the distribution of population on search-space. Only those perturbations are utilized which facilitates the population to converge on the optimum solution. This step-by-step scheme avoids divergence, however, this makes the algorithm slower. Consequently, these proposed algorithms are only valuable when the conventional methods are not able to produce a solution for the PF problem.

The need and rationale of using optimization techniques for solving power flow problem can be appreciated in the following two ways.

- The optimization techniques have advantages of finding all the possible multiple solution accurately required in power system analysis. The optimization algorithm

(especially search based) inherently have high chance of convergence due to their formulations and techniques.

- The optimization techniques have also over the times resolved in several theoretical bottlenecks thereby easing out their implementation but also improving performance.

- The above advantages though were obvious at all times, however their practical implementation were subject to contemporary computational advancements. In the present times the computational resources have improved quite significantly (or exponentially increased). This has lead to several successful implementations of computationally demanding algorithms as apparent from literature. Thus it is imperative to revisit and explore the performance of algorithmss vis-a-vis contemporary computational resource scenario.

With advent of new technologies, the modern distribution systems and tools to examine them are updating themselves. Conventional algorithms of power flow problems fail to provide a solution. As an alternative, optimization algorithms are becoming popular in this area.

In this chapter, two different optimization methods are designed to deal with the PF problem of ill-conditional test systems. The first one, referred to as Butterfly Constrained Optimizer (BCO), is a constrained optimization algorithm which employs the multi-order LM based mutation with υ-constrained handling routine to deal with the constraints of PF problems. The other one, named as Spherical Search (SS), is a bound-constrained optimization algorithm which can be utilized to calculate initial seed for conventional PF algorithms.

The major contributions of this work are summarized as follows:

1. It introduces two novel evolutionary-based PF algorithms, SS and BCO, to address the PF problem of ill-conditioned test systems.

2. It includes an evolutionary-based method to determine the initial seed for the conventional PF algorithm whose performance is dependent on the initial seed.

3. It presents a powerful methods to determine the maximum loadability limit for distribution test systems. This can be applied to investigate the voltage stability of

the system buses of distribution test systems.

4. It provides an authentic PF algorithm for the distribution test systems by establishing two optimization algorithms which diminish the active and reactive power discrepancies. The optimization algorithms have been validated on the distribution test systems to establish that these algorithms can reduce the active and reactive power mismatch.

3.2 Power Flow Formulation as a Constrained Optimization Problem

In this section, the PF problem is formulated as Constrained Optimization Problem (COP) based on power injection.

3.2.1 Formulation based on Power Injection.

The PF problem can be represented by the power balance equation at each bus. Reactive and active power are specified at each PQ buses (load buses) and active power is only specified at PV buses (generator buses). These active and reactive powers can also be calculated using bus voltages and Ybus, which are termed as calculated power. The solution to this PF problem is bus voltages where the difference of specified power and calculated power at each bus becomes zero or within the tolerance limit. Consequently, the main objective of PF is to calculate the voltage magnitude and angles of the system buses which reduce the differences between the specified power and the calculated power at each bus of the system. Hence, the PF problem can be treated as a system of non-linear equations.

In polar co-ordinates, the power balance equation at k-th bus can be represented by the following equations.

$$P_k - \sum_{i=1}^{N} |V_k||V_i||Y_{ki}|cos(\delta_k - \delta_i - \theta_{ki}) = 0, \tag{3.1}$$

$$Q_k - \sum_{i=1}^{N} |V_k||V_i||Y_{ki}|sin(\delta_k - \delta_i - \theta_{ki}) = 0, \tag{3.2}$$

where $P_k(= P_{g,k} - P_{l,k})$ and $Q_k(= Q_{g,k} - Q_{l,k})$ are total active and reactive power injected at k-th bus, respectively, $V_k(|V_k|\angle\delta_k)$ represents the bus voltage at k-th bus, and $Y_{ki}(|Y_{ki}|\angle\theta_{ki})$ represents the ki-th element of admittance matrix. Here, $P_{g,k}$ and $Q_{g,k}$ are total generated active and reactive power at k-th bus, respectively, $P_{l,k}$ and $Q_{l,k}$ represent total active and reactive load at k-th bus.

3.2.2 Formulation as a Constrained Optimization Problem

In this section, PF problem of ill-conditioned test system has been formulated as a COP which is proposed to be solved using the evolutionary algorithms.

A PF problem can be formulated as a COP:

$$\text{Minimize } f = \sum_{(i \in S_{pq} \cup S_{pv})} (P_i - P_{i,g})^2 + \sum_{(j \in S_{pq})} (Q_i - Q_{i,l})^2 + \sum_{(k \in S_{pv})} \left(|V_k| - \sqrt{V_{rk}^2 + V_{mk}^2} \right)^2 \tag{3.3}$$

subject to.

$$\begin{aligned} V_{ri} \sum_{j=1}^{N} (V_{rj} G_{ij} - V_{mj} B_{ij}) + V_{mi} \sum_{j=1}^{N} (V_{rj} B_{ij} + V_{mj} G_{ij}) - P_i = 0, \\ V_{mi} \sum_{j=1}^{N} (V_{rj} G_{ij} - V_{mj} B_{ij}) - V_{ri} \sum_{j=1}^{N} (V_{rj} B_{ij} + V_{mj} G_{ij}) - Q_i = 0, \\ Vr_{lb} < V_{rj} < Vr_{ub}, \ Vm_{lb} < V_{mj} < Vm_{ub} \\ P_{lb} < P_i < P_{ub}, \ Q_{lb} < Q_i < Q_{ub}, \end{aligned} \tag{3.4}$$

where, S_{pq} and S_{pv} are set of PQ and PV buses, respectively. $P_{i,g}$ and $Q_{i,g}$ are generated real and reactive power at i-th bus and $P_{i,l}$ and $Q_{i,l}$ are real and reactive load at i-th bus. G_{ij} and B_{ij} are active and reactive part of ijth element of Ybus matrix and N is the total number of buses in the system. In this problem, the variables are V_{rj}, V_{mj}, P_j, and Q_j where $j = 2, ..., N$. Therefore, total number of variables are $4 \times (N - 1)$.

3.3 Spherical Search

In this section, the mathematical modeling of the SS algorithm is discussed and developed.

SS algorithm is a swarm based meta-heuristics proposed to solve the non-linear bound-constrained global optimization problems. It shows some properties similar to

other popular meta-heuristics, particularly PSO and DE. In the SS algorithm, the search space is represented in the form of vector space where the location of each individual in space is a position vector representing a candidate solution to the problem.

In a D-dimension search space, for each individual, $(D-1)$-spherical boundary is prepared towards the target direction in every iteration before generating the trial location of the individual. Here the target direction is the main axis of the spherical boundary and the individual lies on the surface of the spherical boundary. Trial solutions appear on the 1-spherical boundary. Thus, in every iteration, the trial location for each individual is generated on the surface of $(D-1)$-spherical boundary. An objective function value determines the fitness value of a location. On the basis of the fitness value of the trial locations, better locations pass on into the next iteration as individual locations.

In the SS algorithm, solution update procedure and spherical search movement balance the ability of exploration and exploitation. When the $(D-1)$-spherical boundary is small, exploitation of search-space is emphasized in the algorithm. On the other hand, in case of larger $(D-1)$-spherical boundary, exploration of the space gets emphasized. It is evident that when the target location of a respective individual is far-off, the individual has a tendency to explore, as the spherical boundary is large. This is advantageous as in such conditions it is better to explore the larger search space. On the contrary, when the target locations of a respective individual are nearby, the individual has a tendency to exploit as the spherical boundary becomes small. This is advantageous as in such situations it is better to exploit in a small search space.

At the end of every iteration, the location having the best fitness value is saved as the best solution. Stopping criteria is achieved when the number of function evaluations reaches to a specified number or when the value of the best solution reaches near to the predefined solution within a specified tolerance. For the reported experimental work of this chapter, both the stopping criteria have been used.

3.3.1 Initialization of Population

At the k^{th} iteration, population P_x is represented as follows.

$$P_x^{(k)} = [\bar{x_1}^{(k)}, \bar{x_2}^{(k)}, ...\bar{x_N}^{(k)}] \tag{3.5}$$

where

$$\bar{x_i}^{(k)} = [x_{i1}^{(k)}, x_{i2}^{(k)}, ...x_{iD}^{(k)}]^T \tag{3.6}$$

here, x_{ij} is the value of j^{th} element (parameter) of i^{th} solution and D is the total number of elements (parameters). So, $\bar{x_i}$ is actually representing a point on $D-$dimensional search space. Here, x_{ij}^0 is initialized using random uniform distribution between pre-specified lower and upper bounds of j^{th} element as follows:

$$x_{ij}^0 = (x_{hj} - x_{lj}) * rand(0, 1] + x_{lj}, \tag{3.7}$$

where x_{hj} and x_{lj} represent the upper and lower bounds of j^{th} element respectively. Also, $rand(0, 1]$ generates random number from uniform distribution within the limit $(0, 1]$.

3.3.2 Spherical Surface and Trial Solutions

In the case of population-based optimization algorithms, in every iteration, there will be a need to calculate potential new solutions that compete with the old solution to become a part of the population for the next iteration. In this algorithm, the name, trial solution, is used to represent these potential new solutions. In SS algorithm, for each solution, a $(D-1)$-spherical boundary is prepared where the search direction passes through the main axis of boundary i.e. search direction crosses the center of $(D-1)$-spherical boundary.

In SS algorithm, following equation is used to generate a trial solutions for $i-$th solution.

$$\bar{y_i}^{(k)} = \bar{x_i}^{(k)} + c_i^{(k)} P_i^{(k)} \bar{z_i}^{(k)}, \tag{3.8}$$

where, P_i is a projection matrix, which decides the value of $\bar{y_i}^k$ on the $(D-1)$-spherical boundary. For a particular solution, $\bar{x_i^{(k)}}$, different possible values of $P_i^{(k)}$ yield different values of $\bar{y_i}^{(k)}$. Locus of $\bar{y_i}^{(k)}$ gives $(D-1)$ spherical boundary.

To define all the iterative steps of the SS algorithm, the calculation procedure of $\bar{z_i}^{(k)}$, $c_i^{(k)}$ and $P_i^{(k)}$ are discussed in following sections.

Calculation of search direction, $\bar{z_i}^{(k)}$

In optimization algorithms, quality of new solution highly depends upon the balance between exploration and exploitation of search space. Emphasis on exploration of search space increases the diversity of candidate solutions but slows the optimization process

resulting in delayed or no convergence. Whereas, emphasis on exploitation may accelerate the optimization process which may lead to premature convergence trapped in local minima.

Search direction, $\bar{z_i}^{(k)}$, should be generated in such a way that it guides the $i-$th solution towards the better solutions. Points $\bar{x}_t$, r_1 and r_2 are needed to calculate the search direction as follows.

$$\bar{z_i}^{(k)} = (\bar{x_t}^{(k)} + r_1^{(k)} - r_2^{(k)}) - \bar{x_i}^{(k)}, \tag{3.9}$$

where, $\bar{x}_t$ is the target point. In equation (3.9), two random solutions r_1 and r_2 are selected from the current set of solutions (population). So, the actual search direction deviates by some angle from target direction.

In this chapter, two methods are introduced to calculate the search direction, namely *towards-rand* and *towards-best*. Method *towards-rand* has a better exploration capability and *towards-best* improves the exploitation capability. So, to provide a good balance between the exploration and exploitation of search space, for the half population of better solution, calculation of search direction can be done by *towards-rand* and for the rest half of the population, *towards-best* is used to calculate the search direction thereby forcing diversity in the set of better solutions and forcing the inferior solutions to strive for improved fitness.

In *towards-rand*, the search direction, $\bar{z_i}^{(k)}$, for i^{th} solution at k^{th} iteration is calculated using following equation.

$$\bar{z}_i^{(k)} = \bar{x}_{p_i}^{(k)} + \bar{x}_{q_i}^{(k)} - \bar{x}_{r_i}^{(k)} - \bar{x}_i^{(k)}, \tag{3.10}$$

where

p_i, q_i, and r_i are randomly selected indices from among 1 to N such that $p_i \neq q_i \neq r_i \neq i$.

In *towards-best*, the search direction, $\bar{z_i}^{(k)}$, for i^{th} solution at k^{th} iteration is calculated using following equation.

$$\bar{z}_i^{(k)} = \bar{x}_{pbest_i}^{(k)} + \bar{x}_{q_i}^{(k)} - \bar{x}_{r_i}^{(k)} - \bar{x}_i^{(k)}, \tag{3.11}$$

where $x_{pbest_i}^{(k)}$ represents the randomly selected individual from among the top p solutions searched so far.

Here, $\bar{x}_{p_i}$ and $\bar{x}_{pbest_i}$ represent the target points in *towards-rand* and *towards-best* respectively. Difference term $(\bar{x_q} - \bar{x_r})$ is common in both *towards-rand* and *towards-best* which represents $\bar{r}_1 - \bar{r}_2$ (equation 3.9), which is an approximation of distribution of

difference of solutions in a population. In calculation of new search direction, difference term $(\bar{x_q} - \bar{x_r})$ makes the population to evolve maintaining the diversity of solution thereby avoiding convergence to local minima.

Projection matrix, P is a symmetrical matrix which is used for linear transformation from search space to itself such that $P^2 = P$ i.e. whenever P transforms a point twice, it provides the same point. Projection matrix, $P = A' diag(\bar{b_i}) A$, has been used in equation (3.8) to linearly transform $c_i \bar{z_i} + \bar{x_i}$ to generate trial solution $\bar{y_i}$ on the circular (1-spherical) boundary. Here, A and $\bar{b_i}$ are the orthogonal matrix and binary vector respectively. The total number of combinations of possible binary vectors is finite but in case of orthogonal matrix, A, the possible combinations are infinite. Therefore, all the possible projections of $c_i \bar{z_i} + \bar{x_i}$ create a $(D-1)$-spherical boundary on search space.

Method to compute elements of P along with c has been illustrated as follows.

Orthogonal matrix, A

At the start of k^{th} iteration, an orthogonal matrix, A, is generated randomly such that

$$AA' = I. \tag{3.12}$$

Binary diagonal matrix, $diag(\bar{b_i})$

Binary diagonal matrix, $diag(\bar{b_i})$, are calculated randomly in such a way that,

$$0 < \text{rank}(diag(\bar{b_i})) < D \tag{3.13}$$

Step-size control vector, $\bar{c}$

A step-size control vector, $\bar{c}^{(k)} = [c_1^{(k)}, c_2^{(k)}, ...c_N^{(k)}]$, consists of step-size control parameter used for generation of all the possible trial-solutions where $c_i^{(k)}$ represents the step-size control parameter for i^{th} trial-solution at k^{th} iteration.

At the start of k^{th} iteration, the elements of $\bar{c}^{(k)}$ are calculated randomly in range of [0.5 0.7], arrived by experiments.

3.3.3 Selection of New Population for Next Iteration

Greedy selection procedure is applied to select new set of population for next iteration. To update the i^{th} solution of the population, following criteria is applied. If the objective function value of trial solution, $f(\bar{y_i}^{(k)})$, is lower than the objective function value of solution, $f(\bar{x_i}^{(k)})$ then y_i replaces x_i.

Mathematically,

$$\bar{x_i}^{(k+1)} = \begin{cases} \bar{y_i}^{(k)}, & \text{if } f(\bar{y_i}^{(k)}) \leq f(\bar{x_i}^{(k)}) \\ \bar{x_i}^{(k)}, & \text{otherwise} \end{cases} \tag{3.14}$$

3.3.4 Stopping Criteria

Termination of iterations depends upon two criteria: i) the maximum number of function evaluations and ii) convergence of solution i.e solution is not getting updated for specified number of consecutive iterations.

3.3.5 Steps of Spherical Search Algorithm

The main steps of the proposed algorithm are summarized as follows:

- **Step 1:** Initialize the population P.
- **Step 2:** Calculate the objective function of each solution of P.
- **Step 3:** The best solution of population is selected as best solution.
- **Step 4:** Calculate the search direction for each solution of population P.
- **Step 5:** Calculate the orthogonal matrix, A.
- **Step 6:** Calculate parameters: c_i and *rank of projection matrix*.
- **Step 7:** Calculate trial solution for each solution of population P.
- **Step 8:** Update the population using greedy selection operator.
- **Step 9:** If the stopping criterion is satisfied then the algorithm will be stopped, otherwise it will return to **Step 3**.
- **Step 10:** Return the best optimal solutions, after stopping criteria is satisfied.

Table 3.1: Mean and SD of best error value obtained in 51 independent runs by SS, PSO, BB-PSO, CLPSO, APSO, and OLPSO on 30-D CEC2014 problem suite (Mean: Mean of best error, SD: Standard deviation of best error, W: result of Wilcoxon signed rank test).

Nos	SS		PSO			BB-PSO			CLPSO			APSO			OLPSO		
	Mean	**SD**	**Mean**	**SD**	**W**	**Mean**	**SD**	**W**	**Mean**	**SD**	**W**	**Mean**	**SD**	**W**	**Mean**	**SD**	**W**
f01	**8.75E+03**	**6.70E+03**	5.14E+07	2.24E+07	+	2.40E+06	1.97E+06	+	7.82E+06	2.44E+06	+	2.69E+09	3.28E+08	+	6.12E+06	3.58E+06	+
f02	**0.00E+00**	**0.00E+00**	2.42E+08	4.23E+08	+	1.84E+03	7.68E+03	+	8.93E+01	2.33E+02	+	1.02E+11	2.29E+09	+	1.28E+03	1.48E+03	+
f03	**1.03E-07**	**2.81E-07**	5.97E+04	1.07E+04	+	6.23E+03	1.40E+04	+	2.03E+02	1.85E+02	+	1.19E+06	1.25E+06	+	3.23E+02	5.69E+02	+
f04	**0.00E+00**	**0.00E+00**	1.66E+02	8.29E+01	+	5.99E+01	3.45E+01	+	6.92E+01	2.06E+01	+	2.49E+04	1.54E+03	+	8.64E+01	2.22E+01	+
f05	2.09E+01	5.88E-02	2.08E+01	9.01E+01	=	**2.01E+01**	**5.20E-02**	-	2.04E+01	4.13E-02	-	2.13E+01	5.61E-02	+	2.03E+01	1.28E-01	-
f06	**2.79E-01**	**5.86E-01**	2.58E+01	6.40E+01	+	1.17E+01	2.12E+00	+	1.23E+01	1.47E+00	+	4.80E+01	1.79E+00	+	5.09E+00	1.48E+00	+
f07	**0.00E+00**	**0.00E+00**	9.28E+01	1.23E+01	+	2.73E-02	2.71E-02	+	3.43E-06	4.28E-06	+	1.06E+03	3.85E+01	+	1.02E-13	3.47E-14	=
f08	1.59E+02	1.00E+01	5.09E-02	1.11E+00	-	1.02E-03	8.96E-04	-	**0.00E+00**	**0.00E+00**	-	5.03E+02	3.02E+01	+	**0.00E+00**	**0.00E+00**	-
f09	1.61E+02	1.04E+01	3.18E+01	1.28E+02	-	**3.16E+01**	**8.10E+00**	-	5.22E+01	6.38E+00	-	4.78E+02	6.30E+00	+	4.06E+01	7.02E+00	-
f10	6.32E+03	2.55E+02	7.61E+02	7.61E+02	-	1.59E+00	1.42E+00	-	3.11E+00	1.60E+00	-	9.30E+03	5.68E+02	+	**8.72E-02**	**2.04E-01**	-
f11	6.57E+03	3.04E+02	6.83E+03	1.93E+03	+	**2.11E+03**	**4.38E+02**	-	2.33E+03	3.19E+02	-	9.24E+03	4.86E+02	+	2.28E+03	4.66E+02	-
f12	2.29E+00	3.10E-01	2.86E+00	2.77E+01	+	**1.66E-01**	**5.61E-02**	-	3.94E-01	5.53E-02	-	5.91E+00	1.32E+00	+	2.28E-01	6.38E-02	-
f13	2.49E-01	3.21E-02	6.40E-01	4.44E-01	+	**2.38E-01**	**5.24E-02**	=	3.17E-01	3.75E-02	+	1.03E+01	7.53E-01	+	2.59E-01	3.20E-02	+
f14	2.51E-01	3.53E-02	4.21E-01	1.57E-01	+	5.75E-01	2.78E-01	+	2.51E-01	2.85E-02	=	3.95E+02	2.22E+01	+	**2.41E-01**	**2.66E-02**	=
f15	1.39E+01	7.80E-01	**4.47E+00**	**1.92E+00**	-	7.82E+00	3.03E+00	-	7.49E+00	1.02E+00	-	1.05E+06	0.00E+00	+	6.67E+00	1.62E+00	-
f16	1.19E+01	3.28E-01	1.29E+01	4.82E-01	+	**9.13E+00**	**1.08E+00**	-	1.04E+01	3.72E-01	-	1.42E+01	2.37E-01	+	1.17E+01	5.48E-01	=
f17	**4.80E+02**	**2.34E+02**	3.26E+05	2.57E+05	+	6.44E+05	6.17E+05	+	9.59E+05	4.41E+05	+	2.86E+08	1.28E+08	+	7.98E+05	4.13E+05	+
f18	**7.33E+01**	**2.28E+01**	1.02E+06	2.95E+06	+	6.46E+03	8.74E+03	+	1.01E+02	4.67E+01	+	8.75E+09	3.11E+09	+	3.58E+02	5.12E+02	+
f19	**5.37E+00**	**6.72E-01**	2.82E+02	1.98E+01	+	7.43E+00	1.29E+00	+	7.39E+00	6.27E-01	+	8.45E+02	1.15E+02	+	6.13E+00	8.20E-01	+
f20	**5.77E+01**	**2.14E+01**	1.08E+04	2.18E+03	+	3.02E+03	2.91E+03	+	3.14E+03	1.40E+03	+	1.59E+07	1.37E+07	+	5.58E+03	4.01E+03	+
f21	**4.85E+02**	**1.96E+02**	7.54E+05	4.21E+05	+	2.28E+05	3.29E+05	+	8.46E+04	5.35E+04	+	1.33E+08	7.50E+07	+	1.07E+05	8.33E+04	+
f22	2.29E+02	1.06E+02	8.24E+02	5.24E+02	+	2.43E+02	2.10E+02	+	2.08E+02	7.41E+01	+	1.31E+04	9.38E+03	+	**2.20E+02**	**1.07E+02**	=
f23	3.15E+02	6.61E-03	3.42E+02	6.24E+00	+	3.15E+02	1.87E-12	+	3.15E+02	2.02E-06	+	**2.00E+02**	**0.00E+00**	-	3.15E+02	1.23E-10	+
f24	2.21E+02	7.79E+00	2.05E+02	2.41E-01	-	2.28E+02	4.97E+00	+	2.25E+02	4.53E-01	+	**2.00E+02**	**0.00E+00**	-	2.24E+02	5.47E-01	+
f25	2.03E+02	2.74E-01	2.20E+02	4.51E+00	+	2.06E+02	2.27E+00	+	2.08E+02	1.06E+00	+	**2.00E+02**	**0.00E+00**	-	2.09E+02	1.75E+00	+
f26	1.00E+02	3.24E-02	1.00E+02	2.42E-01	=	1.00E+02	5.49E-02	+	1.00E+02	6.42E-02	+	1.86E+02	2.68E+01	+	1.00E+02	4.44E-02	+
f27	3.34E+02	4.34E+01	2.51E+03	4.82E+02	+	6.53E+02	5.06E+01	+	4.14E+02	4.92E+00	=	**2.00E+02**	**0.00E+00**	-	3.26E+02	3.80E+01	=
f28	8.47E+02	9.35E+01	1.81E+03	4.91E+02	+	9.10E+02	2.59E+01	+	9.08E+02	3.97E+01	+	**2.00E+02**	**0.00E+00**	-	8.73E+02	2.97E+01	+
f29	8.24E+02	6.91E+01	8.77E+07	3.24E+07	+	1.70E+06	3.47E+06	+	9.71E+02	9.14E+01	+	**2.00E+02**	**0.00E+00**	-	1.36E+03	2.82E+02	+
f30	1.74E+03	8.95E+02	4.11E+05	1.87E+04	+	7.94E+03	1.07E+03	+	3.39E+03	7.88E+02	+	**2.00E+02**	**0.00E+00**	-	2.39E+03	5.99E+02	+
+/=/-			23/2/5			21/1/8			20/2/8			23/0/7			18/5/7		

3.3.6 Validation of Spherical Search on Benchmark Problems

In this section, to analyze the performance, SS are benchmarked on 30 real-parameter single objective bound-constrained optimization problems used in a special session of IEEE CEC-2014 [122]. Detailed information and characteristics of these problems are available in [122]. To evaluate the performance of SS on the CEC 2014 problem suite, the results are compared with other state-of-the-art algorithms. State-of-the-art algorithms are divided into four groups:

1. *Group-I:-* Variants of PSO: Basic PSO [123], BB-PSO [124], CLPSO [125], APSO [126], OLPSO [127].

2. *Group-II:-* Variants of DE: CoBiDE [128], FCDE [129], RSDE [130], POBLADE [131], DE-best [132].

3. *Group-III:-* Variants of CMA-ES: Basic CMA-ES [133], I-POP-CMAES [134], LS-CMAES [135], CMSAES [136], (1+1)cholesky-CMAES [137].

4. *Group-IV:-* Recently proposed optimization algorithms: GWO [138], GOA [139], MVO [140], SCA [141], SHO [142], SSA [143], SOA [144], WOA [145].

PSO, DE, and CMA-ES are the popular classical Meta-heuristics. Popular variants of classical algorithms are also taken from the literature to show the effectiveness of the SS.

In this experiment, the population size, N, is set to 80, the dimension of search space for all problems, D, is fixed to 30, and allowed maximum function evaluation, MaxFES, is fixed to 300,000 for 51 independent runs. The parameters of other algorithms are set to their default values as reported in their referred paper.

Tables 3.1-3.9 summarize the mean and standard deviation (SD) of the error values obtained by the algorithms over 51 independent runs for each problem. We also performed the Wilcoxon Signed Ranks Test in this experiment. The statistical results are also summarized in Tables 3.1-3.9, where '+' denotes the performance of the SS is better than other algorithms, '-' denotes the performance of other method is better than the SS, and '=' denotes that there is no significant difference in performance. We also rank all algorithms along with the SS using Friedman ranking test based on the mean of error

Table 3.2: Mean and SD of best error value obtained in 51 independent runs by SS, CoBiDE, FCDE, RSDE, POBL_ADE, and DE_best on 30-D CEC2014 problem suite (Mean: Mean of best error, SD: Standard deviation of best error, W: result of Wilcoxon signed rank test).

Nos	SS		CoBiDE			FCDE			RSDE			POBL_ADE			DE_best		
	Mean	SD	Mean	SD	W	Mean	SD	W	Mean	SD	W	Mean	SD	W	Mean	SD	W
f01	8.75E+03	6.70E+03	**3.24E+00**	**3.24E+00**	-	1.05E+05	9.10E+04	+	1.50E+03	1.70E+03	-	1.60E+04	1.22E+04	+	2.46E+07	9.27E+06	+
f02	**0.00E+00**	**0.00E+00**	1.12E-02	5.54E-03	+	**0.00E+00**	**0.00E+00**	=	**1.19E-09**	**5.99E-09**	=	3.14E+02	7.52E+02	+	**0.00E+00**	**0.00E+00**	=
f03	**1.03E-07**	**2.81E-07**	5.17E-07	4.32E-07	=	1.09E+02	4.04E+02	+	4.74E-02	1.16E-01	+	**6.43E-10**	**4.59E-09**	=	3.32E-05	2.00E-05	-
f04	**0.00E+00**	**0.00E+00**	1.85E+01	6.45E-01	+	2.99E+01	3.05E+01	+	3.05E+00	1.34E+01	+	6.34E+01	2.63E+01	+	7.68E+01	2.42E+01	+
f05	2.09E+01	5.88E-02	2.06E+01	5.12E-02	-	2.09E+01	7.67E-02	=	**2.03E+01**	**9.88E-02**	-	2.06E+01	5.11E-02	-	2.09E+01	4.56E-02	=
f06	2.79E-01	5.86E-01	2.74E+01	1.45E+00	+	2.14E+01	3.56E+00	+	5.16E+00	2.01E+00	+	5.19E+00	1.64E+00	+	1.39E+00	1.31E+00	+
f07	**0.00E+00**	**0.00E+00**	6.74E-07	2.39E-06	+	2.79E-02	2.74E-02	+	8.46E-04	1.59E-03	+	2.37E-02	2.31E-02	+	5.46E-03	6.61E-03	+
f08	1.59E+02	1.00E+01	2.81E+01	3.15E+00	-	9.49E+01	2.23E+01	-	**2.04E+01**	**7.04E+00**	-	5.59E+01	1.10E+01	-	8.90E+01	2.22E+01	-
f09	1.61E+02	1.04E+01	1.42E+02	1.35E+01	-	1.35E+02	3.14E+01	-	**5.80E+01**	**1.65E+01**	-	8.46E+01	9.06E+00	-	1.81E+02	1.12E+01	+
f10	6.32E+03	2.55E+02	2.74E+03	1.84E+01	-	2.27E+03	5.35E+02	-	**3.29E+02**	**2.47E+02**	-	2.17E+03	4.92E+02	-	1.71E+03	1.06E+03	-
f11	6.57E+03	3.04E+02	5.68E+03	2.43E+02	-	3.49E+03	6.80E+02	-	**2.74E+03**	**6.44E+02**	-	3.86E+03	3.52E+02	-	6.41E+03	2.93E+02	=
f12	2.29E+00	3.10E-01	1.05E+00	1.56E-01	-	1.37E+00	5.49E-01	-	**4.44E-01**	**1.66E-01**	-	9.51E-01	1.35E-01	-	2.09E+00	2.42E-01	=
f13	**2.49E-01**	**3.21E-02**	4.56E-01	4.52E-02	+	5.68E-01	1.16E-01	+	3.05E-01	5.50E-02	+	2.86E-01	6.10E-02	+	3.79E-01	4.26E-02	+
f14	2.51E-01	3.53E-02	2.65E-01	2.45E-02	+	4.44E-01	2.27E-01	+	2.36E-01	3.37E-02	=	**2.26E-01**	**4.28E-02**	-	3.90E-01	2.08E-01	+
f15	1.39E+01	7.80E-01	1.35E+01	1.24E+00	=	1.54E+01	6.70E+00	+	**5.92E+00**	**2.59E+00**	-	7.73E+00	1.04E+00	-	1.66E+01	1.26E+00	+
f16	1.19E+01	3.28E-01	1.36E+01	1.85E-01	+	1.22E+01	5.74E-01	+	1.06E+01	7.70E-01	=	**1.04E+01**	**4.58E-01**	=	1.22E+01	2.73E-01	+
f17	**4.80E+02**	**2.34E+02**	1.68E+03	1.45E+02	+	6.54E+03	8.72E+03	+	1.24E+03	3.79E+02	+	1.10E+03	4.14E+02	+	7.64E+05	2.61E+05	+
f18	7.33E+01	2.28E+01	**4.69E+01**	**6.34E+00**	-	1.23E+02	6.70E+01	+	9.54E+01	4.34E+01	+	1.10E+02	3.81E+01	+	1.68E+03	1.30E+03	+
f19	**5.37E+00**	**6.72E-01**	1.25E+01	8.54E-01	+	1.32E+01	1.18E+01	+	5.65E+00	1.46E+00	+	8.88E+00	1.21E+01	+	6.29E+00	1.28E+03	+
f20	5.77E+01	2.14E+01	**2.64E+01**	**3.45E+00**	-	1.33E+02	7.99E+01	+	3.73E+01	2.55E+01	-	3.89E+01	2.21E+01	-	1.14E+02	1.65E+01	+
f21	4.85E+02	1.96E+02	7.16E+02	1.45E+02	+	3.01E+03	3.32E+03	+	4.71E+02	2.34E+02	=	**3.86E+02**	**1.91E+02**	-	3.45E+04	1.49E+04	+
f22	2.29E+02	1.06E+02	2.49E+02	7.98E+01	+	4.57E+02	1.68E+02	+	1.91E+02	1.19E+02	-	2.31E+02	8.16E+01	+	**1.55E+02**	**1.10E+02**	-
f23	3.15E+02	6.61E-03	**3.14E+02**	**2.85E-09**	-	3.15E+02	1.24E-12	+	3.15E+02	1.40E-06	+	3.15E+02	5.74E-14	+	3.15E+02	4.02E-13	+
f24	**2.21E+02**	**7.79E+00**	2.43E+02	1.56E+01	+	2.50E+02	6.86E+00	+	2.24E+02	1.65E+00	+	2.22E+02	7.48E+00	+	2.23E+02	7.13E+00	+
f25	2.03E+02	2.74E-01	**2.00E+02**	**6.58E-04**	-	2.07E+02	4.01E+00	+	2.03E+02	1.17E-01	+	2.04E+02	3.22E+00	+	2.09E+02	1.77E+00	+
f26	**1.00E+02**	**3.24E-02**	1.00E+02	4.56E-02	+	1.01E+02	1.20E-01	+	1.00E+02	4.14E-02	+	1.39E+02	4.91E+01	+	1.00E+02	6.13E-02	+
f27	**3.34E+02**	**4.34E+01**	1.10E+03	6.71E+01	+	6.47E+02	2.50E+02	+	4.69E+02	9.46E+01	+	4.21E+02	4.64E+01	+	3.45E+02	4.44E+01	+
f28	8.47E+02	9.35E+01	**3.72E+02**	**6.37E-01**	-	1.60E+03	5.92E+02	+	9.05E+02	1.21E+02	+	9.16E+02	1.63E+02	+	7.74E+02	1.03E+02	-
f29	8.24E+02	6.91E+01	**2.16E+02**	**9.50E+01**	-	7.55E+05	2.62E+06	+	6.52E+05	2.66E+06	+	3.39E+05	2.41E+06	+	3.57E+03	1.97E+03	+
f30	1.74E+03	8.95E+02	7.36E+02	1.02E+02	-	2.98E+03	1.26E+03	+	1.70E+03	8.67E+02	=	1.29E+03	5.14E+02	-	2.24E+03	6.54E+02	+
+/=/-			14/2/14			23/2/5			15/5/10			19/2/9			21/4/5		

values obtained by the algorithms over 51 independent runs. The statistical results of the Friedman test are reported in Table 3.10.

1. *SS vs Group-I's algorithms:* Table 3.1 summarizes the results obtained by algorithms SS, and Group-I's algorithms: PSO, BB-PSO, CLPSO, APSO, and OLPSO on the CEC-2014 problem suite. It is seen from Table 3.1 that the SS is showing better performance than PSO, BB-PSO, CLPSO, APSO and OLPSO on 23, 21, 20, 23, and 18 problems out of 30, respectively, performance of SS worse than PSO, BB-PSO, CLPSO, APSO and OLPSO on five, eight, eight, seven, and seven problems respectively, and SS is significantly equal to the PSO, BB-PSO, CLPSO, and OLPSO for 2, 1, 2, and 5 problems of CEC-2014 problem suite respectively.

2. *SS vs Group-II's algorithms:* Table 3.2 summarizes the results of the algorithms SS, and Group-II's algorithms: CoBiDE, FCDE, RSDE, POBL_ADE, and DE_best. As shown in Table 3.2, SS have better performance than CoBiDE, FCDE, RSDE, POBL_ADE, and DE_best on 14, 23, 15, 19, and 21 problems out of 30 respectively, performance of SS worse than CoBiDE, FCDE, RSDE, POBL_ADE, and DE_best on 14, five, 10, nine, and five problems respectively, and SS provides performance similar to the CoBiDE, FCDE, RSDE, POBL_ADE, and DE_best for two, two, five, two and seven problems of CEC-2014 problem suite respectively.

3. *SS vs Group-III's algorithms:* Table 3.3 presents the results of the algorithms SS, and Group-III's algorithms: CMA-ES, I-POP-CMAES, LS-CMAES, CMSAES, and (1+1)cholesky-CMAES. when examined the last column of Table 3.3, SS shows better performs then CMA-ES, I-POP-CMAES, LS-CMAES, CMSAES, and (1+1)Cholesky-CMAES on 25, 18, 22, 30, and 23 problems out of 30 respectively, performance of SSO worse than CMA-ES, I-POP-CMAES, LS-CMAES, and (1+1)Cholesky-CMAES on five, nine, eight, and six problems respectively, and SSO is significantly similar to the I-POP-CMAES, and (1+1)Cholesky-CMAES for three, and one problems of CEC-2014 problem suite respectively.

4. *SS vs Group-IV's algorithms:* In Tables 3.4 and 3.9, the outcomes of SS and Group-IV's algorithms are presented. The last rows of Tables 3.4 and 3.9 summarizes the results of WT. It is seen from Tables 3.4 and 3.9 that the performance of SS is

Table 3.3: Mean and SD of best error value obtained in 51 independent runs by SS, CMA-ES, I-POP-CMAES, LS-CMAES, CMSAES, and (1+1)cholesky_CMAES on 30-D CEC2014 problem suite (Mean: Mean of best error, SD: Standard deviation of best error, W: result of Wilcoxon signed rank test).

Nos	SS		CMA-ES			I-POP-CMAES			LS-CMAES			CMSAES			(1+1)cholesky CMAES		
	Mean	SD	Mean	SD	W	Mean	SD	W	Mean	SD	W	Mean	SD	W	Mean	SD	W
f01	8.75E+03	6.70E+03	8.16E+04	2.66E+04	+	**0.00E+00**	**0.00E+00**	-	2.54E+08	1.37E+08	+	7.56E+08	1.40E+08	+	**0.00E+00**	**0.00E+00**	-
f02	**0.00E+00**	**0.00E+00**	4.59E+10	9.72E+09	+	**0.00E+00**	**0.00E+00**	=	6.98E+04	3.25E+04	+	6.85E+10	5.93E+09	+	**0.00E+00**	**0.00E+00**	=
f03	1.03E-07	2.81E-07	2.96E+03	1.29E+03	+	**0.00E+00**	**0.00E+00**	-	2.15E-02	1.90E-02	+	1.26E+05	1.75E+04	+	**0.00E+00**	**0.00E+00**	-
f04	**0.00E+00**	**0.00E+00**	4.71E+03	1.33E+03	+	**0.00E+00**	**0.00E+00**	=	5.50E+00	1.62E+01	+	1.01E+04	1.63E+03	+	1.27E+00	9.10E+00	+
f05	2.09E+01	5.88E-02	**2.00E+01**	**3.70E-04**	-	2.11E+01	7.69E-02	+	2.01E+01	2.18E-01	-	2.10E+01	4.38E-02	+	2.00E+01	5.85E-03	-
f06	**2.79E-01**	**5.86E-01**	6.50E+01	1.57E+00	+	9.48E+00	7.65E+00	+	2.47E+01	3.55E+00	+	3.95E+01	1.04E+00	+	5.02E+01	4.68E+00	+
f07	**0.00E+00**	**0.00E+00**	1.12E+02	1.16E+01	+	**0.00E+00**	**0.00E+00**	=	4.45E-02	1.90E-02	+	6.01E+02	5.27E+01	+	1.11E-02	9.66E-03	+
f08	1.59E+02	1.00E+01	8.98E+02	1.83E+02	+	**1.25E+02**	**1.20E+02**	-	3.41E+02	1.02E+02	+	3.67E+02	1.66E+01	+	4.38E+02	7.76E+01	+
f09	1.61E+02	1.04E+01	9.14E+02	4.24E+00	+	**3.70E+01**	**6.27E+01**	-	3.85E+02	1.84E+02	+	4.31E+02	2.35E+01	+	6.14E+02	1.37E+02	+
f10	6.32E+03	2.55E+02	**1.09E+03**	**5.78E+02**	-	3.47E+03	2.02E+03	-	3.81E+03	5.94E+02	-	7.28E+03	2.80E+02	+	4.96E+03	7.40E+02	-
f11	6.57E+03	3.04E+02	**2.16E+02**	**1.11E+02**	-	2.74E+03	2.92E+03	-	3.38E+03	5.21E+02	-	7.19E+03	2.31E+02	+	5.19E+03	8.58E+02	-
f12	2.29E+00	3.10E-01	**1.20E-01**	**1.16E+00**	-	4.39E+00	1.18E+00	+	2.16E-01	5.88E-02	-	2.29E+00	2.91E-01	+	1.47E+00	7.07E-01	-
f13	**2.49E-01**	**3.21E-02**	1.31E+00	1.70E-01	+	4.67E-01	6.16E-01	+	3.38E-01	4.88E-02	+	6.61E+00	4.79E-01	+	5.86E-01	1.44E-01	+
f14	2.51E-01	3.53E-02	1.57E+01	4.61E+00	+	8.89E-01	2.34E+00	+	**1.79E-01**	**3.12E-02**	-	2.01E+02	2.24E+01	+	4.21E-01	2.12E-01	+
f15	1.39E+01	7.80E-01	1.51E+03	1.48E+00	+	2.95E+05	2.04E+06	+	**8.21E+00**	**1.97E+00**	-	1.30E+06	4.74E+05	+	2.70E+01	1.34E+01	+
f16	1.19E+01	3.28E-01	1.62E+01	6.85E+00	+	**1.09E+01**	**1.99E+00**	-	1.28E+01	4.30E-01	+	1.31E+01	1.79E-01	+	1.43E+01	3.80E-01	+
f17	**4.80E+02**	**2.34E+02**	4.42E+03	9.19E+02	+	5.35E+06	2.59E+07	+	6.98E+04	3.19E+05	+	2.25E+07	8.63E+06	+	1.77E+03	3.91E+02	+
f18	**7.33E+01**	**2.28E+01**	2.50E+03	2.66E+02	+	7.94E+02	3.68E+03	+	4.47E+04	3.15E+05	+	9.95E+08	3.53E+08	+	1.43E+02	4.82E+01	+
f19	**5.37E+00**	**6.72E-01**	2.04E+02	2.19E+01	+	3.68E+01	1.01E+02	+	9.82E+00	1.42E+00	+	2.78E+02	3.94E+01	+	3.42E+01	4.02E+01	+
f20	**5.77E+01**	**2.14E+01**	2.76E+03	2.45E+02	+	1.92E+03	9.92E+03	+	5.40E+02	3.42E+02	+	9.63E+04	3.81E+04	+	3.84E+02	1.24E+02	+
f21	**4.85E+02**	**1.96E+02**	3.53E+03	1.22E+03	+	1.81E+06	1.24E+07	+	4.35E+04	2.65E+05	+	5.48E+06	2.46E+06	+	1.15E+03	3.80E+02	+
f22	2.29E+02	1.06E+02	5.17E+03	1.94E+02	+	**2.19E+02**	**1.00E+02**	-	4.98E+02	1.41E+02	+	1.43E+03	1.85E+02	+	8.63E+02	3.30E+02	+
f23	3.15E+02	6.61E-03	**2.81E+02**	**1.43E+01**	-	3.15E+02	2.30E-13	+	3.14E+02	8.99E+00	-	7.45E+02	7.97E+01	+	3.15E+02	4.09E-08	+
f24	2.21E+02	7.79E+00	2.76E+02	1.22E-01	+	2.28E+02	1.47E+01	+	**2.16E+02**	**2.32E+01**	-	4.06E+02	1.29E+01	+	4.78E+02	3.61E+02	+
f25	**2.03E+02**	**2.74E-01**	2.09E+02	9.14E+00	+	2.05E+02	3.61E+00	+	2.07E+02	9.31E+00	+	2.63E+02	7.69E+00	+	2.26E+02	1.61E+01	+
f26	**1.00E+02**	**3.24E-02**	2.75E+02	4.28E+01	+	1.24E+02	6.59E+01	+	1.00E+02	9.08E-02	+	1.06E+02	6.60E-01	+	1.93E+02	1.73E+02	+
f27	3.34E+02	4.34E+01	4.50E+03	8.76E+02	+	**3.02E+02**	**2.40E+00**	-	4.19E+02	1.40E+02	+	8.82E+02	8.61E+01	+	9.03E+02	4.26E+02	+
f28	**8.47E+02**	**9.35E+01**	5.98E+03	1.36E+02	+	9.72E+02	2.01E+02	+	2.54E+03	9.65E+02	+	3.58E+03	5.23E+02	+	7.88E+03	3.12E+03	+
f29	**8.24E+02**	**6.91E+01**	1.27E+07	6.28E+06	+	2.42E+05	1.71E+06	+	3.59E+03	2.89E+03	+	8.34E+07	3.53E+07	+	4.19E+06	1.17E+07	+
f30	**1.74E+03**	**8.95E+02**	7.18E+05	2.96E+05	+	4.92E+04	2.35E+05	+	7.65E+03	3.29E+03	+	8.96E+05	2.79E+05	+	4.36E+03	1.62E+03	+
+/=/-			25/0/5			18/3/9			22/0/8			30/0/0			23/1/6		

better than GWO, GOA, MVO, SCA, SHO, SSA, SOA, and WOA on 22, 28, 21, 23, 22, 21, 21, and 23 out of 30 problems, respectively. The performance of SS is outperformed by GWO, GOA, MVO, SCA, SHO, SSA, SOA, and WOA on seven, zero, eight, three, six, eight, seven, and seven out of 30 problems , respectively.

In addition, the Friedman Test (FT) is also used to detect the significant differences between SS and the other 23 algorithms on all 30 problems of CEC-2014 problem suite. The detailed results of the FT for all 24 algorithms are shown in Table 3.10. From Table 3.10, it can be found that SS is ranked first by FT among all 24 algorithms. Variants of PSO: BB-PSO, CLPSO, OLPSO, and Variants of DE: CoBiDE, RSDE, POBL-ADE, and DE-best are very competitive with the SS but the performance of SS is slightly better than them. Similarly, variants of CMA-ES: I-POP-CMAES and LS-CMAES are also well performed on the CEC-2014 problem suite, but they could not outperforms the performance of SS. In the case of recently proposed algorithms, MVO, SOA, WOA, SSA, and GWO perform very well, but the performance of SS is significantly better than them. Compared with the rest of other algorithms, SS is significantly outperformed them.

3.3.7 Application of SS Algorithm for Initial Seed for Power Flow

SS Algorithm can be utilized (by minimizing the objective function described in Equation 3.3) to calculate the initial seed for conventional PF algorithm. In ill-conditioned test systems or heavily loaded systems, the steady-state PF solution is far from flat start. Consequently, the conventional algorithms diverges or converges at a very low rate on these problems because of flat start.

In this section, SS algorithm is used to calculate the initial seed for conventional NR algorithm. This approach is named as Spherical Search with Three Phase Current Injection Method (SSTCIM) for further reference. Test systems and algorithms described in Chapter 2 are considered for analyzing the performance of SSTCIM.

Validation of Algorithm

CASE25 is considered to validate the accuracy of the algorithm. The loading condition of this test system is increased to a level (700%) where TCIM diverges.

Table 3.4: Mean and SD of best error value obtained in 51 independent runs by SS, GWO, GOA, MVO, and SCA on 30-D CEC2014 problem suite (Mean: Mean of best error, SD: Standard deviation of best error, W: result of Wilcoxon signed rank test).

Nos	SS		GWO			GOA			MVO			SCA		
	Mean	**STD**	**Mean**	**STD**	**WT**	**Mean**	**STD**	**WT**	**Mean**	**STD**	**WT**	**Mean**	**STD**	**WT**
1	**8.75E+03**	**6.70E+03**	4.22E+07	2.57E+07	+	1.99E+09	1.73E+09	+	1.96E+07	2.54E+07	+	1.58E+08	1.06E+08	+
2	**0.00E+00**	**0.00E+00**	1.06E+09	1.33E+09	+	8.13E+10	6.70E+10	+	4.58E+08	1.17E+09	+	1.01E+10	7.71E+09	+
3	**1.03E-07**	**2.81E-07**	2.52E+04	8.00E+03	+	1.30E+06	2.57E+06	+	9.61E+03	1.27E+04	+	3.16E+04	8.77E+03	+
4	**0.00E+00**	**0.00E+00**	1.85E+02	4.27E+01	+	2.36E+04	2.00E+04	+	1.29E+02	5.98E+01	+	6.69E+02	4.17E+02	+
5	2.09E+01	5.88E-02	2.09E+01	5.92E-02	=	2.12E+01	2.13E-01	+	2.04E+01	4.35E-01	-	2.09E+01	5.67E-02	=
6	**2.79E-01**	**5.86E-01**	1.20E+01	3.08E+00	+	3.37E+01	1.81E+01	+	1.01E+01	2.95E+00	+	2.48E+01	1.09E+01	+
7	**0.00E+00**	**0.00E+00**	7.62E+00	4.23E+00	+	7.56E+02	6.17E+02	+	3.03E+00	4.57E+00	+	8.74E+01	6.84E+01	+
8	1.59E+02	1.00E+01	**6.81E+01**	**1.99E+01**	-	3.21E+02	2.08E+02	+	7.07E+01	2.05E+01	-	1.69E+02	8.60E+01	=
9	1.61E+02	1.04E+01	**8.77E+01**	**2.62E+01**	-	4.11E+02	2.58E+02	+	9.17E+01	2.79E+01	-	2.04E+02	9.14E+01	+
10	6.32E+03	2.55E+02	1.90E+03	5.38E+02	-	6.43E+03	3.73E+03	=	2.33E+03	6.69E+02	-	4.31E+03	2.05E+03	-
11	6.57E+03	3.04E+02	**2.60E+03**	**6.05E+02**	-	6.68E+03	3.37E+03	=	2.79E+03	6.06E+02	-	5.20E+03	2.18E+03	-
12	2.29E+00	3.10E-01	1.70E+00	1.12E+00	-	4.55E+00	2.44E+00	+	**8.37E-01**	**1.06E+00**	-	2.21E+00	8.28E-01	=
13	**2.49E-01**	**3.21E-02**	3.55E-01	8.61E-02	+	6.62E+00	5.12E+00	+	4.03E-01	8.31E-02	+	1.89E+00	1.24E+00	+
14	**2.51E-01**	**3.53E-02**	5.76E-01	5.66E-01	+	2.46E+02	2.05E+02	+	5.08E-01	2.95E-01	+	2.70E+01	2.24E+01	+
15	1.39E+01	7.80E-01	6.22E+01	2.75E+02	+	1.16E+07	1.24E+07	+	**1.09E+01**	**7.81E+00**	-	1.86E+03	2.69E+03	+
16	1.19E+01	3.28E-01	1.07E+01	7.17E-01	-	1.29E+01	1.81E+00	+	1.12E+01	7.05E-01	-	1.19E+01	1.11E+00	=
17	**4.80E+02**	**2.34E+02**	1.06E+06	1.35E+06	+	1.91E+08	1.99E+08	+	4.33E+05	6.98E+05	+	4.22E+06	3.53E+06	+
18	**7.33E+01**	**2.28E+01**	5.69E+06	1.70E+07	+	5.34E+09	4.89E+09	+	1.42E+06	7.13E+06	+	8.57E+07	8.46E+07	+
19	**5.37E+00**	**6.72E-01**	2.59E+01	1.76E+01	+	6.81E+02	6.08E+02	+	1.74E+01	1.47E+01	+	6.19E+01	3.52E+01	+
20	**5.77E+01**	**2.14E+01**	1.28E+04	8.64E+03	+	9.40E+06	1.70E+07	+	5.95E+03	8.75E+03	+	1.34E+04	5.86E+03	+
21	**4.85E+02**	**1.96E+02**	5.42E+05	1.16E+06	+	9.40E+07	9.20E+07	+	2.85E+05	8.76E+05	+	1.14E+06	1.11E+06	+
22	2.29E+02	1.06E+02	3.79E+02	1.87E+02	+	1.34E+04	2.32E+04	+	3.65E+02	1.47E+02	+	6.32E+02	2.64E+02	+
23	3.15E+02	6.61E-03	3.27E+02	4.28E+00	+	1.28E+03	8.31E+02	+	3.20E+02	5.67E+00	+	3.54E+02	2.64E+01	+
24	2.21E+02	7.79E+00	**2.00E+02**	**1.01E-03**	-	4.04E+02	1.67E+02	+	2.15E+02	1.49E+01	=	2.00E+02	2.69E-01	-
25	**2.03E+02**	**2.74E-01**	2.10E+02	3.07E+00	+	3.34E+02	1.07E+02	+	2.07E+02	3.24E+00	+	2.20E+02	1.01E+01	+
26	**1.00E+02**	**3.24E-02**	1.16E+02	3.66E+01	+	2.42E+02	1.35E+02	+	1.16E+02	3.66E+01	+	1.11E+02	2.96E+01	+
27	**3.34E+02**	**4.34E+01**	5.83E+02	1.16E+02	+	1.33E+03	6.36E+02	+	5.41E+02	1.24E+02	+	6.65E+02	2.52E+02	+
28	**8.47E+02**	**9.35E+01**	9.61E+02	1.47E+02	+	5.30E+03	3.58E+03	+	9.97E+02	2.04E+02	+	1.58E+03	6.04E+02	+
29	**8.24E+02**	**6.91E+01**	8.97E+04	1.91E+05	+	4.89E+08	4.37E+08	+	9.42E+05	3.12E+06	+	8.13E+06	8.72E+06	+
30	**1.74E+03**	**8.95E+02**	2.95E+04	2.16E+04	+	6.43E+06	6.54E+06	+	1.54E+04	1.80E+04	+	1.57E+05	1.18E+05	+
+/-/=			22/1/7			28/2/0			21/1/8			23/4/2		

Table 3.5: Initial seed obtained by SS for CASE25 test system

Bus	$\lvert V_a \rvert$	$\angle_a$	$\lvert V_b \rvert$	$\angle_b$	$\lvert V_c \rvert$	$\angle_c$
1	1.0000	0.0000	1.0000	-120.0000	1.0000	120.0000
2	0.9627	-0.2581	0.9634	-120.2113	0.9617	119.7596
3	0.9510	-0.2880	0.9503	-120.2504	0.9503	119.7224
4	0.9454	-0.2769	0.9440	-120.2889	0.9454	119.7125
5	0.9440	-0.2422	0.9421	-120.2575	0.9440	119.7595
6	0.9492	-0.1879	0.9519	-120.1742	0.9465	119.8961
7	0.9382	-0.1416	0.9430	-120.1587	0.9333	119.9966
8	0.9468	-0.1644	0.9495	-120.1403	0.9443	119.9356
9	0.9346	-0.1146	0.9402	-120.1761	0.9285	120.0467
10	0.9328	-0.0914	0.9384	-120.2034	0.9250	120.0902
11	0.9318	-0.0814	0.9375	-120.2194	0.9235	120.1141
12	0.9311	-0.0763	0.9364	-120.2247	0.9225	120.1296
13	0.9318	-0.0741	0.9371	-120.2304	0.9230	120.1223
14	0.9298	-0.1317	0.9356	-120.1310	0.9243	120.0071
15	0.9258	-0.1250	0.9319	-120.1207	0.9207	120.0080
16	0.9374	-0.1362	0.9425	-120.1518	0.9323	120.0185
17	0.9291	-0.1279	0.9354	-120.1407	0.9232	120.0141
18	0.9413	-0.1632	0.9397	-120.0547	0.9404	119.9511
19	0.9326	-0.0640	0.9318	-119.9427	0.9327	120.1612
20	0.9370	-0.1131	0.9355	-119.9851	0.9363	120.0538
21	0.9355	-0.0805	0.9325	-119.9294	0.9336	120.1154
22	0.9322	-0.0403	0.9277	-119.8592	0.9299	120.2074
23	0.9405	-0.1736	0.9386	-120.2086	0.9409	119.8227
24	0.9377	-0.1045	0.9352	-120.1619	0.9380	119.9003
25	0.9340	-0.0334	0.9318	-120.1282	0.9346	119.9908

Table 3.6: Power Flow solution obtained using SSTCIM for CASE25 test system

Bus	$\|V_a\|$	$\angle_a$	$\|V_b\|$	$\angle_b$	$\|V_c\|$	$\angle_c$
1	1.0000	0.0000	1.0000	-120.0000	1.0000	120.0000
2	0.9227	-1.4532	0.9262	-121.0821	0.9378	118.3006
3	0.9051	-1.8118	0.9096	-121.3556	0.9240	117.8898
4	0.8964	-1.9860	0.9017	-121.5027	0.9179	117.7016
5	0.8937	-1.9832	0.8992	-121.4928	0.9156	117.6988
6	0.8827	-1.4361	0.8865	-120.9406	0.9020	118.2451
7	0.8481	-1.4268	0.8523	-120.7969	0.8704	118.1928
8	0.8773	-1.4304	0.8813	-120.9200	0.8972	118.2392
9	0.8321	-1.4260	0.8361	-120.7363	0.8563	118.1686
10	0.8204	-1.4268	0.8234	-120.6928	0.8453	118.1519
11	0.8148	-1.4282	0.8175	-120.6759	0.8403	118.1495
12	0.8121	-1.4243	0.8142	-120.6664	0.8376	118.1635
13	0.8129	-1.4239	0.8150	-120.6730	0.8382	118.1554
14	0.8324	-1.4208	0.8371	-120.7164	0.8553	118.1648
15	0.8266	-1.4144	0.8316	-120.6936	0.8503	118.1588
16	0.8453	-1.4237	0.8496	-120.7859	0.8679	118.1898
17	0.8292	-1.4124	0.8344	-120.7105	0.8518	118.1695
18	0.8902	-1.8089	0.8950	-121.3038	0.9103	117.8768
19	0.8777	-1.7954	0.8844	-121.2805	0.8995	117.9027
20	0.8838	-1.8098	0.8893	-121.2838	0.9045	117.8736
21	0.8812	-1.7924	0.8855	-121.2807	0.9008	117.9060
22	0.8763	-1.7857	0.8794	-121.2644	0.8958	117.9301
23	0.8880	-1.9842	0.8945	-121.4938	0.9115	117.6906
24	0.8829	-1.9836	0.8898	-121.4983	0.9073	117.6852
25	0.8768	-1.9690	0.8852	-121.5176	0.9025	117.6946

The obtained initial seed using SS is reported in Table 3.5. TCIM algorithm uses this initial seed to solve the PF problem of CASE25. Consequently, TCIM converges within 4 iterations. The obtained PF solution is reported in Table 3.6.

From the outcomes, it can be concluded that the proposed approach improves the performance of conventional algorithms. For further analysis, this approach is also analyzed on the test systems with different loading condition with different R/X ratio of lines.

Test systems with high loading conditions

In this section, the stability of the proposed approach is evaluated on various test systems with different loading conditions. The loading level at the buses of the different test systems is gradually increased to their maximum loading limit. Two test systems, CASE37

Table 3.7: Total Number of iterations required for different Power Flow algorithms in heavily loaded ill-conditioned systems.(LF: Loading Factor, NC: Not Converged)

CASE37						
LF(%)	CINR	LMPF	RK4PF	SSTCIM	TCIM	iTCIM
200	2	3	16	3	3	3
600	2	3	17	3	3	3
1000	2	3	18	3	3	3
1400	3	4	18	3	4	4
1800	4	21	59	4	NC	NC
2200	4	24	87	4	NC	NC
2400	NC	26	88	4	NC	NC
2500	NC	37	91	4	NC	NC

CASE84						
LF(%)	CINR	LMPF	RK4PF	SSTCIM	TCIM	iTCIM
100	3	2	26	3	6	4
200	4	4	28	3	13	7
300	6	5	29	3	20	9
400	9	6	29	3	33	11
500	17	9	29	4	69	15
600	NC	40	43	4	NC	NC
700	99	38	63	4	NC	NC
800	31	35	87	4	NC	NC

and CASE84, are considered for this analysis. A total number of iterations required by different algorithms for CASE37 and CASE84 are reported in Table 3.7.

It is observed from this table that the proposed approach improves the performance of TCIM. In CASE37, the performance of SSTCIM is better or at least competitive with the algorithms discussed in chapter 2.

Test systems with high R/X ratio

The sensitivity of the proposed approach is validated for different R/X ratios of the lines of test systems and the performance of the proposed approach is compared with other algorithms. In this study, CASE37 and CASE84 are considered with different R/X ratios.

Number of iterations required to converge by proposed algorithms with other algorithms are reported in Table 3.8. It can be observed that the proposed approach improves the performance of TCIM.

Table 3.8: Total Number of iterations required for different Power Flow algorithms in ill-conditioned systems with high R/X ratios.(NC: Not Converged)

CASE37						
R/X	CINR	LMPF	RK4PF	SSTCIM	TCIM	iTCIM
2	2	3	15	3	3	3
6	2	4	15	3	3	3
10	2	5	15	3	3	3
14	3	6	15	4	4	4
18	3	18	50	4	NC	NC
22	3	29	77	4	NC	NC
24	4	22	78	4	NC	NC
25	8	38	77	4	NC	NC

CASE84						
R/X	CINR	LMPF	RK4PF	SSTCIM	TCIM	iTCIM
1	3	2	26	3	6	4
4	4	4	28	3	14	6
7	5	5	27	4	26	8
10	6	7	27	4	48	10
13	16	16	27	3	NC	20
14	21	43	59	4	NC	NC
15	21	57	87	4	NC	NC
16	21	39	94	4	NC	NC

3.4 Butterfly Constrained Optimizer

BCO is a dual population based method for solving constrained optimization problems. BCO uses υ-Constrained method for handling constraints of the problem. In this section, details of different processes of BCO are described. Afterwards, the complete process of BCO is presented.

3.4.1 Dual-population of BCO

In BCO, there are two populations based on their feasibility. First population, Type-I, contains solutions to minimize the constraint violation and second population, Type-II, contains solution to minimize the constraint violation and optimize the objective function value. Type-I population is defined as a N, D-dimensional vector. If k denotes the iteration, the type-I population, P_1, at k^{th} iteration consist of :

$$P_1^k = [\bar{x}_1^k, \bar{x}_2^k ....\bar{x}_N^k] \tag{3.15}$$

$$\bar{x}_i^k = [x_{i1}^k, x_{i2}^k, x_{i3}^k ....x_{iD}^k]^T, i = 1, 2, ...N \tag{3.16}$$

The Type-II population is defined as N, D-dimensional vector. If k denotes the iteration, the Type-II population, P_2 at k^{th} iteration consist of :

$$P_2^k = [\bar{mx}_1^k, \bar{mx}_2^k ....\bar{mx}_N^k] \tag{3.17}$$

$$\bar{mx}_i^k = [mx_{i1}^k, mx_{i2}^k, mx_{i3}^k ....mx_{iD}^k]^T, i = 1, 2, ...N \tag{3.18}$$

where N is the size of population.

The idea behind the BCO is to take advantage of perching and patrolling modes to search new solution for each $\bar{x}_i^k$ and $\bar{mx}_i^k$. The set of solution $\bar{mx}_i^k$ and $\bar{x}_i^k$ is associated with i^{th} individual at k^{th} iteration. Initial dual solutions of each individual are randomly generated with in the search space. At every iteration, before perching or patrolling, a cris-cross neighbor vector $\bar{cc}$ of length N is calculated by reshuffling the integers from 1 to N. The vector $\bar{cc}$ consists of :

$$\bar{cc} = \{cc_1, cc_2, ...cc_i\}, i = 1, 2, N \tag{3.19}$$

Table 3.9: Mean and SD of best error value obtained in 51 independent runs by SS, SHO, SSA, SOA, and WOA on 30-D CEC2014 problem suite (Mean: Mean of best error, SD: Standard deviation of best error, W: result of Wilcoxon signed rank test).

Nos	SS		SHO			SSA			SOA			WOA		
	Mean	STD	Mean	STD	WT	Mean	STD	WT	Mean	STD	WT	Mean	STD	WT
1	**8.75E+03**	**6.70E+03**	1.80E+07	2.65E+07	+	1.94E+07	2.56E+07	+	5.58E+07	1.15E+07	+	1.97E+07	1.81E+07	+
2	**0.00E+00**	**0.00E+00**	4.58E+08	1.17E+09	+	4.58E+08	1.17E+09	+	1.21E+08	1.36E+06	+	1.26E+08	1.20E+07	+
3	**1.03E-07**	**2.81E-07**	9.99E+03	1.24E+04	+	1.15E+04	1.13E+04	+	4.04E+04	1.35E+03	+	1.87E+04	2.03E+04	+
4	**0.00E+00**	**0.00E+00**	1.19E+02	6.55E+01	+	1.34E+02	5.71E+01	+	1.58E+02	4.68E-01	+	1.19E+02	5.68E+01	+
5	2.09E+01	5.88E-02	2.04E+01	4.58E-01	-	**2.04E+01**	**4.28E-01**	-	2.09E+01	3.12E-02	=	2.09E+01	7.09E-02	-
6	**2.79E-01**	**5.86E-01**	2.20E+01	8.92E+00	+	1.63E+01	5.97E+00	+	1.24E+01	2.27E-02	+	1.74E+01	3.35E+00	+
7	**0.00E+00**	**0.00E+00**	3.00E+00	4.59E+00	+	2.99E+00	4.60E+00	+	7.65E+00	1.50E-02	+	1.88E+00	2.68E-02	+
8	1.59E+02	1.00E+01	8.80E+01	2.32E+01	-	9.90E+01	3.48E+01	-	8.16E+01	4.92E-01	-	1.48E+00	2.31E-01	-
9	1.61E+02	1.04E+01	1.25E+02	3.56E+01	-	1.13E+02	3.88E+01	-	8.68E+01	5.12E-01	-	9.63E+01	2.40E+01	-
10	6.32E+03	2.55E+02	1.98E+03	5.42E+02	-	2.99E+03	1.09E+03	-	2.08E+03	2.65E+00	-	**1.34E+03**	**5.27E+02**	-
11	6.57E+03	3.04E+02	3.37E+03	9.00E+02	-	3.34E+03	8.63E+02	-	2.11E+03	5.12E+00	-	2.46E+03	4.95E+02	-
12	2.29E+00	3.10E-01	1.05E+00	9.54E-01	-	1.02E+00	9.93E-01	-	1.54E-01	1.94E-03	-	1.56E-01	4.62E-02	-
13	**2.49E-01**	**3.21E-02**	4.38E-01	1.17E-01	+	4.51E-01	1.23E-01	+	4.44E-01	9.16E-03	+	5.33E-01	1.27E-01	+
14	**2.51E-01**	**3.53E-02**	3.88E-01	2.16E-01	+	4.49E-01	2.52E-01	+	7.34E-01	4.21E-02	+	3.37E-01	1.03E-01	+
15	1.39E+01	7.80E-01	3.47E+01	1.92E+01	+	1.12E+01	7.76E+00	-	1.91E+01	1.02E-01	+	1.75E+01	1.02E+01	+
16	1.19E+01	3.28E-01	1.18E+01	1.02E+00	=	1.14E+01	8.39E-01	-	**1.06E+01**	**1.57E-03**	-	1.12E+01	6.77E-01	-
17	**4.80E+02**	**2.34E+02**	4.17E+05	7.01E+05	+	4.76E+05	6.84E+05	+	6.52E+05	8.23E+04	+	1.34E+06	2.13E+06	+
18	**7.33E+01**	**2.28E+01**	1.41E+06	7.13E+06	+	1.42E+06	7.13E+06	+	1.23E+04	3.84E+01	+	1.99E+03	3.70E+03	+
19	**5.37E+00**	**6.72E-01**	2.18E+01	1.69E+01	+	1.92E+01	1.38E+01	+	1.23E+01	5.87E-03	+	2.67E+01	3.44E+01	+
20	**5.77E+01**	**2.14E+01**	8.22E+03	7.59E+03	+	6.09E+03	8.66E+03	+	8.75E+03	5.84E+01	+	5.84E+03	1.93E+00	+
21	**4.85E+02**	**1.96E+02**	2.81E+05	8.78E+05	+	3.00E+05	8.74E+05	+	6.95E+05	2.15E+04	+	8.60E+05	7.85E+05	+
22	2.29E+02	1.06E+02	5.73E+02	2.48E+02	+	3.91E+02	1.62E+02	+	3.65E+02	2.56E+01	+	5.69E+02	2.06E+02	+
23	3.15E+02	6.61E-03	3.19E+02	5.88E+00	+	3.20E+02	5.67E+00	+	3.54E+02	1.15E-01	+	3.16E+02	1.01E+00	+
24	2.21E+02	7.79E+00	2.17E+02	1.38E+01	=	2.17E+02	1.55E+01	=	**2.00E+02**	**2.34E-04**	-	2.15E+02	5.15E+00	+
25	**2.03E+02**	**2.74E-01**	2.11E+02	3.43E+00	+	2.11E+02	3.70E+00	+	2.09E+02	5.96E-03	+	2.11E+02	4.59E+00	+
26	**1.00E+02**	**3.24E-02**	1.49E+02	4.93E+01	+	1.10E+02	2.99E+01	+	1.00E+02	2.02E-02	=	1.51E+02	5.13E+01	+
27	**3.34E+02**	**4.34E+01**	7.31E+02	3.32E+02	+	6.40E+02	1.53E+02	+	5.62E+02	1.04E+00	+	7.62E+02	1.98E+02	+
28	**8.47E+02**	**9.35E+01**	2.53E+03	1.47E+03	+	9.85E+02	1.41E+02	+	1.72E+03	4.63E-01	+	1.51E+03	4.53E+02	+
29	**8.24E+02**	**6.91E+01**	5.78E+05	2.14E+06	+	1.05E+06	3.49E+06	+	9.68E+03	1.43E+01	+	8.68E+05	2.67E+06	+
30	**1.74E+03**	**8.95E+02**	1.34E+04	1.90E+04	+	1.77E+04	1.73E+04	+	3.16E+04	6.56E+02	+	1.38E+04	1.98E+02	+
+/-/=			22/2/6			21/1/8			21/2/7			23/0/7		

Table 3.10: Ranking of Algorithm according to Friedman ranking based on mean error value. (FR: Friedman Ranking)

S.N.	Algorithm	FR	Rank	S.N.	Algorithm	FR	Rank
1	**SS**	**5.4667**	**1**	13	I-POP-CMAES	11.4000	10
2	PSO	15.5667	19	14	LS-CMAES	10.6500	9
3	BB-PSO	8.4833	6	15	CMSAES	21.4333	23
4	CLPSO	7.4167	4	16	(1+1)cholesky CMAES	14.0167	18
5	APSO	18.2333	21	17	GWO	14.0000	16
6	OLPSO	7.1000	3	18	GOA	22.5500	24
7	CoBiDE	8.7833	7	19	MVO	12.4500	12
8	FCDE	11.6667	11	20	SCA	18.3167	22
9	RSDE	5.6500	2	21	SHO	14.0000	17
10	POBL_ADE	7.4833	5	22	SSA	13.8333	15
11	DE_best	9.7000	8	23	SOA	12.6500	13
12	CMA-ES	15.8333	20	24	WOA	13.3167	14

3.4.2 Perching

Perching can be explained by dividing its functions into five processes: Cris-cross Modification, Exponential Crossover, Solution Repair, Selection-I and Selection-II.

Cris-cross modification

Cris-cross modification process generates the initial form of perching trial positions vector, $t\bar{x}_i^{k+1}$.

$$t\bar{x}_i^{k+1} = m\bar{x}_{cc_i}^{k} + F(m\bar{x}_{q_i}^{k} - \Re(\bar{x_{r_i}}^{k}, m\bar{x}_{r_i}^{k})) \tag{3.20}$$

where F is the scaling factor which controls the amplitude of the search direction, cc_i is the cris-cross neighbour of i^{th} butterfly. Index q_i and r_i are randomly selected neighbour for i^{th} butterfly. Random selection of indices q_i and r_i are done in such a manner that it satisfies equation 3.21

$$i \neq cc_i \neq q_i \neq r_i \tag{3.21}$$

$\Re(a, b)$ is random selection operator, where probability of selection of a and b is equal. $F \in [0, 1]$ is a real constant.

Exponential recombination

Exponential recombination process generates the final form of perching trial position vector, $t\bar{x}_i^{k+1}$. For exponential recombination, the starting recombination point is selected

randomly from 1 to D, and l circular consecutive elements are not changed in $t\bar{x}_i$ and other elements are taken from $m\bar{x}_i$ and replaced to $t\bar{x}_i$. The pseudo code to generate l is

$l = 0$

$while((rand(0,1) \leq Cr)\&\&(l \leq D))$

$Do\{l = l + 1\}$

where Cr is recombination probability, D is the problem dimension $rand(0,1)$ is a uniformly distributed random number generator. Final form of $t\bar{x}_i$ is generated as

$$t\bar{x}_i{}^{k+1} = \begin{cases} t\bar{x}_i^{k+1}, \text{ for } j = r, r+1, r+2.....r+l-1 \\ m\bar{x}_i^k, \text{for other} j\epsilon[1, D] \end{cases} \tag{3.22}$$

Solution Repair

In solution repair, firstly the feasibility of the perching trial solution, $t\bar{x}_i$ is checked. If the solution, $t\bar{x}_i$, is feasible then solution repair is not required and it switches to next process. If solution, $t\bar{x}_i$, is infeasible, then generate a random number in range of $[0, 1]$ and compare with p_r. If random number is less than P_r, then this solution is repaired by multi-order Levenberg Marquardt method. Otherwise, it switches to next process without repairing the solution.

Selection-I

Selection-I process generates the Type-I population, P_1, of next iteration. Selection of $t\bar{x}_i{}^k$ in place of $\bar{x}_i{}^k$ at k^{th} iteration is decided by the constraint violation. In selection-I, individual having lower constraint violation is selected for the next iteration. Procedure of selection-I is given by equation 3.23

$$\bar{x}_i^{k+1} = \begin{cases} t\bar{x}_i^k, & \text{if } \phi^{(v)}(t\bar{x}_i^k) \leq \phi^{(v)}(\bar{x}_i^k) \\ \bar{x}_i^k, & \text{otherwise.} \end{cases} \tag{3.23}$$

Selection-II

Selection-II is the last process of the perching. It generates the the type-II population, P_2, of next iteration. Selection of $t\bar{x}_i^k$ in place of $m\bar{x}_i^k$ at k^{th} iteration is decided by v-level

comparison. It is done by equation 3.24

$$m\bar{i}x_i^{k+1} = \begin{cases} t\bar{i}x_i^k, & \text{if } (f(t\bar{i}x_i^k), \phi^{(\upsilon)}(t\bar{i}x_i^k)) \leq_\upsilon (f(\bar{i}x_i^k), \phi^{(\upsilon)}(\bar{i}x_i^k)) \\ m\bar{i}x_i^k, & \text{otherwise.} \end{cases} \tag{3.24}$$

3.4.3 Patrolling

Patrolling can be explained by its function into four processes: Towards-best modification, exponential recombination, Selection-I, Selection-III.
Exponential recombination and selection-I is same as perching. So, Towards-best modification and Selection-III are discussed below.

Towards-best modification

This process generates initial form of patrolling trial position vectors, $u\bar{i}x_i^{k+1}$.

$$u\bar{i}x_i^{k+1} = m\bar{i}x_i^k + F(m\bar{i}v_i^k + m\bar{i}x_{maxuv_i}^k - m\bar{i}x_i^k) \tag{3.25}$$

where F is scaling factor, $maxuv_i$ is the most attractive neighbour of i^{th} butterfly.

Selection-III

Selection-III is same as selection-II, but only difference is selection-III also update the velocity vector, $m\bar{i}v_i^k$. Velocity vector updating is done by equation 3.26

$$m\bar{i}v_i^{k+1} = \begin{cases} u\bar{i}x_i^k - m\bar{i}x_i^k, \\ \text{if } (f(t\bar{i}x_i^k), \phi^{(\upsilon)}(t\bar{i}x_i^k)) \leq_\upsilon (f(\bar{i}x_i^k), \phi^{(\upsilon)}(\bar{i}x_i^k)) \\ F(m\bar{i}v_i^k + m\bar{i}x_{cc_i} - m\bar{i}x_i^k), \\ \text{otherwise.} \end{cases} \tag{3.26}$$

3.4.4 Selection of Perching and Patrolling Operator

Selection of Perching and Patrolling operator depends upon the probability vector of operator selection, $Prob$.

$$Prob^k = [prob_1^k, prob_2^k .....prob_N^k] \tag{3.27}$$

where $prob_i^k$ is the probability of operator selection of i^{th} individual at k^{th} iteration. it is the ratio of total number of successful Selection-II run, $suc1_i^k$, and sum of total number of successful selection-II run, $suc1_i^k$ and selection-III run, $suc2_i^k$. It is given by:

$$prob_i^k = \frac{suc1_i^k}{suc1_i^k + suc2_i^k} \tag{3.28}$$

For every individual, a uniformly distributed random number of range $[0, 1]$ is generated. If this number is less than $prob_i^k$, then i^{th} individual selects Perching operator. Otherwise, i^th individual selects Patrolling operator.

3.4.5 Selection of Maximum Attractive Butterfly, $maxuv_i$

Selection of max attractive butterfly, $maxuv_i$ is done in patrolling. Three different neighbour is selected for every individual after every 10 patrolling attempts. Their ranking is done by according to objective function values and constraint violation. Best rank of them is selected as the $maxuv_i$ of i^{th} iteration.

3.4.6 Controlling of the υ-level

A simple way of controlling of the ϵ-level is described in [146]. A similar procedure is used in this study to control the υ-level. The initial υ-level is the ratio of constraint violation of top θ^{th} individual and total number of constraint.

$$\upsilon(0) = \frac{\phi(\bar{mx}_\theta)}{n_h + n_g} \tag{3.29}$$

where n_h and n_g are total number of equality and inequality constraint of problem respectively.

The υ-level is decreasing with increase of the iterations and become zero after current iteration T_c. The υ-level updating is done by equation 3.30

$$\upsilon(k) = \begin{cases} \upsilon(0)(1 - \frac{k}{T_c})^{cp}, & \text{if } 0 \leq k \leq T_c \\ 0, & \text{otherwise.} \end{cases} \tag{3.30}$$

where $\theta = 0.2N$, cp is the parameter to control the speed of decreasing of value, $\upsilon(k)$.

3.4.7 Reflecting Back and Cutting-off

If an individual moves outside the search space, there is need to apply operations like reflecting back and cutting off. Reflecting back and cutting off generate new solution inside the search space. In this study both methods are used.

Reflecting back operation

$$x_{ij}^k = \begin{cases} l_j + (l_j - x_{ij}^k) - \lfloor \frac{l_j - x_{ij}^k}{u_j - l_j} \rfloor (u_j - l_j), & \text{if } x_{ij}^k \leq l_j \\ u_j + (x_{ij}^k - u_j) + \lfloor \frac{x_{ij}^k - u_j}{u_j - l_j} \rfloor (u_j - l_j), & \text{if } x_{ij} \geq u_j \\ x_{ij}^k, & \text{otherwise.} \end{cases} \tag{3.31}$$

where $\lfloor z \rfloor$ is a floor function. Reflecting back operations used in Perching.

Cutting off

$$x_{ij}^k = \begin{cases} l_j, & \text{if } x_{ij}^k \leq l_j \\ u_j, & \text{if } x_{ij}^k \geq u_j \\ x_{ij}^k, & \text{otherwise.} \end{cases} \tag{3.32}$$

This operation is applied to Patrolling.

3.4.8 Validation of Butterfly Constrained Optimizer on Benchmark Problems

In this section, BCO is used to solve the problems presented in CEC 2006 [147] to verify the performance of BCO on different type of constrained problems. Results obtained from experiments are compared with the results of other state of arts constrained optimization techniques for comparative analysis. Constrained variant of other meta-heuristics are grouped based on their underlying techniques: PSO, GA, ES, CMA-ES, and DE etc.

In the experiments, parameter tuning of BCO is done by preliminary parameter analysis and parameter setting of BCO is given in Discussion section.

Experimental Settings

The properties of the benchmark problems given in CEC 2006 are given in Table 3.11. Table 3.11 shows that the benchmark problems containing different types of problems:

$g10, g20, g21, g22, g23$, and $g24$ are linear, $g02, g08, g13, g14, g16, g17$, and $g19$ are non-linear, $g03$, and $g09$ are polynomial, $g05$, and $g06$ are cubic, and $g01, g04, g07, g11, g12, g15$, and $g18$ are quadratic. In the Table 3.11, ρ represent the estimated feasible region in search space and it is calculated by the 1000000 solution samples. Most of the benchmark problems have very low feasible region and also hard to locate the even feasible region. Benchmark problems have different type of constraints which includes linear inequality(LI), non-linear inequality(NI), linear equality(LE), and non-linear equality(NE) constraint. The number of constraint is also very from 1 to 38.

For test function $g20$, an improved best known infeasible solution has been reported in this paper. The best known infeasible solution reported in [147] for test function $g20$ is $x^* = [1.285823e-18, 4.834603e-34, 0, 0, 6.304599e-18, 7.571925e-34, 5.033507e-34, 9.282681e-34, 0, 1.767234e-17, 3.556861e-34, 2.994139e-34, 0.158143, 2.296018e-19, 1.061069e18, 1.319683e-18, 0.530903, 0, 2.891483e-18, 3.348921e-18, 0, 0.311000, 5.412446e-05, 4.849931e-16]$ with $f(x^*) = 0.2049794002$. This solution violates the 11 (10 equality and 1 inequality) constraints with total constraint violation $3.975737e14$. The improved solution found in this paper for test function $g20$ is $x^* = [1.29089e-01, 6.009131e-14, 1.448197e-11, 1.856528e-12, 1.512278e-01, 3.056017e-11, 3.664426e-12, 8.944519e-13, 4.294914e-13, 3.773682e-12, 1.367320e-11, 1.085285e-11, 3.992256e-01, 2.428499e-05, 2.428468e-05, 5.741080e-05, 3.202754e-01, 7.140807e-05, 2.611374e-05, 1.1993356e-10, 1.426029e-11, 3.447475e-05, 1.925004e-05, 2.511113e-05]$ with $f(x^*) = 0.1592683574$. This solution violates only 1 inequality constraint with total constraint violation 0.481498.

General performance of BCO

Twenty five independent runs were performed for each test problems using 5×10^5 FES at most, and the tolerance value δ for the equality constraint was set to 0.0001 as suggested by Liang [147]. The best, median, worst, mean and standard deviation of the error value $(f(x) - f(x^*))$ for the best so far solution after 5×10^3, 5×10^4, and 5×10^5 FEs in each run are recorded in Tables 4.7-3.15.

Tables 4.7-3.15 show that the 3 out of 24 test problems (i.e.$g08$, $g12$, and $g24$) are converged on the feasible optimum solution in every independent run by using 5×10^3 FEs. In 5×10^4 FEs, 12 out of 24 test problems (i.e. $g01$, $g04$, $g06$, $g08$, $g10$, $g11$, $g12$, $g13$, $g15$, $g16$, $g17$, and $g24$) are converged on the feasible optimum solution in every run.

Table 3.11: Properties of benchmark problems given in CEC 2006 [147]

prob	**D**	**Type of Problem**	$\rho(\%)$	**LI**	**NI**	**LE**	**NE**	a
$g01$	13	quadratic	0.0111	9	0	0	0	6
$g02$	20	nonlinear	99.9971	0	2	0	0	1
$g03$	10	polynomial	0.0000	0	0	0	1	1
$g04$	5	quadratic	51.1230	0	6	0	0	2
$g05$	4	cubic	0.0000	2	0	0	3	3
$g06$	2	cubic	0.0066	0	2	0	0	2
$g07$	10	quadratic	0.0003	3	5	0	0	6
$g08$	2	nonlinear	0.8560	0	2	0	0	0
$g09$	7	polynomial	0.5121	0	4	0	0	2
$g10$	8	linear	0.0010	3	3	0	0	0
$g11$	2	quadratic	0.0000	0	0	0	1	1
$g12$	3	quadratic	4.7713	0	1	0	0	0
$g13$	5	nonlinear	0.0000	0	0	0	3	3
$g14$	10	nonlinear	0.0000	0	0	3	0	3
$g15$	3	quadratic	0.0000	0	0	1	1	2
$g16$	5	nonlinear	0.0204	4	34	0	0	4
$g17$	6	nonlinear	0.0000	0	0	0	4	4
$g18$	9	quadratic	0.0000	0	13	0	0	0
$g19$	15	nonlinear	33.4761	0	5	0	0	0
$g20$	24	linear	0.0000	0	6	2	12	16
$g21$	7	linear	0.0000	0	1	0	5	6
$g22$	22	linear	0.0000	0	1	8	11	19
$g23$	9	linear	0.0000	0	2	3	1	6
$g24$	2	linear	79.6556	0	2	0	0	2

prob: Benchmark Problem.

D: Number of dimension of problem.

ρ: Feasibility ratio.

LI: Number of linear inequality constraint.

NI: Number of non-linear inequality constraint.

LE: Number of linear equality constraint.

NE: Number of non-linear equality constraint.

a: Number of active inequality constarint.

Rest of the problems are converged on feasible optimum solution with in 5×10^5 FEs for every independent run except $g20$ and $g22$.

To test problem $g20$, the best known solution is slightly infeasible i.e. feasible optimum solution is not available. Proposed method, BCO, is converged on improved solution. For test problem $g22$, 3 runs out of 25 converged on the best known feasible solution by

Table 3.12: Error Values achieved when FEs are 5000, 50000, and 500000 for test function $g01 - g06$

FES		g01	g02	g03	g04	g05	g06
5.0E+03	Min	1.9674E+00	2.0521E-01	4.3547E-01	3.5106E+01	5.1546E+00	**9.0900E-13**
	Median	5.7809E+00	3.1561E-01	7.8524E-01	1.1499E+02	7.6736E+01	**7.2760E-12**
	Worst	8.7350E+00	3.8456E-01	1.0004E+00	2.0169E+02	6.1227E+02	5.7557E+03
	Mean	5.9698E+00	3.0886E-01	7.5429E-01	1.1587E+02	1.3059E+02	1.0047E+03
	Std	1.7661E+00	3.7480E-02	1.7647E-01	4.5865E+01	1.6333E+02	2.1447E+03
5.0E+04	Min	**9.2000E-14**	1.4730E-02	4.5313E-03	**8.4971E-07**	2.1418E-04	**9.0900E-13**
	Median	**9.8400E-13**	3.1546E-02	1.0079E-02	**1.5282E-05**	1.1020E-03	**5.4570E-12**
	Worst	**1.7494E-11**	9.5223E-02	4.0296E-02	2.3949E-04	2.2037E+01	**1.9099E-11**
	Mean	**3.4191E-12**	3.6746E-02	1.2963E-02	**3.6582E-05**	1.3000E+00	**4.6564E-12**
	Std	**4.9143E-12**	2.1116E-02	7.8858E-03	**5.5316E-05**	4.7936E+00	**3.9673E-12**
5.0E+05	Min	**0.0000E+00**	**3.7372E-09**	**0.0000E+00**	**0.0000E+00**	**0.0000E+00**	**9.0900E-13**
	Median	**0.0000E+00**	**1.9797E-08**	**0.0000E+00**	**0.0000E+00**	**0.0000E+00**	**5.4570E-12**
	Worst	**0.0000E+00**	**6.4743E-08**	**0.0000E+00**	**0.0000E+00**	**0.0000E+00**	**1.9099E-11**
	Mean	**0.0000E+00**	**2.6136E-08**	**0.0000E+00**	**0.0000E+00**	**0.0000E+00**	**4.6564E-12**
	Std	**0.0000E+00**	**1.7600E-08**	**0.0000E+00**	**0.0000E+00**	**0.0000E+00**	**3.9673E-12**

Table 3.13: Error Values achieved when FEs are 5000, 50000, and 500000 for test function $g07 - g12$

FES		g07	g08	g09	g10—	g11—	g12—
5.0E+03	Min	3.0814E+01	**3.4510E-12**	1.4601E+01	4.1756E+01	**3.3075E-05**	**1.9717E-08**
	Median	8.5137E+01	**3.9054E-07**	1.2292E+02	2.6334E+03	2.0188E-04	**6.4211E-07**
	Worst	5.6623E+02	7.5612E-04	5.5246E+04	9.8834E+03	1.2911E-01	**4.6084E-06**
	Mean	1.3221E+02	**4.6842E-05**	2.3881E+03	3.2797E+03	8.6365E-03	**9.8570E-07**
	Std	1.2725E+02	1.6050E-04	1.1014E+04	2.9060E+03	2.8965E-02	**1.0977E-06**
5.0E+04	Min	9.1488E-02	**0.0000E+00**	1.1040E-03	**3.5108E-08**	**0.0000E+00**	**0.0000E+00**
	Median	3.4234E-01	**0.0000E+00**	4.3227E-03	**1.5823E-05**	**0.0000E+00**	**0.0000E+00**
	Worst	6.5021E-01	**0.0000E+00**	7.9238E-03	1.2318E-02	**2.0000E-15**	**0.0000E+00**
	Mean	3.6243E-01	**0.0000E+00**	4.1607E-03	6.2102E-04	**1.6000E-16**	**0.0000E+00**
	Std	1.2355E-01	**0.0000E+00**	1.9215E-03	2.4589E-03	**4.7258E-16**	**0.0000E+00**
5.0E+05	Min	**0.0000E+00**	**0.0000E+00**	**0.0000E+00**	**0.0000E+00**	**0.0000E+00**	**0.0000E+00**
	Median	**0.0000E+00**	**0.0000E+00**	**0.0000E+00**	**0.0000E+00**	**0.0000E+00**	**0.0000E+00**
	Worst	**0.0000E+00**	**0.0000E+00**	**0.0000E+00**	**0.0000E+00**	**2.0000E-15**	**0.0000E+00**
	Mean	**0.0000E+00**	**0.0000E+00**	**0.0000E+00**	**0.0000E+00**	**1.6000E-16**	**0.0000E+00**
	Std	**0.0000E+00**	**0.0000E+00**	**0.0000E+00**	**0.0000E+00**	**4.7258E-16**	**0.0000E+00**

using 5×10^5 FEs.

The result achived by the BCO are very close to or even equal to feasible optimal

Table 3.14: Error Values achieved when FEs are 5000, 50000, and 500000 for test function $g13 - g18$

FES		g13	g14	g15	g16	g17	g18
5.0E+03	Min	1.0850E-02	2.0450E+00	5.9225E-04	8.1472E-02	4.0694E+00	1.1620E-01
	Median	1.2786E-01	5.8555E+00	4.4350E-02	3.0432E-01	5.3215E+01	4.1838E-01
	Worst	9.4729E-01	7.7918E+00	2.2955E+00	7.8726E-01	2.7754E+02	8.5155E-01
	Mean	3.9709E-01	5.6844E+00	3.0686E-01	3.4297E-01	7.4573E+01	4.5509E-01
	Std	3.7967E-01	1.5406E+00	6.3742E-01	2.1835E-01	6.9016E+01	2.3651E-01
5.0E+04	Min	**4.1100E-13**	2.7052E-04	**0.0000E+00**	**3.4311E-06**	**5.2751E-11**	3.2056E-03
	Median	**3.9797E-11**	8.0241E-04	**0.0000E+00**	**1.1654E-05**	**8.5856E-10**	9.3977E-03
	Worst	**2.2570E-08**	2.5207E-03	**9.0900E-13**	**3.7942E-05**	**8.4520E-07**	4.7111E-01
	Mean	**1.3131E-09**	9.1837E-04	**1.4540E-13**	**1.5270E-05**	**5.3349E-08**	2.9085E-02
	Std	**4.6360E-09**	5.8709E-04	**2.2128E-13**	**1.0031E-05**	**1.8432E-07**	9.2273E-02
5.0E+05	Min	**0.0000E+00**	**1.4000E-14**	**0.0000E+00**	**4.0000E-15**	**3.6380E-12**	**0.0000E+00**
	Median	**0.0000E+00**	**1.4000E-14**	**0.0000E+00**	**4.0000E-15**	**3.6380E-12**	**0.0000E+00**
	Worst	**0.0000E+00**	**7.1000E-14**	**9.0900E-13**	**4.0000E-15**	**3.6380E-12**	**0.0000E+00**
	Mean	**0.0000E+00**	**1.8240E-14**	**1.4540E-13**	**4.0000E-15**	**3.6380E-12**	**0.0000E+00**
	Std	**0.0000E+00**	**1.1443E-14**	**2.2128E-13**	**1.6103E-30**	**8.2445E-28**	**0.0000E+00**

Table 3.15: Error Values achieved when FEs are 5000, 50000, and 500000 for test function $g19 - g24$

FES		g19	g20	g21	g22	g23	g24
5.0E+03	Min	4.6250E+01	3.3233E-01	4.5408E+01	2.3643E+02	5.0931E+01	**3.3000E-14**
	Median	7.5536E+01	8.7700E-01	1.1814E+02	1.1161E+04	1.7079E+02	**3.5000E-14**
	Worst	1.4028E+02	2.7133E+00	4.7765E+02	1.9764E+04	3.3621E+02	**6.3000E-14**
	Mean	7.9671E+01	9.5601E-01	1.9748E+02	1.0220E+04	1.8187E+02	**4.0160E-14**
	Std	2.3452E+01	4.6699E-01	1.4443E+02	6.1985E+03	7.0989E+01	**1.0499E-14**
5.0E+04	Min	8.8876E-01	5.2239E-03	1.0848E-02	2.7760E+01	1.1941E+01	**3.3000E-14**
	Median	1.9566E+00	3.0857E-02	2.3503E-02	5.6483E+02	9.3792E+01	**3.3000E-14**
	Worst	3.6198E+00	6.5630E-02	7.5191E-02	4.7803E+03	4.2806E+02	**6.3000E-14**
	Mean	2.0812E+00	2.9412E-02	2.7678E-02	1.0215E+03	1.2093E+02	**3.4200E-14**
	Std	7.4010E-01	1.7922E-02	1.6356E-02	1.2441E+03	9.7208E+01	**6.0000E-15**
5.0E+05	Min	**1.2800E-13**	**1.3662E-10**	**0.0000E+00**	**0.0000E+00**	**0.0000E+00**	**3.3000E-14**
	Median	**4.1254E-11**	**1.4826E-08**	**0.0000E+00**	3.6988E+03	**0.0000E+00**	**3.3000E-14**
	Worst	**4.0478E-08**	**9.7700E-06**	**0.0000E+00**	1.8277E+04	**2.1237E-10**	**6.3000E-14**
	Mean	**4.6628E-09**	**7.7288E-07**	**0.0000E+00**	6.1451E+03	**1.1155E-11**	**3.4200E-14**
	Std	**1.0834E-08**	**2.1255E-06**	**0.0000E+00**	5.6814E+03	**4.3122E-11**	**6.0000E-15**

solution for 23 test problem in all run, except test problem $g22$ (only 3 out of 25 run, result is equal to known feasible optimal solution).

Table 3.16: Best, Median, worst, mean, and standard deviation of NFES to achieve the fixed accuracy level. $((f(x) - f(x^*)) \leq 0.0001)$, feasibility rate, success rate and successful performance over 25 runs of BCO on the CEC 2006 [147]

Prob.	Min	Max	median	Mean	STD	FR	SR	SP
g01	19758	24259	22245	22034	1088	100	100	22034
g02	120145	183451	158284	158293	14441	100	100	158293
g03	65224	89439	81640	80632	5769	100	100	80632
g04	39213	48906	44509	44488	2015	100	100	44488
g05	47230	59218	53852	54437	3287	100	100	54437
g06	258	6166	4050	3784	1425	100	100	3784
g07	179375	206245	197446	196558	7325	100	100	196558
g08	1412	4514	3617	3492	759	100	100	3492
g09	67591	81014	75322	74973	4100	100	100	74973
g10	22443	45100	34998	34192	5103	100	100	34192
g11	468	5902	4083	3705	1381	100	100	3705
g12	120	279	173	198	53	100	100	198
g13	879	18118	14178	13345	4039	100	100	13345
g14	55595	66731	62183	62221	2710	100	100	62221
g15	5415	15677	12365	11761	2911	100	100	11761
g16	34337	41579	38472	38373	2008	100	100	38373
g17	23173	31630	27209	27450	1873	100	100	27450
g18	106449	150370	129525	129224	12341	100	100	129224
g19	212636	265169	245241	241430	14914	100	100	241430
g20	22323	210350	172071	152074	59050	0	100	152074
g21	104454	119499	111879	112507	3858	100	100	112507
g22	250708	297360	284473	277514	92303	32	12	2312617
g23	142823	400000	222973	253267	78025	100	100	253267
g24	132	561	403	360	146	100	100	360

Comparison with other state-of-the-art on CEC 2006 test problems

The NFES required for reaching the optimum value is reported in Table 6.11. Table 6.11 shows the best, worst, median, mean, and standard deviation of NFES to achieve the fixed accuracy level, $(f(\bar{x}) - f(\bar{x}^*)) \leq 0.0001)$, Feasible Rate (FR), Success Rate (SR), and Success Performance (SP) over 25 runs of BCO on the cec 2006 [147]. FR denotes the percentage of runs where atleast one feasible solution is found in 5×10^5 by algorithm. SR denotes percentage of run where atleast one solution satisfies success condition. SP denotes the ratio of mean of NFES required to find optimal feasible solution and SR.

As shown in table 6.11, FR of BCO for every test cases is 100% except problems $g20$, and $g22$. In case of problem $g20$, the optimal solution is slightly infeasible. Problem $g22$ is hard to solve, so in case of BCO only 32% FR is recorded. Regarding SR of BCO,

Table 3.17: Mean NFES to achieve the accuracy level $(f(x) - f(x*)) \leq 0.0001$ and SR over 25 runs on the CEC 2006 [147]

Proposed Work			DE															
Prob.	BCO		EPS-DE [146]		MPDE [132]		GDE [148]		MDE [149]		jDE-2 [150]		DPDE [151]		ICDE [152]		(mu+lm)CDE [153]	
	NFES	SR	NFES	SR	NFES	SR	NFES	SR	NFES	SR	NFES	SR	NFES	SR	NFES	SR	NFES	SR
g01	**22034**	100	59308	100	43430	100	40519	100	75373	100	50386	100	42180	100	105776	100	89000	100
g02	158293	100	149825	100	280573	92	107684	72	96222	16	123490	92	**95102**	94	283528	100	277379	96
g03	80632	100	89407	100	209298	84	143086	4	**44988**	100	–	0	88260	100	212657	100	111025	100
g04	44488	100	26216	100	20883	100	**15281**	100	41562	100	40728	100	25160	100	36770	100	30620	100
g05	54437	100	97431	100	216469	100	178023	92	**21306**	100	206620	68	100506	100	27933	100	165079	100
g06	**3784**	100	7381	100	10574	100	6503	100	5202	100	29488	100	13400	100	13040	100	11032	100
g07	196558	100	74303	100	**57400**	100	123996	100	194202	100	127740	100	99060	100	134789	100	141038	100
g08	3492	100	1139	100	1515	100	1469	100	**918**	100	3236	100	1960	100	1943	100	2010	100
g09	74973	100	23121	100	21044	100	30230	100	**16152**	100	54919	100	31820	100	37929	100	39953	100
g10	**34192**	100	105234	100	48628	100	82604	100	164160	100	146150	100	143300	100	325007	100	188725	100
g11	3705	100	16420	100	22422	96	8460	100	**3000**	100	49700	96	90310	100	4404	100	79475	100
g12	**198**	100	4124	100	4238	100	3149	100	1308	100	6356	100	5626	100	6488	100	4908	100
g13	**13345**	100	34738	100	356433	48	336306	40	21732	100		0	81980	100	34325	100	148237	100
g14	62221	100	113439	100	**42715**	100	220921	96	291642	100	97845	100	107480	100	85758	100	176671	100
g15	11761	100	84216	100	200174	100	71889	96	10458	100	222460	96	94600	100	**10074**	100	130622	100
g16	38373	100	12986	100	13063	100	13224	100	**8730**	100	31695	100	18650	100	25001	100	19154	100
g17	27450	100	98861	100	204791	28	343740	16	26364	100	**17971**	4	128690	100	103230	100	183962	100
g18	129224	100	59153	100	**44045**	100	364861	76	103482	100	104460	100	80280	100	138998	100	215068	100
g19	241430	100	**35635**	100	118274	100	202648	88	–	0	199850	100	163080	100	296145	100	268374	100
g20	152074	100	–	0		0	–	0	–	0	–	0	–	0	–	0	**148506**	100
g21	112507	100	135143	100	142159	68	347653	60	112566	100	**107080**	92	164068	92	317447	100	209896	92
g22	**277514**	12	–	0	–	0	–	0	–	0	–	0	–	0	–	0	–	0
g23	253267	100	**200765**	100	210661	100	425342	40	360420	100	302550	92	204450	94	364806	100	263695	100
g24	**360**	100	2952	100	4342	100	3059	100	1794	100	10196	100	5860	100	574	100	5059	100

Proposed Work			PSO						Others							
Prob.	BCO		PSO		COPSO [154]		PESO [155]		AP-CMA-ES [156]		ASR-ES [157]		PCX [158]		Shade [159]	
	NFES	SR	NFES	SR	NFES	SR	NFES	SR	NFES	SR	NFES	SR	NFES	SR	NFES	SR
g01	**22034**	100	73314	100	95397	100	101532	100	181110	52	35406	100	55204	100	50386	100
g02	158293	100	–	0	179395	73	231193	56	–	0	–	0	**87900**	64	123490	92
g03	80632	100	–	0	315123	100	450644	100	**18302**	100	–	0	34937	100	–	0
g04	44488	100	37802	100	65087	100	79876	100	**4992**	100	15104	100	30989	100	40728	100
g05	54437	100	366824	100	315257	100	452256	100	82365	100	**19281**	100	94765	100	206620	68
g06	3784	100	37802	100	53410	100	56508	100	**3269**	100	9603	100	33821	100	29488	100
g07	196558	100	405156	100	233400	100	352592	96	**14445**	100	76782	8	117121	100	127740	100
g08	3492	100	3656	100	6470	100	6124	100	1661	100	**1027**	100	2826	100	3236	100
g09	74973	100	103677	100	79570	100	97544	100	**5882**	100	30618	100	46527	100	54919	100
g10	34192	100	487525	100	224740	100	452575	16	**24891**	100	–	0	89028	100	146150	100
g11	3705	100	**33073**	100	315000	100	450100	100	25803	100	**2792**	100	38688	100	49700	96
g12	**198**	100	6906	100	6447	100	8088	100	31247	100	2996	100	8960	100	6356	100
g13	13345	100	–	0	315547	100	450420	100	–	0	**11292**	84	53735	100	–	0
g14	62221	100	–	0	326900	3	–	0	**14477**	100	92820	8	59237	100	97845	100
g15	11761	100	267821	100	315100	100	450100	100	131822	100	**8519**	100	46936	100	222460	96
g16	38373	100	56612	100	40960	100	49040	100	**6106**	100	16179	100	30395	100	31695	100
g17	27450	100	–	0	**316609**	76	–	0	–	0	**21491**	76	136110	100	17971	4
g18	129224	100	238706	100	167089	90	214322	92	**68741**	100	40840	92	70027	100	104460	100
g19	241430	100	426101	100	264414	47	–	0	**75669**	100	–	0	129676	100	199850	100
g20	**152074**	100	–	0	–	0	–	0	–	0	–	0	–	0	–	0
g21	112507	100	–	0	–	0	–	0	184302	56	–	0	**38217**	100	107080	92
g22	277514	12	–	0	–	0	–	0	–	0	–	0	–	0	–	0
g23	253267	100	–	0	–	0	–	0	200158	84	–	0	**167119**	100	302550	92
g24	360	100	**1986**	100	19157	100	19980	100	**1663**	100	3638	100	11646	100	10196	100

All the results are taken from their corresponding papers.

–: NFES is not available.

Table 3.18: Ranking based on the SP of all algorithm over 25 runs on the CEC 2006 [147]

Prob.	BCO	EPS-DE	MPDE	GDE	MDE	jDE-2	DPDE	ICDE	(mu+lm)CDE	PSO	COPSO	PESO	AP-CMA-ES	ASR-ES	PCX	Shade
g01	1	9	5	3	11	6	4	15	12	10	13	14	16	2	8	6
g02	7	6	11	5	13	2	1	9	10	14	8	12	14	14	4	3
g03	4	6	9	12	3	13	5	8	7	13	10	11	1	13	2	13
g04	6	14	4	3	13	11	5	9	7	10	15	16	1	2	8	11
g05	4	7	11	10	2	12	8	3	9	15	14	16	5	1	6	13
g06	2	5	7	4	3	11	10	9	8	14	15	16	1	6	13	11
g07	12	3	2	6	11	7	4	9	10	15	13	14	1	16	5	7
g08	13	3	5	4	1	11	8	7	9	14	16	15	6	2	10	11
g09	13	4	3	5	2	11	7	8	9	16	14	15	1	6	10	11
g10	2	6	3	4	10	8	7	13	11	14	12	15	1	16	5	8
g11	3	6	7	5	2	12	14	4	13	9	15	16	8	1	10	11
g12	1	5	6	4	2	9	8	12	7	13	11	14	16	3	15	9
g13	1	5	11	12	3	13	7	4	8	13	9	10	13	2	6	13
g14	4	9	2	11	12	6	8	5	10	15	14	15	1	13	3	6
g15	4	7	11	6	3	12	8	2	9	14	15	16	10	1	5	13
g16	13	3	4	5	2	11	7	9	8	16	14	15	1	6	10	11
g17	2	4	12	13	1	10	6	5	8	14	9	14	14	3	7	10
g18	10	3	1	16	7	8	6	11	13	15	12	14	4	2	5	8
g19	9	1	3	8	14	6	5	11	10	12	13	14	2	14	4	6
g20	2	3	3	3	3	3	3	3	1	3	3	3	3	3	3	3
g21	2	6	8	12	3	5	7	10	9	13	13	13	11	13	1	4
g22	1	2	2	2	2	2	2	2	2	2	2	2	2	2	2	2
g23	6	2	3	12	10	8	4	11	7	13	13	13	5	13	1	9
g24	1	6	9	7	4	12	11	2	10	5	15	16	3	8	14	12
sum	123	125	142	172	137	209	155	181	207	292	288	319	140	162	157	211
rank	1	2	5	9	3	12	6	10	11	15	14	16	4	8	7	13

BCO is capable to provide 100% SR in every test cases except problem $g22$. In problem $g22$, BCO only provide 12% SR. In Table 6.11, SP indicates that the BCO requires less than 4×10^3 FEs for 5 problems, 1×10^5 FES for 16 problems, 2.6×10^5 for 23 problems, to achieve the success condition of optimum.

SR and Mean FEs of BCO required to solve CEC 2006 problems against state-of-the-art that do not use the traditional techniques to solve constrained problems are compared. For convenience, we grouped all the state-of-the-art in three groups: DE-based, PSO-based, and other metaheuristic which is based on CMA-ES and hybrid variant of DE. Most of the state-of-art methods, has taken for comparison, are DE and PSO based because perching and patrolling follows the similar procedure to DE and PSO respectively. Besides metaheuristics, these state-of-the- arts also use different type of constraint-handling techniques to solve COP. Most of the state-of-arts use ϵ-constraint handling, three feasibility rules, and penalty function to handle the constraint. So, effectiveness of proposed constraint handling techniques is also analysed as compared to other constraint handling technique.

Table-3.17 shows the comparison of performance of BCO with other state-of-arts in

Table 3.19: Average ranking of the Friedman test

Algorithm	Average Ranking
BCO	5.4375
EPS-DE	5.8333
MPDE	6.4375
GDE	7.6875
MDE	6.3125
jDE-2	9.6875
DPDE	6.9792
ICDE	8.0625
(μ+λ)CDE	8.875
PSO	13.0833
COPSO	12.6875
PESO	14.0833
AP-CMA-ES	6.5
ASR-ES	7.5833
PCX	7.0625
Shade	9.6875

χ^2- distribution : 114.64614.
P-value : 0.

terms of NFES and SR. In table-3.17, the bold face in NFES shows the best performance in terms of NFES. Table-3.18 shows the ranking basad on the SP of all algorithms. In Table-3.19, result of Friedman ranking test is reported. Average ranking of the Friedman test is done based on the SP of all the algorithms on every problem of CEC 2006 [147].

Comparison with DE-based state-of-arts

To compare the performance of BCO with respect to the popular DE-based state-of-arts, eight different algorithms EPS-DE, MPDE, GDE, MDE, jDE-2, DPDE, ICDE, and (mu+lm)-CDE are chosen. The results of these algorithms are used in comparison is same as reported in their original paper.

A closer examination of Table-3.17 at the first sub-table, reveals that the performance of BCO in terms of NFES and SR is better than the DE-based state-of-art design. Performance of BCO as compared to other DE-based state-of-arts are summarized below:

- *Comparison based on NFES:* In case of seven problems $g01$, $g06$, $g10$, $g12$, $g13$, $g22$, and $g24$, BCO are converged fastly on feasible optimum value i.e. takes less

number of NFES to achieve the accuracy level $(f(x) - f(x^*)) \leq 0.0001$, as compared to others algorithms. Other algorithms like EPS-DE, MPDE, GDE, MDE, jDE-2, DPDE, ICDE and (mu+lm)-CDE take less number of NFES in case of 2 ($g19, g23$), 3 ($g07, g14, g18$), 1 ($g04$), 6 ($g03, g05, g08, g09, g11, g16$), 2 ($g17, g21$), 1 ($g02$), 1 ($g15$) and 1 ($g20$) problems respectively.

- *Comparison based on SR:* In case of all test problems except $g22$ (12%), BCO achieve 100% SR. It can seen from Table- 3.17, BCO outperforms all the DE-based state-of-arts in terms of SR. It is interesting to note that only BCO can found feasible optimal solution for test problem $g22$. Owing to its special characteristic, test problem $g22$ is very hard to solve for different DE-based state-of-arts.

Through this comprehensive comparison with chosen DE-based state-of-art designs, BCO can be considered very competitive with respect to the chosen DE-based state-of-art in case of COPs.

Comparison with PSO-based state-of-art designs

Three PSO-based state-of-the-art design PSO, COPSO, and PESO, are chosen to compare the performance of BCO. The results of these algorithm is directly taken from their original paper. All the chosen PSO-based algorithms use the three feasibility rule as a constraint handling technique.

Second sub-table of Table-3.17, shows that the BCO performs better than chosen PSO-based state-of-art design in terms of NFES and SR. Performance of BCO as compared to chosen PSO-based state-of-the-arts are summarized below:

- *Comparison based on NFES:* In case of test problem except $g04$, BCO are converged fastly i.e. takes less number of NFES to find feasible optimal value. In case of test problem $g04$, PSO converges fastly than BCO.

- *Comparison based on SR:* As shown in second sub-table of Table-3.17, for test problems $g20$, $g21$, $g22$, and $g23$, PSO-based algorithms did not converge on feasible optimum value for any run out of 25 independent run i.e. SR is zero. The performance of BCO is effectively much better than PSO-based algorithms in terms of SR is case of test problems $g02$, $g03$, $g13$, $g14$, $g17$, $g19$, $g20$, $g21$, $g22$, and $g23$.

Based on the above comparison result, we conclude that the performance of BCO is far better than the performance of PSO-based state-of-art designs in case of COPs.

Table 3.20: Multiple solution obtained using BCO for ill-conditioned CASE13

solution-1								solution-2						
Bus	V_a	$\angle_a$	V_b	$\angle_b$	V_c	$\angle_c$		Bus	V_a	$\angle_a$	V_b	$\angle_b$	V_c	$\angle_c$
1	1.00	0.00	1.00	-120.00	1.00	120.00		1	1.00	0.00	1.00	-120.00	1.00	120.00
2	0.99	-0.25	0.99	-120.18	0.99	119.98		2	0.99	-0.25	0.99	-120.18	0.99	119.98
3					0.62	102.02		3					0.92	122.58
4			0.94	-120.73	1.01	119.59		4			0.94	-120.73	1.01	119.59
5			0.92	-121.05	1.02	119.46		5			0.92	-121.05	1.02	119.46
6	0.93	-13.74						6	0.27	-33.10				
7	0.96	-13.96	1.07	-118.37	0.64	104.44		7	0.39	-34.92	1.21	-131.26	0.93	123.30
8	0.93	-15.18	1.08	-118.95	0.63	104.21		8	0.31	-41.56	1.22	-132.73	0.94	123.20
9	0.96	-13.96	1.07	-118.37	0.64	104.44		9	0.39	-34.92	1.21	-131.26	0.93	123.30
10	0.95	-14.05			0.63	103.39		10	0.35	-35.99			0.93	123.21
solution-3								solution-4						
Bus	V_a	$\angle_a$	V_b	$\angle_b$	V_c	$\angle_c$		Bus	V_a	$\angle_a$	V_b	$\angle_b$	V_c	$\angle_c$
1	1.00	0.00	1.00	-120.00	1.00	120.00		1	1.00	0.00	1.00	-120.00	1.00	120.00
2	0.99	-0.25	0.99	-120.18	0.99	119.98		2	0.99	-0.25	0.99	-120.18	0.99	119.98
3					0.97	96.51		3					0.26	90.58
4			0.94	-120.73	1.01	119.59		4			0.94	-120.73	1.01	119.59
5			0.92	-121.05	1.02	119.46		5			0.92	-121.05	1.02	119.46
6	1.14	9.45						6	0.09	-39.62				
7	1.16	9.39	0.15	-164.30	0.98	97.52		7	0.42	-44.17	1.28	-124.24	0.32	97.82
8	1.15	9.41	0.15	-183.44	0.99	96.91		8	0.37	-50.61	1.29	-125.05	0.29	95.65
9	1.16	9.39	0.15	-164.30	0.98	97.52		9	0.42	-44.17	1.28	-124.24	0.32	97.82
10	1.16	9.23			0.97	97.08		10	0.32	-48.98			0.29	97.47

Comparison with Other State-of-Art Designs

To broaden our comparative analysis, we considered some other state-of-art designs AP-CMA-ES, ASR-ES, and PCX and SHADE that combine a population-based algorithm (DE, PSO, and GA) with other programming techniques for example SQP. The performance of BCO as compared to other state-of-art designs are summarized below.

- *Comparison based on NFES:* In the case of five problems $g01$, $g12$, $g20$, $g22$, and $g24$, BCO has provided optimum feasible solutions with minimum Mean NFES as compared to other algorithms. The performance of AP-CMA-ES and ASR-ES on the basis of Mean NFES is better than the performance of BCO. Mean NFES of AP-CMA-ES and ASR-ES is better than BCO for 9 ($g03$, $g04$, $g06$, $g07$, $g09$, $g10$,

$g14$, $g16$, and $g19$) and 6 ($g05$, $g08$, $g11$, $g13$, $g15$, and $g18$) problems respectively. BCO outperforms the PCX and Shade on the basis of Mean NFES.

- *Comparison based on SR:* It can seen from Table-3.17, BCO outperform all the state-of-art designs on the basis of SR. AP-CMA-ES and ASR-ES, PCX, and Shade provides 100% SR on 16, 11, 21, and 13 problems respectively.

Based on the above discussion, we can conclude that the ASR-ES and AP-CMA-ES are having better convergence speed as compared to BCO, but the problem-solving capability of these algorithms are poorer than the BCO. PCX algorithm has the better problem-solving capability with good convergence speed, but BCO outperforms this algorithm on the basis of both property. The BCO also outperforms the performance of Shade.

Ranking of all the selected state-of-art algorithms along with BCO on the basis of Success Performance

Rank based on SP of all competitive algorithms are reported in Table 3.18. It is clear from the Table 3.18, the overall normalized rank of BCO is 1, and the performance of the BCO is better than all other competitive algorithms. In the table 3.18, the number in boldface represents the normalized rank of all ranks. From Table 3.18, Performance of BCO on test problems $g01$, $g12$, $g13$, $g22$, and $g24$ based on SP, is better than all another state of art designs and takes the top position in the ranking table 3.18 of these test problems.

ϵ-DE is obvious at the second rank in Ranking Table 3.18, because it is the winner of CEC-2006. In support of Ranking, non-parameter Friedman test is reported in Table 3.18. In Table 3.18, BCO is globally at the first rank with the minimum value. P-value and χ^2 distribution of Friedman test are also reported at the bottom of Table 3.19. It is clear from these values; there is a significant difference in the performance of all competitive algorithm and Ranking is valid.

3.4.9 BCO based Power Flow for Loadability Evaluation

BCO can be used to obtain multiple solution of PF problems. Multiple PF solutions can be useful in voltage stability analysis of power system. In this section, validation of performance of BCO is done on CASE13 test system.

Four different PF solutions of CASE13 are obtained using BCO and are reported in Table 3.20. It can be seen from Table 3.20 that the solutions are low voltage solutions of PF problem which can be used in voltage stability analysis.

For further analysis of performance of BCO, voltage profile of less stable buses of the system at different loading condition is obtained. In this analysis, CASE11 and CASE25 are considered as test systems. In CASE13, bus 7c, 8c, 9c, and 10c are the least stable buses in which voltage level reduces rapidly with increase of load. Similarly, bus 7a, 9a, 10a, 11a, 12a, 13a, 14a, 15a, 16a, and 17a are least stable buses in CASE25. Voltage profile of these buses with different loading condition are depicted in Figure 3.1, 3.2 and 3.3.

It can be seen from Figure 3.1 that after the loading factor of 10, bus voltage start decreasing due to insufficient power generation. After loading factor of 11.291, the voltage collapses because this point is critical point of CASE13 under defined operating conditions.

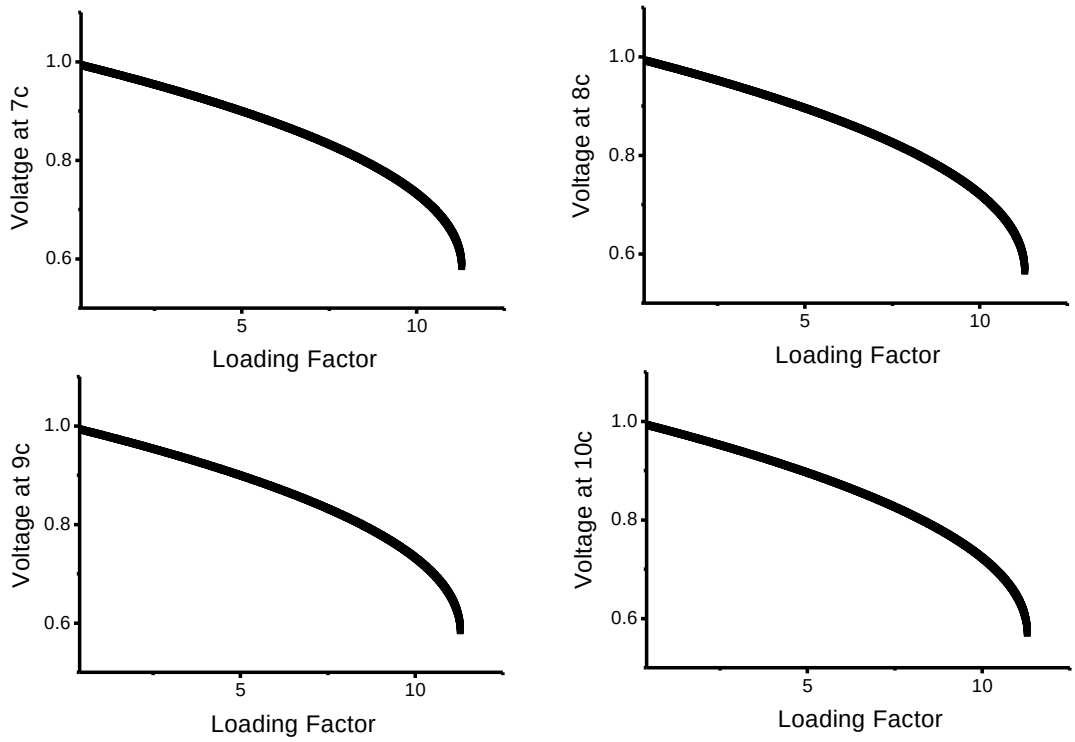

Figure 3.1: Voltage profile of Bus 7c, 8c, 9c, and 10c of CASE13 for different loading condition.

From Figures 3.2 and 3.3, it can be seen that the voltages start reducing rapidly

after loading factor of 11 and voltage collapses at loading factor of 12.612. Therefore, loading factor of 12.612 is the critical point of CASE25 under given operating condition.

3.5 Summary

The SS algorithm has been proposed in this chapter. The SS algorithm is an unconstrained optimization algorithm that can be used to calculate initial seed for the conventional PF algorithms. SS based initial seed can not be the competitor to the flat start used in conventional algorithms but it becomes necessary to use this in the situations where flat start does not converge. From the extensive analysis of the proposed approach, it can be concluded that this approach improves the performance of the conventional algorithm on the heavily loaded and ill-conditioned test systems.

In this chapter, a PF problem is also formulated as a COP to compute the PF solutions of the system at critical points (notch points). To solve this non-convex and highly non-linear COP, the BCO algorithm is proposed for PF. BCO is able to provide multiple solutions specially low voltage solutions for the PF problems. From the extensive study of the performance of BCO as a PF tool, it can be concluded that the BCO can provide continuation PF solutions for the distribution networks.

In the case of the islanded operation of microgrids, the system frequency and power generations at a distribution generation are not pre-defined before PF analysis. Therefore, the proposed algorithms of this chapter cannot be applicable to the PF problems of islanded microgrids. In the next chapter, novel algorithms are proposed to solve the PF problems of islanded microgrids.

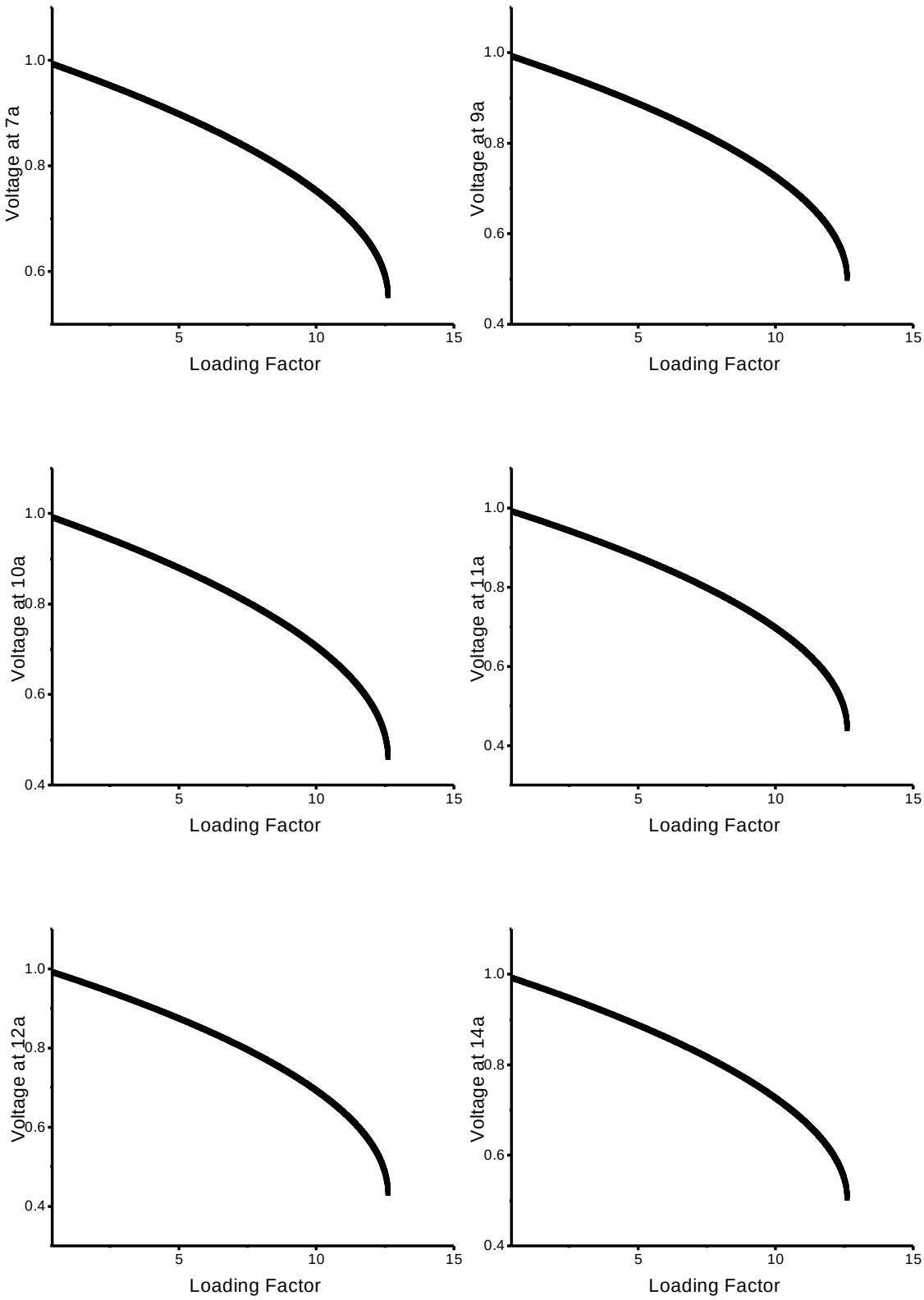

Figure 3.2: Voltage profile of Bus 7a, 9a, 10a, 11c, 12a and 14c of CASE25 for different loading condition.

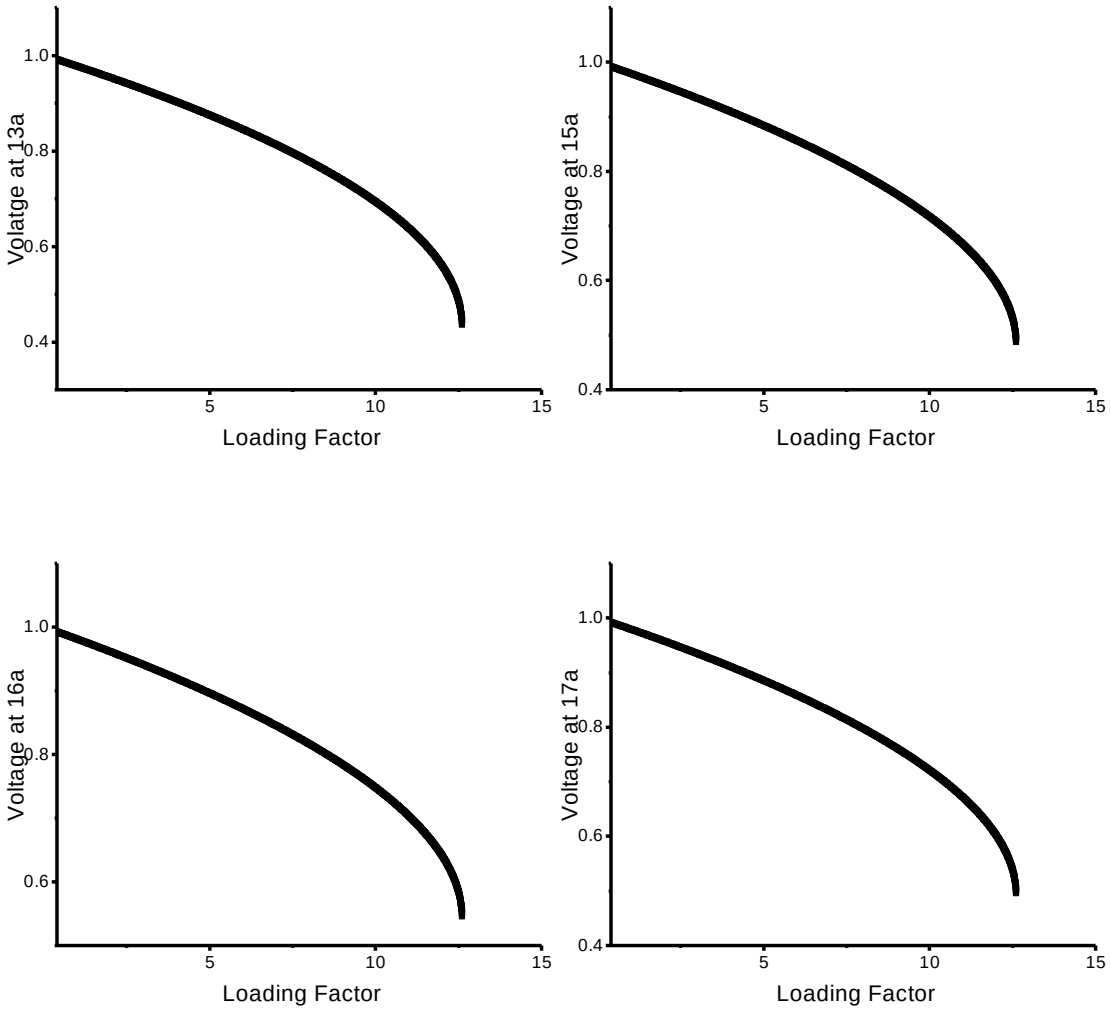

Figure 3.3: Voltage profile of Bus 13a, 15a, 16a, and 17a of CASE25 for different loading condition.

Chapter 4

Power Flow Algorithms for Islanded Microgrids

4.1 Introduction

The PF analysis of DCIMGs is a growing research area. Several algorithm have been proposed to solve the PF problem of the DCIMG. The conventional PF techniques have issues in handling DCIMG due to the nonexistence of reference bus (slack bus) in the system. To address this issue, different novel algorithms are proposed in this chapter for solving the PF problem of DCIMG.

The smart grid architecture based electrical distribution systems are mainly distinguished by higher penetration of DGs. In microgrids, this increasing penetration of DGs with adequate generation can bear the active and reactive power requirement for all or most of its local loads. According to US Department of Energy definition of a microgrid "A group of interconnected loads and distributed energy resource within clearly defined electrical boundaries that acts as a single controllers entity with respect to the grid and that connects [to] and disconnects from such [a] grid to enable it to operate in both grid-connected and island mode" [160].

For the operational analysis of microgrid, there is a requirement of suitable PF tool. In islanded microgrid system, operating frequency value is not constant thus frequency is also a PF variable and Ybus is also not constant due to the reactance of the lines being frequency dependent [93, 161–163]. In a conventional grid-connected system, DGs buses are working as a PQ or PV buses and the excess power is fed from the slack

bus [56,94,95,164]. But such phenomena are not applicable in the islanded system because there is no slack bus in the system. Thus, conventional PF method is not applicable in islanded microgrid [165, 166].

To determine the PF solution for DCIMG, new algorithms have been introduced. These techniques have considered linear equations of the droop characteristics of DGs. The NTR method has been proposed [56] to solve equations obtained after consolidating (i) linear droop bus equations, and (ii) PF equation. In [94], a new PF method that employs PSO is introduced to solve the PF problem of DCIMG. The modified NR method has been used in [2] to solve the power flow problem of DCIMG.

In literature, several works address the power flow problem of a DCIMG. However, these works cannot be applied effectively to the PF problem of DCIMG.

This chapter proposes new algorithms for solving the PF problem of DCIMG using different approaches. In these approaches, any droop bus is considered as an Angle Reference (AR) bus and voltage magnitude of this AR bus and operating system frequency are updated according to the droop characteristics of DGs in the outer loop of the algorithms. Voltages of all buses except AR bus are updated in every iteration by solving the non-linear current-injection based power flow equations. To verify the execution of the proposed power flow approaches on power flow problem of a DCIMG, the outcomes have been compared with the outcomes of optimization algorithm NTR [56], PSCAD [167], MNR algorithm, Direct Backward/Forward Sweep (DBFS) algorithm , and Modified Backward/Forward Sweep (MBFS) algorithm [2].

To sum up, the major contributions of the present work are as follows:

1. This chapter proposes current-injection based NR algorithm, and Nested Backward/Forward Sweep (NBFS) algorithm to solve the PF problem of DCIMG.

2. The proposed algorithms overcome the issues and limitations of NR-based algorithms MNR and NTR, and the need for a gradient of the Ybus with respect to frequency in the Jacobian matrix. The proposed algorithm updates the system frequency in every loop without using the gradient of the Ybus or any other variable with respect to frequency.

3. A closed loop formulation is proposed to evaluate the values of voltage magnitude of AR bus and system frequency, which results in fast convergence in the algorithm.

4. In this chapter, approach of closed loop design has been investigated for convergence through various tests, designed for the purpose.

5. This chapter also investigates the robustness and efficacy of the proposed algorithm for ill-conditional test systems having higher loading conditions and r/x ratios.

4.2 Modeling of Distributed Generations and Different Loads

The modeling of the system components influences the PF solutions. The models of DG and loads are presented in the following subsection.

4.2.1 Modeling of Distributed Generation

The penetration of DGs has been increasing commonly in the distribution systems. A wide category of technologies viz. wind turbines, photovoltaic systems, energy storage systems, fuel cells, and micro-turbines have been incorporated as types of DGs. Consequently, there is a requirement of modeling schemes to handle these DGs in the power flow analysis of DCIMG systems. The electrical characteristics of DGs are based on energy converter utilized in them. The different models for DG are proposed in literature based on electrical characteristics such as constant voltage model (PV), voltage-dependent power factor model (PQ(v)), constant current model (PI), and constant power factor model (PQ), as shown in Table 4.1. In a DCIMG operating mode, these DG units with battery energy storage systems and droop controllers are designed to control the system frequency and voltage while sharing the load demand [168]. In DCIMGs, droop-controlled DG units are designed to imitate the droop characteristics of synchronous generators operating in parallel. Generally, conventional droop settings are capable of providing accurate power-sharing among DG units in DCIMGs.

To model the DGs, based on the output impedance seen by the DGs and r/x ratio of the line, three different droop equations (conventional droop, inverse droop and mixed droop) are considered [104,105]. For the inductive network, DGs operating in conventional droop [163, 169] can be modelled as:

$$|V_k| = |V_{0,k}| - n_k(Q_{G,k} - Q_{0,k}) \tag{4.1}$$

Table 4.1: Component modelling of microgrid in Power Flow algorithm

Primary Energy Resource	Energy Conv.	Model	
		Grid Connected	Islanded
Wind turbine	Double feed induc. gen.	PQ	droop
	Syn. Gen. (Slip control)	PQ	droop
Photo-voltaic system	Current/voltage controlled inverter	PV	droop
Fuel cell	St. pwr. conv. (voltage controlled)	PV	droop
CHP	St. pwr. conv. (power factor controlled)	PQ	droop
	St. pwr. conv. (voltage controlled)	PV	droop
Energy storage	St. pwr. conv. (voltage controlled)	PV	droop
Gas Turbine	St. pwr. conv. (voltage controlled)	PV	droop
Microturbine	Induc. Gen. + St. pwr. conv.	PQ	droop
Geothermal/Ocean Energy/ I.C Engine	Syn. Gen. (Constant Excit. Voltage)	PQ	droop

$$\omega = \omega_0 - m_k(P_{G,k} - P_{0,k}) \tag{4.2}$$

where,

$P_{G,k}$ and $Q_{G,k}$ are the active and reactive power output of k^{th} DG respectively. n_k and m_k are the voltage and frequency droop coefficients of k^{th} DG respectively. $Q_{0,k}$ and $P_{0,k}$ are the power set points at k^{th} DG respectively.

For the resistive network, DGs operating in inverse droop [170, 171] can be modelled as:

$$|V_k| = |V_{0,k}| - n_k(P_{G,k} - P_{0,k}) \tag{4.3}$$

$$\omega = \omega_0 - m_k(Q_{G,k} - Q_{0,k}) \tag{4.4}$$

In practical applications, different DGs can be located a little far from each other and can be paralleled through lines, which contain significant line impedances. The performance of above-mentioned droop characteristics (for fully resistive and fully inductive case) is not satisfactory in case complex impedance and power-sharing among the DGs is not efficient due to active and reactive power coupling. Hence, a mixed droop characteristics [104, 105] is considered. Modelling of DG operating in mixed droop can be expresses as;

$$|V_k| = |V_{0,k}| - n_k(P_{G,k} + Q_{G,k}) \tag{4.5}$$

$$\omega = \omega_0 - m_k(P_{G,k} - Q_{G,k}) \tag{4.6}$$

A dominant DG (typically synchronous generator based DGs) can be operated in isochronous mode, thereby functioning as a non-ideal slack bus i.e., providing constant

frequency and voltage at its terminals regardless of the connected load. Other DGs can operate according to their droop settings. To model isochronously controlled DG, the same droop equations can be adopted by setting droop coefficients to zero, i.e., $|V_k| = |V_{0,k}|$ and $\omega = \omega_0$.

In this chapter, two parameter x and y are considered to obtain all above-mentioned four droop equation of DGs in single composite droop equation. This single composite droop equation can be written as follows:

$$\omega = \omega_0 - m_k(x_k(P_{G,k} - P_{0,k}) - y_k(Q_{G,k} - Q_{0,k})) \tag{4.7}$$

$$|V_k| = |V_{0,k}| - n_k(y_k(x_k(P_{G,k} - P_{0,k}) + x_k(Q_{G,k} - Q_{0,k})) \tag{4.8}$$

In equations (4.7) and (4.8), values of x and y are considered to be either 1 or 0. Hence, there are four possible combination of x and y and each combination represents different droop operation of DGs. If $x = 1$ and $y = 0$, the droop equations are reduced to equations 4.1 and 4.2 i.e. the conventional droop. While $\{x, y\} = \{0, 1\}$ and $\{x, y\} = \{1, 1\}$ represents the inverse droop and mixed droop operation respectively. The last combination, $\{x, y\} = \{0, 0\}$, represents that the DG is acting either as a isochronously controlled or it is operating in grid connected system.

4.2.2 Load Modelling

In static load model, active and reactive power absorbed by the load depends upon the bus voltage and system frequency. Voltage and frequency based active and reactive loads can be represented as given in equations (4.9) and (4.10) respectively.

$$P_{l,k} = P_{0,l,k}(a_p + b_p|V_k| + c_p|V_k|^2 + d_p|V_k|^{\alpha})(1 + e_p(\omega - \omega_0)) \tag{4.9}$$

$$Q_{l,k} = Q_{0,l,k}(a_q + b_q|V_k| + c_q|V_k|^2 + d_q|V_k|^{\beta})(1 + e_q(\omega - \omega_0)) \tag{4.10}$$

where, $a_p + b_p + c_p + d_p = 1$ and $a_q + b_q + c_q + d_q = 1$; ω_0 is the nominal system frequency; e_p and e_q are the frequency dependability coefficient for active and reactive load respectively; ω is the operating system frequency; $P_{0,l,k}$ and $Q_{0,l,k}$ are active and reactive load demand at bus k, when system is operating at nominal frequency and bus voltage; α and β are the active and reactive power exponents respectively.

Nowadays, a large number of Plug-in Hybrid Electric Vehicles (PHEVs) are connected to the modern distribution system. The influence of PHEV loads can be estimated by using different models based on their electrical characteristics which are mainly depended on their different charging operations of the chargers. In this chapter, three different voltage-dependent load models of PHEVs are considered for power flow analysis of DCIMG.

The first type of PHEV load model is represented by a polynomial load (PHEVI) model. In PHEVI, active and reactive power are represented by the following equations.

$$P_{EVI,k} = P_{0,EVI,k}(a_p + b_p|V_k| + c_p|V_k|^2), \tag{4.11}$$

and

$$Q_{EVI,k} = Q_{0,EVI,k}(a_q + b_q|V_k| + c_q|V_k|^2). \tag{4.12}$$

PHEVI has coefficients a_q, b_q, and c_q for the reactive power and a_p, b_p, and c_p for the active power.

In case of the second type of PHEV load model, active power and reactive power are represented by using equations 4.13 and 4.14, respectively considering fast charging station as defined in [172].

$$P_{EVII,k} = P_{0,EVII,k}(a_p + b_p|V_k|^{\alpha}), \text{and} \tag{4.13}$$

$$Q_{EVII,k} = P_{EVII,k}tan(\theta), \tag{4.14}$$

where, a, b, and α represent power constant, exponent constant, and exponent of the voltage magnitude, respectively.Parameter θ is power factor which is equal to 0.97 [172].

The third type of PHEV load model, PHEVIII, is represented by the constant current load. In this case, reactive power and active power are obtained by using polynomial load model, where $P_{EVIII,k}$ of PHEVIII is calculated as follows.

$$P_{EVIII,k} = P_{0,EVIII,k}|V_k|^2, \text{and} \tag{4.15}$$

reactive power,

$$Q_{EVIII,k} = 0. \tag{4.16}$$

The above defined PHEV load models can be handled by using equations (4.9) and (4.10).

4.3 Current Injection Newton-Raphson Algorithm for DCIMG

In this section, a novel algorithm, called CINR, is introduced to solve the PF problem of DCIMG.

In the case of DCIMGs, conventional PF techniques cannot solve the PF problem to provide the steady-state value of system variables for further investigation. In MNR and NTR, some elements of the Jacobian matrix contain the derivative of elements of the bus admittance matrix with respect to the frequency. Reference [2] (where MNR is proposed) provides a brief description of the calculation procedure of the Jacobian matrix. However, in [2], the mutual coupling of the line parameter has not been addressed in the computation procedure of derivative of elements of the bus admittance matrix. In the case of DCIMG having a mutual coupling of the line parameter, we cannot calculate the derivative of the admittance matrix analytically. In such cases, finite difference approximation of the derivatives can be used in place of the analytical derivative, but finite difference step size is to be chosen properly so that the convergence property of Newton-based algorithms [173] is maintained. Various methods have been proposed to select the value of finite difference step-size [173], but these methods increase the time and space complexity of the algorithm and it may also be impractical to solve the power flow problem of a large DCIMG system using these algorithms.

It is interesting to note that non-derivative based PF techniques, DBFS [98] and MBFS [174], are also proposed to solve the power flow problem of DCIMG and they use inner and outer loop approach to update the frequency and voltage magnitude of the slack bus. A similar approach, loop-based frequency update technique, is also given with NR algorithm in [101] to solve the PF problem of DCIMG, but this approach cannot handle the high r/x ratio of the lines.

It is observed that an update of the system frequency separately outside the structure of NR-based algorithms provides better performance on PF problem for DCIMG system having mutually coupled line as compared to the finite difference based approaches. However, a robust and efficient approach for updating the system frequency has not been investigated for existing NR-based algorithms for PF problem of DCIMG system having mutually coupled line impedances. So a new NR-based algorithm, called CINR, with a

loop-based approach to update the frequency is proposed in this work to address this issue.

4.3.1 Classification of Bus-Types

In order to formulate the PF formulation of DCIMG, the primary step is to classify the buses operating in the system. In proposed formulation, classification of buses as follows.

1. Droop bus: The buses where droop controlled DGs are connected.
2. AR bus: One of the droop buses is selected as AR bus.
3. PQ bus: The buses where active and reactive powers are known.
4. PV bus: The buses where voltage magnitude and active power are known.

It is to be noted that an AR bus is needed to provide a reference for the voltage angles of the other buses; voltage angle of AR bus is assummed zero.

4.3.2 Current-injection based Power Flow Formulation

The current mismatch equations are given as follows.

$$\triangle I_{r,i} = \sum_{i=1}^{Nbus} (G_{ij}V_{r,j} - B_{ij}V_{m,j}) - \frac{V_{r,i}P_k^{sp} + V_{m,i}Q_k^{sp}}{V_{r,i}^2 + V_{m,i}^2} = 0 \tag{4.17}$$

$$\triangle I_{m,i} = \sum_{i=1}^{Nbus} (B_{ij}V_{r,j} + G_{ij}V_{m,j}) - \frac{V_{m,i}P_k^{sp} - V_{r,i}Q_k^{sp}}{V_{r,i}^2 + V_{m,i}^2} = 0 \tag{4.18}$$

where P_k^{sp} and Q_k^{sp} are the specified real and reactive power injection at bus k respectively. G_{ij} and B_{ij} are the real and imaginary part of the $\{i,j\}^{th}$ element of bus admittance matrix $(Y - bus)$. While, $V_{r,j}$ and $V_{m,j}$ are respectively the real and imaginary part of voltage of the j^{th} bus . Assuming the slack bus as an AR bus, the current mismatches are calculated for the remaining buses as follows:

$$\triangle = [\triangle I_r^T \triangle I_m^T]^T \tag{4.19}$$

Calculation procedure of $\triangle I_r$ and $\triangle I_m$ for different types of buses is given in [22]. To calculate the Jacobian matrix, equations (4.17) and (4.18) are differentiated with respect

to real and imaginary part of all the bus voltages. For system having all four type of buses, the Jacobian matrix, J, is represented as follows.

$$J = \begin{bmatrix} J_{dr-dr} & J_{dr-pq} & J_{dr-pv} \\ J_{pq-dr} & J_{pq-pq} & J_{pq-pv} \\ J_{pv-dr} & J_{pv-pq} & J_{pv-pv} \end{bmatrix} \tag{4.20}$$

The elements of sub-matrices of the Jacobian matrix are given in Table (4.2). After

Table 4.2: Representation of elements of Jacobian Matrix

Diagonal Element	
J_{dr-dr}	$J1 = G_{kk} - \frac{P_{g,k}(V_{m,k}^2 - V_{r,k}^2) - 2V_{r,k}V_{m,k}Q_{g,k}}{V_k^4} - \frac{V_{r,k}}{V_k^3}\left(\frac{y_k V_{r,k}}{m_k x_k^2 + n_k y_k^2} + \frac{x_k V_{m.k}}{n_k x_k^2 - m_k y_k^2}\right)$
	$J2 = -B_{kk} - \frac{Q_{g,k}(V_{r,k}^2 - V_{m,k}^2 - 2V_{r,k}V_{m,k}P_{g,k})}{V_k^4} - \frac{V_{m,k}}{V_k^3}\left(\frac{y_k V_{r,k}}{m_k x_k^2 + n_k y_k^2} + \frac{x_k V_{m,k}}{n_k x_k^2 - m_k y_k^2}\right)$
	$J3 = B_{kk} - \frac{Q_{g,k}(V_{r,k}^2 - V_{m,k}^2) - 2V_{r,k}V_{m,k}P_{g,k}}{V_k^4} - \frac{V_{m,k}}{V_k^3}\left(\frac{y_k V_{m,k}}{m_k x_k^2 + x_k y_k^2} - \frac{x_k V_{r,k}}{n_k x_k^2 - m_k y_k^2}\right)$
	$J4 = G_{kk} - \frac{P_{g,k}(V_{r,k}^2 - V_{m,k}^2) + 2V_{r,k}V_{m,k}Q_{g,k}}{V_k^4} - \frac{V_{r,k}}{V_k^3}\left(\frac{y_k V_{m,k}}{m_k x_k^2 + n_k y_k^2} - \frac{x_k V_{r,k}}{n_k x_k^2 - m_k y_k^2}\right)$
J_{pq-pq}	$J_1 = G_{kk} - \frac{(P_k^{sp})(V_{mk}^2 - V_{rk}^2) - 2V_{rk}V_{mk}(Q_k^{sp})}{V_k^4} + \frac{-P_{0k}V_{rk}^2(\beta_p + 2\gamma_p V_k) - Q_{0k}V_{rk}V_{mk}(\beta_q + 2\gamma_q V_k)}{V_k^3}$
	$J_2 = -B_{kk} - \frac{(Q_k^{sp})(V_{rk}^2 - V_{mk}^2) - 2V_{mk}V_{rk}(P_k^{sp})}{V_k^4} + \frac{-P_{0k}V_{rk}V_{mk}(\beta_p + 2\gamma_p V_k) - Q_{0k}V_{mk}^2(\beta_q + 2\gamma_q V_k)}{V_k^3}$
	$J_3 = B_{kk} - \frac{(Q_k^{sp})(V_{rk}^2 - V_{mk}^2) - 2V_{mk}V_{rk}(P_k^{sp})}{V_k^4} + \frac{-P_{0k}V_{mk}^2(\beta_p + 2\gamma_p V_k) + Q_{0k}V_{rk}V_{mk}(\beta_q + 2\gamma_q V_k)}{V_k^3}$
	$J_4 = G_{kk} - \frac{(P_k^{sp})(V_{rk}^2 - V_{mk}^2) + 2V_{rk}V_{mk}(Q_k^{sp})}{V_k^4} + \frac{-P_{0k}V_{mk}^2(\beta_p + 2\gamma_p V_k) + Q_{0k}V_{rk}V_{mk}(\beta_q + 2\gamma_q V_k)}{V_k^3}$
J_{pv-pv}	$J_1 = -B_{kk} - \frac{V_{mk}I_{rk}^{calc} - V_{rk}I_{mk}^{calc}}{V_k^2} - \frac{V_{mk}}{V_{rk}}\left(G_{kk} - \frac{P_k^{sp}}{V_k^2}\right)$
	$J_2 = -\frac{V_{mk}}{V_k^2}$
	$J_3 = G_{kk} + \frac{P_k^{sp}}{V_k^2} - \frac{V_{mk}}{V_{rk}}\left(B_{kk} - \frac{V_{mk}I_{rk}^{calc} - V_{rk}I_{mk}^{calc}}{V_k^2}\right)$
	$J_4 = \frac{V_{rk}}{V_k^2}$

Off-diagonal Elements			
J_{dr-dr}, J_{dr-pq},	$J1 = G_{km}$	J_{dr-pv}	$J1 = -B_{km} - \frac{V_{m,k}}{V_{r,k}}G_{km}$
J_{pq-dr}, J_{pq-pq},	$J2 = -B_{km}$	J_{pq-pv}	$J2 = 0$
J_{pv-dr}, J_{pv-pq},	$J3 = B_{km}$	J_{pv-pv}	$J3 = G_{km} - \frac{V_{m,k}}{V_{r,k}}B_{km}$
	$J4 = G_{km}$		$J4 = 0$

calculating the Jacobian Matrix in $(i+1)^{th}$ iteration, the real and imaginary part of bus voltages can be calculated by using following equation.

$$v^{i+1} = v^i + J^{-1}\triangle, \tag{4.21}$$

where

$$v = [V_r^T V_m^T]^T, \tag{4.22}$$

and V_r and V_m are the vectors of real and imaginary parts of voltages of all the system buses except the AR bus.

It is worth mentioning that the NR algorithm can be utilized to solve the PF of DCIMG as proposed in [2, 56, 99, 100] and [101]. For CINR to be able to solve the PF of islanded microgrid implemented with the droop control, few aspects need to be discussed. Firstly, the voltage magnitude of the AR bus is not fixed. Secondly, the system frequency is variable. To resolve these issues, this chapter introduces an iterative approach to update the system frequency and voltage magnitude of AR bus.

4.3.3 Update of the System Frequency and AR Bus Voltage

To determine the PF of DCIMG using CINR algorithm, AR bus is assumed as slack bus. So, the operating states (voltage magnitude) of the AR bus and system frequency must be fixed prior to applying the CINR for performing PF analysis. To address this issue, a loop of operations is proposed in this paper. The objective of this loop is to regulate the voltage of the AR bus and system frequency in order to satisfy the droop characteristics of DCIMG.

The proposed loop-based methodology is shown in figure 4.1 and following steps are performed to solve the PF problem of droop control based islanded microgrids using CINR.

1. At the first step, the initial operating condition is determined. In this step, one droop bus is selected as an AR bus. Variables ω_{grid} and V_s are initialized on their nominal value, ω_0 and $V_{0,s}$ respectively.

2. Afterward, calculate the bus admittance matrix at the system frequency ω_{grid}. In addition, the scheduled generation of active and reactive power at droop buses are calculated using equations (4.7) and (4.8)

3. In this step, PF analysis is done using the CINR algorithm. The main aim of this step is to determine the total injected real and reactive powers in all droop buses including AR bus. These injected real and reactive powers will be further used to update the system frequency and voltage magnitude at AR bus.

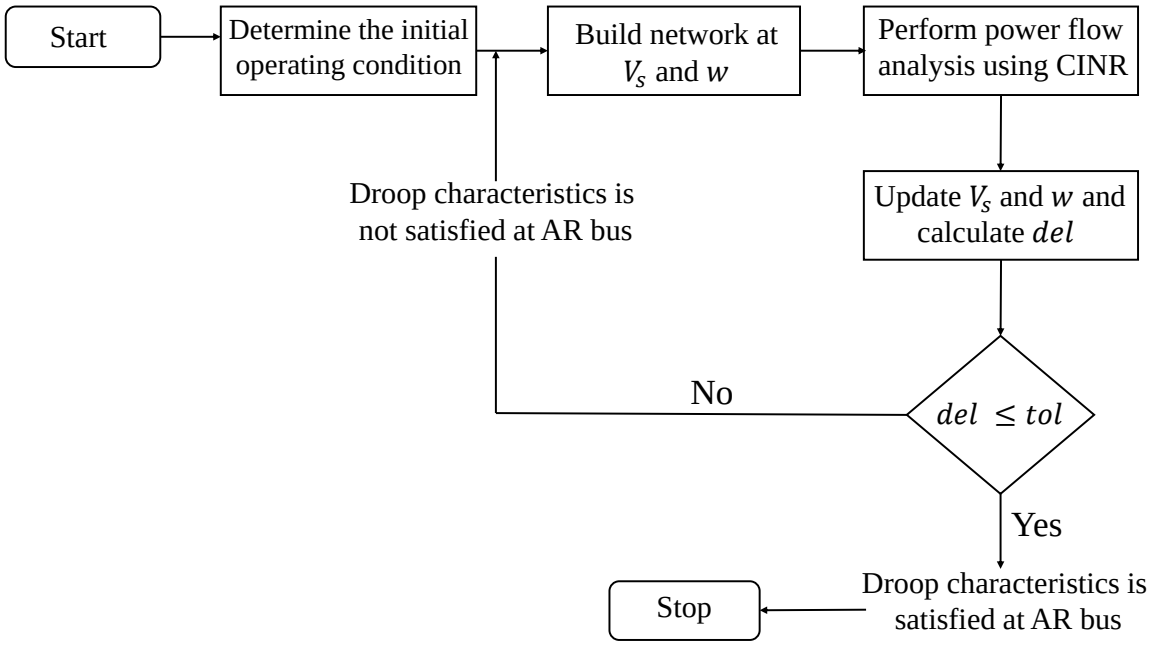

Figure 4.1: Flow chart of CINR

4. In this approach, the system frequency is updated using following equation.

$$w_{grid}^{i+1} = w_0 - \left(\sum_{k=1} \frac{1}{m_k(x_k P_{G,k} - y_k Q_{G,k})} \right)^{-1} \tag{4.23}$$

5. The magnitude of voltage at AR bus is updated as follows.

$$V_s^{i+1} = (1-\alpha)(V_s^i) + \alpha(|V_{0,s}| - n_s(y_s P_{G,s} + x_s Q_{G,s})) \tag{4.24}$$

6. After updating the system frequency and voltage magnitude of AR bus, a variable *del* is calculated using equation (4.25) to check the termination criteria.

$$del = max\{|w_{grid}^{i+1} - w_{grid}^{i}|, |V_s^{i+1} - V_s^i|\} \tag{4.25}$$

7. If the value of *del* is smaller than the pre-specified tolerance, the iterative loop is terminated and the previous PF results are selected as the final PF solution.

8. While, if the value of *del* is not smaller than tolerance, the next loop is performed with updated values and this procedure continues until the value of *del* becomes smaller than the tolerance.

Table 4.3: Data required for modeling of the six bus test system in time-domain

m_p (rad/s/W)	n_q (V/VAR)	w^* (rad/sec)	V^* (V)
$9.4E-05$	$1.3E-03$	377	127

Line parameters			
From bus	To bus	$R_{line}(\Omega)$	$L_{line}(mH)$
1	2	0.43	0.32
1	4	0.30	0.35
2	5	0.20	0.25
2	3	0.15	1.84
3	6	0.05	0.05

Load parameter		
bus number	$R_{load}(\Omega)$	$L_{load}(mH)$
1	6.95	12.20
3	5.01	9.40

4.3.4 Validation of CINR

To confirm the applicability and accuracy of the proposed power flow algorithm, the obtained results are compared with the time-domain model of a droop control based islanded microgrid. For algorithm validation, a six-bus test system (shown in Fig. (4.5)) is considered. The detailed time domain model of this system has been simulated in PSCAD/EMTDC, a time-domain simulation environment as discussed in [163] and [169]. The data used to model this system in time-domain is presented in Table-4.3 . This system has three droop control based DG which are working in an islanded mode.

To solve the power flow of this test system using CINR, the algorithm has been developed in MATLAB. The result obtained from PSCAD and CINR are depicted in Table-4.4. As shown in Table-4.4, the maximum errors in voltage magnitude and angle are 0.0081% and 0.26% respectively. This good agreement within the obtained results validates the accuracy of the CINR in solving the power flow of droop control based islanded MG. Moreover, PSCAD requires approximately 172s to attain the steady-state, while the CINR requires 0.04s.

Table 4.4: Validation of results obtained for six-bus test system.

Bus	Voltage magnitude (V)		Angle (rad)		Active Power (kw)		Reactive Power (kvr)	
	PSCAD	CINR	PSCAD	CINR	PSCAD	CINR	PSCAD	CINR
1	121.92	121.92	0.0078	0.0078	-0.0189	-0.0189	-0.0125	-0.0125
2	123.51	123.51	-0.0013	-0.0013	0	0.000	0	0.0000
3	122.42	122.42	-0.0388	-0.0389	-0.0253	-0.0253	-0.0179	-0.0179
4	125.37	125.37	0.0065	0.0065	0.0151	0.0151	0.0075	0.0075
5	125.74	125.74	0*	0*	0.0151	0.0151	0.0058	0.0058
6	123.11	123.10	-0.0420	-0.0421	0.0151	0.0151	0.0179	0.0179
err	0.0081%		0.26%		0.0005%		0.0003%	
freq	376.6645	376.6645						
Time	172s	0.04s						

4.3.5 Performance Analysis of CINR

Comparison of CINR with MNR and NTR

In this section, four radial (CASE6, CASE22, CASE38, and CASE69) and one meshed (CASE160) distribution systems are considered to compare the results obtained from CINR with the results obtained from MNR and NTR. The extensive data of these test systems are reported in Appendix-II. Four different cases including: 1) conventional droop, 2) inverse droop, 3) mixed droop, and 4) isochronous mode of operation are studied to demonstrate the robustness of the proposed algorithm for the different operating modes of droop-based DGs.

All the algorithms are executed on MATLAB R2017b in PC with an INTEL Core i7 @ 3.2 GHz, 8 GB of RAM. The flat start is considered as an initial solution in all algorithms (for operating frequency the flat start is 1.0 p.u.). The stopping criteria for all the algorithms are same and selected in a way that either the gradient norm or the total number of iterations does not exceed the specified value. The solutions for CASE22, CASE38, and CASE69 including bus powers have been given in appendix IV.

It is to be noted that the NTR algorithm is implemented only for case 1 and MNR is not implemented for case 4 (isochronous operation). Therefore, the power flow results for these cases are not available. For case 1 (conventional droop), all the algorithms are applicable and the power flow results obtained from the algorithms are similar except MNR which fails to provide a solution in case of CASE69 and CASE160. Similarly, in cases 2, 3, and 4, CINR and MNR provide similar power flow results for CASE22, and CASE38 but MNR fails to provide a solution for CASE69 and CASE160. For case 5, only

Table 4.5: Computation time required to solve power flow for different cases considering CINR, MNR and NTR algorithm. (NC: Not Converged, NA: Not Applicable, CT: Computation Time, %: Percentage improvement in computation time.)

System	Cases	CINR	MNR		NTR	
		CT(s)	CT(s)	%	CT(s)	%
CASE22	1	4.96E-03	6.35E-02	1180.16	1.77E-02	256.63
	2	5.58E-03	4.84E-02	767.82	NA	NA
	3	4.22E-03	4.98E-02	1080.50	NA	NA
	4	3.81E-03	NA	NA	NA	NA
CASE38	1	2.22E-02	1.46E-01	556.68	3.48E-02	56.83
	2	1.42E-02	1.59E-01	1020.27	NA	NA
	3	2.28E-02	1.64E-01	621.31	NA	NA
	4	2.36E-02	NA	NA	NA	NA
CASE69	1	1.33E-02	NC	NC	1.43E-01	970.79
	2	1.72E-02	NC	NC	NA	NA
	3	1.82E-02	NC	NC	NA	NA
	4	1.81E-02	NA	NA	NA	NA
CASE160	1	6.08E-02	NC	NC	5.10E-01	738.64
	2	4.99E-02	NC	NC	NA	NA
	3	4.47E-02	NC	NC	NA	NA
	4	6.03E-02	NA	NA	NA	NA

CINR can provide the power flow solutions because MNR and NTR are not defined for an isochronous mode of operation.

To analyze the performance of MNR, NTR, and CINR in terms of computation time, the time required to obtain the power flow solution is recorded for all the cases and reported in Table 4.9. It is found that expected execution time for the cases CASE22 and CASE38, CINR is almost 10 times faster than MNR. Similarly, CINR is approximately 3, 2, and 9 times faster than NTR for the cases CASE22, CASE38, and CASE69, respectively.

From the above analysis, it can be concluded that the solutions obtained by CINR converges faster in comparison to MNR and NTR without compromising the accuracy. Additionally, CINR can also be used to perform power flow analysis for the systems

having DGs with several types of droop characteristics including the isochronous mode of operation.

Robustness of CINR

The performance of power flow algorithms depends on the r/x ratio of lines and the loading condition of the system. Hence, it is also desired to investigate the robustness of the proposed algorithm for different system loading conditions and various r/x ratio of lines. The CASE38 is considered for the study which has a radial structure with lines having a high r/x ratio and zone wise voltage dependent loads. The performance of CINR, MNR, and NTR in terms of computation time for different r/x ratios of line and system loading condition is shown in Figures (4.2) and (4.3) respectively. It is clear from Figures (4.2) and (4.3) that the CINR requires less computation time to obtain the power flow solution of CASE38 for different cases, while MNR requires more computation time as MNR is not designed to deal with the voltage dependent loads.

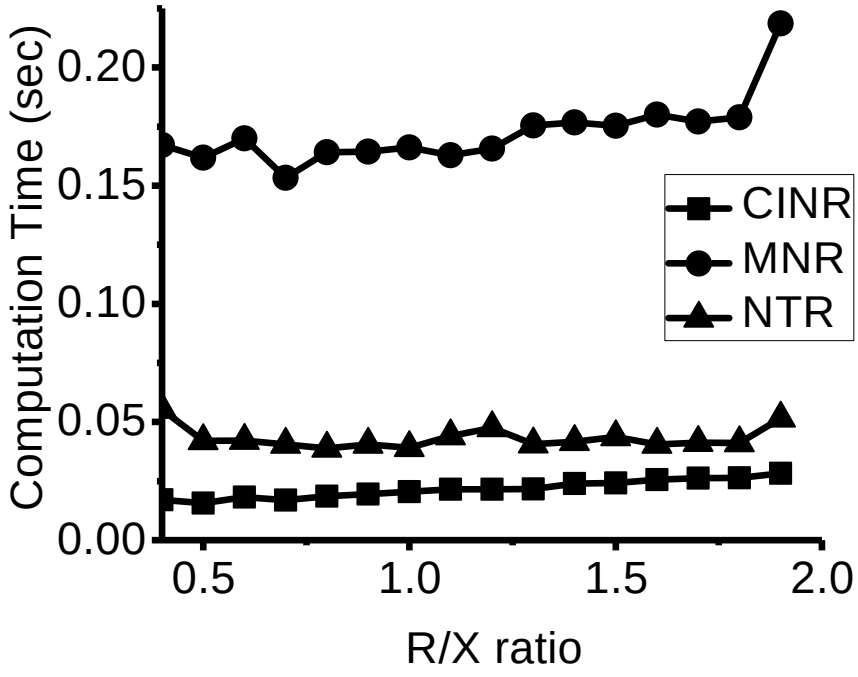

Figure 4.2: r/x ratio vs computation time (sec) for CASE38 test systems.

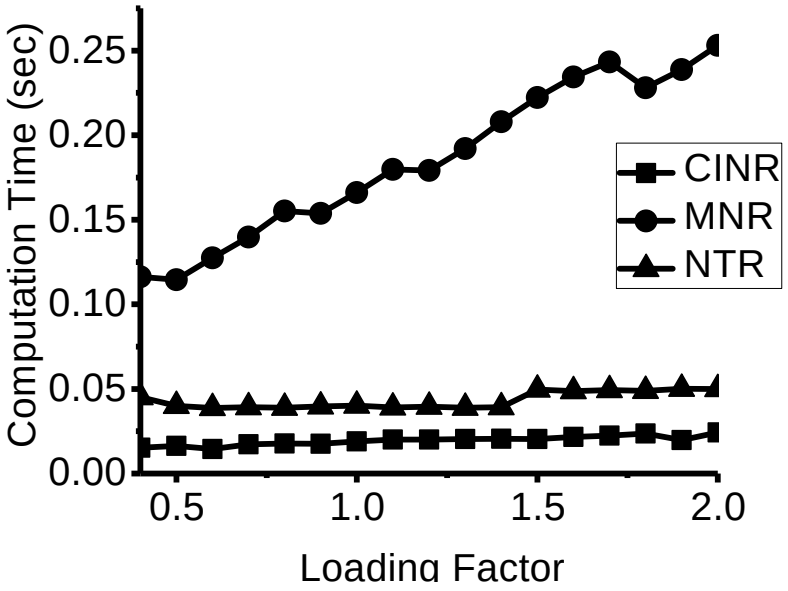

Figure 4.3: Loading factor vs computation time (sec) for CASE38 test systems.

4.4 Nested Backward/Forward Sweep Algorithm for DCIMG

In this section, the main steps of the NBFS algorithm is discussed in detailed. The proposed algorithm is divided into three steps: modified backward sweep, modified forward sweep, and system frequency & reference voltage update. To calculate the initial value of the power flow variables, initialization of parameters including system frequency and node voltages are required. Initialization, modified backward sweep, modified forward sweep and the system frequency & reference voltage update procedure are as follows:

4.4.1 Initialization

The first step of initialization is to select one of the droop buses as a AR bus. Then, the system frequency and voltage of every bus are initialized at 1 pu. Tolerance value for both (voltage and frequency) loops are set to 10^{-8}.

4.4.2 Modified Backward Sweep

The backward sweep is the first sweep applied in conventional BFS algorithm. In this sweep, the branch current is calculated based on the assumption that the voltage of all

the buses are known. Therefore, the branch currents are calculated using the apparent power injected to the buses and the bus voltages. In the case of PQ buses, the apparent injected power is calculated as:

$$S_i = P_i + jQ_i = (P_{g,i} - P_{l,i}) + j(Q_{g,i} - Q_{l,i}) \tag{4.26}$$

Since, in the case of droop buses, the generation depends on the bus voltage and the system frequency. To calculate the apparent power at each droop buses equation (4.27) is formulated using equations (4.7), (4.8), and (4.26) which is given as:

$$\begin{aligned} S_i = (P^o_{g,i} + m_{P,i}(w_o - w) - P_{l,i}) + j(Q^o_{g,i} + n_{Q,i}(|V_o| - \\ |V_i|) - Q_{l,i}) \end{aligned} \tag{4.27}$$

The apparent power (calculated as per equation 4.27) is applied to calculate the bus current which is as follows:

$$I_i = \left(\frac{S_i}{V_i}\right)^* \tag{4.28}$$

These bus currents (equation 4.28) are summed in the backward direction from the farthest buses towards the reference bus to calculate the branch currents and this procedure is described using the following equation:

$$[\mathbf{I}_{ij}] = [\mathbf{BIBC}][\mathbf{I}_i] \tag{4.29}$$

where, the transformation matrix **BIBC** is defined in subsection 4.4.4.

4.4.3 Modified Forward Sweep

In conventional algorithm, the forward sweep is applied to update the bus voltages using the calculated branch current of the backward sweep. This step includes the calculation of voltages from the AR bus to lower stream buses using branch impedances and branch currents. In other words, the bus voltages can be also calculated using the reference voltage, branch impedance, and branch current which is represented as:

$$[\mathbf{V}] = [\mathbf{V}_{ref}] - [\mathbf{BCBV}][\mathbf{I}_{ij}] \tag{4.30}$$

where, the transformation matrix BCBV is used to calculate voltages using branch currents and the computation of this matrix is described in detail in subsection 4.4.4. $[\mathbf{V}_{ref}]$ and $[\mathbf{V}]$ represent the voltage of AR bus and rest other buses in the system respectively.

As we know that in the conventional droop control technique, reactive power sharing among the sources are not proportional as per their rating. Due to disproportional reactive power sharing among the sources, there may be a chance that the obtained current reaches very high value in some cases. This may cause a larger deviation in voltage from the operating point. This larger deviation in voltage may diverge the solution. To overcome this issue, a decelerating factor (β) in the voltage update equation is proposed in this paper which is given in equation (4.31).

$$[\mathbf{V}]^{k+1} = (1-\beta)[\mathbf{V}]^{k} + \beta([\mathbf{V}_{ref}] - [\mathbf{BCBV}][\mathbf{I}_{ij}]) \tag{4.31}$$

where, the value of β must be in range of 0 to 1. The role of β is to adjust the length of voltage correction vector ($[\triangle\mathbf{V}]^{k+1} = [\mathbf{V}]^{k} - [\mathbf{V}_{ref}] + [\mathbf{BCBV}][\mathbf{I}_{ij}]$) to overcome the larger deviation in the voltage correction vector. In the manuscript, the value of β is set to 0.5 for all the cases. It is to be noted that the value β is not optimal at 0.5 for every test system. Although, it performs very well on a wide range of problems.

4.4.4 Calculation of BIBC and BCBV

The first step is to calculate the node incidence matrix, A. Upon calculation of A, the matrices **BIBC** and **BCBV** are calculated. The size of matrix A is $(N_b \times N)$ where, N_b and N indicate the number of branches and nodes of the system respectively. The $(i\text{-}j)^{th}$ element of A, a_{ij}, is:

1. $a_{ij} = +1$ when current leaves the node j from branch i
2. $a_{ij} = -1$ when current flows towards the node j from branch i
3. $a_{ij} = 0$ when there is no connection between the node j and branch i

According to the network theory, branch and node currents are associated as:

$$[\mathbf{I}_i] = A^t[\mathbf{I}_{ij}] \tag{4.32}$$

where, $[\mathbf{I}_i]$ and $[\mathbf{I}_{ij}]$ represent the node and branch current vectors respectively and superscript t indicates the transpose of the matrix.

However, in the backward sweep, the branch currents are required to calculate from the bus injected currents. Therefore, from equation (4.32).

$$[\mathbf{I}_{ij}] = (A^t)^{-1}[\mathbf{I}_i] \tag{4.33}$$

where $(\ldots)^{-1}$ indicates the inverse of a matrix.

In general, $N_b \neq N$, so the matrix A is non-invertible. However, in the case of a radial system ($N_b = N - 1$), by eliminating the first column from A, corresponding to AR bus, the branch currents can be directly computed from the node currents. It may be noted that the first column of A (corresponding reference node) can be eliminated because this node is not a participant of the backward process of BFS.

After comparing the equations (4.29) and (4.33), the specific procedure to build **BIBC** on the basis of network theory indicates that $\mathbf{BIBC} = (A^t)^{-1}$.

For the special case of a square incidence matrix A graph theory shows that:

$$[\mathbf{V}_i] = (A)^{-1}[\mathbf{V}_{ij}] \tag{4.34}$$

where, $[\mathbf{V}_i]$ and $\mathbf{V}_{ij}$ indicate the node and branch voltage vector respectively.

$[\mathbf{V}_{ij}]$ can be obtained as:

$$[\mathbf{V}_{ij}] = diag([\mathbf{Z}_{ij}])[\mathbf{I}_{ij}] \tag{4.35}$$

where, $diag([\mathbf{Z}_{ij}])$ indicates the diagonal matrix of the branch impedances. Accordingly, the bus voltages in the forward sweep is calculated as:

$$[\mathbf{V}_i] = [\mathbf{V}_{ref}] - (A)^{-1} diag([\mathbf{Z}_{ij}])[\mathbf{I}_{ij}] \tag{4.36}$$

From equations (4.30) and (4.36), it can be found that $\mathbf{BCBV} = (A)^{-1} diag([\mathbf{Z}_{ij}])$. The detailed description about the formation of the matrices **BIBC** and **BCBV** can be found in [36-37].

4.4.5 Frequency and AR Bus Voltage Update

This step is basically a correction step of system frequency and the reference voltage. The system frequency and voltage of AR bus is a global variable in the case of DCIMGs. Therefore, these values must be adjusted after each iteration until the convergence is reached. The AR bus is also the droop bus but it behaves like the upstream bus. Hence, the droop characteristics of AR bus is also satisfied at the equilibrium state. Based on the mismatch of droop characteristics of AR bus, the value of system frequency and voltage of AR bus is updated. In droop controlled MGs, the system frequency depends on the total active power-sharing of the DGs, where all the DGs behave as a single source with

equivalent frequency droop . The equivalent droop ($m_{P,equ}$) of the system is calculated as:

$$m_{P,equ} = \frac{1}{\sum_{k\epsilon DB} \frac{1}{m_{P,k}}}$$

where, DB is a set of all droop buses and $m_{P,k}$ is a droop coefficient corresponding to $P-\omega$ droop for k^{th} bus. The new system frequency is obtained as:

$$w^{m+1} = w_o - \frac{1}{m_{P,equ}} \left(\sum_{k\epsilon DB} (P^o_{g,k} - P^{m+1}_{g,k}) \right) \tag{4.37}$$

where, m indicates the loop index.

The change in system frequency causes the change in the line reactance which is modified as:

$$X^{m+1}_{ij} = w^{m+1} L_{ij} \tag{4.38}$$

In addition, the net imbalance of voltage droop, $\triangle V$, at the AR bus is used to update the voltage of the AR bus. The $\triangle V$ is calculated using equation (4.39) and the voltage of AR bus is updated using equation (4.40).

$$\triangle V^{m+1} = (V_o - |V_{AR}|^m) + \frac{1}{n_{Q,AR}} \left(Q^o_{g,AR} - Q^{m+1}_{g,AR} \right) \tag{4.39}$$

$$V^{m+1}_{ref} = V^m_{ref} + \alpha \triangle V^{m+1} \tag{4.40}$$

where, V_o is a nominal voltage of AR bus and α is declaration factor whose value lies between 0.3 to 1.5. The flow chart of the proposed algorithm is shown in Fig. (4.4).

4.4.6 Validation of NBFS

In this section, the proposed algorithm NBFS is validated on a small 6-bus test system (Fig. 4.5). Details of the system including droop parameters, line and load data, rated voltage and system frequency is given in Table 4.3. To illustrate its effectiveness and accuracy, the result obtained from the proposed algorithm is compared with the result obtained from the time-domain model of the test system. The NBFS is implemented to obtain the load flow solution of the network. The time-domain model of the test system is simulated in the PSCAD/EMTDC and results are presented in Table 4.6.

The result shows that the NBFS provides a similar corresponding value of voltage and angle in comparison to the solution obtained from PSCAD/EMTDC which shows the

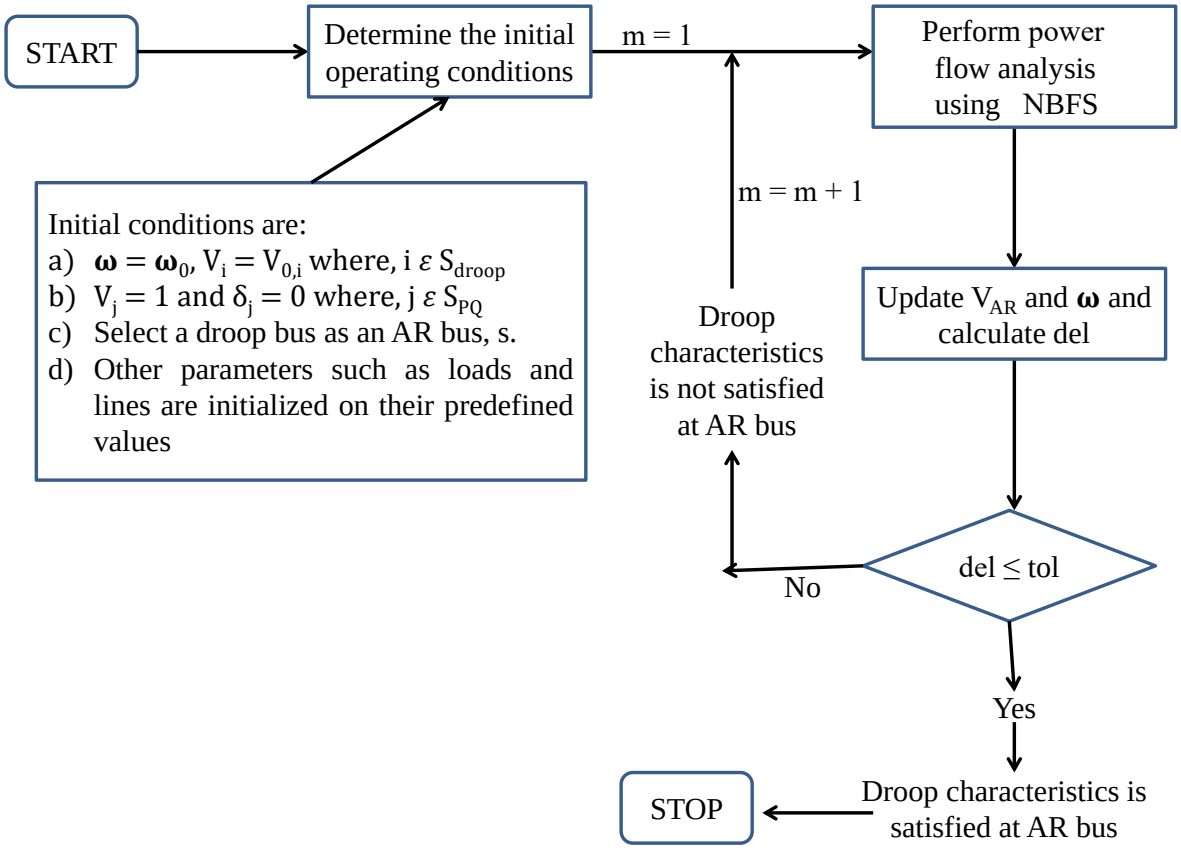

Figure 4.4: Flow chart of NBFS

accuracy of the proposed algorithm. It is to be noted that to achieve the converged solution, NBFS takes execution time approximately 0.008 sec which is very less as compared to the required simulation time of PSCAD.

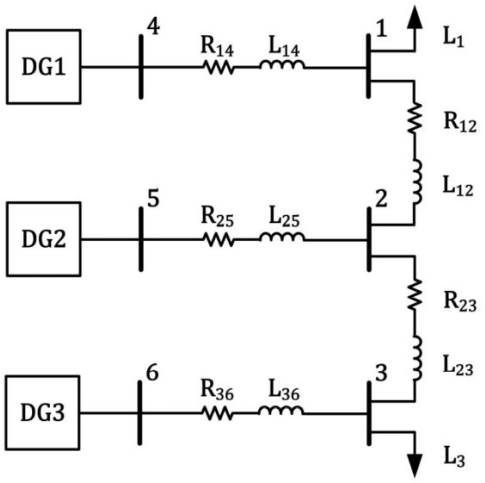

Figure 4.5: 6-bus MG [2].

Table 4.6: Validation of obtained result of the six-bus test system

Bus	Voltage magnitude (V)		Angle (rad)	
	PSCAD	NBSF	PSCAD	NBSF
1	121.92	121.92	0.0078	0.0078
2	123.51	123.51	-0.0013	-0.0013
3	122.42	122.42	-0.0388	-0.0389
4	125.37	125.37	0.0065	0.0065
5	125.74	125.74	0*	0*
6	123.11	123.10	-0.0420	-0.0421
err	0.0081%		0.26%	
freq	376.6645	376.6645		
Time	172s	0.009s		

4.4.7 Performance Analysis of NBFS

Comparison of NBFS with DBFS and MBFS

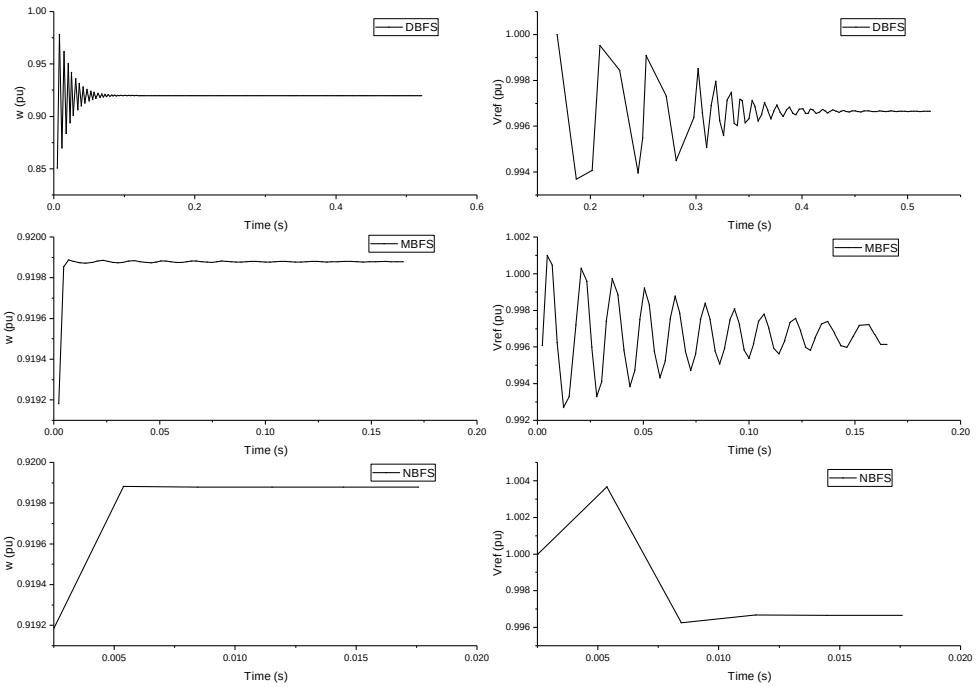

Figure 4.6: Convergence of the solution with respect to computation time for CASE33 system

In this section, a detailed comparison among the load flow solutions (obtained for droop based islanded microgrid) applying NBFS, DBFS, and MBFS are presented.

CASE33 radial distribution test system is adopted to compare result of the proposed algorithm with the DBFS [98] and MBFS [174]. The droop parameter and test settings are directly adopted from [174] and [98] for fair comparison. Additionally, results of PSCAD/EMTDC are also included for validation. Table 4.7 shows the results given

Table 4.7: NBFS algorithm versus DBFS, MBFS, and PSCAD/EMTDC results for CASE33 system. (1* represents the AR bus)

Bus	Voltage Magnitude (pu)				Active Load (pu)				Reactive Load (pu)			
	DBFS	MBFS	PSCAD	NBFS	DBFS	MBFS	PSCAD	NBFS	DBFS	MBFS	PSCAD	NBFS
1*	0.996	0.997	0.997	0.997	0.00	0.00	0.00	0.00	0.00	0.00	0.00	0.00
2	0.996	0.996	0.996	0.996	0.20	0.20	0.20	0.20	0.12	0.12	0.12	0.12
3	0.993	0.993	0.993	0.993	0.18	0.18	0.18	0.18	0.08	0.08	0.08	0.08
4	0.992	0.992	0.992	0.992	0.24	0.24	0.24	0.24	0.16	0.16	0.16	0.16
5	0.991	0.992	0.992	0.992	0.12	0.12	0.12	0.12	0.06	0.06	0.06	0.06
6	0.991	0.991	0.991	0.991	0.12	0.12	0.12	0.12	0.04	0.04	0.04	0.04
7	0.990	0.990	0.990	0.990	0.40	0.40	0.40	0.40	0.20	0.20	0.20	0.20
8	0.990	0.990	0.990	0.990	0.40	0.40	0.40	0.40	0.20	0.20	0.20	0.20
9	0.992	0.992	0.992	0.992	0.12	0.12	0.12	0.12	0.04	0.04	0.04	0.04
10	0.994	0.994	0.994	0.994	0.12	0.12	0.12	0.12	0.04	0.04	0.04	0.04
11	0.995	0.995	0.995	0.995	0.09	0.09	0.09	0.09	0.06	0.06	0.06	0.06
12	0.996	0.995	0.995	0.995	0.12	0.12	0.12	0.12	0.07	0.07	0.07	0.07
13	1.001	1.001	1.001	1.001	0.12	0.12	0.12	0.12	0.07	0.07	0.07	0.07
14	0.999	0.999	0.999	0.999	0.24	0.24	0.24	0.24	0.16	0.16	0.16	0.16
15	0.998	0.997	0.997	0.997	0.12	0.12	0.12	0.12	0.02	0.02	0.02	0.02
16	0.997	0.996	0.996	0.996	0.12	0.12	0.12	0.12	0.04	0.04	0.04	0.04
17	0.995	0.994	0.994	0.994	0.12	0.12	0.12	0.12	0.04	0.04	0.04	0.04
18	0.994	0.994	0.994	0.994	0.18	0.18	0.18	0.18	0.08	0.08	0.08	0.08
19	0.995	0.995	0.995	0.995	0.18	0.18	0.18	0.18	0.08	0.08	0.08	0.08
20	0.992	0.992	0.992	0.992	0.18	0.18	0.18	0.18	0.08	0.08	0.08	0.08
21	0.991	0.991	0.991	0.991	0.18	0.18	0.18	0.18	0.08	0.08	0.08	0.08
22	0.990	0.991	0.990	0.990	0.18	0.18	0.18	0.18	0.08	0.08	0.08	0.08
23	0.992	0.992	0.992	0.992	0.18	0.18	0.18	0.18	0.10	0.10	0.10	0.10
24	0.990	0.990	0.990	0.990	0.84	0.84	0.84	0.84	0.40	0.40	0.40	0.40
25	0.991	0.991	0.991	0.991	0.84	0.84	0.84	0.84	0.40	0.40	0.40	0.40
26	0.990	0.990	0.990	0.990	0.12	0.12	0.12	0.12	0.05	0.05	0.05	0.05
27	0.989	0.990	0.989	0.989	0.12	0.12	0.12	0.12	0.05	0.05	0.05	0.05
28	0.985	0.986	0.986	0.986	0.12	0.12	0.12	0.12	0.04	0.04	0.04	0.04
29	0.983	0.984	0.984	0.984	0.24	0.24	0.24	0.24	0.14	0.14	0.14	0.14
30	0.983	0.984	0.983	0.983	0.40	0.40	0.40	0.40	1.20	1.20	1.20	1.20
31	0.985	0.986	0.986	0.986	0.30	0.30	0.30	0.30	0.14	0.14	0.14	0.14
32	0.987	0.988	0.988	0.988	0.42	0.42	0.42	0.42	0.20	0.20	0.20	0.20
33	0.990	0.990	0.990	0.990	0.12	0.12	0.12	0.12	0.08	0.08	0.08	0.08
Max Error	0.001	0.001	–	0.000	0.00	0.00	–	0.00	0.00	0.00	–	0.00
					Active Generation (pu)				Reactive Generation (pu)			
1	0.996	0.997	0.997	0.997	2.494	2.502	2.502	2.502	0.978	0.967	0.967	0.967
6	0.991	0.991	0.991	0.991	0.981	0.980	0.980	0.980	0.904	0.909	0.909	0.909
13	1.001	1.001	1.000	1.000	1.707	1.701	1.701	1.701	0.931	0.893	0.893	0.893
25	0.991	0.991	0.991	0.991	0.981	0.980	0.980	0.980	0.904	0.909	0.909	0.909
33	0.990	0.990	0.990	0.990	1.304	1.301	1.301	1.300	0.916	0.948	0.948	0.948
Max Error	0.001	0.001		0.000	0.008	0.000		0.000	0.038	0.000	0.000	0.000
					Pg	Qg	Pl	Ql	Ploss	Qloss	freq	CT(s)
				DBFS	7.467	4.633	7.430	4.600	0.037	0.033	0.919	0.521
				MBFS	7.464	4.626	7.430	4.600	0.034	0.026	0.920	0.165
				PSCAD	7.463	4.625	7.430	4.600	0.035	0.027	0.920	462.142
				NBFS	7.463	4.626	7.430	4.600	0.035	0.026	0.920	0.018

in [98] and [174] in addition to the results obtained from NBFS and PSCAD/EMTDC.

For a fair comparison, the nominal power of all DGs is set at $0.9 + j0.9$ pu and bus 1 is considered as the AR bus. Therefore, the power reported in Table 4.7 is an apparent power which is the sum of nominal power and the power generated due to drop in frequency and voltage. It is clearly seen from Table 4.7, the obtained system frequency is similar for all the algorithms, while there is some difference in the magnitude of bus voltages. The maximum mismatch of voltage magnitude, real power, and reactive power are also reported in Table 4.7. This maximum mismatch is calculated after considering the result of PSCAD/EMTDC as a standard solution of PF problem. From Table 4.7, it can say that the solution of NBFS is nearer to the solution of PSCAD/EMTDC as compared to other solutions obtained with application of other algorithms. Hence, the obtained solution of NBFS is more accurate than the solution of MBFS and NBFS.

In DBFS, the obtained reactive power generation of DGs is slightly different from the result obtained from MBFS and NBFS. DBFS uses an inner and outer loop update schemes in such a way that the voltage of DG is updated in the inner loop using BFS while the voltage magnitude of reference bus remains constant [98]. When the inner loop converges, the voltage magnitude of AR bus is updated based on the reactive power mismatch and the voltages of other buses according to the droop law. On the other hand, MBFS and NBFS are governed by the droop law of the DGs, so their output reactive power are closer to the results obtained in the time domain simulation in PSCAD/EMTDC.

To further analyze difference between the performance of NBFS, MBFS, and DBFS; the dynamics of system frequency and voltage magnitude of AR bus (Bus 1) with respect to time is depicted in Fig 4.6. It is clearly seen from Fig. 4.6 that in comparison to MBFS and DBFS, the required computation time is very less in NBFS to achieve the converged power flow solution. The main reason behind this difference in computation time and dynamics is the variations in the basic structure of the algorithms. In NBFS, there is one loop where the system frequency and voltage magnitude of reference bus are updated to satisfy the droop characteristics of DG connected to the reference bus. For the other DGs, the generated power is updated in backward sweep step of BFS according to their droop characteristics. This structure of NBFS reduces the computational burden and increases the convergence speed as compared to MBFS and NBFS. Since the generated power of all the droop controlled DGs are updated outside the loop of BFS in MBFS and DBFS, in DBFS, different loops are utilized to update the real and reactive power separately which

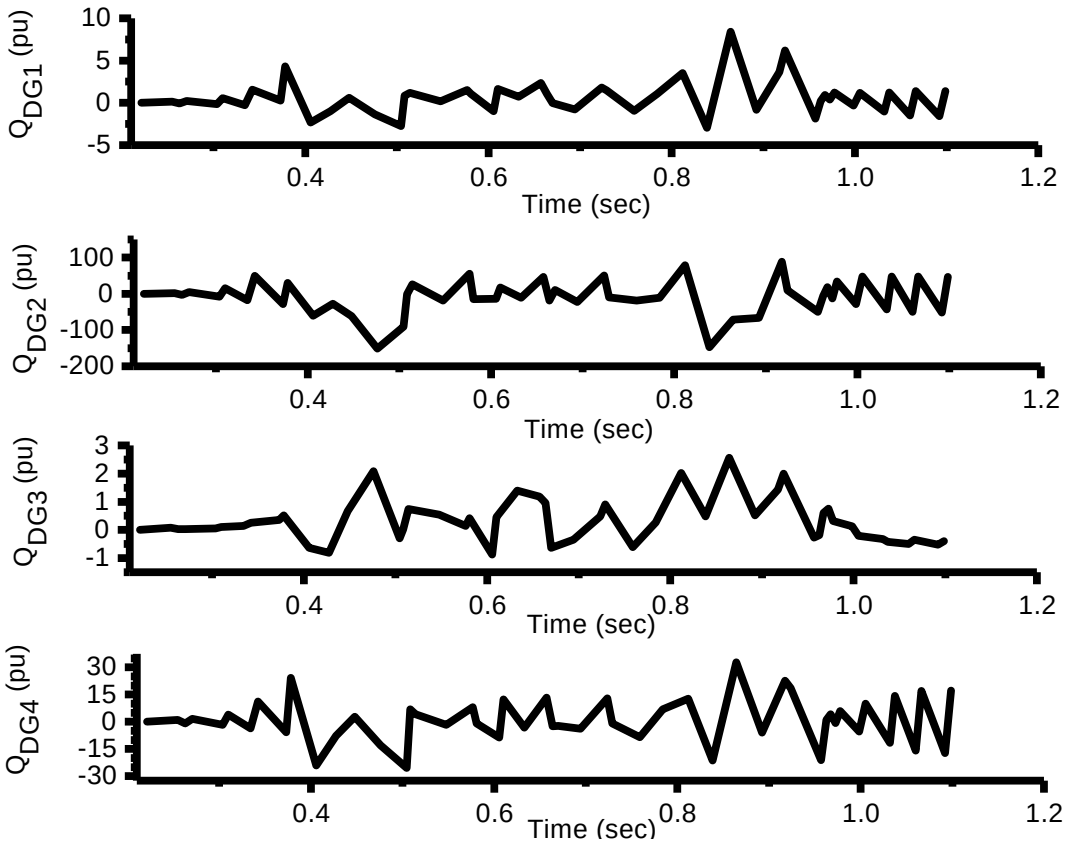

Figure 4.7: Divergence of MBFS for 33-bus test system

increases the computation burden which ultimately increases the convergence time to achieve the solution. It can be seen in the Fig. 4.6 that the deviation in system frequency and voltage magnitude of reference bus before the convergence is higher in DBFS while in the case of NBFS deviation is very less. This oscillatory behavior of MBFS and DBFS delays the convergence and also makes the algorithm unstable for hard PF problems. According to the discussed points, we can say that the efficiency and robustness of NBFS is better than the MBFS and DBFS.

Comparison of NBFS with NTR and MNR

In this section, to examine the robustness of the proposed algorithm to achieve the power flow solution, a comparative study among the proposed algorithm and Jacobian based algorithms (NTR and MNR) is performed.

Three test systems including CASE22, CASE38, and CASE69 are chosen to analyze the performance of DBFS, MBFS, NTR, MNR, and NBFS. The data for the droop controlled DGs are given in Table 4.8. The convergence time to achieve the PF solution for

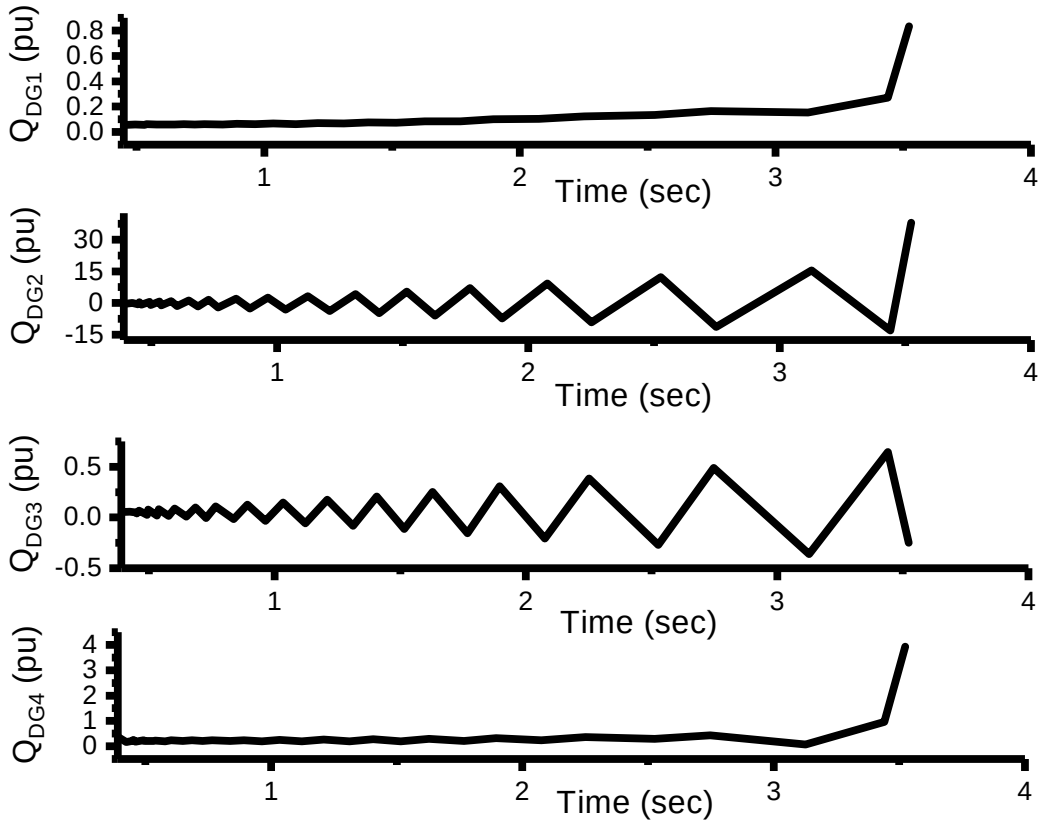

Figure 4.8: Divergence of DBFS for 33-bus test system

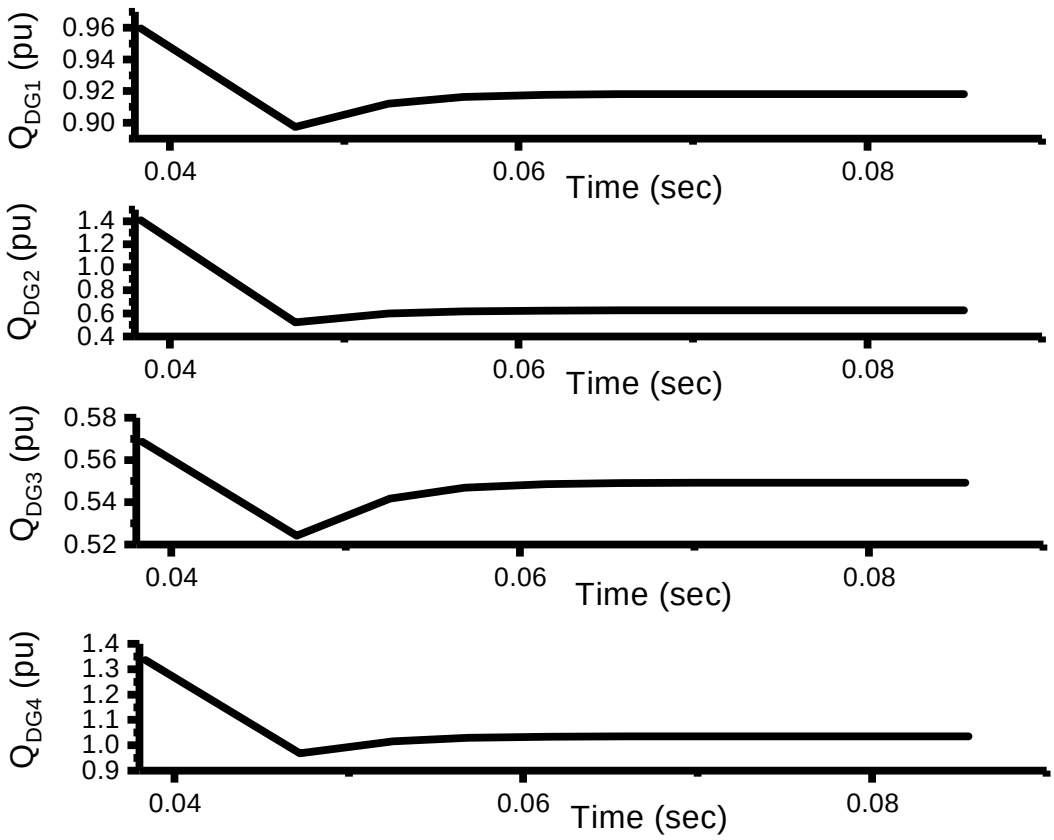

Figure 4.9: Convergence of NBFS for 33-bus test system

Table 4.8: Droop gains, nominal values and operative mode of DGs and Q_{max} limit for the 22-bus, 38-bus, and 69-bus test system.

Test System	Bus Number	m	n	w_0	$\|V_0\|$	Q_{max}
22-bus	5	0.005102	0.05	1	1	0.2
	13	0.001502	0.03	1	1	0.3
	15	0.004506	0.01	1	1	0.4
	21	0.001502	0.02	1	1	0.4
38-bus	34	0.005102	0.02	1	1.01	0.9
	35	0.001502	0.03333	1	1.01	0.6
	36	0.004506	0.02	1	1.01	0.9
	37	0.002253	0.05	1	1.01	0.3
	38	0.002253	0.05	1	1.01	0.3
69-bus	1	0.005102	0.05	1	1.01	0.35
	25	0.004506	0.05	1	1.01	0.45
	29	0.002253	0.01	1	1.01	0.9
	50	0.002253	0.1	1	1.01	0.6
	60	0.005102	0.1	1	1.01	1.5
	65	0.001502	0.03	1	1.01	0.9

Table 4.9: Computation time (in second) required to solve power flow for 22-bus, 38-bus, and 69-bus systems considering NBFS, MNR, NTR, MBFS, and NBFS algorithm. (NC: Not Converged)

System	NBFS	MNR	NTR	MBFS	DBFS
22-bus	4.96E-03	6.35E-02	1.77E-02	NC	NC
38-bus	3.01E-02	1.46E-01	3.48E-02	NC	NC
69-bus	4.33E-02	NC	1.43E-01	NC	NC

all the three systems are obtained for each algorithm (MBFS, DBFS, MNR, NTR, and NBFS) which are given in Table 4.9. It is clearly seen from the Table 5 that the MBFS and DBFS did not converge on a single test system due to their dynamics characteristic which is discussed in the previous section. In all test systems, the required time to

converge is lesser in case of NBFS as compared to MNR and NTR because:

- NBFS does not require calculation of the Jacobian matrix to achieve the PF solution.
- In MNR and NTR, bus admittance matrix is calculated at every iteration due to change in frequency, while NBFS does not require bus admittance matrix.
- In the case of MNR, CASE69 system does not reach convergence because MNR operates at the boundary of the solvable and unsolvable region in this case.

Discussion

The performance of the proposed algorithm NBFS is compared fairly with the performance of algorithms MBFS, DBFS, MNR, and NTR on three test system. It is found that among three test system, the MBFS and DBFS achieve the PF solution for only one test system. Hence, the performance of NBFS is only analyzed for the CASE33 test system in comparison with MBFS and DBFS and it is found that the NBFS is more efficient and robust than the MBFS and NBFS.

It is already discussed that the main reason behind the diversion of MBFS and DBFS is the oscillatory dynamics of system frequency and voltage magnitude of the reference bus. To show this behavior, MBFS and DBFS are applied on a CASE33 radial test system with droop parameter $\{0.005, 0.1, 0.01, 0.1, 0.02\}$. The resultant dynamics of reactive power generation of droop based DGs are shown in Figs. 4.7, 4.8 and 4.9 for MBFS, DBFS and NBFS respectively. It is clearly seen from the Figs. 4.7 and 4.8 that the generated reactive power of all droop controlled DGs are increased beyond the limit of the solvable region which leads the divergence in case of MBFS and DBFS. On the other hand, NBFS uses the deceleration factors α and β which behaves as a damper to the oscillation of system variables. This is the main reason behind the convergence of the NBFS algorithm in case of hard problems.

Both the MNR and NTR algorithms are Jacobian-based algorithm, in which the admittance matrix is also calculated to achieve the solution. The inverse of Jacobian Matrix is computationally bulky and increases with the increase of the size of the system. The effect of this computational burden is also shown in Table 4.9 where computation time for the convergence increases with the increase of the size of the system. Besides inverse of a Jacobian matrix, calculation of admittance matrix at every iteration also increases

the computational burden and complexity. In NBFS, these complex calculations are not required, so the algorithm requires less time to converge as compared to Jacobian based algorithms. Additionally, the system size does not affect the computation time much in the case of NBFS which is also seen from Table 4.9.

Performance of NBFS on weakly meshed islanded microgrid

In this sub-section, to show the robustness of the proposed algorithm for achieving the power flow solution of weakly meshed islanded microgrids, a comparative study among the algorithms NBFS, NTR, and MNR has been performed.

Table 4.10: The computation time (in second) required to solve power flow problem of CASE160 test system for NBFS, MNR, and NTR

System	NBFS	MNR	NTR
CASE160	6.08E-02	8.36E-01	5.10E-01

A 160-bus test system is selected to analyze the performance of NBFS, NTR, and MNR. The system data of this test system is adapted from [175]. In NBFS, the calculation procedure of matrices BIBC and BCBV are modified for weakly-meshed islanded system. The convergence time required to achieve the solutions are obtained for each algorithm (NBFS, NTR, and MNR) and are reported in Table 4.10. It is clearly seen from the Table 4.10 that the NBFS requires least time to converge in comparison to the MNR and NTR.

Comparison with conventional BFS on grid-connected microgrid

In this section, to examine the robustness of the proposed step of BFS of NBFS (pBFS) algorithm to achieve the PF solution of grid-connected microgrid, a comparative study between pBFS and conventional BFS (cBFS) algorithm is performed.

The CASE38 test system is selected to analyze the performance of pBFS and cBFS. The line and load data of the test system are adapted from [176]. System loads are increased from its base value (reported in [176]) by a different factor (λ) to analyze the robustness of the proposed pBFS algorithm in comparison to cBFS. The number of iterations and convergence time required to achieve the PF solution for the test system under different loading conditions is obtained for both the algorithms (pBFS and cBFS)

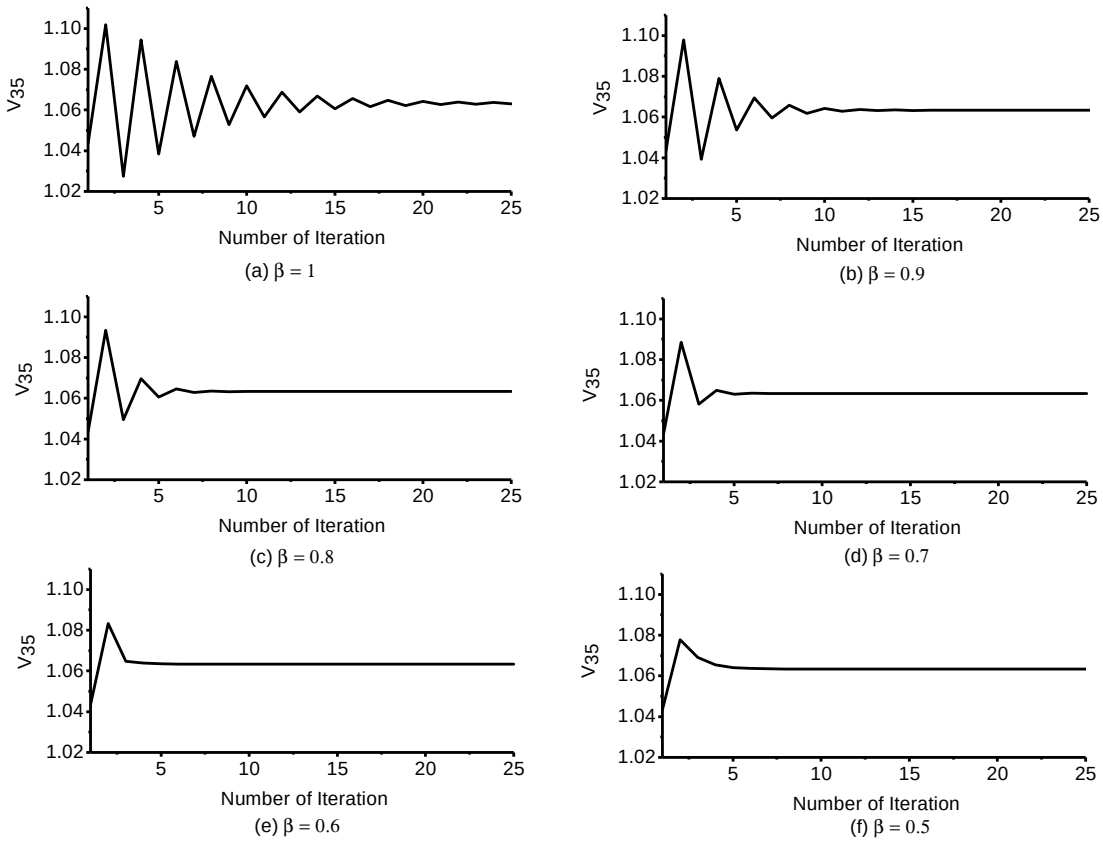

Figure 4.10: Effect of the value of β on the convergence of voltage magnitude of bus 35 of CASE38 test system in the case of $\lambda = 4$.

which are given in Table 4.11. It is clearly seen from Table 4.11 that the pBFS requires less number of iteration and less convergence time in comparison to cBFS for every loading condition. In addition, cBFS did not converge for the cases when $\lambda > 3$ due to the large variations of bus voltages in the initial iterations, while pBFS successfully converge for all the cases because the modified forward sweep uses a decelerating factor β to overcome the issue of the large variation in bus voltages in the initial few iterations. In the next subsection, the role of the parameter β is discussed.

Significance of the parameter β

The robustness of the proposed pBFS (step of NBFS) is highly improved as compared to the cBFS (conventional BFS) due to the parameter β which is used in equation (4.31) of the modified forward sweep. It is to be noted that the pBFS is reduced to cBFS for the value of $\beta = 1$. In this subsection, we have discussed the impact of β on the convergence behavior of the pBFS.

Table 4.11: Number of iteration and computation time (in second) required to solve power flow problem of CASE38 test system for different value of λ considering pB-FS and cBFS. (fail: fail to supply solution within 50 iteration, NC: Not Converged, NA: Not Available, It: Number of iteration, CT: Computation Time (in second))

λ	pBFS		cBFS	
	It	CT	It	CT
1.0	8	3.24E-03	11	4.72E-03
1.5	10	4.02E-03	15	7.03E-03
2.0	12	4.72E-03	20	8.12E-03
2.5	13	5.01E-03	26	1.12E-02
3.0	15	6.01E-03	35	1.52E-02
3.5	17	6.24E-03	fail	NA
4.0	19	7.35E-03	fail	NA
4.5	20	8.01E-03	fail	NA
5.0	21	8.23E-03	NC	NA

CASE38 test system with $\lambda = 4$ is considered to analyze the effect of β. In conventional BFS algorithm, the variation in the magnitude of bus voltages of the system is highly oscillating in initial iterations and this oscillation is gradually damped out in later iterations as shown in figure 4.10-(a). It is clearly seen from the figure 4.10-(a) that the voltage magnitude of bus 35 highly oscillates in the initial iterations and as iteration increases, this oscillation damps out gradually. The parameter β is used to adjust the length of voltage correction vector ($[\triangle \mathbf{V}]^{k+1} = [\mathbf{V}]^k - [\mathbf{V}_{ref}] + [\mathbf{BCBV}][\mathbf{I}_{ij}]$) to damp out the oscillation in voltage magnitude. The convergence of the voltage magnitude of bus 35 of the CASE38 test system is shown in figure 4.10 for different values of β ($\beta = 0.5, 0.6, 0.7, 0.8, 0.9$). It is clearly seen from the figure 4.10 that the oscillation in voltage magnitude can be damped out quickly by taking the value of β smaller than 1. As the value of β decreases, the damping in oscillation in the voltage magnitude increases. However, the very low value of β increases the convergence time (settling time). Therefore, the value of β must be set carefully to provide the trade-off between the oscillation and convergence time. In this work, the value of β is chosen 0.5, which provides the balance between oscillation and convergence time in most of the case studies.

4.5 Application of Proposed Approach for DG Modeling and Frequency Update in NTR and MNR

As discussed in the previous subsection, the robustness of NTR and CINR is similar but the NTR algorithm cannot be applied to the systems having (i) DGs with mixed droop characteristics, (ii) DG with isochronous mode of operation and (iii) coupling between the lines. In this work, these issues of NTR are addressed and a new DG model and procedure for updating operating frequency are proposed. These procedures are in general structure and can also be employed with NTR to improve the versatility of the algorithm. In this section, to observe the versatility of the NTR, the modified algorithm is implemented on different types of DCIMGs.

4.5.1 Significance of Proposed DG Model in NTR

The proposed DG model is implemented in NTR by modifying the non-linear equations used in [56]. These non-linear equations are modified in line with the equations proposed in this work. The modified NTR, named NTR-pDMm, can perform the power flow analysis for different cases (discussed in section 4.3.5). The accuracy of the obtained solution of NTR-pDMm is similar to the obtained solution of CINR for all the cases. However, computation time is still the issue in the NTR-pDMm due to the high complexity of the steps of the conventional Newton-Trust algorithm. The results obtained using the proposed DG model in NTR (NTR-pDGm) and CINR in terms of execution time are shown in Table 4.12. It is found that the computation time to converge on a steady-state value in CINR is less than the NTR-pDGm due to the low complexity of the steps required in CINR.

It can be concluded from the above result and discussion that the proposed DG model can be implemented on other Newton-based algorithms to improve their versatility. Also, the convergence rate of CINR is better than modified NTR (NTR-pDGm) due to its simple steps.

Table 4.12: Computation time required to solve power flow for different cases considering CINR, NTR-pDGm algorithm. (NC: Not Converged, CT: Computation Time, %: Percentage improvement in computation time.)

System	Cases	CINR	NTR-pDGm	
		CT(s)	CT(s)	%
CASE22	2	5.58E-03	1.79E-02	220.84
	3	4.22E-03	1.97E-02	365.86
	4	3.81E-03	1.73E-02	353.31
CASE38	2	1.42E-02	3.50E-02	147.17
	3	2.28E-02	3.53E-02	54.77
	4	2.36E-02	4.41E-02	87.21
CASE69	2	1.72E-02	1.40E-01	716.45
	3	1.82E-02	1.38E-01	658.41
	4	1.81E-02	1.50E-01	729.12
CASE160	2	4.99E-02	6.39E-01	1178.58
	3	4.47E-02	5.27E-01	1078.50
	4	6.03E-02	5.20E-01	763.13

4.5.2 Significance of Proposed Frequency Update Procedure in NTR and MNR

The approach taken in the present work is further reinforces its superiority by applying modification in MNR and NTR (MNR-mod and NTR-mod). The modifications made are in line with the approach considered in this paper. For the systems with coupling between the lines, the derivative of admittance matrix cannot be calculated analytically as there is no explicit expression. However, the derivatives of the elements of admittance matrix can be calculated using finite differences method. The frequency terms which are embedded in the elements of the admittance matrix are removed (assuming frequency to be constant). However, the updation of frequency is performed in the outer loop as shown in figure (4.1). The results obtained using proposed modifications in MNR and NTR (MNR-mod and NTR-mod) are shown in table (4.13). The table (4.13) also depicts the results when the elements of Jacobian are calculated using finite differences method (MNR-fd and

NTR-fd). The table (4.13) indicates that significant reduction in computation time can be achieved when the modification are done as per the proposed approach as compared to those obtained using their corresponding finite difference version viz MNR-fd and NTR-fd. further, Table 4.13 also shows that CINR is faster than MNR-mod and NTR-mod, establishing that even if MNR, NTR is adopted for the framework proposed in this work, the CINR outperforms.

Table 4.13: Computational effort of MNR-mod, MNR-fd, NTR-pr, NTR-fd, and CINR for solving different test cases. (iter: number of iterations, CT: Computation Time)

Test Cases	MNR-mod		MNR-fd		NTR-mod		NTR-fd		CINR	
	iter	CT(s)	iter	CT(s)	iter	CT(s)	iter	CT(s)	iter	CT(s)
CASE22	33	0.0205	3	0.3246	37	0.0198	4	0.2932	27	0.0049
CASE33	39	0.0372	3	0.6091	34	0.0297	4	0.5682	24	0.0063
CASE69	37	0.1666	4	0.9351	39	0.1433	5	0.8702	28	0.0133
CASE160	34	0.577	4	3.0717	32	0.5482	4	2.8126	25	0.0608
CASE1458	35	3.656	5	8.2825	37	3.2735	6	7.6835	27	0.3852
CASE3139	38	7.9334	5	17.9729	35	7.1374	6	16.673	29	0.8257

4.6 Summary

In this chapter, a nested-iterative approach, CINR and NBFS are proposed to obtain the power flow solution of droop-based islanded microgrid. A loop-based approach is employed to update the system frequency and voltage of the angle reference bus after every iteration. To analyze the effectiveness of CINR and NBFS, the algorithms are implemented on several test systems including CASE6, CASE22, CASE38, CASE69 and CASE160. In each case study, the load dependency and droop characteristics of DGs are considered. The solutions obtained from the proposed CINR and NBFS are analysed and compared with the solutions obtained from MNR, NTR, DBFS, MBFS and PSCAD. It is found that the solutions obtained from CINR and NBFS show superior convergence in comparison to MNR, NTR, DBFS, MBFS and PSCAD.

Furthermore, the efficacy and robustness of the proposed technique are also analyzed by modifying the operational conditions of DCIMG from well-conditioned to ill-

conditioned by changing the r/x ratio of the lines and the loading conditions. The proposed algorithms converge under various ill-conditions. The proposed techniques also show superior performance in terms of computational time and accuracy in comparison to the performance of NTR and MNR methods of PF analysis.

The effectiveness of the proposed algorithm is also analyzed for the PF analysis of more complicated DCIMG system after considering the isochronous operation of one of the DG in the system. The proposed algorithms also converge for the isochronous operation of the DCIMG. Since, CINR and NBFS are conventional techniques to solve power flow of distribution system, so modeling of different type of droop buses is also considered. The main contributions of proposed approach are as follows:

1. The proposed algorithms, CINR and NBFS, deal with the issues and limitations related to the Newton-based algorithms including MNR and NTR. It also deals with the need of a gradient of the bus admittance matrix with respect to the system frequency in the Jacobian matrix.

2. The proposed algorithms update the system frequency in every loop without using the gradient of the bus admittance matrix or any other variable with respect to the system frequency.

3. A closed loop formulation is proposed to evaluate the values of voltage magnitude of the AR bus and system frequency, which results in fast convergence in the algorithm.

4. The proposed algorithms also converge for the isochronous mode of operation of DCIMG systems.

5. In the proposed approach, DG model and procedure for updating the system frequency is utilized in NTR and MNR to improve its versatility.

The algorithms show rigid convergence characteristics for various conditions of DCIMG. The performance of the proposed algorithms are better in comparison to NTR and MNR approach in terms of computation time and applicability under various operating conditions. Testing of the proposed algorithms on unbalanced DCIMG systems may be the scope of future work.

Chapter 5

Differential Evolution and MAES for Power Flow Problem of Droop Controlled Islanded Microgrids

5.1 Introduction

Conventional PF algorithms are not effective in analyzing the of islanded microgrid as the system frequency and voltage of the slack bus is assumed to be constant. Such assumptions are not applicable in the operation of islanded microgrid as DGs provide the real and reactive power to adjust the load demands as well as maintain the voltage magnitude and system frequency in the absense of the main grid. To solve the power flow of islanded microgrid, a novel formulation as a constrained optimization problem is proposed in this thesis.

A MG has been recognized as a collection of DGs which are interconnected with thermal and electrical loads, and energy storage units. In addition, it functions as a single small scale low-voltage distribution system. Due to the use of power electronic controls and interfaces in MGs, system reliability, security, and power electronic controls can be enhanced [177, 178]. An MG may run in islanded or grid-connected mode. In an islanded mode, controllers of DGs are capable of voltage and frequency regulation along with controlling active and reactive power. While in a grid-connected mode the frequency and voltages of MGs are managed by the main grid.

In practice, different type of control strategies for MGs have been proposed such as

distributed, decentralized, and centralized; any hybrid structure of these models is also feasible. Strategies based on centralized control need to transfer data using stable communication environment. In the case of large MGs, these strategies are not suitable where DGs are placed far from each other [179–181]. Large MGs are usually controlled using decentralized strategies, such as DCIMGs, where communication of significant information is not needed [178]. In droop controller based strategies, local variables can be utilized for effective sharing of loads of loads among DGs. Here, the frequency and magnitude of the voltage of MGs are used as local variables [182].

In DCIMGs, DGs are connected to MGs using suitable control approach using power electronic converters [183–186]. For designing the effective and efficient control strategy, a power flow analysis model is required to calculate the steady-state variables, especially for an islanded MGs. Design of droop control strategies use power flow solutions to test its efficacy. This is more so in the case of MGs operated in islanded mode.

To address the characteristics of MGs and distribution systems, a number of methods have been introduced for PF analysis. Some of such algorithms are derived from the NR approach [23, 43], while others are based on the basic electric circuit laws [51]. In [187], a modified algorithm, called BFS method, has been proposed for solving the power mismatches equations of radial power systems. In [27], an implicit ZBus algorithm based on the superposition principle of electric circuits is proposed to solve the power flow problem.

In [56], a model of three-phase PF problem is proposed which adopt the real characteristics of islanded MGs similar to three-phase distribution systems. In the model proposed in [56], the problem is formulated as a non-linear optimization problem and this problem is solved by NTR technique. But, it is highly sensitive to the initial solutions of variables of the PF problem. In addition, a number of studies of PF analysis for droop controlled islanded MGs based on a nature-inspired optimization algorithm have been developed.

In general, Jacobian based PF algorithms, such as NR, and FD may not produce PF solution for power mismatch equations of distribution systems having a high value of R/X. To solve this problem, a number of methods [183–186] have been introduced. In addition, to present an adequate platform for PF analysis, modeling of distributed slack bus has also been studied [28, 53, 100].

In current practices, DG having the highest capacity is considered as a slack bus which operates like an infinite bus at a constant voltage to provide system frequency, and other DGs are treated as either PV or PQ buses. However, this assumption cannot be considered feasible in the case of islanded MGs. For example, the generation capacity of DGs in MGs is not usually high enough to allow them to act as an infinite bus. In addition, voltage swelling may occur in the buses of MG when a DG is acting as a slack bus. In such a situation, slack bus (DGs) must provide power independently for the whole power losses of MG which is not an effective state of operation for MG [43]. Therefore, in an islanded MG, considering a DG as a slack bus is not appropriate for PF analysis.

In order to resolve this issue, one way is to consider that all DG units operate using droop controllers where all DGs locally tune the voltage and frequency of islanded MG [179]. In such operation, active power generation and voltage magnitude of each DG is required to be fixed according to droop characteristics of controllers. This operation of MG creates a new type of bus, called droop bus, in addition to PQ and PV buses in the system. It is worth to note here that grid-connected MG behaves like a simple distribution system having a slack bus operating as a infinite bus. Other problems related to power flow analysis of islanded MGs can be outlined as dealing with the reactive power scheduling of DGs, and singularity of the Jacobian matrix which causes failure in convergence of PF [185].

In order to resolve these issues, this thesis proposes a new PF formulation for islanded microgrids. This formulation is expressed in form of constrained optimization problem which models different mode of operations of DGs (such as PV, PQ, and droops operations). In order to solve this constrained optimization problem, two novel optimization algorithms are proposed.

The main contributions of this chapter are summarized as follows.

- It introduces a novel formulation as a constrained optimization problem for PF analysis of islanded MGs.
- It proposes PF constraint based on the droop characteristics of distributed slack buses to deal with the droop buses in power flow analysis. In addition, system frequency is also considered as an extra variable of the PF problem.
- It provides an adequate method to share reactive and active power among DGs

based on the droop characteristics in the PF analysis.

- It provides the PF solutions for the islanded MGs using the proposed optimization algorithms.

This chapter is organized as follows. In the second section, the microgrid system and load are modeled. This is followed by formulating the constrained optimization problem for power flow analysis of islanded MGs. In the fourth section, the main steps of the optimization algorithm are proposed. Finally, the validation of the proposed algorithm on the power flow problem of islanded MGs is discussed.

5.2 Modelling of Droop Controlled Microgrid

5.2.1 Modeling of Frequency and Voltage Dependent Loads

Generally, loads are assumed to be independent of the value of voltage and therefore, the active and reactive power demands of loads are treated as constant parameters. However, such premises are not true in practice, especially in MGs where power demand of some loads are depended on the values of frequency and voltages. Mathematically, voltage-dependent loads can be defined as

$$P_l = P_{l,0}\left(\frac{V}{V_0}\right)^{\alpha}, \tag{5.1}$$

and

$$Q_l = Q_{l,0}\left(\frac{V}{V_0}\right)^{\beta} \tag{5.2}$$

where $Q_{l,0}$ and $P_{l,0}$ represent the reactive and active power, respectively, at nominal voltage; Q_l and P_l represent reactive and active power respectively, at operating voltage; V and V_0 represent the magnitude of voltage and nominal voltage, respectively, at load buses; β and α represent the exponent parameters for reactive and active powers, respectively, for the model [188].

In similar way, frequency dependent load can be defined as

$$P_l = P_{l,0}\left(\frac{V}{V_0}\right)^{\alpha}(1 + k_{pf}\triangle f) \tag{5.3}$$

and

$$Q_l = Q_{l,0}\left(\frac{V}{V_0}\right)^{\beta}(1 + k_{qf}\triangle f) \tag{5.4}$$

where $\triangle f$ is the deviation in system frequency with respect to the nominal frequency; k_{qf} and k_{pf} represent frequency dependent parameter, where their values are defined in range $(-2, 0)$ and $(0, 3)$, respectively [189].

5.2.2 Modeling of Lines in Islanded MGs

Line impedance of islanded MGs can be defined as, $z = r + jx(w)$ where, r and x represent the resistance and reactance of the line, respectively. Here, the value of reactance, x, depends on the operating frequency. Therefore, small deviation in frequency can change the reactance of the lines.

5.2.3 Modeling of DGs in Islanded MGs

In grid-connected MGs, DGs can operate to provide pre-specified active and reactive generation to satisfy the power demands of system loads. In such operation, the difference in total load demand and power generated by DGs are supplied or absorbed by the main grid to keep the system frequency and voltages of the buses constant. Similar to conventional power systems, in grid-connected MGs, DGs can be modeled as a PV and PQ bus [190, 191]. However, this cannot be valid in the case of islanded MGs, as shown below:

1. There is no slack bus in islanded MGs.
2. System frequency is not consant.
3. Reference voltage does not exist in islanded MGs to calculate the voltage of all system buses.
4. In an islanded mode, the deviation between power generation and demands may be fixed by changing the system frequency and magnitude of the voltage using droop controllers.

Therefore, the power flow problem of islanded MGs will be solved without considering the slack bus in the system. In order to formulate the PF problem of islanded MGs, in place of a slack bus, multiple droop buses are modeled based on the droop characteristics to share the power demand among the DGs. According to the droop characteristics of

the controllers, an increment in reactive power and active power demand follows from a decrement in magnitude of the voltage and operating frequency, respectively. So, in the case of droop bus, reactive and active power generation of a DG can be calculated using the following equations.

$$P_i = \frac{1}{np_i}(w_i^* - w) \tag{5.5}$$

$$Q_i = \frac{1}{mq_i}(V_i^* - V_i) \tag{5.6}$$

where V_i^* and w_i^* represent the nominal values of voltage magnitude and frequency, respectively; mq_i and np_i represent the reactive and active power static droop gains, respectively.

Based on the IEEE Standard 1547.7 [184], equations (5.5) and (5.6) are valid for islanded MGs where the output impedance of converter is assumed inductive. Figures (5.2) and (5.4) show the sharing of active and reactive power among the DGs.

5.3 Power Flow Formulation

In general, four variables are involved in a conventional power flow viz. active power, reactive power, voltage magnitude, and voltage angle. In the case of PQ bus, the value of voltage angle and voltage magnitude are unknown. In case of PV bus, voltage magnitude and reactive power are unknown. But, in the case of droop bus, all these variables are unknown. Conventional techniques cannot be applied to the power flow problem of islanded MGs as a frequency is not considered constant. In islanded MGs, the operating frequency is also an unknown variable for the power flow problem. Therefore, new equations should be derived for the PV, PQ, and droop buses are presented in the following section.

5.3.1 Modeling of Droop Bus

The value of active and reactive power injection of bus i can be defined as

$$P_i = P_{i,dg} - P_{i,l} \tag{5.7}$$

$$Q_i = Q_{i,dg} - Q_{i,l} \tag{5.8}$$

where, $P_{i,dg}$ and $Q_{i,dg}$ are calculated using equations (5.5) and (5.6). Here, P_i and Q_i can be calculated using following equations.

$$P_i = V_{ri}\sum_{j=1}^{N}(V_{rj}G_{ij} - V_{mj}B_{ij}) + V_{mi}\sum_{j=1}^{N}(V_{rj}B_{ij} + V_{mj}G_{ij}) \tag{5.9}$$

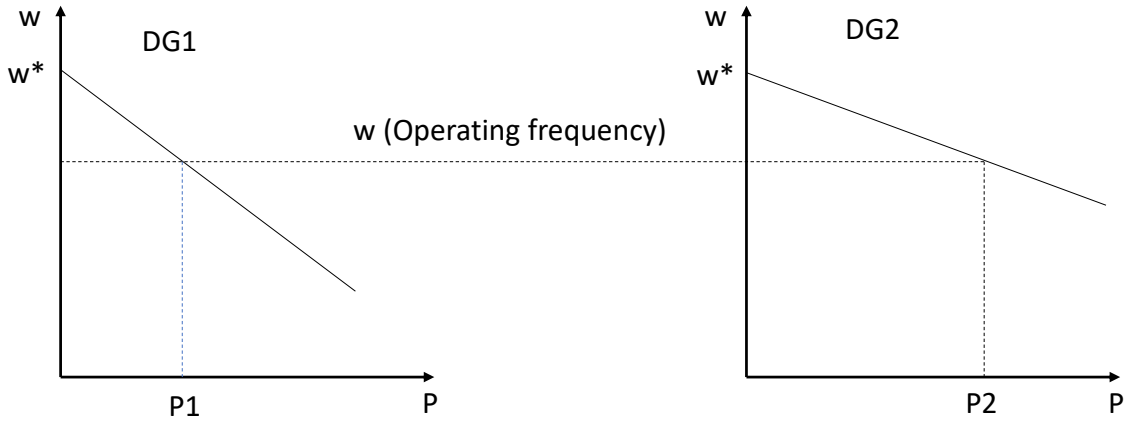

Figure 5.1: Sharing of active power among DGs using droop based controller

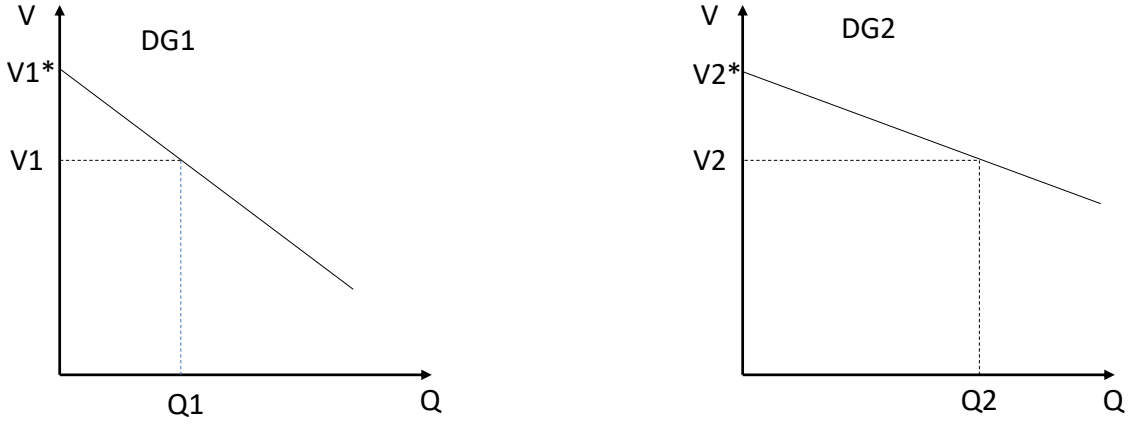

Figure 5.2: Sharing of reactive power among DGs using droop based controller

$$Q_i = V_{mi}\sum_{j=1}^{N}(V_{rj}G_{ij} - V_{mj}B_{ij}) - V_{ri}\sum_{j=1}^{N}(V_{rj}B_{ij} + V_{mj}G_{ij}) \tag{5.10}$$

Power flow equations for droop bus can be derived using equations (5.5), (5.6), (5.7), (5.8), (5.9), and (5.10), which are given below.

$$\frac{1}{np_i}(w_i^* - w) - P_{i,l} = V_{ri}\sum_{j=1}^{N}(V_{rj}G_{ij} - V_{mj}B_{ij}) + V_{mi}\sum_{j=1}^{N}(V_{rj}B_{ij} + V_{mj}G_{ij}) \tag{5.11}$$

$$\frac{1}{mq_i}(V_i^* - V_i) - Q_{i,l} = V_{mi}\sum_{j=1}^{N}(V_{rj}G_{ij} - V_{mj}B_{ij}) - V_{ri}\sum_{j=1}^{N}(V_{rj}B_{ij} + V_{mj}G_{ij}) \tag{5.12}$$

5.3.2 Modeling of PQ Bus

The active and reactive power injection are known in PQ buses, so PQ buses can be defined by following equations

$$P_k = V_{rk}\sum_{j=1}^{N}(V_{rj}G_{kj} - V_{mj}B_{kj}) + V_{mk}\sum_{j=1}^{N}(V_{rj}B_{kj} + V_{mj}G_{kj}) \tag{5.13}$$

$$Q_k = V_{mk}\sum_{j=1}^{N}(V_{rj}G_{kj} - V_{mj}B_{kj}) - V_{rk}\sum_{j=1}^{N}(V_{rj}B_{kj} + V_{mj}G_{kj}) \tag{5.14}$$

5.3.3 Modeling of PV bus

The active power and voltage magnitude are known in PV buses, so PV buses can be defined as given below

$$P_k = V_{rk}\sum_{j=1}^{N}(V_{rj}G_{kj} - V_{mj}B_{kj}) + V_{mk}\sum_{j=1}^{N}(V_{rj}B_{kj} + V_{mj}G_{kj}) \tag{5.15}$$

$$V_k^2 = V_{rk}^2 + V_{mk}^2 \tag{5.16}$$

To solve this proposed power flow formulation, a constrained optimization problem shall be discussed later in the chapter to optimize objective function corresponding to power flow.

5.3.4 Objective Function

The objective function can be formulated as the sum of square error of mismatch equations of droop bus (equations (5.11) and (5.12)) i.e.

$$\text{Minimize, } f = \sum_{k\epsilon S_{dr}}(\triangle P_k^2 + \triangle Q_k^2) \tag{5.17}$$

where

$$\triangle P_i = \frac{1}{np_i}(w_i^* - w) - P_{i,l} - V_{ri}\sum_{j=1}^{N}(V_{rj}G_{ij} - V_{mj}B_{ij}) - V_{mi}\sum_{j=1}^{N}(V_{rj}B_{ij} + V_{mj}G_{ij}) \quad (5.18)$$

and

$$\triangle Q_i = \frac{1}{mq_i}(V_i^* - V_i) - Q_{i,l} - V_{mi}\sum_{j=1}^{N}(V_{rj}G_{ij} - V_{mj}B_{ij}) + V_{ri}\sum_{j=1}^{N}(V_{rj}B_{ij} + V_{mj}G_{ij}) \quad (5.19)$$

The objective function, defined in equation 5.17, has $(2 \times N + 1)$ variables. This objective function is to be optimized subject to following constraints.

1. Equality constraints related to k-th PQ bus:

$$P_k - V_{rk}\sum_{j=1}^{N}(V_{rj}G_{kj} - V_{mj}B_{kj}) - V_{mk}\sum_{j=1}^{N}(V_{rj}B_{kj} + V_{mj}G_{kj}) = 0 \quad (5.20)$$

   and

$$Q_k - V_{mk}\sum_{j=1}^{N}(V_{rj}G_{kj} - V_{mj}B_{kj}) + V_{rk}\sum_{j=1}^{N}(V_{rj}B_{kj} + V_{mj}G_{kj}) = 0 \quad (5.21)$$

2. Equality constraints related to k-th PV bus:

$$P_k - V_{rk}\sum_{j=1}^{N}(V_{rj}G_{kj} - V_{mj}B_{kj}) - V_{mk}\sum_{j=1}^{N}(V_{rj}B_{kj} + V_{mj}G_{kj}) = 0 \quad (5.22)$$

   and

$$V_k^2 - V_{rk}^2 - V_{mk}^2 = 0 \quad (5.23)$$

3. Bound constraints:

$$V_{k,min} \leq V_k \leq V_{k,max} \quad (5.24)$$

   and

$$w_{min} \leq w \leq w_{max} \quad (5.25)$$

In the later sections, two novel constrained optimization algorithms are discussed which have been used to solve the above-mentioned objective for corresponding to power flow problem.

5.4 Differential Evolution with Gauss-Newton based Mutation

The DE [132] algorithm is a popular global optimization technique used in different problems of the power system. The DE relatively more robust and efficient technique as compared with other evolutionary algorithms. Several latest variants of DE have been judged as top-ranked algorithms in recent IEEE congress on evolutionary computation competitions [122, 192]. However, DE may not be directly applied to the constrained optimization problem. A constraint handling technique is required to evaluate the fitness of the solutions on the basis of feasibility and objective function value. In this chapter, epsilon-based constraint handling technique [146] has been employed with the operators of DE to solve the constrained optimization problems. In addition, it is also challenging for EAs to determine a feasible solution for a constrained problem with many equality constraints. For handling the equality constraints, most of the EAs convert equality constraints into relaxed inequality constraints. As a result, the feasibility of the obtained solutions is inadequate. In order to address this issue, this thesis introduces an algorithm to solve the problem with many equality constraints by introducing a Gauss-Newton (GN) based mutation operator that finds a feasible solution from an infeasible solution using the GN [193] algorithm. The proposed algorithm is named as ϵDE-GN and main operators of ϵDE-GN are summarized in the following sub-sections.

5.4.1 Differential Evolution

DE is a search-based global optimization algorithm proposed by Storn and Price [132]. DE can be applied to different type of optimization problems viz. Non-convex, non-differentiable, non-linear and multi-modal problems. In literature, it is shown that DE is robust and efficient on these types of problems. In DE, initial solutions are generated randomly within the lower and upper bound of search space and these solutions form an initial population. Each solution consists of n elements as decision parameters of the problem. At each iteration, all solutions of the population are selected as parents. Offspring generation for each parent is done as follows. The mutation process begins with the random selection of 3 solutions (different from the parent) from the population. The first solution out of 3 is considered as base vector. Other two solutions are utilized

to generate a difference vector. The difference vectors are weighted using parameter s_F and added to the base vector. The resulting solution is then passed through a process of crossover with parent solution. The probability of crossover is guided using a parameter CR (Crossover Rate). The crossover scheme returns a trial solution. Finally, for selection of solution for the next iteration, the trail solution is accepted if the trail vector is better than the parent. In algorithm ϵDE-GN, an exponential crossover is implemented. Another variant of crossover, Binomial Crossover, has been studied well in literature. However, exponential crossover performs better in constrained optimization problem as compared to binomial crossover. Hence, the exponential crossover is adopted in this work.

5.4.2 Gauss-Newton Mutation

The GN mutation is an operator used to calculate a feasible solution for an infeasible solution using gradient information of constraints, $\nabla C(x)$. The constraint vector, $C(x)$, the constraint violation vector, $\triangle C(x)$, and increment expected in point x, $\triangle x$, to satisfy constraints are related in the following manner [193]:

$$\triangle x = -\frac{\nabla C(x)^T \triangle C(x)}{\nabla C(x)^T \nabla C(x)} \tag{5.26}$$

where,

$$\triangle C(x) = [\triangle g_1(x)...\triangle g_n(x), \triangle h_{n+1}(x)...\triangle h_m(x)]^T, \triangle g_i(x) = max\{0, g_j(x)\} \tag{5.27}$$

The relation 5.26 is utilized whenever an infeasible solution, x^{infea}, is encountered. This mutation operation, $x^{fea} = x^{infea} + \triangle x$, is executed where x^{infea} is an infeasible solution.

5.4.3 ϵ-Constrained Handling Technique

In ϵ-constraint handling technique establishes an ϵ-level comparison to compare the solutions [146]. The ϵ-level comparison is defined using lexicographic order in which constraint violation, $\phi(x)(= \sum_{i=1}^{m} \triangle C_i(x))$, precedes objective function value, $f(x)$ as described in following paragraph [146].

Let $\{\phi_1, \phi_2\}$ and $\{f_1, f_2\}$ be the constraint violation value and the function values at points $\{x_1, x_2\}$ respectively. Then, the ϵ level comparisons are defined as follows:

$$(f_2, \phi_2) <_\epsilon (f_1, \phi_1) \Leftrightarrow \begin{cases} f_2 < f_1, & \text{if } (\phi_1, \phi_2 \leq \epsilon) \text{ or } (\phi_1 == \phi_2) \\ \phi_2 < \phi_1, & \text{otherwise} \end{cases} \tag{5.28}$$

$$(f_2, \phi_2) \leq_\epsilon (f_1, \phi_1) \Leftrightarrow \begin{cases} f_2 \leq f_1, & \text{if } (\phi_1, \phi_2 \leq \epsilon) \text{ or } (\phi_1 == \phi_2) \\ \phi_2 \leq \phi_1, & \text{otherwise} \end{cases} \tag{5.29}$$

Generally, ϵ level may not be controlled for most of the constrained optimization problems. However, constrained problems with equality constraints should be solved using controlled ϵ level. A simple way to control the ϵ-level is proposed in [146], which is defined using following equations.

$$\epsilon(t) = \begin{cases} \phi(x_\theta)(1 - \frac{t}{T_c})^{cp}, & 0 < t < T_c \\ 0, & T_c \leq t \end{cases} \tag{5.30}$$

where x_θ represents the top $\theta-$th individuals and cp represent parameter to control the speed of reduction of the ϵ-level.

5.4.4 The Algorithm: ϵDE-GN

The algorithm ϵDE-GN is based on DE/rand/1/exp [146]. The main steps of algorithm ϵDE-GN are as follows.

- **Step 1:** *Initialization*- In this step, initial population, P^0, of N_p solutions is initialized within the bound of search-space using following equation.

$$x_i^0 = (x_U - x_L)rand + x_L, \ i = 1, 2, ...N \tag{5.31}$$

  where x_U and x_L are the upper and lower bounds of search space respectively and *rand* represents the random number from uniform distribution within the range $(0, 1)$. An initial value of $\epsilon-$level, $\epsilon(0)$, is calculated using equation (7.18).

- **Step 2:** *Mutation*- For each solution x_i^k, three different solution x_{r1}^k, x_{r2}^k, and x_{r3}^k are selected from population, P^k, at k-th iteration. A new mutant solution, v_i^k, is calculated using x_{r1}^k, x_{r2}^k, and x_{r3}^k as follows.

$$v_i^k = x_{r1}^k + s_F(x_{r2}^k - x_{r3}^k), \text{ where } (r1 \neq r2 \neq r3 \neq i) \tag{5.32}$$

  where sF is a parameter called scaling factor.

- **Step 3:** *Crossover*- The mutant solution v_i^k, is used as a donor solution in crossover operation for solution x_i^k to generate a trial solution, u_i^k. A crossover point, l, is randomly selected from 1 to D, where D is the dimension of the problem. The element

corresponding $l-th$ dimension of the trail solution u_i^k is taken from the element corresponding to $l-th$ dimension of donor solution v_i^k. Subsequent elements of trial solution u_i^k are taken from donor solution v_i^k with exponentially decreasing probability (calculated using crossover rate CR). Rest of the elements of trial solution u_i^k are taken from the elements of solution x_i^k.

- **Step 4:** *Gauss-Newton Mutation-* If the generated trial solution u_i^k is infeasible (does not satisfy the all constraint), u_i^k is updated using GN. This process is repeated until the number of trials of GN reaches to N_{gn} or solution u_i^k becomes feasible solution. If after N_{gn} number of trials, infeasible trail solution does not become feasible the trial infeasible solutions is discarded in favor of previous feasible solution.

- **Step 5:** *Selection-* If the trial solution u_i^k is better than solution x_i^k on the basis of $\epsilon-$ level comparison, the trial solution u_i^k replaces the solution x_i^k for the next iteration.

- **Step 6:** $\epsilon-$ *level control-* The value of $\epsilon-$ level is updated using equation (7.18).

- **Step 7:** *Termination Condition-* If the total number of iteration becomes greater than maximum allowed iteration (T_{max}), the algorithm is terminated. Otherwise go to **Step 2**.

The performance of ϵDE-GN has been validated on benchmark problems and reported in Appendix-III.

5.5 Matrix Adaptation Evolution Strategy

The performance of Evolutionary Algorithms (EAs) can be heavily undermined in case of COPs where several constraints limit the feasible regions. For example, CMA-ES, one of the most efficient algorithms for unconstrained optimization, cannot readily be extended to solve COPs. Although some attempts of adopting CMA-ES for COPs have been made [156, 157], it is not yet competitive on these types of problems as compared to other popular algorithms like DE, GA, and PSO. There are two main reasons behind the relatively bleaker performance of CMA-ES on COPs: (i) conventional recombination approach of the algorithm cannot be suitable for the search space of COPs due to the

ranking of solutions based on the objective function value and (ii) the self-adaptation of the parameters of the algorithm is not suitable for COPs due to lower volume of the feasible region in search space especially in case of COPs involving several equality constraints.

To overcome these limitations of CMA-ES, we introduce here (i) a constraint handling technique, called υ-level penalty function to modify the fitness value of solutions while ranking the solutions in the algorithm and (ii) a solution repair scheme, called Broyden-based mutation, to handle the feasibility issue of solutions during the optimization process.

Firstly we introduce the υ-level penalty function and Broyden based mutation, then the main steps and framework of the proposed algorithm are discussed.

To solve the COPs, a new constraint handling technique called υ-level penalty function, is proposed in this section.

5.5.1 υ-level Modification in Constraints

Although, ϵ-level comparison of ϵ-constrained method shows good performance as a constraint handling technique with several EAs on COPs [1,146,194], its capability of relaxing infeasible solutions is more prominent in case the solutions violate a lower number of constraints as compared to the situation when several constraints are violated (as illustrated in Figure 5.3). The relaxed feasible region can be represented using Eqn. 5.33.

$$\phi(x) \leq \epsilon \implies \phi(x) - \epsilon \leq 0, \tag{5.33}$$

where $\phi(x)$ represents the value of constraint violation at solution x and it can be calculated as follows.

$$\phi(x) = \sum_{j=1}^{q} (max\{0, g_j(x)\}) + \sum_{j=q+1}^{m} (max\{0, |h_j(x)|\}) \tag{5.34}$$

It is seen from Eqn. (5.33), a fixed value of ϵ is used to modify the feasible region for each constraint violation without considering the number of violated constraints. This ϵ value is shared among the violated constraints. Therefore, the infeasible region with a low number of violated constraints is getting more sharing of ϵ as compared to the infeasible region with a higher number of violated constraints. This may strongly degrade the performance on COPs with a higher number of constraints with the optimum solution at active constraints.

To demonstrate this issue, a pictorial representation of a simple COP having five linear constraints are shown in figure 5.3. It can be seen from figure 5.3 that the ϵ-level feasible region has a very low volume of relaxed feasible region nearer to the optimum value as compared to the volume of the relaxed feasible region of other areas. Since the main function of this relaxed feasible region is to facilitate the population to search solutions at the boundary of the feasible region then the very low volume of relaxed feasible region nearer to the optimum solution cannot be the best situation. In [195] and [196], relaxed equality and inequality constraint functions are used to create separate surrogate models for all constraints. Further, these surrogate models are utilized to generate new solutions for expansive COPs. The performance of these surrogate assisted algorithms is highly improved after using relaxed equality and inequality constraint functions in place of actual constraint functions [195].

To sum up, the separate relaxation of constraints can provide a sufficient volume of the relaxed feasible region, which is beneficial to explore the optimum solutions nearer to the boundaries of feasible regions. Nevertheless, this approach has been discovered in surrogate modeling but has not been utilized in constrained handling techniques by existing constrained optimizations EAs. To overcome the limitation of ϵ-level modification without losing its core properties and to utilize the features of separate relaxation of constraints, a υ-level modification is proposed in this study.

In υ-level modification, the boundaries of all the feasible regions are modified. It is done by subtracting υ from all the constraints of the problem as shown below:

$$g_i^{(\upsilon)}(x) \leq 0 \implies g_i(x) - \upsilon \leq 0, \tag{5.35}$$

where υ represents the υ-level and its value must be a non-negative number. Usually, there is no need to have υ-level modification in constraints and many problems can be solved where the value of υ-level is set to 0 during the optimization process. However, in case of problems with smaller feasible regions, a high number of active inequality and equality constraints, the υ-level modification in constraint with proper controlling of υ-level would be required to obtain the better quality solutions. The calculation and controlling procedure of υ-level is discussed in the later section.

It is worth noting here that the υ-level modification is applicable to inequality constraints only. As an equality constraint, $h_i(x) = 0$ can be replaced with two inequality

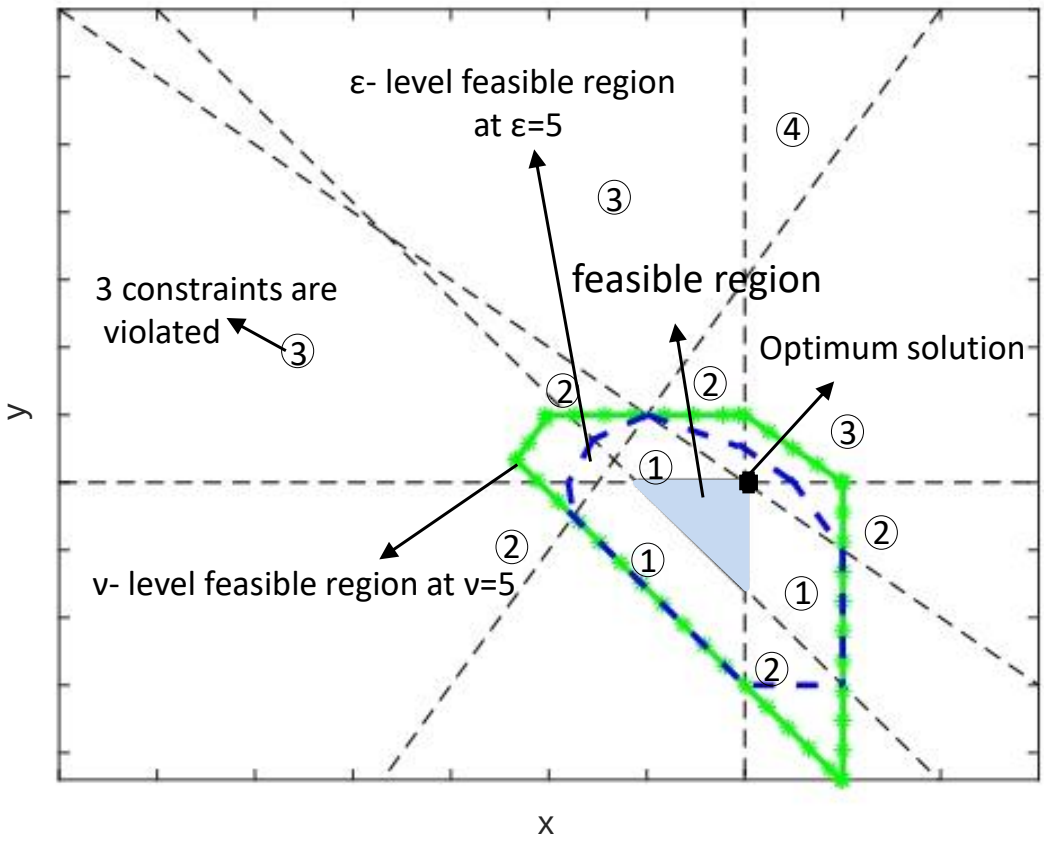

Figure 5.3: Graphical representation of main feature of υ-level modification as compared to ϵ-level comparison on a simple 2-D search space. Green solid line and blue dotted line represent the boundaries of υ-level and ϵ-level feasible regions respectively, at $\epsilon = \upsilon = 5$. Numbers within the circle represent the number of violated constraints in their respective area of search space.

constraints $h_i(x) \leq \epsilon_v$ and $-h_i(x) \leq \epsilon_v$, where ϵ_v is set to 10^{-4}. Thus, equality constraints can also be modified by υ-level modification as shown below.

$$|h_i^{(\upsilon)}(x)| \leq \epsilon_v \implies |h_i(x)| - \upsilon \leq \epsilon_v. \tag{5.36}$$

Moreover, we propose a simple procedure to control the υ-level at each iteration. The υ-level is only controlled for the first T iterations. After that, the υ-level is set to 0. The υ-level for each iteration is calculated as follows.

$$\upsilon_0 = \frac{\sum_{i=1}^{\theta\lambda} \phi_{i:\theta\lambda}}{\theta\lambda},$$

$$\upsilon^k = \begin{cases} \upsilon_0 \left(1 - \frac{k}{T}\right)^{\gamma} & , \ 0 < k \leq T, \\ 0 & , \ k > T, \end{cases} \tag{5.37}$$

where $\phi_{i:\theta N_p}$ represents the constraint violation of top i^{th} individual, $\theta = 0.9$, γ represents a parameter to control decay of the υ-level, and λ represents the population size. In this approach, it is presumed that the υ-level is equal to 10^{-5} (very small) at $k = 0.95T$. Now from Eqn. (5.37), this assumption can be reflected in the following way.

$$\upsilon^{0.95T} = \upsilon_0 \left(1 - \frac{0.95T}{T}\right)^{\gamma} = 10^{-5}. \tag{5.38}$$

Thus, parameter γ can be tuned according to Eqn. (5.38) and this can be done as shown below:

$$\gamma = max\left\{3, \frac{(-5 - log(\upsilon_0))}{log(0.05)}\right\}, \tag{5.39}$$

where the minimum value of γ is set to 3 to avoid too small a value for γ.

It is worth noting here that the value of T is problem dependent. The value of T can be fixed by using the sensitivity analysis over the wide variety of problems. From sensitivity analysis, it was found that the value of T can be set between 20% to 50% of the maximum allowed number of iterations.

Constraint violation and υ-level penalty function

In the υ-level penalty function, a υ-level constraint violation $\phi^{(\upsilon)}(x)$ is calculated by the sum of all the modified constraints:

$$\phi^{(\upsilon)}(x) = \sum_{j=1}^{q} (max\{0, g_j^{(\upsilon)}(x)\}) + \sum_{j=q+1}^{m} (max\{0, |h_j^{(\upsilon)}(x)| - \epsilon_v\}). \tag{5.40}$$

A v-level penalty function is defined as follows.

$$F(x) = f(x) + \alpha \cdot \phi^{(v)}(x), \tag{5.41}$$

where $f(x)$ and $F(x)$ denote the objective function value and fitness value at x respectively, and α is the penalty factor.

Calculation of the penalty factor α

Solving COPs with population-based EAs requires a balance between the minimization of the objective function and the constraint violation(s) during the optimization process. In [197], the correlation between constraint violation and objective function is calculated to guide the population for finding the feasible region. Although this approach performs well on COPs, a learning stage is required to calculate the correlation between the objective function and constrained violation. However, the correlation gained from the learning stage provides global correlation information and this correlation is not uniform over the search space. During the optimization process, it is more beneficial to use a local correlation between the objective function and constraints. In addition, no learning stage is required to calculate the local correlation between objective function and constraint which reduces the computational overhead. Here, we propose a simple approach to calculate the local correlation between the objective function and constraint violation to update the penalty factor.

Two kinds of relationship exist between constraints and the objective function.

1. The objective function $f(x)$ decreases as the degree of constraint violation $\phi^{(v)}(x)$ decreases.

2. The objective function $f(x)$ does not decreases as the degree of constraint violation $\phi^{(v)}(x)$ decreases.

For case (1), the objective function and constraint violation correlate with each other. In this situation, searching for a solution using constraint violation can easily stagnate the population in the feasible region. Therefore, the objective function value can help the solution to jump from the infeasible region to a feasible region. In such cases, the value of α should be equal to zero.

In the second type of relationship, objective function and constraint violation are not correlated to each other. Under this situation, too much weight to objective function or constraint violation may prevent the solution from stagnating the population. In such cases, the value of α should be tuned to provide proper weight to the objective function and constraint violation in fitness value.

To sum up, the value of α needs to tune according to the correlation between constraints and the objective function to guide the solutions to find the feasible region. However, this correlation information has not been utilized in the existing penalty functions. Hence a new self-adaptive technique is proposed in this chapter to auto-tune the value of α by using the correlation information.

At each iteration, the fitness value of the best solution should be lower than the fitness value of the other solution of the population of current or past iterations (in case of minimization problem). Mathematically, this relation can be represented in the following way:

$$f(y) + \alpha \cdot \phi^{(v)}(y) > f(x^*) + \alpha \cdot \phi^{(v)}(x^*), \tag{5.42}$$

where y represents a solution of population of the current or past generation and x^* represents the best solution found so far. Further, Eqn. (5.42) can be reduced to

$$\alpha > \frac{f(x^*) - f(y)}{\phi^{(v)}(y) - \phi^{(v)}(x^*)}. \tag{5.43}$$

The right hand side of Eqn. (5.43) indicate the relative variation of objective function value with respect to opposite variation of the constraint violation between the best solution and other solutions. When we mine this variation for all solutions of population, it provides the local correlation information between objective function and constraint in terms of relative variation from best solution.

In order to provide better mining of the correlation, an archive of solutions A_r of fixed size is formed which contains the solutions generated in past generations. When the size of this archive exceeds the fixed size, randomly selected solutions are discarded from the archive to maintain the size. From Eqn. (5.43),

$$\alpha^k > \frac{f(x^*) - f(y_i^k)}{\phi^{(v)}(y_i^k) - \phi^{(v)}(x^*)}, \tag{5.44}$$

where y_i^k represents the $i-$th individual of archive A_r and N_{A_r} represents the size of A_r. This information can be utilized to tune the value of penalty factor (α) in each iteration.

In v-level penalty function, we use the following equation to tune the value of α.

$$\alpha^k = max\left\{\frac{f(x^*) - f(y_i^k)}{\phi^{(v)}(y_i^k) - \phi^{(v)}(x^*)}, 0\right\}, \tag{5.45}$$

where $i = 1, 2, ...N_{A_r}$.

5.5.2 Broyden-based Mutation

In this subsection, Broyden-based Mutation is discussed.

Motivation

COPs with non-linear equality constraints can be hard to solve using COEAs. Most of constrained optimization EAs transform equality constraints into relaxed inequality constraints to solve these COPs. Feasible region of the search-space becomes very low due to the involvement of a large number of equality constraints. As a result, the performance of MA-ES (or CMA-ES) has been mediocre on these COPs as compared to other class of EAs. To address this issue, a gradient-based repair method is utilized in [1]. In literature, this repair method has also been utilized with other class of EAs such as in [198] with GA, and in [146] with DE. However, this repair method requires a large number of FEs (multiple of the number of decision variables) to repair a single infeasible solution. The main reason for the requirement of high function evaluations is the evaluation of gradient information (Jacobian matrix) of constraint space in each iteration of the repair process. In order to resolve this issue, a Broyden-based Mutation (BBM) technique is proposed in this chapter that requires only one FE in each iteration except for the first iteration to repair the infeasible solution. For the first iteration of the repairing process, the steps are similar to reported in [1].

Broyden's method

To solve a system of non-linear equations, $F(x) = [f_1(x), f_2(x)....f_n(x)]^T = 0$, where n is the total number of non-linear equations and $x = [x_1, x_2, \ldots .x_n]^T$, Newton's method is the computationaly inefficient due to the requirement of partial derivative of $F(x)$ at x (Jacobian matrix) during each iteration. This method cannot facilitate the reusing of information gained from previous iterations and in some situations determination of

the partial derivatives can be very costly. Finite-difference based calculation of partial derivatives of $F(x)$ at x requires n function evaluations (FEs) per iteration.

To overcome this issue of Newton's method, approximate partial derivatives can be used alternatively, since it provides slightly slower convergence due to approximation but it improves the efficiency overall. A simple and robust way to approximate the partial derivatives is proposed by C. G. Broyden in his seminal work on finding the solution of system of non-linear simultaneous equations [199]. In [199], the following equations are proposed to solve the simultaneous equations.

$$x^{(k+1)} = x^{(k)} - B^{-1(k)}F(x^{(k)}), \tag{5.46}$$

where

$$B^{-1(k)} = B^{-1(k-1)} + \frac{(s^{(k)} - B^{-1(k-1)}y^{(k)})(s^{(k)})^T B^{-1(k)}}{(s^{(k)})^T B^{-1(k-1)}y^{(k)}}, \tag{5.47}$$

$$s^{(k)} = x^{(k)} - x^{(k-1)}, \text{ and} \tag{5.48}$$

$$y^{(k)} = F(x^{(k)}) - F(x^{(k-1)}). \tag{5.49}$$

It can be seen from the above equations that an approximation of the inverse of the matrix of partial derivatives requires only one FE.

Proposed Scheme

Our proposed BBM to repair the infeasible solution is inspired by Broyden's method. The main steps of BBM are as follows:

1. First of all, all the constraints (Inequality, equality and bound constraints) of the COP are transformed into a system of simultaneous equations using slack variables, i.e.

$$g_j(x) + s_j^2 = 0, \ j = 1, ..., q, \tag{5.50}$$

$$h_j(x) = 0, \ j = q+1, ..., m, \tag{5.51}$$

$$x_i - l_i - lb_i^2 = 0, \ i = 1, ..., n, \tag{5.52}$$

$$x_i - u_i + ub_i^2 = 0, \ i = 1, ..., n, \tag{5.53}$$

   where, s_j, lb_i, and ub_i are the slack variables used to transform inequality, lower-bound, and upper-bound constraints into non-linear equations.

2. In second step, above mentioned system of simultaneous equations is solved using BBM (shown in Algorithm 4).

Algorithm 4: BBM(x)

Result: x, FE

Set $Max_{FE} \leftarrow (3D+1)$, and $TolF \leftarrow 10^{-15}$;

Define $s_j \leftarrow 0,\ j = 1, ..., q$, $lb_i \leftarrow \sqrt{x_i - l_i},\ , i = 1, ..., D$, and $ub_i \leftarrow \sqrt{u_i - x_i},\ , i = 1, ..., D$;

Initialize $\hat{x}^{(0)} \leftarrow [x^T, s_1, ..s_q, lb_1, ..lb_D, ub_1, ..ub_D]^T$;

$J \leftarrow$ Calculate Jacobian using Finite-difference approximation;

$FE \leftarrow D$;

$B^{-1(0)} \leftarrow$ PsuedoInverse(J);

$F^{(0)} \leftarrow F(\hat{x}^{(0)})$;

$FEs \leftarrow FEs + 1$;

$k \leftarrow 0$;

while $(FEs < Max_{FE})||(\|F^{(k)}\| > TolF)$ **do**

  $k \leftarrow k + 1$;

  $\hat{x}^{(k+1)} \leftarrow \hat{x}^{(k)} - B^{-1(k)}F^{(k)}$;

  $F^{(k+1)} \leftarrow F(\hat{x}^{(k+1)})$;

  $FE \leftarrow FE + 1$;

  $s^{(k+1)} \leftarrow \hat{x}^{(k+1)} - \hat{x}^{(k)}$;

  $y^{(k+1)} \leftarrow F^{(k+1)-F^{(k)}}$;

  $B^{-1(k+1)} \leftarrow B^{-1(k)} + \frac{(s^{(k+1)} - B^{-1(k)}y^{(k+1)})(s^{(k+1)})^T B^{-1(k)}}{(s^{(k+1)})^T B^{-1(k)} y^{(k+1)}}$;

end

$x \leftarrow \hat{x}^{(k)}_{1:D}$;

5.5.3 Proposed Algorithm: υMA-ESbm

The proposed algorithm, named υMA-ESbm, is described. MA-ES [200] is used as the core optimizer. In order to deal with the constraints of the problem, υ-level penalty function based constraint handling technique with Broyden-based mutation is consolidated in the framework of MA-ES described in [200]. The pseudo code of υMA-ESbm is shown in Algorithm 5.

Algorithm 5: υMA-ESbm

Result: $bestx$, $bestf$, and $bestc$

1 Set λ, μ, σ^0, σ_{max}, T, k_r, and θ_r;
2 Initialize the parameters of MA-ES at their default values as shown in Table 5.1;
3 Initialize $M^0 \leftarrow I$, $P_c \leftarrow 0$, and $X^0 \leftarrow \{x_1^0, x_2^0 .... x_\lambda^0\}$;
4 Evaluate f^0, g^0, and h^0 at each individual of X^0;
5 $FEs \leftarrow \lambda$;
6 $\phi_i^{(0)} \leftarrow \sum_j \max(g_{i,j}^0, 0) + \sum_j \max(|h_{i,j}^0| - e_v, 0)$, $i \in \{1, 2..\lambda\}$;
7 Calculate υ_0, γ, $\phi^{(\upsilon_0)}$, and α^0 using Eqns. (5.37), (5.39), (5.40), and (5.45) respectively ;
8 $F^0 \leftarrow f^0 + \alpha^0 \cdot \phi^{(\upsilon_0)}$;
9 $x_m^0 \leftarrow \sum_{i=1}^{\mu} w_i x_{i:\lambda}$ according to F^0;
10 $bestx \leftarrow x_{1:\lambda}^0$, and $bestf \leftarrow f_{1:\lambda}^0$;
11 $bestc \leftarrow \sum_j \max(g_{1:\lambda}^0, 0) + \sum_j \max(|h_{1:\lambda}^0| - e_v, 0)$;
12 $k \leftarrow 0$;
13 **while** $FEs \leq FE_{max}$ **do**
14 $k \leftarrow k + 1$;
15 $M^{-1} \leftarrow \text{PseudoInverse}(M^k)$;
16 **for** $i \leftarrow 1 : \lambda$ **do**
17 $z_i^k \leftarrow N(0, I)$, $d_i^k \leftarrow M^k z_i^k$ and $\bar{x} \leftarrow x_i^k + \sigma^k d_i^k$;
18 $x_i^{k+1} \leftarrow \text{KeepRange}(\bar{x})$;
19 Evaluate f_i, g_i, and h_i at x_i^{k+1};
20 $FEs \leftarrow FEs + 1$;
21 Calculate $\phi_i^{(\upsilon)}$ using Eqn. (5.40);
22 **if** $(mod(k, D) == 0) || (U(0,1) < \theta_r)$ **then**
23 $[x_i^{k+1}, FE] \leftarrow \text{BBM}(x_i^{k+1})$;
24 $FEs \leftarrow FEs + FE$
25 **end**
26 **if** $\bar{x} \neq x_i^{k+1}$ **then**
27 $d_i^k \leftarrow \frac{x_i^{k+1} - \bar{x}}{\sigma^k}$, $z_i^k \leftarrow M^{-1} d_i^k$;
28 Calculate $\phi_i^{(\upsilon)}$ using Eqn. (5.40);
29 **end**
30 **end**
31 Calculate α using Eqn. (5.45);
32 $F^k \leftarrow f^k + \alpha^k \cdot \phi^{(\upsilon^k)}$;
33 $x_m^{k+1} \leftarrow x_m^k + \sigma^k \sum_{i=1}^{\mu} w_i d_{1:\lambda}^k$ according to F;
34 Update P_c^{k+1}, M^{k+1}, σ^{k+1}, and υ^{k+1} using Eqns. (5.56), (6.48), (5.58), and (5.37);
35 Update $bestx$, $bestf$, and $bestc$ using Deb's rule [201];
36 **end**

The main steps of υMA-ESbm are described as follows.

- **Step 1** (Line 1-3): Firstly, parameters of algorithm are set to their default values and an initial population X^0 of λ solutions are randomly generated within the bounds of the search space using following equation.

$$x_{i,j}^0 = l_j + (u_j - l_j) \cdot \text{U}(0,1), \ \ for\ i = 1, 2.....\lambda, \tag{5.54}$$

Table 5.1: Default value of parameters of MA-ES [1]

1.	$w_i = \frac{ln(\mu+0.5)-ln(i)}{\sum_{j=1}^{\mu}(ln(\mu+0.5)-ln(j))},\ for\ i \in \{1,..,\mu\},$	
2.	$\mu_{eff} = \frac{1}{\sum_{i=1}^{\mu} w_i^2},$	3. $c = \frac{\mu_{eff}+2}{D+\mu_{eff}+5},$
4.	$c_p = \frac{2}{(D+1.3)^2+\mu_{eff}},$	5. $c_z = min\left[1-c_p, \frac{2(\mu_{eff}-2+1/\mu_{eff})}{(D+1)^2+\mu_{eff}}\right].$

where, $x_{i,j}$ represents $j-$th element of x_i^0 and $\mathrm{U}(0,1)$ a uniformly distributed random number in $(0,1)$.

- **Step 2** (Line 4-12): The initial population is used to determine the υ_0 and γ. Then, the initial recombinant, x_m^0, is obtained using weighted recombination of the top μ individuals of population X^0.

- **Step 3** (Line 17-21): By using σ^k and M^k, new solutions are generated for each λ solutions in the mutation operation. If a new solution is sampled outside the bounds of the search space, then that solution is reflected back to search space using Eqn. (5.55) (Line 18, KeepRange function).

$$x_{i,j} = \begin{cases} 2 \times l_j - x_{i,j} - \left\lfloor \frac{l_j - x_{i,j}}{v_i} \right\rfloor v_i, & if \mathrm{x\dot{}i,j\ ¡\ l\dot{}j} \\ x_{i,j} - \left\lfloor \frac{x_{i,j}-v_j}{v_i} \right\rfloor_i, & if \mathrm{x\dot{}i,j¿u\dot{}j} \\ x_{i,j} & else \end{cases} \tag{5.55}$$

where $v_i = (l_j - u_j)$.

- **Step 4** (Line 22-25): If the iteration count, k, becomes multiple of dimension D, BBM operator is used with probability θ_r to generate the feasible solutions to replace the infeasible ones.

- **Step 5** (Line 26-29): The corresponding vectors d_i^k and z_i^k of the readjusted x_i^k are recalculated to the correct value. Inverse of M^k is required for this process.

- **Step 6** (Line 31-34): Calculates the penalty factor α by using Eqn. (5.45). Vector P_c^{k+1} is updated using Eqn. (5.56) and matrix M^{k+1} is updated using P_c^{k+1}, M^k, z^k as shown in Eqn (6.48), and other parameters. Finally, the mutation step-size σ^{k+1} is updated using the value of P_c^{k+1} as shown in Eqn. (5.58).

$$P_c^{k+1} = (1-c)P_c^k + \sqrt{c(2-c)\mu_{eff}} \sum_{i=1}^{\mu} w_i z_{i:\lambda}^k, \tag{5.56}$$

$$M^{k+1} = M^k + \frac{c_p}{2} M^k (P_c^{k+1}(P_c^{k+1})^T - I)...$$
$$+ \frac{c_z}{2} M^k \left(\sum_{i=1}^{\mu} w_i z_{i:\lambda}^k (z_{i:\lambda}^k)^T - I \right), \tag{5.57}$$

$$\sigma^{k+1} = min \left(\sigma^k exp \left[\frac{c}{2} \left(\frac{||P_c^{k+1}||^2}{D} - 1 \right) \right], \sigma_{max} \right), \tag{5.58}$$

where c, c_p, and c_z are learning rate parameters of MA-ES which are set to their default values.

- **Step 7** (Line 35): Best solution with its objective function and constraint violation value are updated using Deb's rule [201] of selection of solution.
- **Step 8** (Line 15): If the inverse of M is ill-conditioned then M is reinitialized to Identity matrix.
- **Step 9** (Line 13): Go to **Step 3**, if the FEs is less than the maximum allowed number of function evaluation.
- **Step 10** (Line 36): Return the best solution with its objective function and constraint violation value.

The performance of υMAESlm has been validated on benchmark problems and reported in Appendix-III.

5.6 Performance of Proposed Algorithm

Two novel algorithms, ϵDE-GN, and υMAESbm, have been implemented to optimize the objective function corresponding to power flow problem. ϵDE-GN algorithm uses DE as a search algorithm with a Gauss-Newton mutation operator. υMAESbm uses MAES as a search algorithm with Broyden mutation operator.

To analyze the accuracy of the obtained results from the proposed algorithms, a comparison of voltages obtained from the proposed algorithms and PSCAD/EMTDC is performed on the 6-bus system. The results obtained from PSCAD, ϵDE-GN, and υMAESbm are depicted in Table-5.2. It is clearly seen from Table-5.2 that the maximum errors in voltage magnitude and angle are 0.0081% and 0.26% respectively. This good agreement within the obtained results validates the accuracy of the ϵDE-GN, and

Table 5.2: Validation of obtained result of the six-bus test system

Bus	Voltage magnitude (V)			Angle (rad)		
	PSCAD	ϵDE-GN	υMAESbm	PSCAD	ϵDE-GN	υMAESbm
1	121.92	121.92	121.92	0.0078	0.0078	0.0078
2	123.51	123.51	123.51	-0.0013	-0.0013	-0.0013
3	122.42	122.42	122.42	-0.0388	-0.0389	-0.0389
4	125.37	125.37	125.37	0.0065	0.0065	0.0065
5	125.74	125.74	125.74	0*	0*	0*
6	123.11	123.10	123.10	-0.0420	-0.0421	-0.0426
err		0.0081%	0.0081%		0.26%	0.26%
freq	376.6645	376.6645	376.6645			
Time	172s	0.4s	0.9s			

Table 5.3: Comparison of results on 33-bus system

Methods	Mean	Stdev	CT
GA	1.48×10^{-04}	1.02×10^{-04}	4.3s
PSO	2.04×10^{-06}	1.83×10^{-06}	2.2s
Newton-trust	1.73×10^{-06}	1.07×10^{-06}	1.7s
ϵDE-GN	1.58×10^{-09}	1.43×10^{-09}	0.8s
υMAESbm	1.25×10^{-10}	1.08×10^{-10}	1.1s

υMAESbm in solving the power flow of droop control based islanded MG. Moreover, PSCAD requires approximately 172s to attain the steady-state, while the ϵDE-GN, and υMAESbm require 0.4s and 0.9s respectively.

Further, a comparison among different optimization algorithms, GA, PSO, Newton-trust region, ϵDE-GN, and υMAESbm has also been done for a 33-bus test system. The values of the means and standard deviations of the objective function with computation time are depicted for each of the algorithms in Table 5.3. This Table shows that the proposed algorithms outperform the other contenders in terms of accuracy and computation time.

5.7 Case Studies

In this section, four case studies were carried out to validate the load flow flow algorithms on different test systems. The framework of these cases studies are as follows:

- **Case study I**: In this case, CASE6 test system was adopted to validate the proposed load flow algorithms. Fig. 5.4 shows topology of CASE6 test system as an islanded microgrid. The load data and line connectivity data used in test systems are reported in Appendix-II. This system consist of three similar droop controlled DGs on buses 4, 5 and 6 and the system is operated in islanded mode. The detailed specifications of droop controls are depicted in Table. 5.4. The effectuation of the proposed load flow algorithms as well as a comparative analysis using PSCAD software [40], the PSO method [23] are depicted in Table 5.4. Following are the observations:

  1. The steady state frequency obtained by proposed algorithms are 0.99924 p.u.
  2. The comparative analysis of the maximum magnitude and maximum phase errors of above specified methods against the proposed methods are 0.0008 and 0.007, respectively .

  Based on the above comparative analysis, it can be concluded that the proposed algorithms perform with acceptable accuracy on droop controlled microgrids in islanded mode of operation.

Table 5.4: Droop control settings of DGs in CASE6 test system [56]

DG	Location	m_p	n_q	ω^*	V^*	S_{max}	Q_{max}
1	4	1.1439×10^{-3}	0.0591	1	1.01	1	0.7
2	5	1.1439×10^{-3}	0.0591	1	1.01	1	0.7
3	6	1.1439×10^{-3}	0.0591	1	1.01	1	0.7

- **Case study II:** The IEEE CASE69 distribution system shown in Fig.5.5 has been considered for this case study as an islanded microgrid. This system is having total active and reactive loads of 3.772 MW and 2.694 MVAr respectively. Bus numbers 50, 27, 35, 46 and 65 are considered for DGs installation. The detailed droop control setting of DGs for the CASE69 distribution system reported in Table 5.6 are adopted

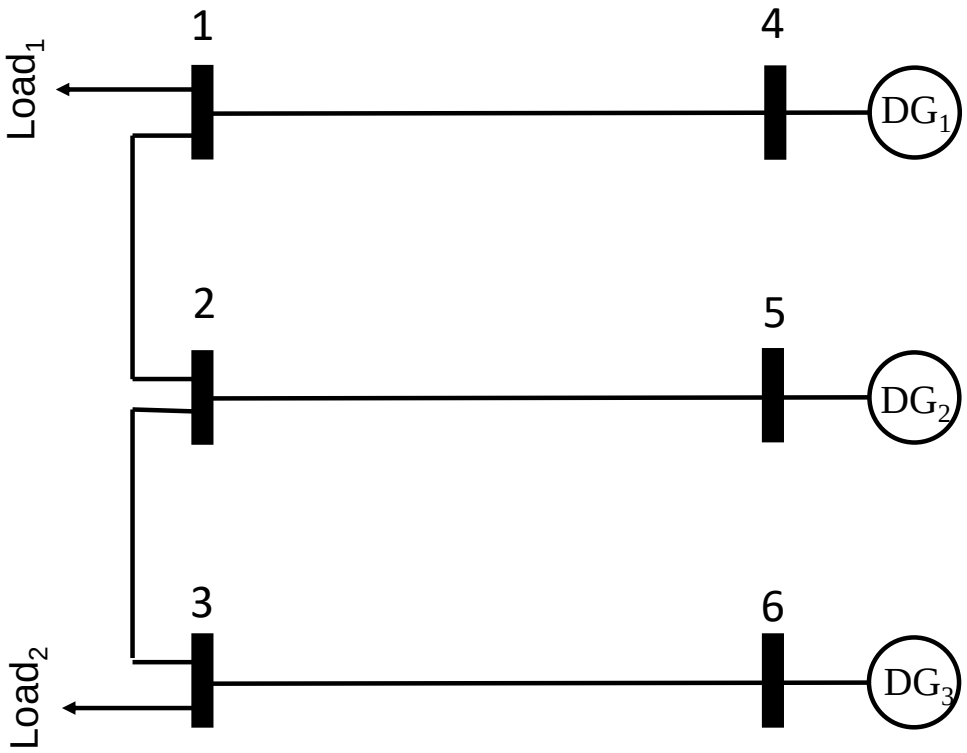

Figure 5.4: Topology of CASE6 test system operated as an islanded microgrid.

Table 5.5: Outcomes of proposed load flow algorithm for a CASE6 test system compared with other methods.

Bus	Time domain Model		ϵDE-GN		υMAESbm		PSO		Newton-trust	
	$\|V\|$	$\angle_V$	$\|V\|$	$\angle_V$	$\|V\|$	$\angle_V$	$\|V\|$	$\angle_V$	$\|V\|$	$\angle_V$
1	0.9605	0	0.9606	0	0.9606	0	0.9607	0	0.9601	0
2	0.9730	-0.537	0.9729	-0.5291	0.9730	-0.5269	0.9728	-0.5292	0.9725	-0.5262
3	0.9643	-2.685	0.9647	-2.6837	0.9646	-2.6828	0.9645	2.6765	0.9638	-2.6822
4	0.9877	-0.0725	0.9875	-0.0726	0.9877	-0.0716	0.9884	-0.0727	0.9873	-0.0722
5	0.9906	-0.452	0.9903	-0.4516	0.9905	-0.4522	0.9883	-0.0454	0.9901	-0.45101
6	0.9698	-2.869	0.9689	-2.8668	0.9698	-2.8659	0.9701	-2.8608	0.9694	-2.8653

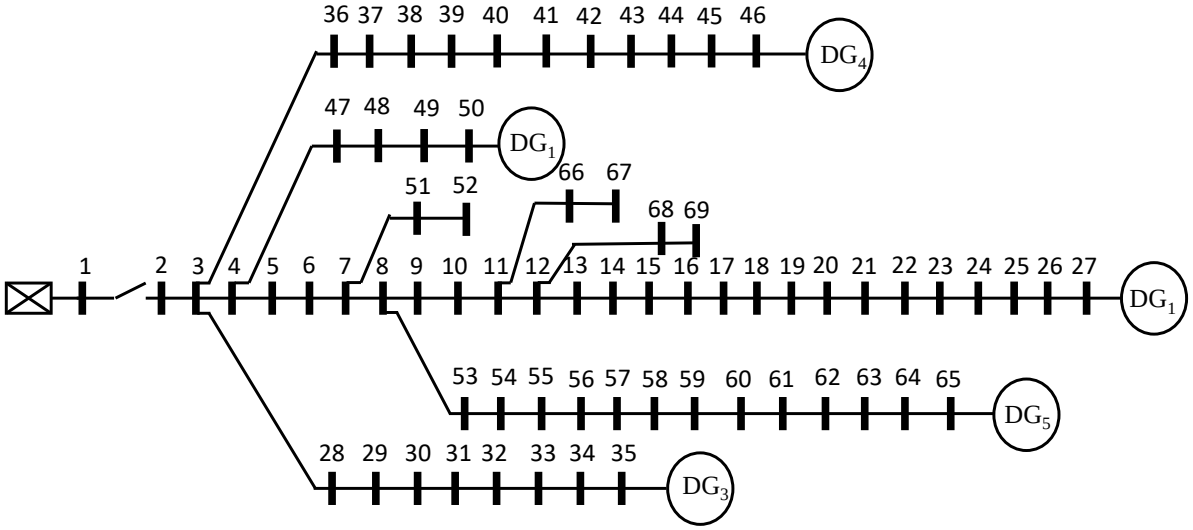

Figure 5.5: Topology of CASE69 test system operated as an islanded microgrid.

for analyses purpose. Tables 5.7 and 5.8 present the detailed voltage profile obtained using ϵDE-GN and υMAESbm, respectively. Following are the observations.

1. The steady state frequency obtained by ϵDE-GN and υMAESbm are 0.9977 p.u and 0.9977 p.u., respectively.
2. The total active power and reactive power load demand on the distribution system are 3.7722 MW and 2.6941 MVAr respectively whereas active and reactive power losses are 0.0868 MW and 0.0424 MVAR.

- **Case study III:** A CASE33 distribution system with bus voltage of 12.66 kV is used in this case study for demonstration of proposed load flow algorithm. The single

Table 5.6: Droop control settings of DGs in CASE69 test system [2]

DG	Location	m_p	n_q	ω^*	V^*	S_{max}	Q_{max}
1	60	1.501×10^{-3}	0.03333	1	1.04	2.0	1.4
2	27	4.504×10^{-3}	0.01	1	1.04	1.0	0.65
3	35	2.308×10^{-3}	0.05	1	1.04	1.2	0.6
4	46	2.308×10^{-3}	0.05	1	1.04	1	0.6
5	65	1.501×10^{-3}	0.03333	1	1.04	1.5	0.9

Table 5.7: Voltage profile obtained from ϵDE-GN for CASE69 distribution system operated as an islanded microgrid.

Bus	$\lvert V\rvert$	$\angle_V$	P	Q	$\lvert I\rvert$	$\angle_I$	Bus	$\lvert V\rvert$	$\angle_V$	P	Q	$\lvert I\rvert$	$\angle_I$	Bus	$\lvert V\rvert$	$\angle_V$	P	Q	$\lvert I\rvert$	$\angle_I$
1	–	–	–	–	–	–	24	0.9711	-0.1277	-0.0280	-0.0200	0.0208	2.2516	47	0.9712	-0.0001	0.0000	0.0000	0.0061	-0.7545
2	0.9710	0.0000	0.0000	0.0000	0.0033	-0.5378	25	0.9870	-0.1356	0.0000	0.0000	0.0032	0.5156	48	0.9730	0.0039	-0.0790	-0.0564	0.0592	2.5486
3	0.9710	0.0000	0.0000	0.0000	0.0063	-0.8331	26	0.9936	-0.1388	-0.0140	-0.0100	0.0105	2.2647	49	0.9815	0.0190	-0.3847	-0.2745	0.2893	2.5477
4	0.9712	-0.0003	0.0000	0.0000	0.0057	-0.8002	27	0.9974	-0.1407	0.4940	0.6374	0.3698	-0.9093	50	0.9872	0.0254	-0.3847	-0.2745	0.6281	-0.3321
5	0.9711	-0.0037	0.0000	0.0000	0.0150	-0.9815	28	0.9706	0.0005	-0.0260	-0.0186	0.0275	2.5083	51	0.9401	-0.0825	-0.0405	-0.0283	0.0292	2.4537
6	0.9571	-0.0377	-0.0026	-0.0022	0.0225	-1.2498	29	0.9648	0.0073	-0.0260	-0.0186	0.0234	2.3300	52	0.9400	-0.0825	-0.0036	-0.0027	0.0029	2.4250
7	0.9433	-0.0737	-0.0404	-0.0300	0.0183	2.8487	30	0.9688	0.0293	0.0000	0.0000	0.0050	-0.6933	53	0.9373	-0.1039	-0.0043	-0.0035	0.0068	-0.8428
8	0.9403	-0.0826	-0.0750	-0.0540	0.0612	2.4732	31	0.9695	0.0332	0.0000	0.0000	0.0047	-0.7149	54	0.9356	-0.1232	-0.0264	-0.0190	0.0095	2.4035
9	0.9390	-0.0874	-0.0300	-0.0220	0.0128	2.4806	32	0.9732	0.0526	0.0000	0.0000	0.0130	-0.6912	55	0.9340	-0.1504	-0.0240	-0.0172	2.1961	-1.3162
10	0.9279	-0.0876	-0.0280	-0.0190	0.0189	2.5090	33	0.9828	0.0986	-0.0140	-0.0100	0.0178	-0.7815	56	0.8995	-0.1475	0.0000	0.0000	0.0503	1.0580
11	0.9256	-0.0877	-0.1450	-0.1040	0.1145	2.4455	34	1.0074	0.1901	-0.0195	-0.0140	0.0215	-0.8037	57	0.7209	-0.0983	0.0000	0.0000	0.0691	1.0531
12	0.9231	-0.0901	-0.1450	-0.1040	0.1109	2.4370	35	1.0335	0.2664	1.0099	-0.9140	0.8479	1.1568	58	0.6334	-0.0694	0.0000	0.0000	0.0415	1.1028
13	0.9295	-0.0969	-0.0080	-0.0055	0.0041	2.1597	36	0.9710	0.0003	-0.0260	-0.0186	0.0275	2.5237	59	0.5996	-0.0571	-0.1000	-0.0720	0.1140	2.2052
14	0.9362	-0.1038	-0.0080	-0.0055	0.0043	2.1304	37	0.9715	0.0051	-0.0260	-0.0186	0.0212	2.5374	60	0.5598	-0.0405	0.4486	1.3111	0.0548	-1.5506
15	0.9434	-0.1109	0.0000	0.0000	0.0018	-0.2209	38	0.9736	0.0094	0.0000	0.0000	0.0038	-0.8084	61	0.5012	-0.0292	-1.2440	-0.8880	1.3428	2.5328
16	0.9447	-0.1122	-0.0455	-0.0300	0.0338	2.4396	39	0.9741	0.0106	-0.0240	-0.0170	0.0187	2.6245	62	0.4991	-0.0287	-0.0320	-0.0230	0.0022	1.2631
17	0.9480	-0.1150	-0.0600	-0.0350	0.0429	2.4945	40	0.9742	0.0107	-0.0240	-0.0170	0.0185	2.6275	63	0.4959	-0.0281	0.0000	0.0000	0.0073	2.4883
18	0.9481	-0.1150	-0.0600	-0.0350	0.0431	2.4941	41	0.9911	0.0405	-0.0012	-0.0010	0.0051	-1.8529	64	0.4807	-0.0251	-0.2270	-0.1620	0.2435	2.5459
19	0.9528	-0.1178	0.0000	0.0000	0.0011	0.2747	42	0.9985	0.0531	0.0000	0.0000	0.0018	-1.5648	65	0.4761	-0.0242	1.4649	0.0565	0.0633	2.5506
20	0.9558	-0.1196	-0.0010	-0.0006	0.0010	0.2978	43	0.9995	0.0547	-0.0060	-0.0043	0.0058	2.6485	66	0.9252	-0.0875	-0.0180	-0.0130	0.0130	2.4392
21	0.9607	-0.1224	-0.1140	-0.0810	0.1141	2.3989	44	0.9997	0.0551	0.0000	0.0000	0.0019	-0.9064	67	0.9252	-0.0875	-0.0180	-0.0130	0.0138	2.4378
22	0.9610	-0.1226	-0.0053	-0.0035	0.0239	-0.7357	45	1.0023	0.0598	-0.0392	-0.0263	0.0442	2.8316	68	0.9210	-0.0894	-0.0280	-0.0200	0.0216	2.4428
23	0.9642	-0.1242	0.0000	0.0000	0.0013	0.7907	46	1.0023	0.0598	0.9767	0.1198	0.5296	0.1773	69	0.9210	-0.0894	-0.0280	-0.0200	0.0218	2.4425
w	0.9977																			

line diagram of distribution system shown in Fig. 5.6 with four DGs on bus number 26, 22, 25 and 9 and this test system is operated in islanded mode. The static droop coefficient of DGs along with relevant specification are depicted in Table. 5.9. The coefficients k_{pf} and k_{qf} (equations 5.3 and 5.4) for all DGs were assumed as 1 and -1 respectively. In this case, analysis have been performed assuming DG1 operates in PV mode, whereas other DGs are operating in droop controlled mode. Often constant power load modeling is taken into load flow formulation, whereas in this work loads are modeled to mimic real scenario in form of commercial, residential and industrial load models which were obtained by using equations 5.3 and 5.4. The

Table 5.8: Voltage profile obtained from υMAESbm for CASE69 distribution system operated as an islanded microgrid.

Bus	$\|V\|$	$\angle_V$	P	Q	$\|I\|$	$\angle_I$	Bus	$\|V\|$	$\angle_V$	P	Q	$\|I\|$	$\angle_I$	Bus	$\|V\|$	$\angle_V$	P	Q	$\|I\|$	$\angle_I$
1	–	–	–	–	–	–	24	0.9711	-0.1277	-0.0280	-0.0200	0.0208	2.2516	47	0.9712	-0.0001	0.0000	0.0000	0.0061	-0.7545
2	0.9710	0.0000	0.0000	0.0000	0.0033	-0.5378	25	0.9870	-0.1356	0.0000	0.0000	0.0032	0.5156	48	0.9730	0.0039	-0.0790	-0.0564	0.0592	2.5486
3	0.9710	0.0000	0.0000	0.0000	0.0063	-0.8331	26	0.9936	-0.1388	-0.0140	-0.0100	0.0105	2.2647	49	0.9815	0.0190	-0.3847	-0.2745	0.2893	2.5477
4	0.9712	-0.0003	0.0000	0.0000	0.0057	-0.8002	27	0.9974	-0.1407	0.4940	0.6374	0.3698	-0.9093	50	0.9872	0.0254	-0.3847	-0.2745	0.6281	-0.3321
5	0.9711	-0.0037	0.0000	0.0000	0.0150	-0.9815	28	0.9706	0.0005	-0.0260	-0.0186	0.0275	2.5083	51	0.9401	-0.0825	-0.0405	-0.0283	0.0292	2.4537
6	0.9571	-0.0377	-0.0026	-0.0022	0.0225	-1.2498	29	0.9648	0.0073	-0.0260	-0.0186	0.0234	2.3300	52	0.9400	-0.0825	-0.0036	-0.0027	0.0029	2.4250
7	0.9433	-0.0737	-0.0404	-0.0300	0.0183	2.8487	30	0.9688	0.0293	0.0000	0.0000	0.0050	-0.6933	53	0.9373	-0.1039	-0.0043	-0.0035	0.0068	-0.8428
8	0.9403	-0.0826	-0.0750	-0.0540	0.0612	2.4732	31	0.9695	0.0332	0.0000	0.0000	0.0047	-0.7149	54	0.9356	-0.1232	-0.0264	-0.0190	0.0095	2.4035
9	0.9390	-0.0874	-0.0300	-0.0220	0.0128	2.4806	32	0.9732	0.0526	0.0000	0.0000	0.0130	-0.6912	55	0.9340	-0.1504	-0.0240	-0.0172	2.1961	-1.3162
10	0.9279	-0.0876	-0.0280	-0.0190	0.0189	2.5090	33	0.9828	0.0986	-0.0140	-0.0100	0.0178	-0.7815	56	0.8995	-0.1475	0.0000	0.0000	0.0503	1.0580
11	0.9256	-0.0877	-0.1450	-0.1040	0.1145	2.4455	34	1.0074	0.1901	-0.0195	-0.0140	0.0215	-0.8037	57	0.7209	-0.0983	0.0000	0.0000	0.0691	1.0531
12	0.9231	-0.0901	-0.1450	-0.1040	0.1109	2.4370	35	1.0335	0.2664	1.0099	-0.9140	0.8479	1.1568	58	0.6334	-0.0694	0.0000	0.0000	0.0415	1.1028
13	0.9295	-0.0969	-0.0080	-0.0055	0.0041	2.1597	36	0.9710	0.0003	-0.0260	-0.0186	0.0275	2.5237	59	0.5996	-0.0571	-0.1000	-0.0720	0.1140	2.2052
14	0.9362	-0.1038	-0.0080	-0.0055	0.0043	2.1304	37	0.9715	0.0051	-0.0260	-0.0186	0.0212	2.5374	60	0.5598	-0.0405	0.4486	1.3111	0.0548	-1.5506
15	0.9434	-0.1109	0.0000	0.0000	0.0018	-0.2209	38	0.9736	0.0094	0.0000	0.0000	0.0038	-0.8084	61	0.5012	-0.0292	-1.2440	-0.8880	1.3428	2.5328
16	0.9447	-0.1122	-0.0455	-0.0300	0.0338	2.4396	39	0.9741	0.0106	-0.0240	-0.0170	0.0187	2.6245	62	0.4991	-0.0287	-0.0320	-0.0230	0.0022	1.2631
17	0.9480	-0.1150	-0.0600	-0.0350	0.0429	2.4945	40	0.9742	0.0107	-0.0240	-0.0170	0.0185	2.6275	63	0.4959	-0.0281	0.0000	0.0000	0.0073	2.4883
18	0.9481	-0.1150	-0.0600	-0.0350	0.0431	2.4941	41	0.9911	0.0405	-0.0012	-0.0010	0.0051	-1.8529	64	0.4807	-0.0251	-0.2270	-0.1620	0.2435	2.5459
19	0.9528	-0.1178	0.0000	0.0000	0.0011	0.2747	42	0.9985	0.0531	0.0000	0.0000	0.0018	-1.5648	65	0.4761	-0.0242	1.4649	0.0565	0.0633	2.5506
20	0.9558	-0.1196	-0.0010	-0.0006	0.0010	0.2978	43	0.9995	0.0547	-0.0060	-0.0043	0.0058	2.6485	66	0.9252	-0.0875	-0.0180	-0.0130	0.0130	2.4392
21	0.9607	-0.1224	-0.1140	-0.0810	0.1141	2.3989	44	0.9997	0.0551	0.0000	0.0000	0.0019	-0.9064	67	0.9252	-0.0875	-0.0180	-0.0130	0.0138	2.4378
22	0.9610	-0.1226	-0.0053	-0.0035	0.0239	-0.7357	45	1.0023	0.0598	-0.0392	-0.0263	0.0442	2.8316	68	0.9210	-0.0894	-0.0280	-0.0200	0.0216	2.4428
23	0.9642	-0.1242	0.0000	0.0000	0.0013	0.7907	46	1.0023	0.0598	0.9767	0.1198	0.5296	0.1773	69	0.9210	-0.0894	-0.0280	-0.0200	0.0218	2.4425
w	0.9977																			

load exponents for commercial, residential and industrial load are given in Table 5.10. Following are the observations:

1. The steady state frequency obtained by ϵDE-GN and υMAESbm for this case are 0.9984 p.u and 0.9984 p.u, respectively.
2. The detailed voltage and load profile of the CASE33 distribution system are presented in Table. 5.11.
3. Reactive power generation reaches maximum when the voltage of bus 22 equals 1.0075 p.u. whereas reactive power generation is fixed at its maximum value, when the voltage of bus 22 equals to 1.01 p.u. keeping the value of reactive power of droop controlled DGs within in their permissible range.

- **Case study IV:** The CASE25, a three phase unbalanced distribution operating in isolated mode, with the rated voltage of 12.66 KV has been adopted for this study. Fig. 5.7 shows typical topology of 25-bus distribution system as an islanded microgrid. The load data, line connectivity and impedances for different type of conductor used in distribution system are given in ref. [202]. Three DGs are installed

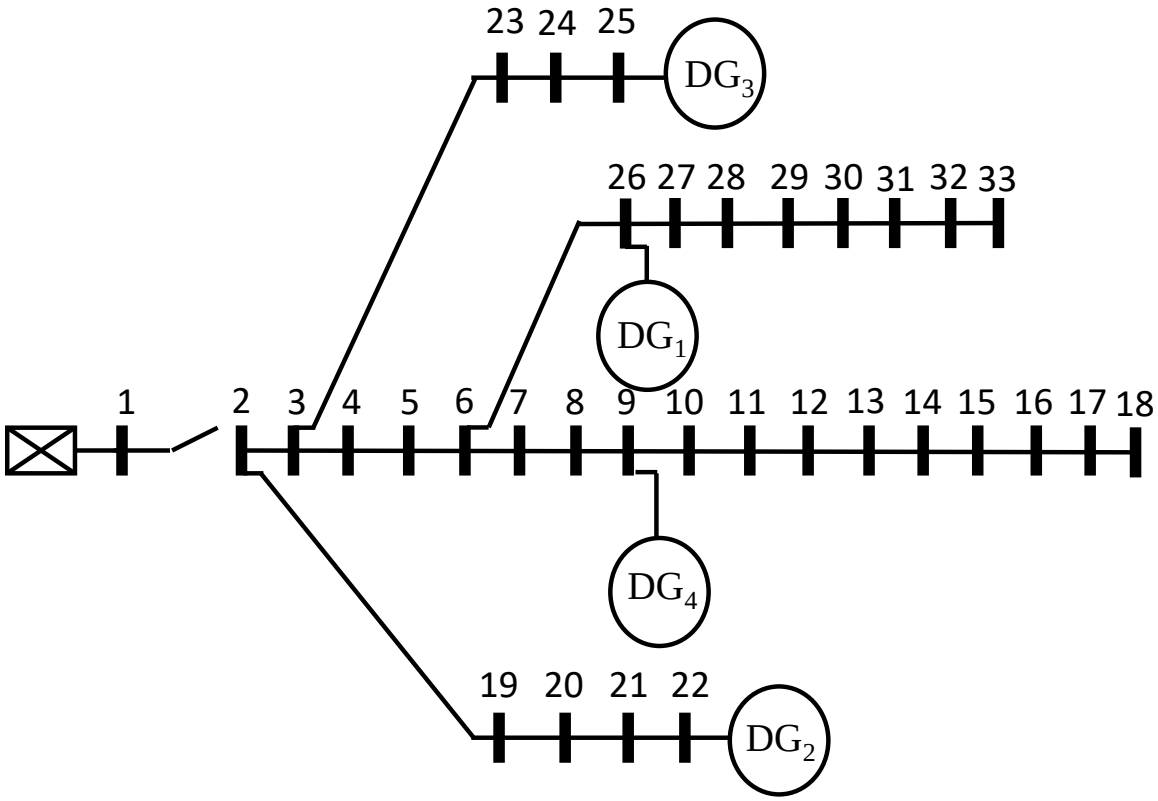

Figure 5.6: Topology of CASE33 system operating in islanded mode

Table 5.9: Droop control settings of DGs in CASE33 system [2]

DG	Location	m_p	n_q	ω^*	V^*	S_{max}	Q_{max}
1	26	0.705×10^{-3}	0.01667	1	1	3.5	1.8
2	22	2.252×10^{-3}	0.05	1	1	1.5	0.6
3	25	4.504×10^{-3}	0.01	1	1	1.5	1.3
4	9	3.003×10^{-3}	0.0667	1	1	1.5	1

Table 5.10: Load exponents of different loads

Load	α	β
constant	0	0
industrial	0.18	6
residential	0.92	4.04
commercial	1.51	3.4

Table 5.11: Voltage profile obtained by ϵDE-GN for CASE33 distribution system operated as an islanded microgrid.

Bus	$\lvert V\rvert$	$\angle_V$	P	Q	$\lvert I\rvert$	$\angle_I$	Bus	$\lvert V\rvert$	$\angle_V$	P	Q	$\lvert I\rvert$	$\angle_I$	Bus	$\lvert V\rvert$	$\angle_V$	P	Q	$\lvert I\rvert$	$\angle_I$
1	–	–	–	–	–	-	12	0.9830	0.0003	-0.1200	-0.0700	0.1413	2.6138	23	0.9906	-0.0015	-0.1800	-0.1000	0.2079	2.6330
2	0.9922	0.0000	-0.2000	-0.1200	0.2351	2.6012	13	0.9773	-0.0011	-0.1200	-0.0700	0.1422	2.6124	24	0.9908	-0.0043	-0.8400	-0.4000	0.9390	2.6929
3	0.9909	-0.0001	-0.1800	-0.0800	0.1988	2.7233	14	0.9752	-0.0023	-0.2400	-0.1600	0.2958	2.5513	25	0.9944	-0.0064	0.4205	1.0644	1.1509	-1.2010
4	0.9905	0.0009	-0.2400	-0.1600	0.2912	2.5545	15	0.9738	-0.0029	-0.1200	-0.0200	0.1249	2.9736	26	0.9912	0.0051	3.0831	1.3764	3.4062	-0.4148
5	0.9906	0.0018	-0.1200	-0.0600	0.1354	2.6798	16	0.9725	-0.0033	-0.1200	-0.0400	0.1301	2.8166	27	0.9888	0.0060	-0.1200	-0.0500	0.1315	2.7528
6	0.9906	0.0043	-0.1200	-0.0400	0.1277	2.8241	17	0.9706	-0.0044	-0.1200	-0.0400	0.1303	2.8154	28	0.9779	0.0073	-0.1200	-0.0400	0.1294	2.8271
7	0.9901	0.0029	-0.4000	-0.2000	0.4517	2.6808	18	0.9701	-0.0046	-0.1800	-0.0800	0.2031	2.7188	29	0.9701	0.0085	-0.2400	-0.1400	0.2864	2.6220
8	0.9896	0.0022	-0.4000	-0.2000	0.4519	2.6801	19	0.9928	0.0002	-0.1800	-0.0800	0.1984	2.7236	30	0.9667	0.0102	-0.4000	-1.2000	1.3085	1.9027
9	0.9907	0.0010	1.3207	0.9988	1.6713	-0.6465	20	1.0000	0.0024	-0.1800	-0.0800	0.1970	2.7258	31	0.9627	0.0089	-0.3000	-0.1400	0.3439	2.7138
10	0.9853	0.0000	-0.1200	-0.0400	0.1284	2.8199	21	1.0024	0.0036	-0.1800	-0.0800	0.1965	2.7269	32	0.9618	0.0085	-0.4200	-0.2000	0.4837	2.7057
11	0.9845	0.0001	-0.0900	-0.0600	0.1099	2.5537	22	1.01	0.0063	1.4410	0.6	1.5769	-0.4285	33	0.9616	0.0084	-0.1200	-0.0800	0.1500	2.5620
w	0.9984																			

at bus number 13, 19 and 25. The static droop coefficient of DGs along with relevant specification are depicted in Table. 5.13. Tables 5.14 and 5.15 show the power flow solution for CASE25 three phase unbalanced distribution by ϵDE-GN and υMAESbm, respectively. As shown in these tables, the voltage magnitudes and angles obtained by ϵDE-GN and υMAESbm are identical.

In Tables 5.14 and 5.15, it is to be noted that for bus 1 and bus 2, voltages and angles for all the phases are identical. This reason behind this as follows. When CASE25 system works in the grid connected mode, bus 1 acts as a root node connected to the

Table 5.12: Voltage profile obtained by υMAESbm for CASE33 distribution system operated as an islanded microgrid.

Bus	$\|V\|$	$\angle_V$	P	Q	$\|I\|$	$\angle_I$	Bus	$\|V\|$	$\angle_V$	P	Q	$\|I\|$	$\angle_I$	Bus	$\|V\|$	$\angle_V$	P	Q	$\|I\|$	$\angle_I$
1	–	–	–	–	–	-	12	0.9830	0.0003	-0.1200	-0.0700	0.1413	2.6138	23	0.9906	-0.0015	-0.1800	-0.1000	0.2079	2.6330
2	0.9922	0.0000	-0.2000	-0.1200	0.2351	2.6012	13	0.9773	-0.0011	-0.1200	-0.0700	0.1422	2.6124	24	0.9908	-0.0043	-0.8400	-0.4000	0.9390	2.6929
3	0.9909	-0.0001	-0.1800	-0.0800	0.1988	2.7233	14	0.9752	-0.0023	-0.2400	-0.1600	0.2958	2.5513	25	0.9944	-0.0064	0.4205	1.0644	1.1509	-1.2010
4	0.9905	0.0009	-0.2400	-0.1600	0.2912	2.5545	15	0.9738	-0.0029	-0.1200	-0.0200	0.1249	2.9736	26	0.9912	0.0051	3.0831	1.3764	3.4062	-0.4148
5	0.9906	0.0018	-0.1200	-0.0600	0.1354	2.6798	16	0.9725	-0.0033	-0.1200	-0.0400	0.1301	2.8166	27	0.9888	0.0060	-0.1200	-0.0500	0.1315	2.7528
6	0.9906	0.0043	-0.1200	-0.0400	0.1277	2.8241	17	0.9706	-0.0044	-0.1200	-0.0400	0.1303	2.8154	28	0.9779	0.0073	-0.1200	-0.0400	0.1294	2.8271
7	0.9901	0.0029	-0.4000	-0.2000	0.4517	2.6808	18	0.9701	-0.0046	-0.1800	-0.0800	0.2031	2.7188	29	0.9701	0.0085	-0.2400	-0.1400	0.2864	2.6220
8	0.9896	0.0022	-0.4000	-0.2000	0.4519	2.6801	19	0.9928	0.0002	-0.1800	-0.0800	0.1984	2.7236	30	0.9667	0.0102	-0.4000	-1.2000	1.3085	1.9027
9	0.9907	0.0010	1.3207	0.9988	1.6713	-0.6465	20	1.0000	0.0024	-0.1800	-0.0800	0.1970	2.7258	31	0.9627	0.0089	-0.3000	-0.1400	0.3439	2.7138
10	0.9853	0.0000	-0.1200	-0.0400	0.1284	2.8199	21	1.0024	0.0036	-0.1800	-0.0800	0.1965	2.7269	32	0.9618	0.0085	-0.4200	-0.2000	0.4837	2.7057
11	0.9845	0.0001	-0.0900	-0.0600	0.1099	2.5537	22	1.01	0.0063	1.4410	0.6	1.5769	-0.4285	33	0.9616	0.0084	-0.1200	-0.0800	0.1500	2.5620
w	0.9984																			

grid. However, when this system is working as an islanded microgrid, bus 1 becomes leaf node (Fig. 5.7) where as per the data specified, there are no load on bus 1 and bus 2. Hence no current flows between these buses in all the phases and due to this voltage magnitudes and angles for all phases at these buses shall be identical..

From the above discussion, it can be concluded that the performance of ϵDE-GN and υMAESbm is satisfactory on unbalanced islanded microgrids.

Table 5.13: Droop control settings of DGs in CASE25 test system.

DG	Location	S_p	S_q	ω^*	V^*	S_{max}	Q_{max}
1	13	0.005	0.05	1	1.01	0.6	0.36
2	19	0.01	0.1	1	1.01	0.3	0.18
3	25	0.005	0.05	1	1.01	0.6	0.18

5.8 Summary

In this chapter, novel algorithms for the power flow problem of an islanded microgrid are introduced. In proposed algorithms, the operating frequency is represented as an additional power flow variable. Various modes of DGs, droop, PV and PQ, are modeled as per the characteristics of islanded microgrids.

The proposed power flow problem is formulated as a constrained optimization problem which is solved by using two proposed algorithms, ϵDE-GN, and υMAESbm. The proposed algorithms are applied to balanced test systems: CASE6, CASE33, CASE69,

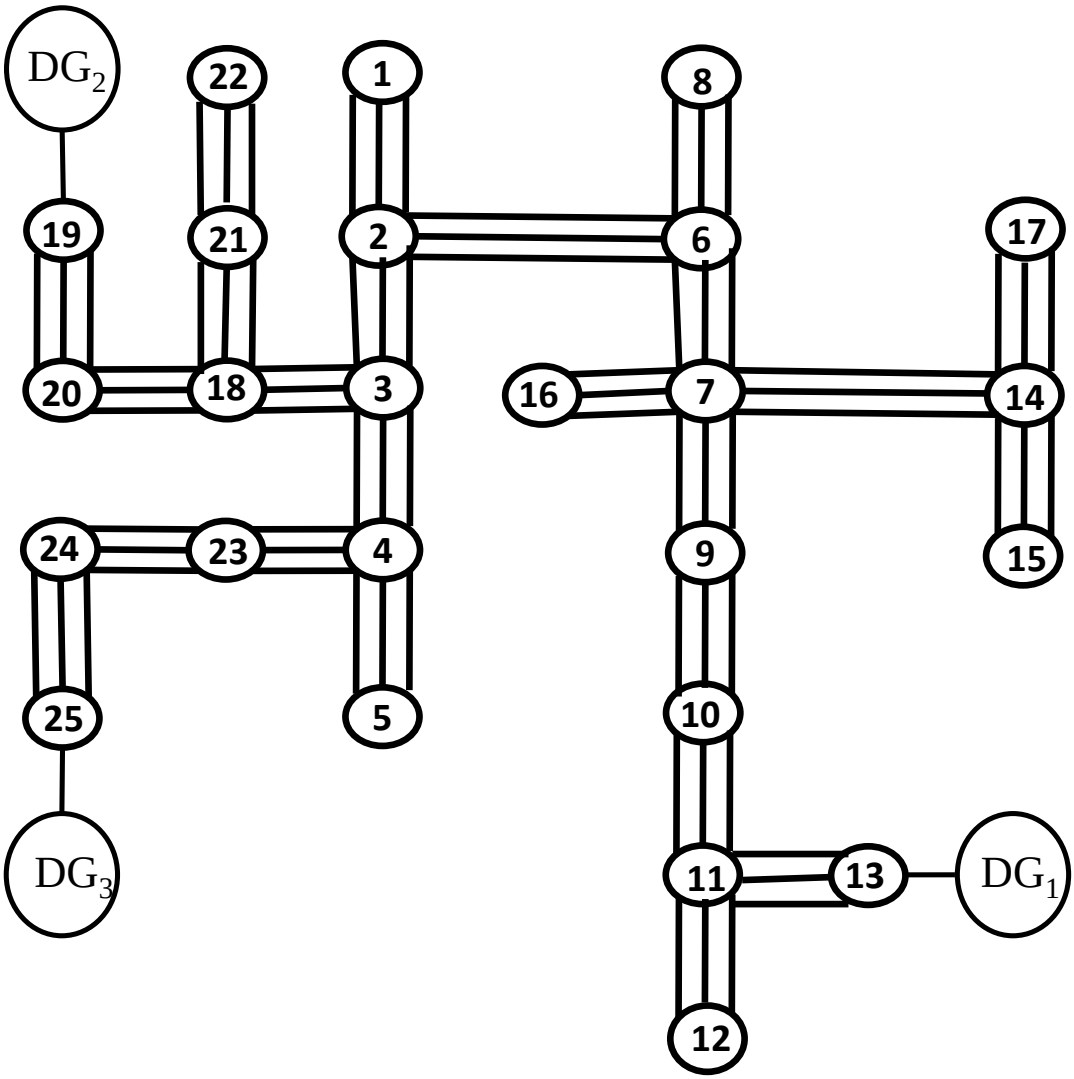

Figure 5.7: Topology of CASE25 test system operated as an islanded microgrid.

Table 5.14: Power flow result obtained by ϵDE-GN for CASE25 unbalanced distribution system operated as an islanded microgrid.

Bus	Phase a				Phase b				Phase c			
	$\|V\|$	$\angle_V$	P	Q	$\|V\|$	$\angle_V$	P	Q	$\|V\|$	$\angle_V$	P	Q
1	0.9894	0.0000	0.0000	0.0000	0.9893	-119.9860	0.0000	0.0000	0.9896	119.9868	0.0000	0.0000
2	0.9894	0.0000	0.0000	0.0000	0.9893	-119.9860	0.0000	0.0000	0.9896	119.9868	0.0000	0.0000
3	0.9901	0.0111	-0.0035	-0.0025	0.9899	-119.9791	-0.0040	-0.0030	0.9902	120.0002	-0.0045	-0.0032
4	0.9908	0.0320	-0.0050	-0.0040	0.9906	-119.9633	-0.0060	-0.0045	0.9908	120.0237	-0.0050	-0.0035
5	0.9904	0.0323	-0.0040	-0.0030	0.9902	-119.9621	-0.0040	-0.0030	0.9905	120.0233	-0.0040	-0.0030
6	0.9881	0.0039	-0.0040	-0.0030	0.9881	-119.9785	-0.0045	-0.0032	0.9885	119.9886	-0.0035	-0.0025
7	0.9876	0.0068	0.0000	0.0000	0.9876	-119.9723	0.0000	0.0000	0.9879	119.9913	0.0000	0.0000
8	0.9875	0.0046	-0.0040	-0.0030	0.9874	-119.9760	-0.0040	-0.0030	0.9879	119.9877	-0.0040	-0.0030
9	0.9892	0.0086	-0.0060	-0.0045	0.9893	-119.9762	-0.0050	-0.0040	0.9895	119.9981	-0.0050	-0.0035
10	0.9914	0.0101	-0.0035	-0.0025	0.9914	-119.9821	-0.0040	-0.0030	0.9914	120.0058	-0.0045	-0.0032
11	0.9929	0.0109	-0.0045	-0.0032	0.9929	-119.9867	-0.0035	-0.0025	0.9928	120.0112	-0.0040	-0.0030
12	0.9926	0.0113	-0.0050	-0.0035	0.9925	-119.9858	-0.0060	-0.0045	0.9925	120.0126	-0.0050	-0.0040
13	0.9953	0.0085	0.0393	0.0278	0.9953	-119.9915	0.0392	0.0286	0.9953	120.0085	0.0399	0.0284
14	0.9857	0.0076	-0.0050	-0.0035	0.9857	-119.9633	-0.0050	-0.0040	0.9860	119.9877	-0.0060	-0.0045
15	0.9850	0.0083	-0.0133	-0.0100	0.9850	-119.9608	-0.0133	-0.0100	0.9854	119.9869	-0.0133	-0.0100
16	0.9872	0.0072	-0.0040	-0.0030	0.9872	-119.9710	-0.0040	-0.0030	0.9876	119.9909	-0.0040	-0.0030
17	0.9853	0.0085	-0.0040	-0.0030	0.9854	-119.9627	-0.0035	-0.0025	0.9856	119.9882	-0.0045	-0.0032
18	0.9902	-0.0047	-0.0040	-0.0030	0.9900	-119.9959	-0.0040	-0.0030	0.9902	119.9881	-0.0040	-0.0030
19	0.9937	-0.0486	0.0159	0.0164	0.9937	-120.0486	0.0166	0.0178	0.9937	119.9514	0.0167	0.0168
20	0.9914	-0.0210	-0.0035	-0.0025	0.9913	-120.0168	-0.0040	-0.0030	0.9913	119.9774	-0.0045	-0.0032
21	0.9891	-0.0028	-0.0040	-0.0030	0.9888	-119.9932	-0.0035	-0.0025	0.9890	119.9915	-0.0045	-0.0032
22	0.9884	-0.0020	-0.0050	-0.0035	0.9880	-119.9912	-0.0060	-0.0045	0.9884	119.9943	-0.0050	-0.0040
23	0.9925	0.0394	-0.0060	-0.0045	0.9924	-119.9590	-0.0050	-0.0040	0.9925	120.0346	-0.0050	-0.0035
24	0.9947	0.0466	-0.0035	-0.0025	0.9945	-119.9563	-0.0045	-0.0032	0.9945	120.0462	-0.0040	-0.0030
25	0.9992	0.0527	0.0373	0.0241	0.9992	-119.9473	0.0387	0.0245	0.9992	120.0527	0.0384	0.0248
w	0.9993											

and unbalanced test systems: CASE25 test systems to analyze the performance of the algorithms. Moreover, the performance of the proposed algorithms is compared with the performance of PSO, GA, NTR, and time-domain software. The obtained results reveal that the performance of the proposed algorithm is superior to others.

Table 5.15: Power flow result obtained by υMAESbm for CASE25 unbalanced distribution system operated as an islanded microgrid.

Bus	Phase a				Phase b				Phase c			
	$\|V\|$	$\angle_V$	P	Q	$\|V\|$	$\angle_V$	P	Q	$\|V\|$	$\angle_V$	P	Q
1	0.9894	0.0000	0.0000	0.0000	0.9893	-119.9860	0.0000	0.0000	0.9896	119.9868	0.0000	0.0000
2	0.9894	0.0000	0.0000	0.0000	0.9893	-119.9860	0.0000	0.0000	0.9896	119.9868	0.0000	0.0000
3	0.9901	0.0111	-0.0035	-0.0025	0.9899	-119.9791	-0.0040	-0.0030	0.9902	120.0002	-0.0045	-0.0032
4	0.9908	0.0320	-0.0050	-0.0040	0.9906	-119.9633	-0.0060	-0.0045	0.9908	120.0237	-0.0050	-0.0035
5	0.9904	0.0323	-0.0040	-0.0030	0.9902	-119.9621	-0.0040	-0.0030	0.9905	120.0233	-0.0040	-0.0030
6	0.9881	0.0039	-0.0040	-0.0030	0.9881	-119.9785	-0.0045	-0.0032	0.9885	119.9886	-0.0035	-0.0025
7	0.9876	0.0068	0.0000	0.0000	0.9876	-119.9723	0.0000	0.0000	0.9879	119.9913	0.0000	0.0000
8	0.9875	0.0046	-0.0040	-0.0030	0.9874	-119.9760	-0.0040	-0.0030	0.9879	119.9877	-0.0040	-0.0030
9	0.9892	0.0086	-0.0060	-0.0045	0.9893	-119.9762	-0.0050	-0.0040	0.9895	119.9981	-0.0050	-0.0035
10	0.9914	0.0101	-0.0035	-0.0025	0.9914	-119.9821	-0.0040	-0.0030	0.9914	120.0058	-0.0045	-0.0032
11	0.9929	0.0109	-0.0045	-0.0032	0.9929	-119.9867	-0.0035	-0.0025	0.9928	120.0112	-0.0040	-0.0030
12	0.9926	0.0113	-0.0050	-0.0035	0.9925	-119.9858	-0.0060	-0.0045	0.9925	120.0126	-0.0050	-0.0040
13	0.9953	0.0085	0.0393	0.0278	0.9953	-119.9915	0.0392	0.0286	0.9953	120.0085	0.0399	0.0284
14	0.9857	0.0076	-0.0050	-0.0035	0.9857	-119.9633	-0.0050	-0.0040	0.9860	119.9877	-0.0060	-0.0045
15	0.9850	0.0083	-0.0133	-0.0100	0.9850	-119.9608	-0.0133	-0.0100	0.9854	119.9869	-0.0133	-0.0100
16	0.9872	0.0072	-0.0040	-0.0030	0.9872	-119.9710	-0.0040	-0.0030	0.9876	119.9909	-0.0040	-0.0030
17	0.9853	0.0085	-0.0040	-0.0030	0.9854	-119.9627	-0.0035	-0.0025	0.9856	119.9882	-0.0045	-0.0032
18	0.9902	-0.0047	-0.0040	-0.0030	0.9900	-119.9959	-0.0040	-0.0030	0.9902	119.9881	-0.0040	-0.0030
19	0.9937	-0.0486	0.0159	0.0164	0.9937	-120.0486	0.0166	0.0178	0.9937	119.9514	0.0167	0.0168
20	0.9914	-0.0210	-0.0035	-0.0025	0.9913	-120.0168	-0.0040	-0.0030	0.9913	119.9774	-0.0045	-0.0032
21	0.9891	-0.0028	-0.0040	-0.0030	0.9888	-119.9932	-0.0035	-0.0025	0.9890	119.9915	-0.0045	-0.0032
22	0.9884	-0.0020	-0.0050	-0.0035	0.9880	-119.9912	-0.0060	-0.0045	0.9884	119.9943	-0.0050	-0.0040
23	0.9925	0.0394	-0.0060	-0.0045	0.9924	-119.9590	-0.0050	-0.0040	0.9925	120.0346	-0.0050	-0.0035
24	0.9947	0.0466	-0.0035	-0.0025	0.9945	-119.9563	-0.0045	-0.0032	0.9945	120.0462	-0.0040	-0.0030
25	0.9992	0.0527	0.0373	0.0241	0.9992	-119.9473	0.0387	0.0245	0.9992	120.0527	0.0384	0.0248
w	0.9993											

Chapter 6

EBOwithCMAR in Optimization of Grid-connected Microgrids

6.1 Introduction

In this part, a technique is proposed to reduce the active and reactive power loss with phase balancing at the main transformer simultaneously in the system by using Single-Phase Distributed Generators (SPDGs) with capacitors. An optimization algorithm, Effective Butterfly Optimizer with Covariance Matrix Adapted Retreat Phase (EBOwithCMAR), is proposed and applied to optimally size and site the SPDGs in power distribution systems for reducing the active and reactive system losses with minimal load unbalance at the primary transformer.

DGs with capacitor banks may be set up locally adjacent to the consumer points. which can significantly support the extra load demand, cut down operational cost, minimize losses, enhance voltage profile and power capability of the system. DGs can be a micro-turbine operated on natural gas, a light synchronous generator driven on diesel, fuel cells, and wind turbines, etc. Several renewable sources such as wind turbine and solar units have further added advantages of low direct emissions. In addition, the evolvement of compact DGs is the principal reason to take advantage of cheaper investment and low space requirement. Although DGs provide many improvements, there are various challenges when these are consolidated with the power distribution system. DG can set up a bidirectional flow of power through the line of the distribution system. If a DG has not been accurately sited and sized, it may substantially increase system losses and

overvoltages at the end of buses.

On the contrary, loads like high rated induction motors, system lines, transformers, and cables are highly inductive. These kinds of loads use VAR as the primary source of power and establish a lagging power factor at the buses which further increases losses and degrades the behaviors of the system. Several DG technologies such as fuel and PV cells can only deliver active power to the systems, while some alternative DG technologies such as wind turbines can operate as a reactive and active power source. Capacitors are simple static devices that can be utilized to provide reactive power support to the system for compensating the lagging VAR. In several studies, it has been established that the shunt capacitors can be utilized to reduce system losses, raise feeder strength and enhance the reliability of the system.

Optimal siting and sizing of DGs are important in enhancing performances of the distribution systems. Several research efforts focused on optimal siting and sizing of DGs to reduce active power losses. Several numerical algorithms [203] and nature-inspired meta-heuristics like GA [204], PSO [205, 206], modified PSO (mPSO) [207], modified Ant Colony Optimization and Artificial Bee Colony [208] have been investigated for different types of DGs. While the impact of size and site of the DG has broadly been investigated, a system containing both elements requires more consideration. Naik et al. [209] took an analytical approach to optimally site and size both DG and capacitor. In [210], PSO is adopted with improved results. In most recent studies, heuristic techniques such as Hybrid Harmony Search method and Particle Artificial Bee Colony [211], Intersect Mutation Differential Evolution [212] and Backtracking Search Algorithm [213] have all been used for optimal size and site of both DGs and capacitors. All the above-mentioned methods aim towards minimizeing active losses without properly addressing other system parameters, such as voltage profile, reactive losses, etc.To reduce search space of the method and hence the computational burden, Naik et al. [209] and Muthukumar et al. [211] approached location optimization based on active power loss sensitivity factors of buses. The bus with largest sensitivity of active power loss is preferred as candidate bus for DG placement.

In this chapter, an optimization method, EBOwithCMAR, is proposed and has been applied to minimize the active and reactive power losses with minimal unbalance at the end of the primary transformer in the distribution network. This study utilizes the unbalanced distribution systems such as CASE11, CASE25, and CASE37 for demonstrating

the effectiveness of the proposed approach. As an optimization algorithm, EBOwithCMAR has several advantages over other popular algorithms and it is the winner of IEEE CEC 2017's competition on bound-constrained optimization problems.

6.2 Problem Formulation

The main objective of this study is to determine the appropriate location and size of SPDGs in the power distribution system that will provide minimal power loss with low phase unbalance at the main transformer. Though, the placement of SPDGs and sizing of SPDGs are long term problem which considers reliability, cost and other aspects, these were not in the scope of the thesis.

The active and reactive power losses in the line connecting buses i and j are computed as follows.

$$P_{loss}(i,j) = R_{ij}\frac{P_i^2 + Q_i^2}{|V_i|^2}, \tag{6.1}$$

$$Q_{loss}(i,j) = X_{ij}\frac{P_i^2 + Q_i^2}{|V_i|^2}, \tag{6.2}$$

where P_{loss} and Q_{loss} represent active and reactive power loss. Total power loss of the system can be determined by summing up all the lines losses of the system as follows.

$$\mathbf{P}_{loss} = \sum_{i=1}^{N}\sum_{j=1}^{N} P_{loss}(i,j), \tag{6.3}$$

and,

$$\mathbf{Q}_{loss} = \sum_{i=1}^{N}\sum_{j=1}^{N} Q_{loss}(i,j) \tag{6.4}$$

where $\mathbf{P}_{loss}$ and $\mathbf{Q}_{loss}$ represent the total active and reactive power loss, respectively. N is the total number of buses in the network.

Current injection at the root node (bus connected to main transformer) can be calculated using the following equations.

$$I_1^s = \left(\frac{S_1^s}{V_1^s}\right)^* \tag{6.5}$$

where I_1^s is current injection at phase s of root node (bus 1), S_1^s is total power transformed at phase s of main transformer, and $s \in \{a, b, c\}$.

Negative-sequence and zero-sequence current injection at main transformer can be calculated as follows.

$$I_1^- = \frac{I_1^a + \alpha^2 I_1^b + \alpha I_1^c}{3}, \tag{6.6}$$

$$I_1^0 = \frac{I_1^a + I_1^b + I_1^c}{3} \tag{6.7}$$

where, I_1^- and I_1^0 are negative-sequence and zero-sequence current injections at main transformer, respectively and $\alpha = 1\angle 120°$.

In this study, SPDGs with capacitor bank are considered to supply single-phase active and reactive power. When an SPDG is connected to s-th phase of i-th bus for delivering power, S_{dg}, the load in that phase changes from S_i^s to $S_i^s - S_{dg}$. To test proposed formulation, a representative distribution system having SPDGs of fixed size at fixed bus locations was needed. However, to have a system with fixed SPDG sizes (capacities) at specified bus locations, we have developed such systems considering the loss minimization and negative- and zero-sequence current minimization for peak loading conditions of the system. The resulting system with fixed SPDG sizes (capacities) at pre-specified locations is considered to be a representative distribution system of the above problem. For creating a representative distribution system, the optimization algorithm must check all possible locations of SPDGs with a different capacity at peak loading condition for minimum losses with minimal phase unbalance at the root node. Therefore, this optimization problem can be defined as follows.

$$\text{Minimize } f(\mathbf{k}, \mathbf{s}, \mathbf{Pdg}, \mathbf{Qdg}) = w_1 \mathbf{P}_{loss} + w_2 \mathbf{Q}_{loss} + w_3 \sqrt{(I_1^-)^2 + (I_1^0)^2} \tag{6.8}$$

where $\mathbf{k} = \{k_1, k_2..., k_n\}$ represents the bus location of SPDGs, $\mathbf{s} = \{s_1, s_2..., s_n\}$ represents the phase location of SPDGs. Similarly, $\mathbf{S}_{dg} = \mathbf{P}_{dg} + j\mathbf{Q}_{dg} = \{S_{dg,1}, S_{dg,1}..., S_{dg,n}\}$ represents the power capacity of SPDGs. Parameters w_1, w_2, and w_3 $(w_1 + w_2 + w_3)$are the weighing factor for different objectives to transform multi-objective optimization problem into single objective optimization problem. This optimization problem is a non-convex, non-linear, and mixed integer bound-constrained optimization problem.

Once the locations and SPDG sizes (capacities) are fixed on a peak loading scenario, then the generation scheduling of SPDG (within the said capacities) and phase switching at the pre-specified buses are determined on hourly basis. For this case, the new optimization problem can be defined as

$$\text{Minimize } f(\mathbf{s}, \mathbf{Pdg}, \mathbf{Qdg}) = w_1 \mathbf{P}_{loss} + w_2 \mathbf{Q}_{loss} + w_3 \sqrt{(I_1^-)^2 + (I_1^0)^2} \tag{6.9}$$

6.3 Proposed Methodology

To solve above-discussed optimization problems, an optimization algorithm, EBOwithCMAR, is proposed in this section. Objective function of these problems can not be directly calculated as bus voltages of the system are not available for different locations of SPDGs. Therefore, power flow analysis is required for calculating bus voltages to evaluate the objective function. In this work, CINR (proposed in chapter 2) is employed for power flow analysis.

6.3.1 EBOwithCMAR

EBOwithCMAR is an optimization algorithm which incorporates Effective Butterfly Optimizer (EBO) with a powerful local search technique, Covariance Matrix Adapted Retreat Phase (CMAR) to improve local search capability of EBO. Before describing the framework of EBOwithCMAR, main steps of EBO and CMAR are presented in following subsections.

EBO

EBO is a dual population-based global optimization algorithm based on the mate-locating behaviors of male butterflies. Two mate-locating behaviors, *Perching* and *Patrolling*, are used in EBO to update the solutions. In EBO, the following rules are utilized to implement mate-locating behaviors of male butterflies.

1. Male butterflies are attracted to the object with the highest UV radiation/reflection.

2. Male butterflies memorize the best perching position by using different cues of the surrounding.

3. Population size is kept constant during the algorithmic process.

4. Position of all male butterflies is updated using one of the mate-locating behaviour viz. *Perching* and *Patrolling*.

Algorithm begins with randomly initialized solutions that form two populations ($X1 = \{\hat{x}1_1, \hat{x}1_2, ...\hat{x}1_{NP_1}\}$, $X2 = \{\hat{x}2_1, \hat{x}2_2, ...\hat{x}2_{NP_2}\}$), where NP_1 and NP_2 are the sizes of the population of the primary and secondary population, respectively. A new set of updated solutions, $Y = \{\hat{y}_1, \hat{y}_2, ...\hat{y}_{NP_1}\}$, is calculated using "towards-best" or "criss-cross" modification operators.

Modification Operators:

In the case of criss-cross modification operator, $\hat{y}_i$ is calculated using the following equation.

$$\hat{y}_i = \hat{x}1_{cc_i} + F * (\hat{x}1_{r1_i} - (X1 \cup X2)_{r2_i}), \tag{6.10}$$

and in case of towards-best modification operator, $\hat{y}_i$ is calculated using the following equation.

$$\hat{y}_i = \hat{x}1_{best_i} + F * (\hat{x}1_{cc_i} - (X1 \cup X2)_{r2_i}), \tag{6.11}$$

where ($\hat{x}1_{cc_i}$, $\hat{x}1_{r1_i}$, and $(X1 \cup X2)_{r2_i}$) are distinct from each other and $r1_i$ and $r2_i$ are randomly chosen index from 1 to NP_1 and 1 to $(NP_1 + NP_2)$, respectively. $\hat{x}1_{best_i}$ represents a best-neighbor of individual i and F is a parameter used to control the evolving rate of solutions. $X1 \cup X2$ represents the combination of both the populations of solutions.

Here, $\hat{x}1_{cc_i}$ is a criss-cross neighbor of the i^{th} solution and cc_i is calculated using Equation 6.12.

$$\{cc_1, cc_2, ...cc_{NP_1}\} = randp(1, NP_1) \tag{6.12}$$

where $randp(1, NP_1)$ is a random permutation of integers between 1 and NP_1. To update each solution, the selection of modification operator is decided using probabilities, P_{perch} and P_{pat}.

Hanging Binomial Crossover:

Hanging Binomial Crossover is a modified version of Binomial Crossover. Crossover rate of each elements j, cr_j, is calculated using equations (6.13) and (6.14).

$$n_j = Rem(D + j - j_{rand}, \frac{D}{2}) \tag{6.13}$$

where D is the total number of decision variable of the problem and $Rem(x, y)$ is a remainder function operator which produces the remainder to the division of x and y. Parameter j_{rand} is randomly selected index from 1 to D.

$$cr_j = CR * e^{-\frac{t}{D} * n_j} \tag{6.14}$$

where t represents a parameter within the range of $[0, 0.5]$. If $t = 0$, then this crossover method is reduced to binomial crossover.

Selection:

Selection of solutions in both the populations for the next iteration is done by the following equations.

$$\hat{x}1_i^{k+1} = \begin{cases} \hat{y}1_i^k, & \text{if } f(\hat{x}1_i^k) > f(\hat{y}1_i^k) \\ \hat{x}1_i^k, & \text{otherwise} \end{cases}, \tag{6.15}$$

and

$$\hat{x}2_i^{k+1} = \begin{cases} \hat{x}1_i^k, & \text{if } f(\hat{x}1_i^k) > f(\hat{y}1_i^k) \\ \hat{x}2_i^k, & \text{otherwise} \end{cases}, \tag{6.16}$$

where, $f(\hat{x}1_i)$ represents the objective function value of solution $\hat{x}1_i$. Note that the objective function value of solution $\hat{x}2_i^{k+1}$ is not evaluated because the objective function value of solution $\hat{x}2_i^{k+1}$ is not utilized in optimization steps of EBO. Step-by-step procedure of EBO is shown in Algorithm-6.

CMAR

CMAR is population based iterative optimization techniques which sample new solutions from probabilistic models. For generating a new sample of the solution, it is essential to calculate the mean and the covariance matrix of the distribution of the probabilistic model. The parameter adaptation procedure of CMAR is adopted from [214]. A brief description of the main steps used to generate new samples is as follows.

1. *Probabilistic Model*: Two probabilistic models are used in CMAR to sample the new solution with a probability of 0.5. The distribution of these two models are individually controlled by its mean m and covariance matrix C. The distribution of these models can be described using the following ways.

$$M1(m, C) \sim m + C^{\frac{1}{2}}.M1(0, I), \tag{6.17}$$

$$M2(m, C) \sim m + C^{\frac{1}{2}}.M2(0, I), \tag{6.18}$$

where $M1$ and $M2$ represent the distribution of probabilistic models, I is an identity matrix, and m and C represent the mean and covariance matrix of the distribution, respectively.

Algorithm 6: Effective Butterfly Optimizer

Initialization;
Fitness evaluation;
while *stopping criteria is not met.* **do**
  /*Modification Operator*/;
  $\{cc_1, cc_2, ..., cc_{NP_1}\} \leftarrow randp(1, NP_1)$;
  for $i = 1$ *to* NP_1 **do**
    $r2_i \leftarrow$ randomly selected solution from $X1 \cup X2$;
    if $rand < P_{perch}$ **then**
      /*Generate $\hat{y}_i$ using criss-cross modification operator8/;
      $r1_i \leftarrow$ randomly selected solution from $X1$;
      $\hat{y}_i \leftarrow \hat{x}1_{cc_i} + F(\hat{x}1_{r1_i} - (X1 \cup X2)_{r2_i})$;
    else
      /*Generate $\hat{y}_i$ using towards-best modification operator*/;
      $\hat{y}_i \leftarrow \hat{x}1_{best_i} + F * (\hat{x}1_{cc_i} - (X1 \cup X2)_{r2_i})$;
    end
  end
  /*Hanging Binomial Crossover*/;
  for $i = 1$ *to* NP_1 **do**
    /*crossover between $\hat{y}_i$ and $\hat{x}1_i$*/;
    $j_{rand} \leftarrow$ randomly selected index from 1 to D;
    for $j = 1$ *to* D **do**
      $n_j \leftarrow Rem(D + j - j_{rand}), \frac{D}{2}$;
      $cr_j \leftarrow CR \times e^{-\frac{t}{D} n_j}$;
      $rand \leftarrow$ randomly generated number from uniform distribution;
      if $(rand \geq cr_j) || (j = j_{rand})$ **then**
        $y_{i,j} \leftarrow x1_{i,j}$;
      end
    end
  end
  Evaluate fitness value on newly updated positions;
  /* Selection*/;
  for $i = 1$ *to* NP_1 **do**
    if $f(\hat{x1}_i^k) > f(\hat{y1}_i^k)$ **then**
      $\hat{x1}_i^{k+1} \leftarrow \hat{y1}_i^k$;
      $\hat{x2}_i^{k+1} \leftarrow \hat{x1}_i^k$;
    end
  end
  $k \leftarrow k + 1$;
end
Result: Best Solution having lowest objective function

2. *Sampling*: The i-th new sample of a solution is generated at k-th iteration by using

following equation.

$$x_i^{(k+1)} \sim \begin{cases} m^{(k)} + \sigma^{(k)} C^{\frac{1}{2}(k)} M1(0, I), & \text{if rand} \leq 0.5 \\ m^{(k)} + \sigma^{(k)} C^{\frac{1}{2}(k)} M2(0, I), & \text{otherwise} \end{cases} \tag{6.19}$$

where, σ is the step-size value and rand is the random number generated from uniform distribution within the range $(0, 1)$.

3. *Mean Calculation*: The mean, m, for the next iteration is calculated using a weighted average of half of the best solutions from the current N samples, $\{x_1, x_2, ..., x_N\}$, as shown in Equation 6.20.

$$m^{(k+1)} = \sum_{i=1}^{\frac{N}{2}} w_i x_{i:N}^{(k)}, \tag{6.20}$$

where $x_{i:N}$ represents the i-th best solution of N samples of solutions. Here, $\sum_{i=1}^{\frac{N}{2}} w_i = 1$ and w_i is calculated by following equation.

$$w_i = \frac{ln(\frac{N}{2} + 1) - ln(i)}{\sum_{j=1}^{\frac{N}{2}} ln(\frac{N}{2} + 1) - ln(j)}, \tag{6.21}$$

where $f(*)$ represents the objective function value at $*$ solution.

4. *Calculation of square root of covariance matrix*: In CMAR, square root of the covariance matrix is adapted in each iteration by using the evolution path, $P_c^{(k)}$, and random numbers, $z_i^{(k)} (= M1(0, I)$ or $M2(0, I))$, used to genrate samples at k-th iteration.

$$P_c^{(k)} = (1 - c_c) P_c^{(k-1)} + hs^{(k)} \sqrt{c_c(2 - c_c)\mu_{eff}}.z_m^{(k)}, \tag{6.22}$$

$$C^{\frac{1}{2}(k+1)} = (1 - c_{cov} - c_1(1 - (1 - hs^{(k)})c_c(2 - c_c)))C^{\frac{1}{2}(k)} \tag{6.23}$$

$$c_1 C^{\frac{1}{2}(k)} \left(P_c^{(k)} (P_c^{(k)})^T\right) + c_{cov} C^{\frac{1}{2}(k)} \sum_{i=1}^{\frac{N}{2}} w_i z_{i:N}^{(k)} \left(z_{i:N}^{(k)}\right)^T, \tag{6.24}$$

where,

$$z_m^{(k)} = \sum_{i=1}^{\frac{N}{2}} w_i z_{i:N}^{(k)}. \tag{6.25}$$

The control parameters N, c_c, c_1, c_{cov}, and μ_{eff} are set by using following equations.

$$N = 4 + \lfloor 3ln(D) \rfloor, \tag{6.26}$$

$$\mu_{eff} = \frac{(\sum_{i=1}^{\frac{N}{2}} w_i)^2}{\sum_{i=1}^{\frac{N}{2}} w_i^2}, \tag{6.27}$$

$$c_c = \frac{4D + \mu_{eff}}{D^2 + 4D + 2\mu_{eff}}, \tag{6.28}$$

$$c_1 = \frac{1}{(D + 1.3)^2 + \mu_{eff}}, \tag{6.29}$$

$$c_{cov} = \min\left(0.5 - c_1, \frac{\mu_{eff}^2 - 2\mu_{eff} + 1}{\mu_{eff}^2 + \mu_{eff}(D+2)^2}\right). \tag{6.30}$$

5. *Step-size adaptation*: The adaptation of step-size are done by using following equation.

$$P_s^{(k+1)} = (1 - c_s)P_s^{(k)} + \sqrt{c_s(2 - c_s)\mu_{eff}}.z_m^{(k)}, \tag{6.31}$$

$$\sigma^{(k+1)} = \sigma^{(k)}.exp\left(\frac{c_s}{d_s}\left(\frac{||P_s^{(k+1)}||}{E_x} - 1\right)\right) \tag{6.32}$$

where, c_s, d_s, and E_x are the control parameters. These parameters can be calculated by using following equations.

$$c_s = \frac{\mu_{eff} + 2}{\mu_{eff} + D + 5}, \tag{6.33}$$

$$d_s = 1 + 2.max\left(0, \sqrt{\frac{\mu_{eff} - 1}{D + 1} - 1}\right) + c_s, \tag{6.34}$$

$$E_x = \sqrt{D}\left(1 - \frac{1}{4D} + \frac{1}{21D^2}\right) \tag{6.35}$$

The parameter hs used in Equation 6.22 is updated in each iteration by using following equation.

$$hs^{(k+1)} = \begin{cases} 1, & \text{if } \frac{||P_s||^2 D}{(1-(1-c_s)^{2(k+1)})} < 2 + \frac{4}{D+1}, \\ 0, & \text{otherwise} \end{cases} \tag{6.36}$$

In the following sections, the framework of EBOwithCMAR is discussed.

Framework of EBOwithCMAR

In EBOwithCMAR, an initial population of size N is randomly generated from the uniform distribution within the bound of solution-space. This population is split into three different populations, X_1, X_2, and X_3 of sizes, N_1, N_2, and N_3, respectively, where the

first two populations are used in EBO and the last population is used in CMAR. Algorithms EBO and CMAR are utilized to update the solutions with probabilities $prob_{EBO}$ and $prob_{CMAR}$, respectively, at a particular iteration. A cycle, cy, of a fixed number of iteration is initialized at the beginning of the optimization process where both of the algorithms are utilized parallelly ($prob_{EBO}$ and $prob_{CMAR}$ are set to 1) for the half of the cycle. At the end of the half cycle, the new values of $prob_{EBO}$ and $prob_{CMAR}$ are updated for the next half of the cycle. The new value of probabilities $prob_{EBO}$ and $prob_{CMAR}$ depends upon the following criteria.

1. Based on the superiority of the best solution obtained using EBO and CMAR, and

2. Based on the diversity of solutions of the populations, X_1 and X_3.

A data sharing between the populations X_1 and X_3 are done at the last of each cycle. Whenever EBOwithCMAR will enter into the next cycle, and similar steps are replicated. To improve the local search potential of EBOwithCMAR, sequential quadratic programming is utilized at the later phases of the optimization process (75% of the optimization process is completed) with a probability of $prob_{ls}$. In case of failure of the SQP algorithm, probability $prob_{ls}$ is reduced to a very small value.

In EBOwithCMAR, some components of EBO are modified. The modified components of EBO are described in the following sections.

Modified component of EBO:

A brief description of the main steps of EBO is discussed earlier. In EBOwithCMAR, modification operators are modified to improve the diversity of the populations X_1 and X_2, and a self-adaptive approach is utilized for the different parameters of EBO.

1. *Modified modification operators*: A modified criss-cross and towards-best modification operators used in EBOwithCMAR are shown in Equation (6.37) and Equation (6.38), respectively.

$$\hat{y}_{i,j} = \begin{cases} \hat{x}1_{i,j} + F_i(\hat{x}1_{cc_i,j} - \hat{x}1_{i,j} + \hat{x}1_{r1_i,j} - (X_1 \cup X_2)_{r2_i,j}), \\ \text{if } (rand_j(0,1) \leq cr_{i,j} \text{ or } j = j_{rand}) \\ \hat{x}1_{i,j}, \\ \text{otherwise.} \end{cases} \tag{6.37}$$

$$\hat{y}_{i,j} = \begin{cases} \hat{x}1_{i,j} + F_i(\hat{x}1_{best_i,j} - \hat{x}1_{i,j} + \hat{x}1_{cc_i,j} - (X_1 \cup X_2)_{r2_i,j}), \\ \text{if } (rand_j(0,1) \leq cr_{i,j} \text{ or } j = j_{rand}) \\ x1_{i,j}, \\ \text{otherwise.} \end{cases} \tag{6.38}$$

where $(cc_i, r1_i, \text{and } r2_i)$ are distinct integers.

2. *Selection of $best_i$*: The $best_i$ is the best solution among the randomly selected D solutions from population X_1. When the size of the population X_1 is less than the $2D$, $best_i$ is randomly selected from the 10% of best solutions.

3. *Calculation of P_{perch} and P_{pat}*: The probabilities P_{perch} and P_{pat} are initially set to 0.5. The improvement rate of objective function values is utilized to modify the value of these probabilities. The improvement rate is estimated using the following equation.

$$I_i^{(k+1)} = \frac{\sum_{z \in S_i}^{PS_1} max(0, f_z^{(k+1)} - f_z^{(k)})}{\sum_{z \in S_i}^{PS_1} f_z^{(k)}}$$

$$\text{where } S_i \text{ is a set of solutions updated by } \begin{cases} perching, & \text{if } i = 1 \\ patrolling, & \text{if } i = 2. \end{cases} \tag{6.39}$$

Now, P_{perch} and P_{pat} are modified using following equation.

$$P_{perch} = max\left(0.1, min\left(0.9, \frac{I_1}{I_1 + I_2}\right)\right), \tag{6.40}$$

$$P_{pat} = 1 - P_{perch} \tag{6.41}$$

4. *Linear Reduction of Size of N_1 and N_2*: Reduction in the size of populations X_1 and X_2 at the end of each iteration is done by using a linear reduction mechanism proposed in [215]. In this approach, the size of X_1 is reduced by eliminating the worst solutions, while the size of X_2 is reduced by eliminating random solutions from the population. The reduced sizes of populations are calculated using the following equations.

$$N_1^{(k+1)} = round\left(\left(\frac{N_{1,min} - N_{1,max}}{FE_{max}}\right) * FEs\right) + N_{1,max} \tag{6.42}$$

$$N_2^{(k+1)} = round\left(\left(\frac{N_{2,min}-N_{2,max}}{FE_{max}}\right)*FEs\right) + N_{2,max} \quad (6.43)$$

where $(N_{1,max}, N_{2,max})$ and $(N_{1,min}, N_{2,min})$ are the maximum and minimum values allowed for N_1 and N_2 respectively. FE_{max} and FEs represent the maximum allowed function evaluation and current function evaluation, respectively.

5. *Adaptation of F, $freq$, CR and T*: In EBOwithCMAR, a parameter adaptation technique is utilized to auto-tune the parameters F, $freq$, CR, and T at each iteration. The following steps are performed to adapt the parameters.

   - A matrix of size $(4 \times H)$, M, is initialized at their default values. The default value of parameters F, CR, $freq$, and T are 0.7, 0.5, 0.5, and 0.1, respectively.
   - The new value of parameters CR_i, F_i, $freq_i$, and T_i associated with solution $\hat{x}1_i$ is calculated by following equations.

$$CR_i = M2(M_{3,r}, 0.1), \quad (6.44)$$

$$freq_i = randci(M_{2,r}, 0.1), \quad (6.45)$$

$$F_i = \begin{cases} \frac{1}{2}\left(\tan(\pi(FEs+1))\frac{FE_{max}-FE}{FE_{max}}+1\right), & \text{if } FEs \le FE_{max} \,\&\, rand \le 0.5 \\ \frac{1}{2}\left(\tan(2\pi freq_i * FEs)\frac{FEs}{FE_{max}}+1\right), & \text{if } FEs \le FE_{max} \,\&\, rand > 0.5 \\ randci(M_{1,r}, 0.1), & \text{otherwise} \end{cases}, \quad (6.46)$$

$$T_i = M2(M_{4,r}, 0.05), \quad (6.47)$$

   where r represents a integer from $[1, H]$, and $randci$ provides the random number from cauchy distribution.

   - The value of $M_{i,d}$ is updated by using the following equation at the end of each iteration.

$$M_{i,d} = \frac{\sum_{\gamma=1}^{4} w_\gamma S_{i,\gamma}^2}{\sum_{\gamma=1}^{4} w_\gamma S_{i,\gamma}}, \quad (6.48)$$

   where, $S_{i,1:\gamma} = (F_i, CR_i, freq_i, T_i)$ and $1 < d < H$ is the index of the memory to be updated. It is initialized to 1, and then increased by 1 whenever an index of memory is updated and if it is greater than H, it is reset to 1. w_γ is calculated by using following equation.

$$w_\gamma^{(k+1)} = \frac{\triangle f_\gamma^{(k+1)}}{\sum_{i=1}^{N_1} \triangle f_\gamma^{(k+1)}} \quad (6.49)$$

and $\triangle f_\gamma = |f_\gamma^{(k)} - f_\gamma^{(k+1)}|$.

- *CMAR*: CMAR starts with a randomly generated initial population of size N_3 ($X_3 = \{x_1, x_2 ... x_{N_3}\}$ from uniform distribution within the solution-space. Initial mean, $m^{(0)}$, is calculated by the arithmetic mean of X_3.

Update of $prob_{EBO}$ ***and*** $prob_{CMAR}$***:***

Two factors are considered to update the probabilities $prob_{EBO}$ and $prob_{CMAR}$. They are the diversity of the population and quality of solutions.

Two quality values, $\hat{Q}_{EBO}$ and $\hat{Q}_{CMAR}$, are calculated at the end of half of cycle by using the following equation.

$$\hat{Q}_i = \frac{f_{best,i}^{\frac{CS}{2}}}{f_{best,EBO}^{\frac{CS}{2}} + f_{best,CMAR}^{\frac{CS}{2}}} \; \forall \, i \in \{EBO, CMAR\}, \tag{6.50}$$

where $f_{best,i}^{\frac{CS}{2}}$ is the best objective function value at the end of half of cycle, $\frac{CS}{2}$ by i-th algorithm.

At the same time, the diversity of the populations X_1 and X_3 are calculated using the following equation.

$$\hat{div}_i = \frac{div_i}{div_{X_1} + div_{X_3}} \; \forall \, i \in \{EBO, CMAR\}, \tag{6.51}$$

where div_i is the diversity rate of population with respect to best solution at the end of half of cycle, $\frac{CS}{2}$ by i-th algorithm.

A progress index, PI_i is calculated by using equation (6.52).

$$PI_i = (1 - \hat{Q}_i) + \hat{div}_i, \; \forall \, i \in \{EBO, CMAR\} \tag{6.52}$$

Now, the probability, $prob_i$ is calculated as shown in equation (6.53).

$$prob_i = max\left(0.1, min\left(0.9, \frac{PI_i}{PI_{EBO} + PI_{CMAR}}\right)\right), \; \forall \, i \in \{EBO, CMAR\} \tag{6.53}$$

If the sum of PI is equal to zero, $prob_{EBO}$ and $prob_{CMAR}$ are set to 1.

Data Sharing:

At the end of every cycle, CS, algorithm having a greater value of probability is considered to be best algorithm of that cycle. If EBO is considered as the best, then population X_3 is replaced by the random solution of population X_1. Parameters of CMAR is also

Algorithm 7: EBOwithCMAR

Define $N \leftarrow N_1 + N_2 + N_3$, $cy \leftarrow 0$, $prob_{EBO} = prob_{CMAR} \leftarrow 1$ and all other parameters required;
for $i = 1$ *to* N **do**
    $X_i \leftarrow$ uniformly distributed D random numbers within the bounds of search-space;
end
Randomly assign N_1, N_2, and N_3 individuals from X to $X_i, \forall i = 1, 2, 3$;
while *termination condition is not satisfied* **do**
    $cy \leftarrow cy + 1$;
    if $cy == \frac{CS}{2}$ **then**
        Calculate $prob_{EBO}$ and $prob_{CMAR}$ using Equation (6.53);
    end
    if $cy == CS$ **then**
        Share Data;
        $prob_{EBO} = 1$, and $prob_{CMAR} = 1$;
        $cy \leftarrow 0$;
    end
    if $rand \leq prob_1$ **then**
        Apply EBO;
        $FEs \leftarrow FEs + N_1$;
    end
    if $rand \leq prob_2$ **then**
        Apply CMAR;
        $FEs \leftarrow FEs + N_3$;
    end
    if $rand \leq prob_{ls}$ & $FEs \geq 0.75 * FE_{max}$ **then**
        Apply SEQ;
        $FEs \leftarrow FEs + FE_{seq}$;
        if *best solution is improved* **then**
            $prob_{ls} \leftarrow 0.1$;
            update X_1 and X_2;
        else
            $prob_{ls} \leftarrow 0.0001$;
        end
    end
    $k \leftarrow k + 1$;
end
Result: Best Solution having lowest objective function

reinitialized at default value except the step size, σ, where σ is calculated as $\sigma = \sigma_{initial} * (1 - cFE/FE_{max})$.

On the other hand, if CMAR emerges as the best, the worst individual in X_1 is replaced by the best individual in X_3. After data sharing, new cycle is again started and process repeated. The step-by-step procedure of EBOwithCMAR is shown in Algorithm-7. The performance of EBOwithCMAR in comparison of state-of-the-art algorithms are

reported in the Appendix.

6.3.2 Evaluation of Objective Function

In any optimization algorithm, objective function for each generated solution needs to be evaluated for improving the solutions. The objective function of the optimization problem discussed in the section 6.2 cannot be evaluated directly. Power flow analysis is needed to obtain the steady-state voltage at each bus of the system because these voltages are used to calculate the objective function defined in Equation 7.5.

CINR algorithm is employed to calculate the steady-state voltage at each bus for every solution of the optimization problem. Each solution contains the location (bus and phase) and power capacity of SPDG. First of all, loads of the system are updated according to the solution (location and capacity of SPDGs). Loads are modified by using following equations.

$$P_{L,i}^{t} = \begin{cases} P_{L,i}^{t} - P_{dg,j}, & \text{if } i == k_j \ \& \ t == s_j \\ P_{L,i}^{t}, & \text{else} \end{cases} \tag{6.54}$$

and,

$$Q_{L,i}^{t} = \begin{cases} Q_{L,i}^{t} - Q_{dg,j}, & \text{if } i == k_j \ \& \ t == s_j \\ Q_{L,i}^{t}, & \text{else} \end{cases} \tag{6.55}$$

where $P_{L,i}^{t}$ and $Q_{L,i}^{t}$ represent the active and reactive load at t-th phase of i-th bus. $\{K_j, s_j, P_{dg,j}, Q_{dg,j}\}$ represents the bus-location, phase-location, active power capacity, and reactive power capacity of j-th SPDG.

After modifying the loads, power flow analysis is performed on this loading condition using CINR to calculate the voltage at each bus. Further these voltages are used to calculate the objective function values.

6.3.3 Proposed Algorithm

The above-discussed optimization problem considers location (in terms of phase and bus) and size (in terms of active and reactive power) of SPDGs as the problem variables. Each solution vector has $4 * M$ elements where M is the total number of SPDGs used in the systems.

The purpose of this problem is to find the optimum location and rating for all the SPDGs so that the objective function is minimized. It is worth mentioning here that the solution variables related to location must be an integer value. Therefore, during the calculation of objective function value, these variables are rounded off to its adjacent integer value.

The following steps are utilized to solve the optimization problem.

1. **Step 1:** Initialization of population of N_p solutions is done as uniformly distributed random points within the bound of each variables.
2. **Step 2:** Power flow Analysis is performed using each solution of current population.
3. **Step 3:** Objective function is evaluated using each solution of current population
4. **Step 4:** Solutions of population are updated using EBOwithCMAR
5. **Step 5:** Check the stopping criteria. If stopping criteria is met, go to **Step 6**, otherwise go to **Step 2**
6. **Step 6:** Best solution on the basis of minimum objective function value is extracted from population to locate and schedule the SPDGs within the system.

6.4 Results and Discussion

In this section, the performance of the proposed approach, as well as comparative analysis are discussed.

In this analysis, three test systems, CASE13, CASE25, and CASE37, are considered. The details of these systems are reported in the Appendix I. Details of the experimental setup are given in Table 6.1. The performance of proposed algorithm has been compared with state-of-the-art algorithms reported in literature. The algorithms chosen for comparative analysis are IMDE [212], Analytical Approach (AA) [209], PSO [210], BSA [213], and IPSO [216].

Four scenario are studied in this work. In first case, only phase-balancing is done i.e. negative-sequence and zero-sequence currents are minimized at root node. In second scenario, minimization of active power loss is considered as objective function. Similarly, reactive power loss is considered as objective function in third scenario. In last scenario,

Table 6.1: The detail of experimental setup

S.N.	Test System	Number of SPDGs	P_{max}	Q_{max}
1.	CASE13	3	2 p.u.	2 p.u.
2.	CASE25	5	2 p.u.	2 p.u.
3.	CASE37	7	2 p.u.	2 p.u.

the weighted objective function with equal weighing factor is considered to minimize all the objective function simultaneously.

6.4.1 Parameter Settings

For EBO, $N_{1,max} = 18D$, $N_{1,min} = 4$,$N_{2,max} = 46.8D$, $N_{2,min} = 10$ $H = 6$. For CMAR, $N_3 = 4 + (3log(D))$ [214], and $\sigma = 0.3$. $CS = 100$. For local search, $prob_{ls} = 0.1$ and $FE_{ls} = 0.25 * FE_{max}$ function evaluations. Here, $D = 4 * M$.

6.4.2 Case Studies

The proposed algorithm with other state-of-the-art algorithms has been run for all the test cases.

CASE13

The best site and size of SPDGs obtained after 100 independent runs using all algorithms are recorded for the weighted objective function. The parameters (negative-sequence current, zero-sequence current, active loss and reactive loss) at the optimal solution obtained from all algorithms are reported in Table 6.2. This table shows that the optimal solutions obtained from all algorithms are different from each other. The proposed algorithm provides better solutions as compared to solutions obtained from other competitive algorithms. From this analysis, it can be concluded that the proposed approach is a better option to solve the optimization problem in case of CASE13.

Further, proposed algorithm is utilized for analyzing the system for all the objective function cases. The optimal size and site of SPDGs for different objective functions (scenarios) are depicted in Table 6.3. From table 6.3, the site of SPDGs for scenario-2,

Table 6.2: Simulation results for CASE13 test system.

Index	EBOwithCMAR	IMDE	AA	PSO	BSA	IPSO
I_1^0	**2.08E-09**	6.72E-06	8.24E-06	7.45E-05	8.25E-06	1.87E-08
I_1^-	**9.23E-10**	2.41E-05	4.21E-05	1.06E-05	5.87E-05	6.83E-09
$\mathbf{P}_{loss}$	7.23E-02	6.23E-02	**5.34E-02**	1.07E-01	8.43E-02	7.54E-02
$\mathbf{Q}_{loss}$	1.51E-01	1.48E-01	**1.45E-01**	1.83E-01	1.73E-01	1.76E-01

scenario-3 and scenario-4 are same, while the size of SPDGs are different to minimize objective functions of these scenarios.

Table 6.3: Results for CASE13 for scenario-4

scenario-1	location	2-b	7-a	10-c
	P_{dg}	3.24E-01	4.73E-01	5.48E-01
	Q_{dg}	2.26E-01	2.04E-01	2.93E-01
scenario-2	location	7-c	8-a	9-b
	P_{dg}	1.02E+00	7.68E-01	3.24E-01
	Q_{dg}	4.28E-01	2.03E-01	3.13E-02
scenario-3	location	7-c	8-a	9-b
	P_{dg}	1.02E+00	9.11E-01	3.16E-01
	Q_{dg}	4.03E-01	3.37E-01	7.40E-02
scenario-4	location	7-c	8-a	9-b
	P_{dg}	7.06E-01	5.83E-01	4.75E-01
	Q_{dg}	1.18E-01	1.00E-02	4.33E-02

Table 6.4: Value of main parameters of system for different cases of CASE13

Index	scenario-1	scenario-2	scenario-3	scenario-4
I_1^0	4.72E-12	8.77E-02	8.87E-02	2.08E-09
I_1^-	2.05E-12	9.17E-02	1.52E-01	9.23E-10
$\mathbf{P}_{loss}$	1.04E-01	4.70E-02	5.04E-02	7.23E-02
$\mathbf{Q}_{loss}$	2.10E-01	6.10E-02	5.40E-02	1.51E-01

CASE25

From 100 independent runs, the best size and site of SPDGs are selected for comparative analysis on CASE25. The parameters of CASE25 at the optimal solution are reported in Table 6.5 for all algorithms. This table shows that the proposed algorithm performs better than other algorithms for this test system. These outcomes conclude that the proposed algorithm provides a better option for solving this optimization problem in this test system.

Table 6.5: Simulation results for CASE25 test system for scenario-4

Index	EBOwithCMAR	IMDE	AA	PSO	BSA	IPSO
I_1^0	**2.65E-11**	1.32E-06	3.56E-06	2.93E-05	2.85E-06	5.85E-06
I_1^-	**2.69E-11**	4.23E-05	3.83E-05	3.08E-05	9.75E-05	4.86E-06
$\mathbf{P}_{loss}$	**2.93E-01**	3.01E-01	3.28E-01	3.18E-01	3.87E-01	2.98E-01
$\mathbf{Q}_{loss}$	**3.35E-01**	3.37E-01	3.85E-01	4.01E-01	4.01E-01	3.38E-01

In addition, EBOwithCMAR is employed to further analyze the CASE25 for different scenarios having different objective function. The experimental outcomes are depicted in Table 6.6. From this table, the site and size of SPDGs are different from each other to minimize all objective functions. Negative-sequence current and zero-sequence current at root node with active and reactive power loss are also reported in Table 6.7 at the optimal solution of all cases of the objective function.

CASE37

The performance of the proposed algorithm is also analyzed on CASE37. Similarly to CASE13 and CASE25, the best solution from 100 independent runs is selected for analysis. Negative-sequence and zero-sequence with active and reactive power loss are reported in Table 6.8 for all solutions obtained by all algorithms. As shown in Table 6.8, the performance of EBOwithCMAR is superior to other algorithms. Therefore, for further analysis only the proposed algorithm is utilized for all objective functions (scenarios).

The optimal site and size of SPDGs for all case of the objective function are reported in Table 6.9. From this table, it can be seen that the location and size of SPDGs are different in all cases. Obtained active and reactive loss with zero-sequence and negative-

Table 6.6: Obtained results for CASE25

scenario-1	location	4-a	5-c	12-c	16-a	17a
	P_{dg}	1.32E+00	1.15E+00	9.02E-01	1.36E+00	1.06E+00
	Q_{dg}	5.65E-01	6.68E-01	5.76E-01	1.03E+00	1.03E+00
scenario-2	location	9-b	10-c	11-a	14-a	15-a
	P_{dg}	2.00E+00	2.00E+00	2.00E+00	2.00E+00	1.26E+00
	Q_{dg}	2.00E+00	2.00E+00	1.63E+00	1.76E+00	4.36E-02
scenario-3	location	11-a	13-b	14-c	23-a	25-c
	P_{dg}	2.00E+00	1.99E+00	2.00E+00	2.00E+00	2.00E+00
	Q_{dg}	2.00E+00	1.90E+00	2.00E+00	2.00E+00	1.12E+00
scenario-4	location	5-c	8-a	10-b	11-c	13-a
	P_{dg}	3.02E-01	2.00E+00	2.45E-01	2.00E+00	2.00E+00
	Q_{dg}	1.15E+00	2.00E+00	1.78E+00	1.86E+00	2.00E+00

Table 6.7: Value of main parameters of system for different cases of CASE25

Index	scenario-1	scenario-2	scenario-3	scenario-4
I_1^0	1.23E-20	9.63E-01	9.30E-01	2.65E-11
I_1^-	9.98E-21	2.06E+00	8.57E-01	2.69E-11
$\mathbf{P}_{loss}$	4.00E-01	2.29E-01	2.48E-01	2.93E-01
$\mathbf{Q}_{loss}$	4.37E-01	2.82E-01	2.68E-01	3.35E-01

sequence current at root node are also shown in Table 6.8 for all cases of the objective function.

6.4.3 24-hour loading scenario

In this loading scenario the optimal SPDG locations obtained in case studies of CASE25 have been fixed. Using these sites for SPDGs along with reactive supports, the optimization for 24-hour load scenarios for objective function stated in equation 6.9 has been considered.

For each of the 24-hour loading scenario the optimal phase and sizes of the SPDGs have been obtained using EBOwithCMAR algorithm. In the following paragraphs the re-

Table 6.8: Simulation results for CASE37 test system of scenario-4

Index	EBOwithCMAR	IMDE	AA	PSO	BSA	IPSO
I_1^0	3.20E-12	6.87E-06	5.90E-06	4.88E-07	3.95E-07	3.94E-06
I_1^-	1.82E-12	4.56E-05	8.36E-05	3.87E-06	2.95E-06	4.69E-06
$\mathbf{P}_{loss}$	8.98E-02	1.05E-01	9.87E-02	1.15E-01	1.13E-01	1.04E-01
$\mathbf{Q}_{loss}$	4.89E-02	8.48E-02	7.84E-02	1.09E-01	1.14E-01	9.25E-02

Table 6.9: Obtained results for CASE37

scenario-1	Location	30-c	31-a	31-b	31-c	32-a	32-b	33-a
	P_{dg}	1.81E-01	5.06E-02	3.91E-02	1.19E-01	5.36E-02	3.73E-02	5.39E-02
	Q_{dg}	1.03E-01	4.61E-02	5.07E-02	1.07E-01	4.67E-02	4.76E-02	4.67E-02
scenario-2	Location	26-a	28-c	30-a	31-a	34-b	35-a	35-c
	P_{dg}	6.38E-02	2.55E-01	1.37E-01	1.22E-01	1.52E-01	1.27E-01	2.19E-01
	Q_{dg}	5.48E-02	9.99E-02	9.35E-02	1.00E-02	9.87E-02	1.18E-01	7.55E-02
scenario-3	Location	5-b	8-a	10-c	12-c	24-c	25-a	34-b
	P_{dg}	2.53E-01	4.49E-01	2.40E-01	1.94E-01	1.70E-01	1.00E-02	8.48E-02
	Q_{dg}	1.02E-01	2.41E-01	1.29E-01	1.38E-01	3.71E-02	1.00E-02	3.66E-02
scenario-4	Location	8-c	12-c	21-a	22-a	25-c	34-b	35-a
	P_{dg}	2.99E-01	1.40E-01	3.01E-02	4.20E-02	4.20E-02	2.55E-01	2.88E-01
	Q_{dg}	1.81E-01	4.88E-02	1.68E-02	2.10E-02	2.10E-02	1.44E-01	1.61E-01

Table 6.10: Value of main parameters of system for different cases of CASE37

Index	case-1	case-2	case-3	case-4
I_1^0	3.94E-22	9.82E-03	1.62E-03	3.20E-12
I_1^-	6.26E-23	3.23E-02	2.00E-03	1.82E-12
$\mathbf{P}_{loss}$	6.96E-02	4.67E-02	6.28E-02	8.98E-02
$\mathbf{Q}_{loss}$	4.39E-02	2.51E-02	3.08E-02	4.89E-02

sults obtained in terms of sequence and phase currents, voltages, losses (real and reactive), and phase utilization index are discussed.

Sequence Currents: The hourly negative- and zero-sequence currents for 24-hours without SPDG and with SPDG are shown in Fig. 6.1. It is observed from the figure that, without SPDG the amount of negative- and zero-sequence currents lie in the range 0.66 pu to 1.90 pu and with DG the negative- and zero-sequence currents are found to be almost negligible.

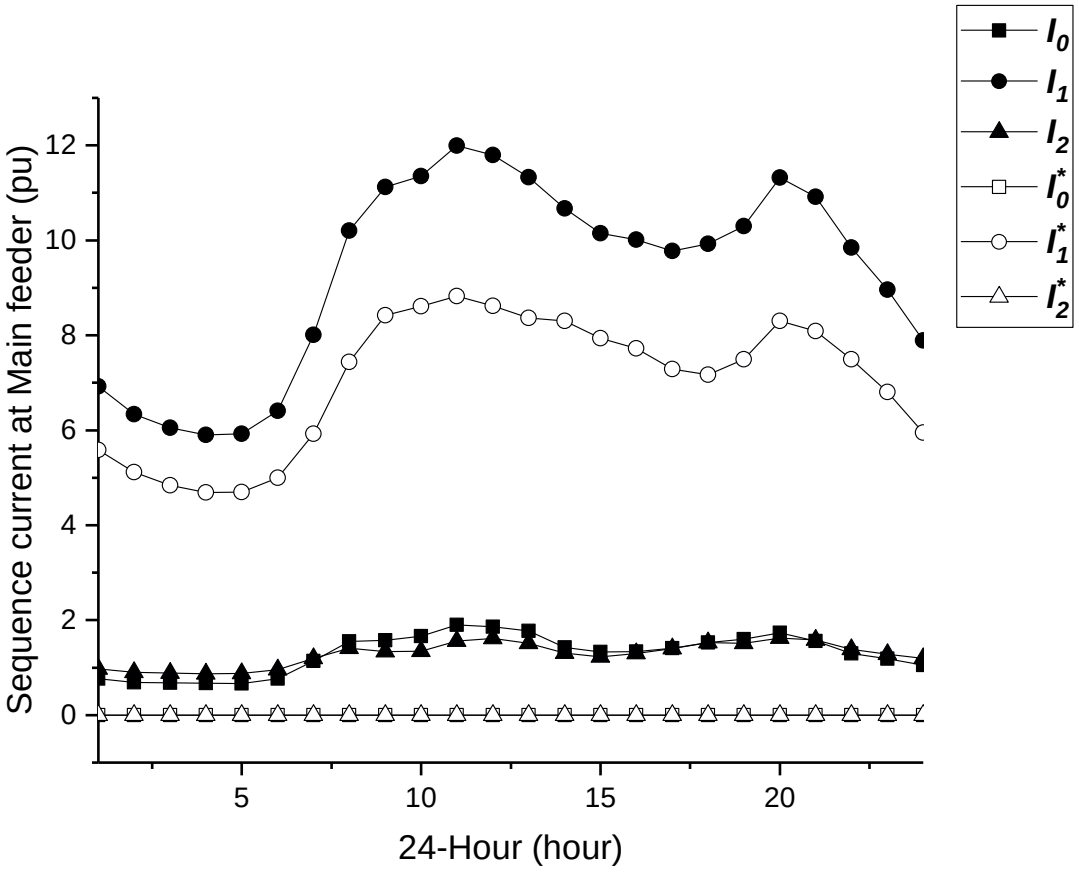

Figure 6.1: Hourly positive-, zero-, negative-sequence currents without and with SPDGs. I_0, I_1, and I_2 indicate sequence currents for the case when SPDGs are not placed. I_0^*, I_1^*, and I_2^* indicate sequence currents for the case when SPDGs are placed.

Phase currents: The effect of reduction in zero- and negative-sequence currents is also reflected in the phase currents at main-substation as shown in Fig. 6.2. Fig. 6.2 shows that the SPDGs provide currents in such a manner that currents in three phases at the main substation get balanced. An important observation made from the figure is that the balanced phase currents of all the three phases at the main-substation are

reduced to the minimum of three phase currents under unbalance (without SPDG). It is to be noted that I_b (minimum of phase current) overlaps with I_a^*, I_b^*, I_c^*. This results in increased MVA margins on the other two phases.

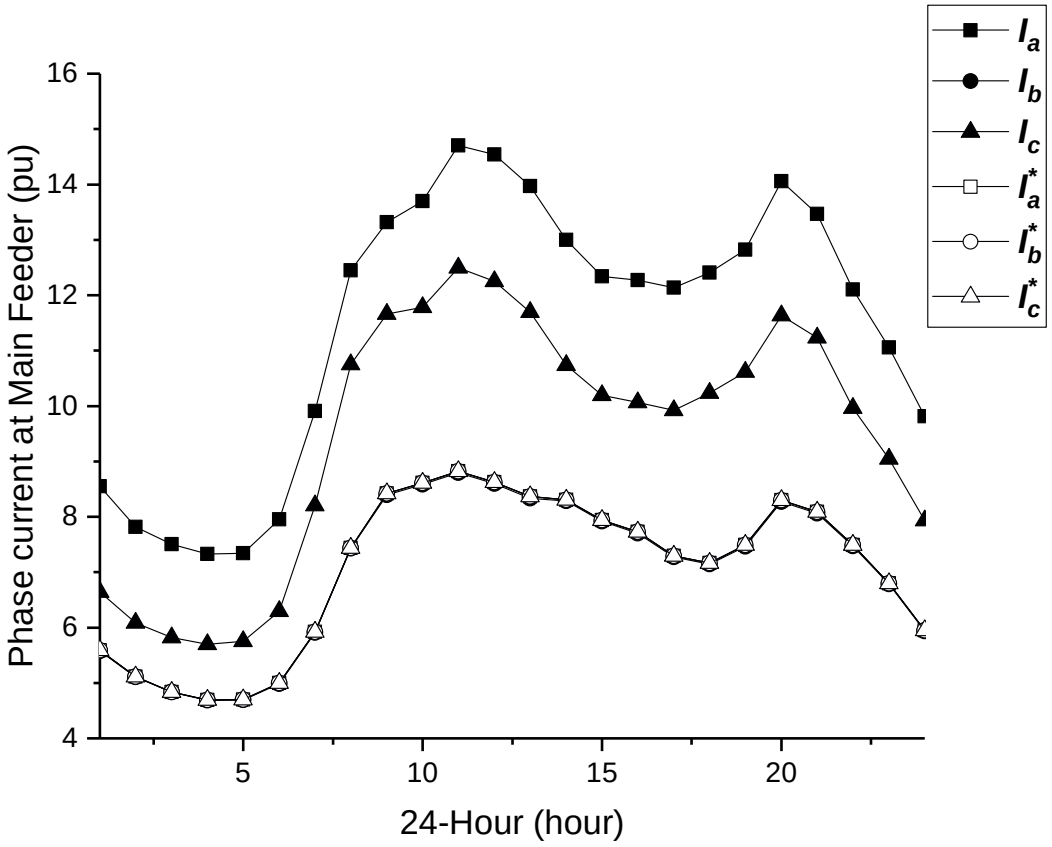

Figure 6.2: Hourly phase currents without and with SPDGs. I_a, I_b, and I_c indicate phase currents for the case when SPDGs are not placed. I_a^*, I_b^*, and I_c^* indicate phase currents for the case when SPDGs are placed.

Voltages: The bus-wise phase voltages for the peak load condition are plotted in Fig. 6.3. From this figure, it is observed that with the use of SPDGs, voltage profile improves and voltages become more balanced as compared to the case without SPDG. It is observed that phase voltages after scheduling SPDGs get pulled up towards the highest phase voltage of the case when SPDGs are not used. Comparison of minimum bus voltage before and after placing the SPDGs at every hour is shown in Fig. 6.4. From Fig. 6.4, minimum bus voltages of the system considerably improve when SPDGs are optimally placed in the system.

Losses: Scheduling of SPDGs in the system also affect the line losses. If SPDGs are

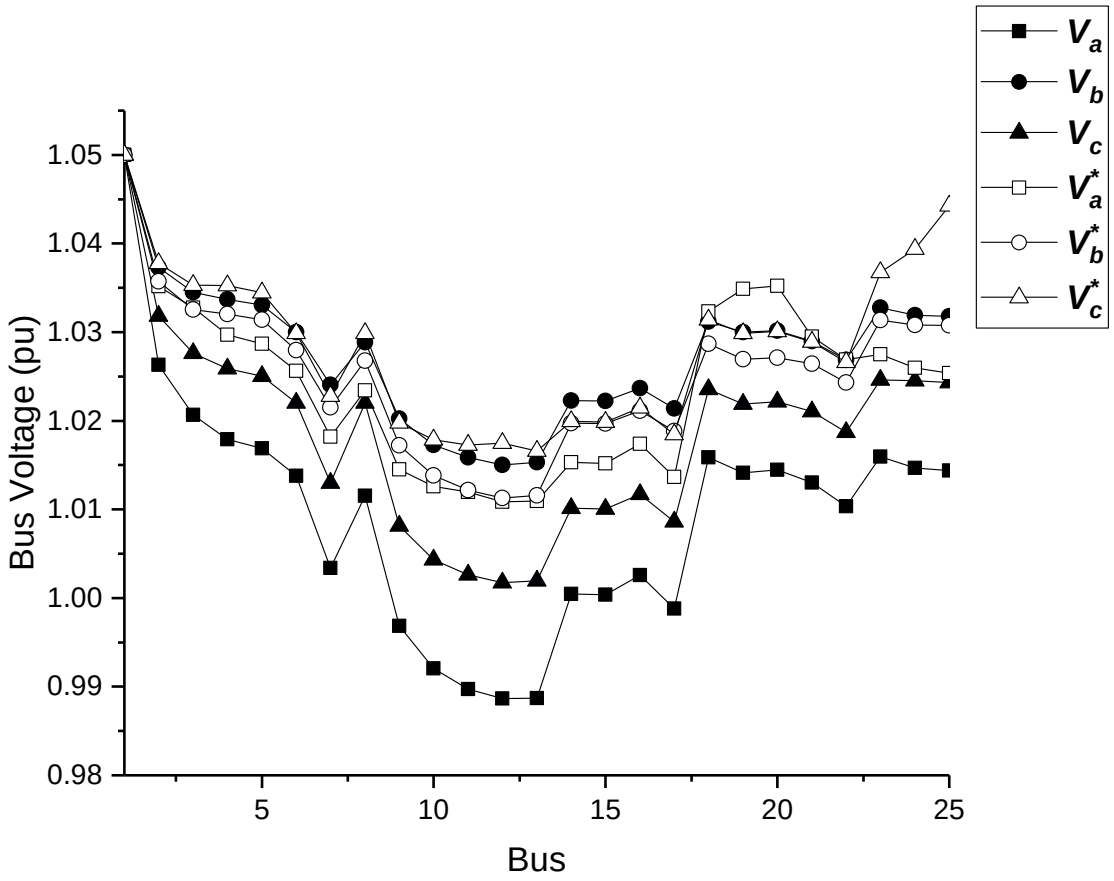

Figure 6.3: Bus voltages without and with SPDGs. V_a, V_b, V_c indicate bus voltages without SPDGs. V_a^*, V_b^*, V_c^* indicate bus voltages with SPDGs.

not suitably placed, losses may increase dramatically. Effect of placement of single-phase SPDGs on the active and reactive line losses is also studied. Active and reactive line losses before and after placing SPDGs for 24-hour are shown in Fig. 6.5. It is clear from Fig. 6.5 that the active and reactive line losses also reduce. Hence, the placement of SPDGs to balance the currents at main feeder does not increase the line losses, instead losses will come down.

Phase Utilization Index (PUI): PUIs before and after placing the SPDGs for 24-hour are shown in Fig. 6.6. Fig. 6.6 clearly shows that the PUIs are negligible when the SPDGs are optimally placed.

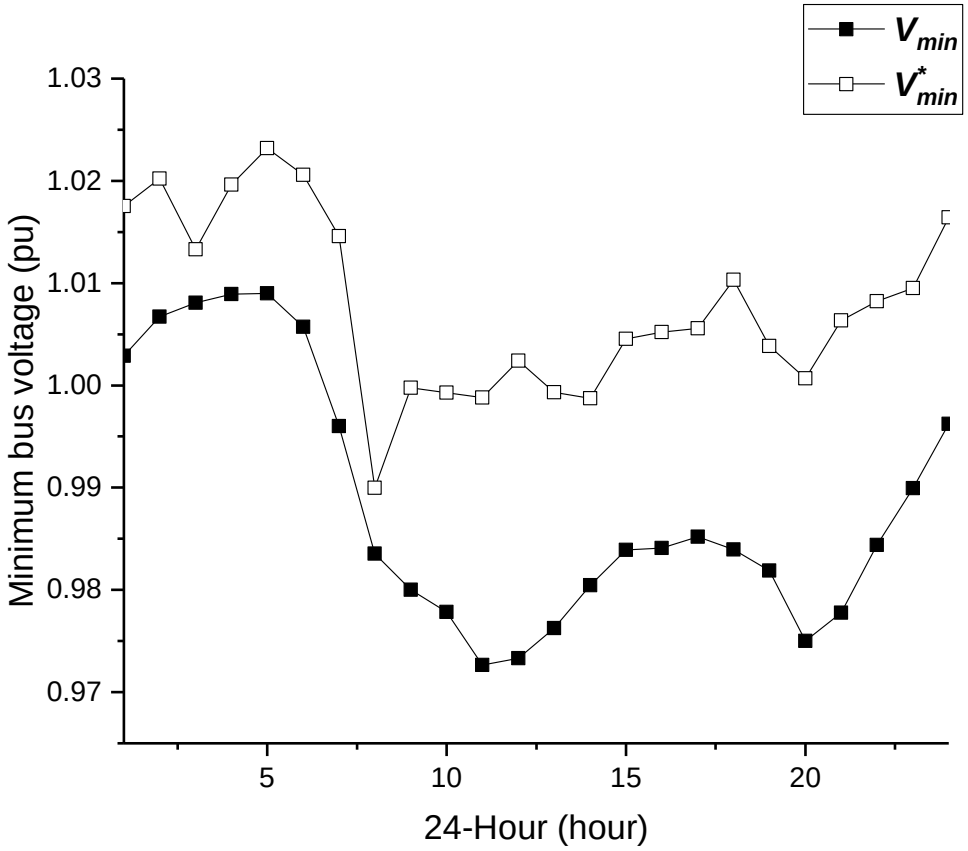

Figure 6.4: Minimum of the all bus Voltages without SPDGs and with SPDGs for 24 hour. V_{min} and V^*_{min} indicate the minimum bus voltage in case of Without SPDGs and with SPDGs respectively.

6.5 Summary

Planning of SPDGs for the purpose of phase balancing and a loss minimization is proposed in this chapter. EBOwithCMAR with CINR algorithm is utilized to solve this problem. CINR is utilized to calculate objective function at each solution. The planning is approached for different objectives. In the first objective function, the optimal SPDG locations (phase and bus) and sizes are obtained for minimum negative-sequence and zero-sequence current at the root node. The location and size are then evaluated for the minimization of active and reactive loss. Also, hourly scheduling of SPDG (in term of phase and size) for 24-hour loading scenario to obtain the phase balancing with minimum active and reactive losses is performed. It has been established that EBOwithCMAR with CINR is an effective algorithm for solving phase balancing and loss minimization problem.

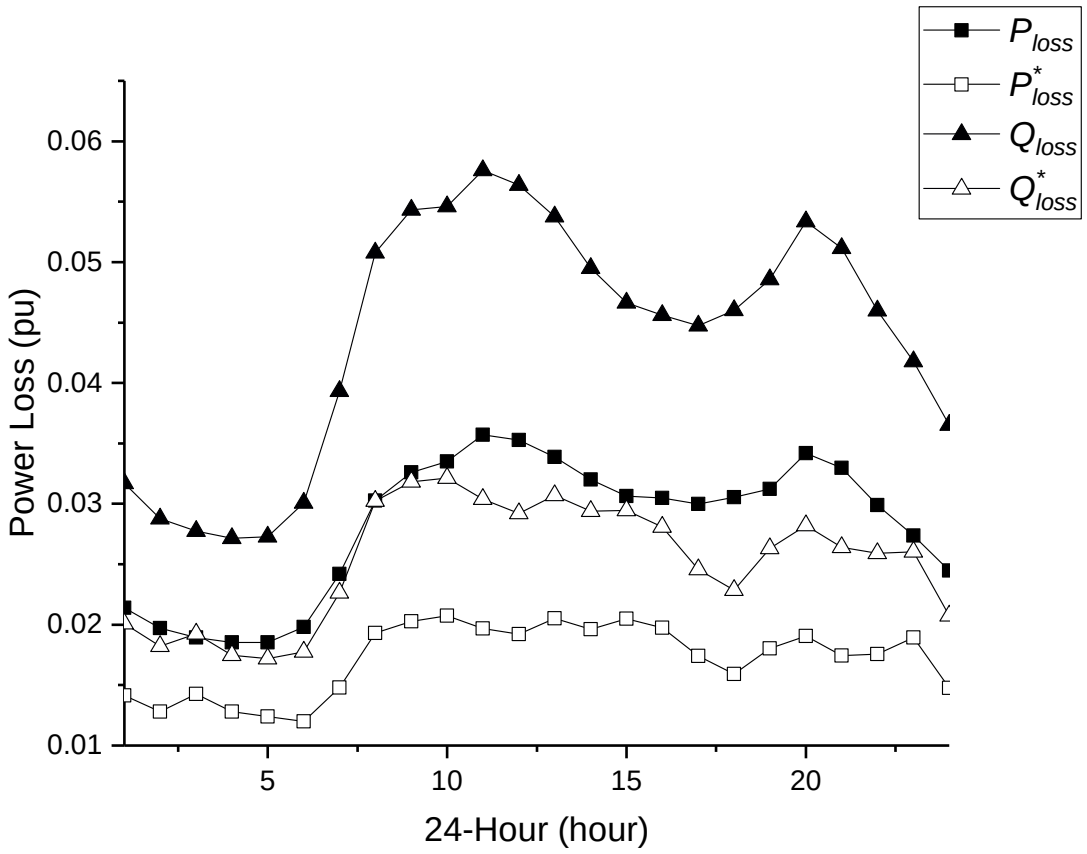

Figure 6.5: Total active and reactive power line loses for 24-hours. P_{loss} and Q_{loss} indicate total active and reactive line losses for the case when SPDGs are not placed. P^*_{loss} and Q^*_{loss} indicate total active and reactive power line loss for the case when SPDGs are placed.

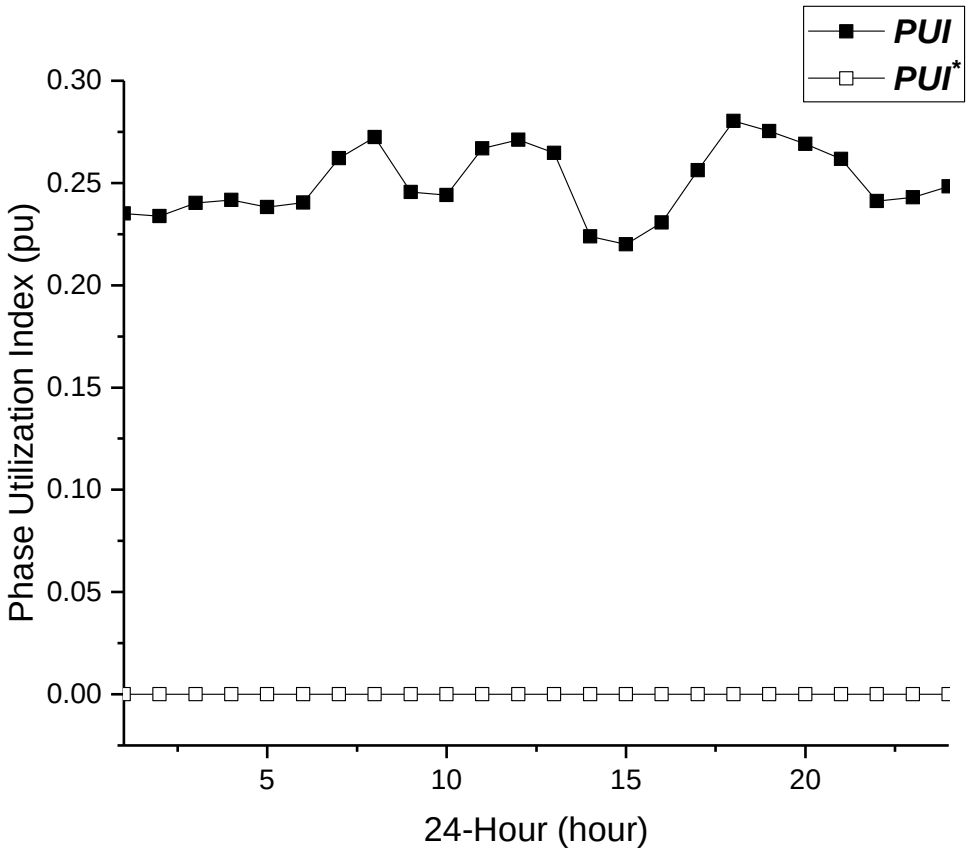

Figure 6.6: Phase Utilization Index at main feeder for 24 hours. PUI and PUI^* indicates the phase utilization index in case of without SPDGs and with SPDGs respectively.

Chapter 7

ESHADE in Optimization of Islanded Microgrids

7.1 Introduction

This chapter presents a method to determine optimal droop settings of DGs in a DCIMG. Minimization of system losses are considered as objective function while droop characteristics and power balance is considered as operational constraints of the DCIMG. The resultant optimization problem is solved using ESHADE and CINR. Here, ESHADE is an enhanced version of SHADE algorithm [217]. SHADE [217] is an acronym for Success-History based Parameter Adaption for Differential Evolution. CINR is used to calculate the objective function and ESHADE is used to calculate the optimal droop setting for all DGs.

An islanded MG is a low or medium voltage distribution system where electrical boundaries are clearly defined and a group of DGs and loads are interconnected without the support of the main grid [84,85,218]. In MG, the group of DGs supports local demands fully or partially of electricity and heat within the electrical boundaries [84,85]. MGs can be seen as a single controllable unit with respect to the main grid. In MGs, the system can operate in islanded or grid-connected mode, or it can operate in a smooth transition state between these two modes [84, 85, 219]. Islanded mode provides following benefits to the utilities as well as customers 1) improved power quality, 2) improved the system reliability, 3) overloads prevention, 4) maintenance of components of systems without interruption of power supply to the customers [220]. In the near future, microgrids are likely to be

operated in an islanded mode for longer time durations due to above-mentioned potential benefits.

For the successful operations of a DCIMG, microgrid's local loads must be shared among the DGs within the limits of the bus voltages and operating frequency. Besides, the line flows should be within acceptable limits. In the literature, several droop control schemes are introduced for power-sharing among the DGS in DCIMG [169, 221, 222]. However, it is essential to operate the microgrids in an islanded mode not only in a stable state but also with optimal settings. From the customer perspective, the system should be operated at a low operating cost without compromising with its performance.

Nowadays, researchers focus on the optimal operation of DCIMG. In [223], an energy management system is proposed for DCIMG to operate stably with low fuel consumption. In [224], an optimization process is proposed to dispatch DGs and storage systems optimally for medium -voltage DCIMG with low operating cost and low emission. In a DCIMG, the operating frequency and bus voltages are been determined by the droop characteristics of DGs and loading conditions of the system. Moreover, the power output of a droop-controlled DGs are not known before the power flow analysis. In [225], a multistage algorithm is proposed to minimize fuel cost by considering constraints on voltage, frequency, and stability for a VSC-based microgrid.

In this thesis, a multi-operator variant of DE, ESHADE, is proposed to calculate the optimal droop settings of DGs for minimizing the operating cost and system losses in DCIMG. The proposed approach integrates the CINR method to perform the power flow analysis calculating the objective function values for each combination of droop settings of DGs. In ESHADE, four mutation strategies are employed with the same self-adaptation scheme of control parameters, but strategies are selected for individuals independently using a probability-based selection. To update the said probability, the success rate of each mutation strategy is utilized. Thus, the larger part of the population will get enrolled gradually in the better performing strategy.

7.2 Problem Formulation

In this work, we presume the existence of a Microgrid Central Controller (MGCC) and a noncritical low-bandwidth communication infrastructure to complement the droop con-

trol scheme. In this paradigm, the optimization of the islanded microgrid operation is performed centrally by a higher level coordinated management function at the MGCC. Using periodic measurements of the islanded microgrid generation and loads, the MGCC updates the DG unit droop settings (i.e., characteristics) in order to optimally dispatch the different DG units in the Islanded microgrids.

The main objective of this chapter is to find an optimal setting for droop controllers to minimize active power losses and reactive power losses.

The active and reactive power losses in the line connecting buses i and j can be calculated using following equations.

$$P_{loss}(i,j) = R_{ij}\frac{P_i^2 + Q_i^2}{|V_i|^2} \tag{7.1}$$

$$Q_{loss}(i,j) = X_{ij}\frac{P_i^2 + Q_i^2}{|V_i|^2} \tag{7.2}$$

where P_{loss} and Q_{loss} are active and reactive power loss. Total power loss of the system can be calculated by summing up all the lines losses of the system, i.e.,

$$\mathbf{P}_{loss} = \sum_{i=1}^{N}\sum_{j=1}^{N} P_{loss}(i,j), \tag{7.3}$$

$$\mathbf{Q}_{loss} = \sum_{i=1}^{N}\sum_{j=1}^{N} Q_{loss}(i,j) \tag{7.4}$$

where $\mathbf{P}_{loss}$ and $\mathbf{Q}_{loss}$ represent the total active and reactive power loss, respectively. N is the total number of buses in the network.

In this study, the optimal values of the droop setting are obtained to calculate for minimizing the active and reactive losses. This problem can be formulated as a bound-constrained optimization problem. During the optimization process, the algorithm must evaluate all feasible settings of droop controllers to provide the minimum losses. For this purpose, the following optimization problem is considered in this study.

$$\text{Minimize } f(\mathbf{m}_p, \mathbf{n}_q) = w_1\mathbf{P}_{loss} + w_2\mathbf{Q}_{loss} \tag{7.5}$$

where $\mathbf{m}_p = \{m_{p1}, m_{p2}..., m_{pn}\}$ and $\mathbf{n}_q = \{n_{q1}, n_{q2}..., n_{qn}\}$ represent the droop settings of active and reactive power of DGs. Index n represents the number of DGs in islanded microgrids. Parameters w_1, and w_2 are the weighing factor for different objectives to

represent multi-objective optimization problem into single objective optimization problem. This optimization problem is a non-convex, and non-linear continuous unconstrained optimization problem.

7.3 Proposed Methodology

To solve the above-discussed optimization problem, an optimization algorithm, ESHADE, is proposed in this section. The objective function of this problem can not be directly calculated because bus voltages of the system are not available for a different setting of droop controllers. Therefore, power flow analysis is required for calculating bus voltages to evaluate the objective function. In this work, CINR (proposed in chapter 4) is considered for power flow analysis.

7.3.1 ESHADE

In this section, the procedures and steps of ESHADE are discussed in detailed form. The self-adaptation mechanism for control parameters is also discussed which is an improved version of success history based parameter adaptation scheme proposed in [217]. The main step of ESHADE Algorithm is shown in Algorithm- 8. Steps, which is not described in Algorithm -8, is discussed in following subsections:

Initialization

In order to start the optimization process, an initial population P^0 should be generated uniformly within the upper and lower bound of the search-space. The Population, P^0 is represented using the following equation:

$$P^0 = [\bar{x}_1^0, \bar{x}_2^0 ..... \bar{x}_{N_p}^0], where \tag{7.6}$$

$$\bar{x}_i^0 = [x_{i1}^0, x_{i2}^0 .... x_{iD}^0]'$$

where, N_p and D are the size of population and dimension of search-space respectively. Here, x_{ij}^0 is initialized randomly as follows:

$$x_{ij}^0 = x_{Lj} + rand(0,1]. \times (x_{Uj} - x_{Lj}) \tag{7.7}$$

where x_{Lj} and x_{Uj} are the lower and upper bound of j^{th}-dimension of search-space. Operator $rand(0,1]$ stands for random number generator from uniform distribution.

Algorithm 8: Framework of ESHADE

Data: Define N_P^0 and all other parameters required
Result: X

Generate an initial population, P^0 of N_P^0 individual;
Objective function evaluation at each individual of population;
$nfes \leftarrow N_P^0$, $g \leftarrow 0$;
$\mu_{sF} \leftarrow 0.5$, $\mu_{cr} \leftarrow 0.5$, $\mu_{prob} \leftarrow 1$, $k \leftarrow 1$;
while *termination condition is not satisfied* **do**
    $g \leftarrow g + 1$;
    for i = *1:*N_P **do**
        % calculation of parameter starts;
        $sF_i \leftarrow$ using Equations 7.14 and 7.15;
        $cr_i \leftarrow$ using Equations 7.16;
        $prob \leftarrow$ using Equations 7.18;
        % Mutation;
        if $rand < 0.5$ **then**
            $r \leftarrow rand()$;
            if $r < prob(1)$ **then**
                $\bar{v}_i \leftarrow$ using **DE1**;
            else if $prob(1) < r < prob(1) + prob(2)$ **then**
                $\bar{v}_i \leftarrow$ using **DE2**;
            else
                $\bar{v}_i \leftarrow$ using **DE3**;
            end
        else
            $\bar{v}_i \leftarrow$ using **DE4**;
        end
        % Crossover;
        $\bar{u}_i \leftarrow$ **BinomialCrossover**($\bar{x}_i$, $\bar{u}_i$, cr_i);
        % Selection;
        objective function evaluate at $\bar{u}_i$;
        $nfes \leftarrow nfes + 1$;
        $\bar{x}_i \leftarrow$ **Selection**($\bar{x}_i$, $\bar{u}_i$);
    end
    Update the k^{th} element of μ for all parameter;
    $\sigma \leftarrow$ describe as in [226];
    $C \leftarrow$ describe as in [226];
    $k \leftarrow rem(k + 1, h)$;
    Resize the Population and Archive using EPSR;
end

Mutation

For each individual, a mutant vector has been generated. In ESHADE, four mutation strategies (modified version of mutation strategies reported in [217, 226, 227]) are used to generate mutant vectors and are as follows:

- DE1: current-to-$p$best with archive [217]:

$$\bar{v}_i^g = \bar{x}_i^g + sF_i \times (\bar{x}_{p\text{best}}^g - \bar{x}_i^g + \bar{x}_{r_1}^g - \hat{x}_{r_2}^g) \tag{7.8}$$

- DE2: current-to-$\phi rand$ [226]:

$$\bar{v}_i^g = \bar{x}_i^g + sF_i \times (\bar{x}_{r_\phi}^g - \bar{x}_i^g + \bar{x}_{\phi\text{best}}^g - \bar{x}_{\phi\text{worst}}^g) \tag{7.9}$$

- DE3: Modified DCMA-ES with archive [227]:

$$\bar{v}_i^g = \mathcal{N}(\bar{x}_m^g, \sigma^2 C^g) + 0.1sF_i \times (\bar{x}_{r_1}^g - \hat{x}_{r_2}^g) \tag{7.10}$$

- DE4: $\phi rand$ [226]:

$$\bar{v}_i^g = \bar{x}_{r_\phi}^g + sF_i \times (\bar{x}_{\phi\text{best}}^g - \bar{x}_{\phi\text{worst}}^g) \tag{7.11}$$

where, $r_1 \neq r_2 \neq i$ are integer with $\bar{x}_{r_1}$ is randomly selected from population P, $\hat{x}_{r_2}$ is randomly selected from union of population and archive. While $p\bar{\text{best}}$ is selected from $p\%$ individuals from best individuals of P. In order to select $\bar{x}_{r_\phi}$, $\bar{x}_{\phi\text{best}}$, and $\bar{x}_{\phi\text{worst}}$; entire population is divided into three clusters, ϕbest, ϕ, and ϕworst (best, better, and worst) of size $p\%$, $(1-2p)\%$ and $p\%$ of N_p respectively. $\bar{x}_{r_\phi}$, $\bar{x}_{\phi\text{best}}$, and $\bar{x}_{\phi\text{worst}}$ are randomly selected from cluster ϕ, ϕbest, and ϕworst respectively. The calculation procedures of σ and C used in equation (7.10) are discussed in Section 6.3.1 in previous chapter.

In ESHADE, all mutation strategies are classified into two classes. In the first class, the three mutation strategies: DE1, DE2, and DE3 are applied with probability $prob(1)$, $prob(2)$, and $prob(3)$ respectively to generate a mutant vector. While in the second class, a mutant vector is generated using DE3. In every iteration, a mutant vector is calculated for every individual of the population using one of the above-mentioned mutation class with equal probability.

Crossover

In this chapter, binomial crossover is employed. In the binomial crossover, the target vector, $\bar{x}_i$, is crossed over with the mutated vector,$\bar{v}_i$, using the binomial experiment scheme, to generate the trial vector, $\bar{u}_i$ for target vector.

$$u_{ij}^g = \begin{cases} x_{ij}^g, & \text{if } (rand_{ij} > cr_i), \\ v_{ij}^g, & \text{if } (rand_{ij} < cr_i) \text{ or } (j == j_{rand}) \end{cases} \tag{7.12}$$

Selection

After trial vector, $\bar{u}_i$, has been calculated, a selection operator is applied to find out the survivor for the next generation [132]. In selection operator, $\bar{x}_i$ is compared with the $\bar{u}_i$ on the basis of their objective function value and the better one is stored in population for the next generation.

$$\bar{x}_i^{g+1} = \begin{cases} \bar{x}_i^g, & \text{if } (f(\bar{x}_i^g) < f(\bar{u}_i^g)), \\ \bar{u}_i^g, & \text{otherwise} \end{cases} \tag{7.13}$$

Parameter adaptation of population size (N_p), scaling factor (sF), and crossover rate (cr)

The performance of DE is highly influenced by the parameter setting. Parameter setting is problem dependent and each problem has its own set of parameter values. In order to resolve this issue, self-adaptation procedures for parameters are proposed in this subsection.

Adaptation procedure for scaling factor, sF:

In order to perform an adaptation for sF, the procedure is composed of two sections. The first section is activated during the initial evolutionary process, while the other section is activated later part of the evolutionary process.

Here, the first section uses the condition : $nfes < 0.2 \times max_nfes$ to activate. In first section of adaptation of scaling factor, sF_i is generated within the range of [0.45, 0.5] using following mathematical equation:

$$sF_i = \begin{cases} 0.5, & \text{if } (\mu_{sF}(j) > 0.5), \\ 0.45 + rand(0, 0.1], & \text{otherwise} \end{cases} \tag{7.14}$$

where $\mu_{sF}(j)$ is the j^{th} element of μ_{sF}. Here, μ_{sF} is a memory where Lehmer mean of successful scaling factor's value of previous generations are stored [217]. Index j is randomly selected for each individual independently from the range $[1, H]$ where H is memory size.

During the second section, the adaptation of scaling factor is done using following equation:

$$sF_i = randc(\mu_{sF}(j), 0.1) \tag{7.15}$$

where *randc* stands for random number generator from Cauchy distribution.

Adaptation procedure for crossover rate, cr:

In ESHADE, the crossover rate, cr_i, is adapted according following equation:

$$cr_i = randn(\mu_{cr}(j), 0.1) \tag{7.16}$$

where, μ_{cr} has similar function of μ_{sF}, but it stores the weighted mean of successful crossover rate's values of previous generations and *randn* stands for normal distribution [217].

Exponential population size reduction for population size, N_p:

In order to improve the performance of ESHADE, exponential population size reduction (EPSR) technique is employed to reduce the population exponentially. In EPSR, the following equation is used:

$$N_p^{g+1} = N_p^0 \times round\left(1 - \gamma \frac{N_p^0 - N_{p,min}}{max_{nfes}}\right)^g \tag{7.17}$$

where γ is a parameter to control the exponential curve, N_p^0 is the initial population size and $N_{p,min}$ is minimum allowed population size which is equal to 4.

The calculation and adaptation procedure of the parameters associated with DE3, σ and C, have already been discussed in Section 6.3.1.

Calculation of *prob*

In order to calculate *prob*, an index, j, is generated randomly within the range $[1, h]$ for every individual. Then, j^{th} element of the historical memory, μ_{prob}, is used to calculate prob using following equation:

$$prob(k) = \frac{\mu_{prob}(j,k)}{\sum_{n=1}^{3} \mu_{prob}(j,n)}, \text{ where } k = 1, 2, 3. \tag{7.18}$$

Updation of historical memory, μ

Elements of the historical memory, μ, is updated using the *success* of the individuals at the end of every iteration. Here at g iteration, the *success* of i^{th} individual is calculated using the following equation:

$$success_i^g = f(\bar{x}_i^g) - f(\bar{x}_i^{g+1}) \tag{7.19}$$

where, $f(.)$ stands for objective function value.

For parameters cr, and sF, k^{th} element of historical memory μ_{cr} and μ_{sF} respectively are calculated using following equations:

$$\mu_{cr}(k) = \frac{\sum_{n=1}^{N_p} w_n^2 cr_n}{\sum_{n=1}^{N_p} w_n cr_n} \tag{7.20}$$

$$\mu_{sF}(k) = \frac{\sum_{n=1}^{N_p} w_n^2 sF_n}{\sum_{n=1}^{N_p} w_n sF_n} \tag{7.21}$$

where,

$$w_i = \frac{success_i}{\sum_{n=1}^{N_p} success_n} \tag{7.22}$$

In case of $prob$, k^{th} elements of historical memory μ_{prob} are calculated using following equation:

$$\mu_{prob}(k,m) = (1-c)\mu_{prob}(k,m) + c\triangle_m \tag{7.23}$$

where c is the learning rate, and $\triangle_m$ is calculated using Equation-(7.24)

$$\triangle_m = \frac{\sum_{n \epsilon S_m} success_n}{\sum_{n=1}^{N_p} success_n} \tag{7.24}$$

where S_m is the set of individuals which are selected for m^{th} mutation strategy (here m can be 1, 2, and 3 which are stand for for DE1, DE2, and DE3 respectively).

7.3.2 Evaluation of Objective Function

In optimization algorithms, evaluation of objective function at each iterations for all the solutions is required for improving the solutions. The objective function considered in this chapter cannot be evaluated directly. Power flow analysis is to be perform to obtain the steady-state voltage at each bus of the system because these voltages are used to calculate the objective function defined in Equation 7.5.

CINR algorithm is utilized to calculate the steady-state voltage at each bus for every solution of the optimization process. Each solution contains the droop settings of all DGs. First of all, power capacity of the DGs are updated according to the solution (droop settings of DGs). Power generation are modified by using following equations.

$$P_{dg,i} = \frac{1}{n_{pi}}(w_i^* - w) \tag{7.25}$$

and,

$$Q_{dg,i} = \frac{1}{m_{qi}}(|V_i|^* - |V_i|) \tag{7.26}$$

where $P_{dg,i}$ and $Q_{dg,i}$ represent the active and reactive power at i-th bus. $\{n_{pi}, m_{qi}\}$ represent the droop characteristics of i-th DG.

After modifying the power capacity equations, power flow analysis is performed using CINR to calculate the voltage at each bus. Further these voltages are used to calculate the objective function values.

7.3.3 Proposed Algorithm

The above-discussed optimization problem considers droop settings (related to active and reactive power output) of DGs as the problem variables. Each solution vector has $2 * M$ elements where M is the total number of DGs in the systems.

The purpose of this problem is to find the optimum droop settings for all the DGs so that the objective function is minimized.

The following steps are utilized to solve the optimization problem.

1. **Step 1:** Initialization of population of N_p solution is done using uniformly distributed in random points within the bound of each variables.

2. **Step 2:** Power flow analysis is performed at each solution of current population.

3. **Step 3:** Objective function is evaluated at each solution of current population

4. **Step 4:** Solutions of population are updated using ESHADE (proposed algorithm)

5. **Step 5:** Check the stopping criteria. If stopping criteria is met go to **Step 6**, otherwise go to **Step 2**

6. **Step 6:** Best solution on the basis of minimum objective function value is extracted from population to set the droop controllers of DGs within the system.

7.4 Results and Discussion

In this section, the proposed optimization algorithm is applied to solve the optimal power flow problem of droop-controlled islanded microgrids through optimal setting of droop parameters.

Before applying this method for optimal power flow problem, the proposed algorithm is validated on standard benchmark problem used in 100-digit challenge at IEEE CEC 2019 [228]. The results corresponding to all problems are given in Appendix III

7.4.1 Parameter Setting

For ESHADE, the parameter are set as follows: $N_p^0 = 18 \times D$, $N_{p,min} = 4$, $\gamma = 5$, and $c = 0.8$.

7.4.2 Case Studies

Three test systems viz. CASE6, CASE22, and CASE38, are considered to analyze the performance of proposed algorithm. The detail of these test systems are reported in Appendix-II.

Proposed algorithm is applied on CASE6 test system to obtained the optimal droop settings for minimal active and reactive power losses.

Table 7.1: Results of optimal power flow problem of CASE6

Without Optimization				Min of $\mathbf{P}_{loss}$				Min of $\mathbf{Q}_{loss}$				Min of $(0.5 * \mathbf{P}_{loss} + 0.5 * \mathbf{Q}_{loss})$			
w	0.9991			w	0.9961			w	0.9941			w	0.9945		
$\mathbf{P}_{loss}$	0.0080			$\mathbf{P}_{loss}$	0.0063			$\mathbf{P}_{loss}$	0.0064			$\mathbf{P}_{loss}$	0.0063		
$\mathbf{Q}_{loss}$	0.0062			$\mathbf{Q}_{loss}$	0.0026			$\mathbf{Q}_{loss}$	0.0025			$\mathbf{Q}_{loss}$	0.0025		
	Bus	$\|V\|$	$V_\angle$		Bus	$\|V\|$	$V_\angle$		Bus	$\|V\|$	$V_\angle$		Bus	$\|V\|$	$V_\angle$
	1	0.9600	0.0000		1	0.9481	0.0000		1	0.9495	0.0000		1	0.9505	0.0000
	2	0.9725	-0.5214		2	0.9646	-0.3301		2	0.9690	-0.3961		2	0.9682	-0.3772
Voltage	3	0.9639	-2.6710	Voltage	3	0.9568	-0.3260	Voltage	3	0.9686	-0.3515	Voltage	3	0.9653	-0.3466
	4	0.9872	-0.0740		4	0.9723	-0.2379		4	0.9714	-0.2098		4	0.9738	-0.2121
	5	0.9901	-0.4461		5	0.9746	-0.5212		5	0.9790	-0.5033		5	0.9778	-0.5185
	6	0.9693	-2.8542		6	0.9645	-0.4217		6	0.9768	-0.4736		6	0.9733	-0.4599
	Bus	P	Q		Bus	P	Q		Bus	P	Q		Bus	P	Q
	1	-0.1487	-0.0984		1	-0.1451	-0.0960		1	-0.1455	-0.0963		1	-0.1458	-0.0965
	2	0.0000	0.0000		2	0.0000	0.0000		2	0.0000	0.0000		2	0.0000	0.0000
Power	3	-0.1993	-0.1409	Power	3	-0.1964	-0.1388	Power	3	-0.2013	-0.1422	Power	3	-0.1999	-0.1413
	4	0.1187	0.0587		4	0.0985	0.0638		4	0.0894	0.0572		4	0.0957	0.0603
	5	0.1187	0.0457		5	0.0546	0.0508		5	0.0591	0.0420		5	0.0548	0.0445
	6	0.1187	0.1411		6	0.1946	0.1228		6	0.2046	0.1418		6	0.2015	0.1355
m_p	0.0075	0.0075	0.0075	m_p	0.0713	0.0200	0.0395	m_p	0.1000	0.0289	0.0661	m_p	0.1000	0.0272	0.0573
n_q	0.2173	0.2173	0.2173	n_q	0.5000	0.2888	0.4343	n_q	0.5000	0.1637	0.5000	n_q	0.5000	0.1971	0.4352

Table 7.1 shows the results of CASE6 after solving the optimal power problem using ESHADE. It can be concluded from Table 7.1 that the active and reactive power losses are reduced by 21.25% and 59.68%, respectively after using the optimal setting of droop

coefficients. In Table 7.1, results of single objective optimal power flow is also reported and these results show that these objectives are also able to reduce the active and reactive power losses with sufficient margins.

The Voltage profile of system is reduced in the system after including optimal droop settings. The main reason behind this issue is that the droop coefficient related to reactive power are increased to minimize the losses. Similarly system operating frequency is also reduced due to increase of droop coefficient related to active power.

Table 7.2: Results of optimal power flow problem of CASE22

Normal		Min of $\mathbf{P}_{loss}$		Min of $\mathbf{Q}_{loss}$		Min of $(0.5 * \mathbf{P}_{loss} + 0.5 * \mathbf{Q}_{loss})$	
w	0.9996	w	0.9994	w	0.9865	w	0.9994
$\mathbf{P}_{loss}$	0.0053	$\mathbf{P}_{loss}$	0.0022	$\mathbf{P}_{loss}$	0.0022	$\mathbf{P}_{loss}$	0.0022
$\mathbf{Q}_{loss}$	0.0027	$\mathbf{Q}_{loss}$	0.0011	$\mathbf{Q}_{loss}$	0.0011	$\mathbf{Q}_{loss}$	0.0011
m_p	0.0051	m_p	0.0043	m_p	0.1000	m_p	0.0041
	0.0015		0.0043		0.1000		0.0041
	0.0045		0.0027		0.0623		0.0025
	0.0015		0.0033		0.0766		0.0031
n_q	0.0500	n_q	0.0103	n_q	0.0100	n_q	0.0103
	0.0300		0.0135		0.0132		0.0135
	0.0100		0.0100		0.0100		0.0100
	0.0200		0.0114		0.0112		0.0113

The outcomes of CASE22 and CASE38 are reported in Tables 7.2 and 7.3, respectively. From these tables, it can be concluded that the active and reactive power losses are reduced after implementing the optimal droop settings into the systems. It is worthwhile to note that the outcomes of all types of objective functions are almost similar in all case studies. This outcome implies that the minimizing of active power and minimizing of reactive power are not conflicting objectives in case of droop controlled islanded microgrids.

7.5 Summary

In this chapter, a new optimization algorithm, ESHADE, is proposed to solve the optimal power flow problem of droop-controlled islanded microgrids where minimization of power losses are the objectives. The proposed algorithm is validated on the standard benchmark

Table 7.3: Results of optimal power flow problem of CASE38

Normal		Min of $\mathbf{P}_{loss}$		Min of $\mathbf{Q}_{loss}$		Min of $(0.5 * \mathbf{P}_{loss} + 0.5 * \mathbf{Q}_{loss})$	
w	0.9982	w	0.9772	w	0.9555	w	0.9579
$\mathbf{P}_{loss}$	0.0053	$\mathbf{P}_{loss}$	0.0841	$\mathbf{P}_{loss}$	0.0845	$\mathbf{P}_{loss}$	0.0842
$\mathbf{Q}_{loss}$	0.1269	$\mathbf{Q}_{loss}$	0.0700	$\mathbf{Q}_{loss}$	0.0685	$\mathbf{Q}_{loss}$	0.0686
	0.0051		0.0291		0.0618		0.0569
	0.0015		0.0452		0.0994		0.0868
m_p	0.0045	m_p	0.0586	m_p	0.1000	m_p	0.1000
	0.0023		0.0565		0.1000		0.1000
	0.0023		0.0153		0.0295		0.0281
	0.0500		0.0684		0.0830		0.0775
	0.0300		0.1000		0.1000		0.1000
n_q	0.0500	n_q	0.1000	n_q	0.1000	n_q	0.1000
	0.0100		0.1000		0.1000		0.1000
	0.1000		0.0423		0.0405		0.0422

problems and obtained results show that the proposed algorithm is effective and robust in comparison to state-of-the-art algorithms.

The results of the optimal power flow show that active and reactive power losses of the system are reduced, while the voltage profile is also reduced to adjust the new setting of droop coefficients related to reactive power generation.

Chapter 8

Conclusions and Future Scope

8.1 Conclusions

- Three numerical power flow algorithms, CINR, LMPF, and RK4PF, are proposed in Chapter-2. These algorithms have been validated on several ill-conditioned test systems. Comparative analysis reveals that the proposed algorithms outperform the other state-of-the-art algorithms viz. TCIM, iTCIM, and BFS in terms of rate of convergence and robustness.

- In Chapter-3, an unconstrained optimization algorithm, Spherical Search, is proposed. This algorithm is used to calculate the initial solution for the load flow algorithms. From the extensive analysis, it has been established that the proposed approach improves the performance of the load flow algorithm for the ill-conditioned and heavily loaded systems in terms of convergence and robustness.

- In Chapter-3, a new formulation of the power flow problem as a non-convex and non-linear constrained optimization problem is proposed to compute the steady-state condition of the system at critical loading conditions. A constrained optimization algorithm, Butterfly Constrained Optimizer (BCO), is proposed to solve this problem. Comparative analysis established that the BCO successfully evaluates continuation power solutions.

- In Chapter-4, nested-iterative approaches, NBFS and CINR, are proposed to solve the power flow problem of a droop-based islanded microgrid. The loop based approach comprises of updating the voltage and system frequency of the angle reference

bus. The algorithms have been implemented on several test systems to establish the effectiveness of algorithms. Further, the comparative analysis shows that proposed algorithms has superior convergence in comparison to state-of-the-art algorithms viz. MNR, NTR, DBFS, MBFS, and PSCAD.

- In Chapter-5, two novels constrained optimization algorithms, ϵDE-GN and υMAESbm, are proposed to solve the power flow problem of droop-controlled islanded microgrids. Further, the power flow problem is formulated as a constrained optimization problem. The proposed algorithm is applied on balanced as well as unbalanced test systems. The outcomes demonstrate that the proposed algorithms perform better than other state-of-the-art algorithms viz. PSO, NTR, and GA.

- In Chapter-6, the phase balancing and loss minimization of single-phase distributed generations has been addressed. This problem is formulated as a mixed-integer nonlinear unconstrained optimization problems. Further, a new method, EBOwithCMAR, has been proposed and has used with CINR to solve this problem. In this approach, CINR is used to calculate objective function at each solution. Four different objectives are considered in this work. From comparative analysis, it has been established that EBOwithCMAR with CINR is an effective algorithm to solve loss minimization and phase balancing problem.

- In Chapter-7, for solving the optimal power flow problem of droop-controlled islanded microgrids, a new optimization algorithm, ESHADE, has been proposed. The minimization of power losses is considered as an objective function in optimal power flow. Proposed formulation is validated on the several test systems and results show that active and reactive power losses are reduced. However, the voltage profile is slightly degraded to adjust the new settings of droop controllers.

8.2 Future Scope

The proposed algorithms can be applied for the planning and analyzing distribution systems. Power flow algorithms can be extended to investigate their applicability to the voltage-stability of the systems. Optimization algorithms can be utilized for economic

dispatch, centralized and decentralized coordination of plug-in vehicles, optimal sizing, and siting of the battery storage system problems of distribution systems.

Appendix I: Data for Test Systems CASE13, CASE25, CASE37, and CASE28

Table I.1: General Data of CASE13

General Data	
Slack	1
Vnom (kV)	4.16
InternationalSystem	0
DeltaLF	0
V_slack_ph_A	1.000
V_slack_ph_B	1.000
V_slack_ph_C	1.000
Ang_slack_ph_A	0
Ang_slack_ph_B	-120
Ang_slack_ph_C	120

Table I.2: Topology of CASE13

Node A	**Node B**	**Length (ft.)**	**Config.**
1	4	500	3
1	2	500	2
4	5	300	3
10	6	800	7
1	7	2000	1
7	10	300	4
7	9	1000	1
10	3	300	5
7	8	500	6

Table I.3: Line Parameter of CASE13

Config	R11	R12	R13	R22	R23	R33
1	0.3465	0.156	0.158	0.3375	0.1535	0.3414
2	0.7526	0.158	0.156	0.7475	0.1535	0.7436
3	–	0	0	1.3294	0.2066	1.3238
4	1.3238	0	0.2066	–	0	1.3294
5	–	0	0	–	0	1.3292
6	0.7982	0.3192	0.2849	0.7891	0.3192	0.7982
7	1.3425	0	0	–	0	–
Config	X11	X12	X13	X22	X23	X33
1	1.0179	0.5017	0.4236	1.0478	0.3849	1.0348
2	1.1814	0.4236	0.5017	1.1983	0.3849	1.2112
3	0	0	0	1.3471	0.4591	1.3569
4	1.3569	0	0.4591	0	0	1.3471
5	0	0	0	0	0	1.3475
6	0.4463	0.0328	-0.0143	0.4041	0.0328	0.4463
7	0.5124	0	0	0	0	0
Config	B11	B12	B13	B22	B23	B33
1	6.2998	-1.9958	-1.2595	5.9597	-0.7417	5.6386
2	5.699	-1.0817	-1.6905	5.1795	-0.6588	5.4246
3	0	0	0	4.7097	-0.8999	4.6658
4	4.6658	0	-0.8999	0	0	4.7097
5	0	0	0	0	0	4.5193
6	96.8897	0	0	96.8897	0	96.8897
7	88.9912	0	0	0	0	0

Table I.4: Load Data of CASE13

Bus	Phase-a		Phase-b		Phase-c	
	KW	KVAr	KW	KVAr	KW	KVAr
2	160	110	120	90	120	90
4	0	0	170	125	0	0
5	0	0	230	132	0	0
6	128	86	0	0	0	0
7	402	230	451	258	672	439
8	485	-10	68	-140	290	12
3	0	0	0	0	170	-20

Table I.5: Load Data of ill-conditioned CASE13

Bus	Phase-a		Phase-b		Phase-c	
	KW	KVAr	KW	KVAr	KW	KVAr
2	1600	1100	1200	900	1200	900
4	0	0	1700	1250	0	0
5	0	0	2300	1320	0	0
6	1280	860	0	0	0	0
7	4886	2795	5481	3136	8007	5335
8	4850	-100	680	-140	2900	120
3	0	0	0	0	1700	-20

Table I.6: General Data of CASE25

General Data	
Slack	1
Vnom (kV)	4.16
International System	0
DeltaLF	0
V_slack_ph_A	1
V_slack_ph_B	1
V_slack_ph_C	1
Ang_slack_ph_A	0
Ang_slack_ph_B	-120
Ang_slack_ph_C	120

Table I.7: Topology of CASE25

Node A	Node B	Length (ft.)	Config.
1	2	1000	1
2	3	500	1
2	6	500	2
3	4	500	1
3	18	500	2
4	5	500	2
4	23	400	2
6	7	500	2
6	8	1000	2
7	9	500	2
7	14	500	2
7	16	500	2
9	10	500	2
10	11	300	2
11	12	200	3
11	13	200	3
14	15	300	2
14	17	300	3
18	20	500	2
18	21	400	3
20	19	400	3
21	22	400	3
23	24	400	2
24	25	400	3

Table I.8: Line Parameters of CASE25

Conf	R11	R12	R13	R22	R23	R33
1	0.3686	0.0169	0.0155	0.3757	0.0188	0.3723
2	0.9775	0.0167	0.0152	0.9844	0.0186	0.981
3	1.928	0.0161	0.0161	1.9308	0.0161	1.9337
Conf	X11	X12	X13	X22	X23	X33
1	0.6852	0.1515	0.1098	0.6715	0.2072	0.6782
2	0.8717	0.1697	0.1264	0.8654	0.2275	0.8648
3	1.4194	0.1183	0.1183	1.4215	0.1183	1.4236
Conf	B11	B12	B13	B22	B23	B33
1	0	0	0	0	0	0
2	0	0	0	0	0	0
3	0	0	0	0	0	0

Table I.9: Load Data of CASE25

Bus	Ph-1 (kW)	Ph-1 (kVAr)	Ph-2 (kW)	Ph-2 (kWAr)	Ph-3 (KW)	Ph-3 (kVAr)
2	0	0	0	0	0	0
3	35	25	40	30	45	32
6	40	30	45	32	35	25
4	50	40	60	45	50	35
18	40	30	40	30	40	30
5	40	30	40	30	40	30
23	60	45	50	40	50	35
7	0	0	0	0	0	0
8	40	30	40	30	40	30
9	60	45	50	40	50	35
14	50	35	50	40	60	45
16	40	30	40	30	40	30
10	35	25	40	30	45	32
11	45	32	35	25	40	30
12	50	35	60	45	50	40
13	35	25	45	32	40	30
15	133.3	100	133.3	100	133.3	100
17	40	30	35	25	45	32
20	35	25	40	30	45	32
21	40	30	35	25	45	32
19	60	45	50	35	50	40
22	50	35	60	45	50	40
24	35	25	45	32	40	30
25	60	45	50	30	50	35

Table I.10: General Data of CASE37

General Data	
Slack	701
Vnom (kV)	4.8
International System	0
DeltaLF	1
V_slack_ph_A	1.0283
V_slack_ph_B	1.0249
V_slack_ph_C	1.0112
Ang_slack_ph_A	-29.5322
Ang_slack_ph_B	-150.52
Ang_slack_ph_C	90.1923

Table I.11: Tolology of CASE37

Node A	Node B	Length	Config.
701	702	960	2
702	705	400	4
702	713	360	3
702	703	1320	2
703	727	240	4
703	730	600	3
704	714	80	4
704	720	800	3
705	742	320	4
705	712	240	4
706	725	280	4
707	724	760	4
707	722	120	4
708	733	320	3
708	732	320	4
709	731	600	3
709	708	320	3
710	735	200	4
710	736	1280	4
711	741	400	3
711	740	200	4
713	704	520	3
714	718	520	4
720	707	920	4
720	706	600	3
727	744	280	3
730	709	200	3
733	734	560	3
734	737	640	3
734	710	520	4
737	738	400	3
738	711	400	3
744	728	200	4
744	729	280	4

Table I.12: Line Parameters of CASE37

Conf	R11	R12	R13	R22	R23	R33
1	0.2926	0.0673	0.0337	0.2646	0.0673	0.2926
2	0.4751	0.1629	0.1234	0.4488	0.1629	0.4751
3	1.2936	0.4871	0.4585	1.3022	0.4871	1.2936
4	2.0952	0.5204	0.4926	2.1068	0.5204	2.0952
5	0	0	0	0	0	0
Conf	X11	X12	X13	X22	X23	X33
1	0.1973	-0.0368	-0.0417	0.19	-0.0368	0.1973
2	0.2973	-0.0326	-0.0607	0.2678	-0.0326	0.2973
3	0.6713	0.2111	0.1521	0.6326	0.2111	0.6713
4	0.7758	0.2738	0.2123	0.7398	0.2738	0.7758
5	1	0	0	1	0	1
Conf	B11	B12	B13	B22	B23	B33
1	159.7919	0	0	159.7919	0	159.7919
2	127.8306	0	0	127.8306	0	127.8306
3	74.8405	0	0	74.8405	0	74.8405
4	60.2483	0	0	60.2483	0	60.2483
5	1	0	0	1	0	1

Table I.13: Load Data of CASE37

Node	Ph-1 (kW)	Ph-1 (kVAr)	Ph-2 (kW)	Ph-2 (kWAr)	Ph-3 (KW)	Ph-3 (kVAr)
701	140	70	140	70	350	175
712	0	0	0	0	85	40
713	0	0	0	0	85	40
714	17	8	21	10	0	0
718	85	40	0	0	0	0
720	0	0	0	0	85	40
722	0	0	140	70	21	10
724	0	0	42	21	0	0
725	0	0	42	21	0	0
727	0	0	0	0	42	21
728	42	21	42	21	42	21
729	42	21	0	0	0	0
730	0	0	0	0	85	40
731	0	0	85	40	0	0
732	0	0	0	0	42	21
733	85	40	0	0	0	0
734	0	0	0	0	42	21
735	0	0	0	0	85	40
736	0	0	42	21	0	0
737	140	70	0	0	0	0
738	126	62	0	0	0	0
740	0	0	0	0	85	40
741	0	0	0	0	42	21
742	8	4	85	40	0	0
744	42	21	0	0	0	0

Table I.14: General Data of CASE28

General Data	
Slack	1
Vnom (kV)	4.16
International System	0
DeltaLF	0
V_slack_ph_A	1
V_slack_ph_B	1
V_slack_ph_C	1
Ang_slack_ph_A	0
Ang_slack_ph_B	-120
Ang_slack_ph_C	120
PV bus	3

Table I.15: Topology of CASE28

Node A	Node B	Length (ft.)	Config.
1	2	1000	1
2	3	500	1
2	6	500	2
3	4	500	1
3	18	500	2
4	5	500	2
4	23	400	2
4	26	1000	1
6	7	500	2
6	8	1000	2
7	9	500	2
7	14	500	2
7	16	500	2
9	10	500	2
10	11	300	2
11	12	200	3
11	13	200	3
14	15	300	2
14	17	300	3
14	27	1000	1
18	20	500	2
18	21	400	3
20	19	400	3
20	28	1000	1
21	22	400	3
23	24	400	2
24	25	400	3

Table I.16: Line Parameters of CASE28

Conf	R11	R12	R13	R22	R23	R33
1	0.3686	0.0169	0.0155	0.3757	0.0188	0.3723
2	0.9775	0.0167	0.0152	0.9844	0.0186	0.981
3	1.928	0.0161	0.0161	1.9308	0.0161	1.9337
Conf	X11	X12	X13	X22	X23	X33
1	0.6852	0.1515	0.1098	0.6715	0.2072	0.6782
2	0.8717	0.1697	0.1264	0.8654	0.2275	0.8648
3	1.4194	0.1183	0.1183	1.4215	0.1183	1.4236
Conf	B11	B12	B13	B22	B23	B33
1	0	0	0	0	0	0
2	0	0	0	0	0	0
3	0	0	0	0	0	0

Table I.17: Load Data of CASE28

Node	Ph-1 (kW)	Ph-1 (kVAr)	Ph-2 (kW)	Ph-2 (kWAr)	Ph-3 (KW)	Ph-3 (kVAr)
2	0	0	0	0	0	0
3	35	25	40	30	45	32
6	40	30	45	32	35	25
4	50	40	60	45	50	35
18	40	30	40	30	40	30
5	40	30	40	30	40	30
23	60	45	50	40	50	35
7	0	0	0	0	0	0
8	40	30	40	30	40	30
9	60	45	50	40	50	35
14	50	35	50	40	60	45
16	40	30	40	30	40	30
10	35	25	40	30	45	32
11	45	32	35	25	40	30
12	50	35	60	45	50	40
13	35	25	45	32	40	30
15	133.3	100	133.3	100	133.3	100
17	40	30	35	25	45	32
20	35	25	40	30	45	32
21	40	30	35	25	45	32
19	60	45	50	35	50	40
22	50	35	60	45	50	40
24	35	25	45	32	40	30
25	60	45	50	30	50	35

Table I.18: Load and Voltage Data of CASE28

Node	Ph-1 (V)	Ph-1 (kW)	Ph-1 (kVAr)	Ph-2 (V)	Ph-2 (kW)	Ph-2 (kWAr)	Ph-3 (V)	Ph-3 (KW)	Ph-3 (kVAr)
26	0.9924	145	0	0.9926	145	0	0.9938	145	0
27	0.9838	65	0	0.984	65	0	0.9854	65	0
28	0.9902	65	0	0.9905	65	0	0.9917	65	0

Appendix II: : Data for Test Systems CASE6, CASE23, CASE38, and CASE33

Table II.1: Line Data of CASE6

Node A	Node B	R	X
1	2	0.267	0.074
1	4	0.186	0.082
2	5	0.124	0.058
2	3	0.093	0.431
3	6	0.031	0.012

Table II.2: Active Load Data of CASE6

Node	Load (kW)	a_p	b_p	c_p	α_p	β_p
1	0.161	0	0	0	1	2
2	0	0	0	0	1	0
3	0.215	0	0	0	1	2
4	0	0	0	0	1	0
5	0	0	0	0	1	0
6	0	0	0	0	1	0

Table II.3: Reactive Load Data of CASE6

Node	Load (kVar)	a_q	b_q	c_q	α_q	β_q
1	0.107	0	0	0	1	2
2	0	0	0	0	1	0
3	0.152	0	0	0	1	2
4	0	0	0	0	1	0
5	0	0	0	0	1	0
6	0	0	0	0	1	0

Table II.4: DG's Data of CASE6

Node	m_p	n_q
5	0.00748	0.217323
6	0.00748	0.217323
4	0.00748	0.217323

Table II.5: Line Data of CASE22

Node A	Node B	R	X
1	2	0.030281	0.014934
2	3	0.004521	0.002331
2	4	0.04476	0.02305
4	5	0.01595	0.008182
5	6	0.108347	0.055802
6	7	0.004942	0.002545
6	8	0.024008	0.012364
4	9	0.061413	0.031628
9	10	0.004521	0.002331
9	11	0.055785	0.028769
11	12	0.004521	0.002331
11	13	0.032579	0.016777
13	14	0.086446	0.044529
14	15	0.001818	0.000959
14	16	0.004521	0.002331
16	17	0.026545	0.013669
17	18	0.007843	0.004033
17	19	0.047438	0.024455
19	20	0.010678	0.005455
20	21	0.007198	0.003719
20	22	0.044041	0.022678

Table II.6: Active Load Data of CASE22

Node	Load (kW)	a_p	b_p	c_p	α_p	β_p
1	0	0	0	0	1	0
2	0.00336	0	0	0	1	0
3	0.00336	0	0	0	1	0
4	0.00676	0	0	0	1	0
5	0.00292	0	0	0	1	0
6	0.0021	0	0	0	1	0
7	0.00176	0	0	0	1	0
8	0.00288	0	0	0	1	0
9	0.00386	0	0	0	1	0
10	0.00288	0	0	0	1	0
11	0.00326	0	0	0	1	0
12	0.00326	0	0	0	1	0
13	0.01642	0	0	0	1	0
14	0.00694	0	0	0	1	0
15	0.00694	0	0	0	1	0
16	0.01606	0	0	0	1	0
17	0.00992	0	0	0	1	0
18	0.00992	0	0	0	1	0
19	0.00876	0	0	0	1	0
20	0.00746	0	0	0	1	0
21	0.00746	0	0	0	1	0
22	0.0062	0	0	0	1	0

Table II.7: Reactive Load Data of CASE22

Node	Load (kVar)	a_q	b_q	c_q	α_q	β_q
1	0	0	0	0	1	0
2	0.00418	0	0	0	1	0
3	0.00418	0	0	0	1	0
4	0.00746	0	0	0	1	0
5	0.0025	0	0	0	1	0
6	0.00284	0	0	0	1	0
7	0.00234	0	0	0	1	0
8	0.00372	0	0	0	1	0
9	0.00518	0	0	0	1	0
10	0.00372	0	0	0	1	0
11	0.0039	0	0	0	1	0
12	0.0039	0	0	0	1	0
13	0.01434	0	0	0	1	0
14	0.00602	0	0	0	1	0
15	0.00602	0	0	0	1	0
16	0.01402	0	0	0	1	0
17	0.00956	0	0	0	1	0
18	0.00956	0	0	0	1	0
19	0.00778	0	0	0	1	0
20	0.0072	0	0	0	1	0
21	0.0072	0	0	0	1	0
22	0.00588	0	0	0	1	0

Table II.8: DG's Data of CASE22

Node	m_p	n_q
5	0.005102	0.05
13	0.001502	0.03
15	0.004506	0.01
21	0.001502	0.02

Table II.9: Line Data of CASE38

Node A	Node B	R	X
1	2	0.000574	0.000293
2	3	0.00307	0.001564
3	4	0.002279	0.001161
4	5	0.002373	0.001209
5	6	0.0051	0.004402
6	7	0.00116	0.003853
7	8	0.00443	0.001464
8	9	0.006411	0.004668
9	10	0.006501	0.004608
10	11	0.001224	0.000405
11	12	0.002331	0.000771
12	13	0.009141	0.007192
13	14	0.003372	0.004439
14	15	0.00368	0.003275
15	16	0.004647	0.003394
16	17	0.008026	0.010716
17	18	0.004558	0.003574
2	19	0.001021	0.000974
19	20	0.009366	0.00844
20	21	0.00255	0.002979
21	22	0.004414	0.005836
3	23	0.002809	0.00192
23	24	0.005592	0.004415
24	25	0.005579	0.004366
6	26	0.001264	0.000644
26	27	0.00177	0.000901
27	28	0.006594	0.005814
28	29	0.005007	0.004362
29	30	0.00316	0.00161
30	31	0.006067	0.005996
31	32	0.001933	0.002253
32	33	0.002123	0.003301
8	34	0.012453	0.012453
9	35	0.012453	0.012453
12	36	0.012453	0.012453
18	37	0.003113	0.003113
25	38	0.003113	0.003113

Table II.10: Active Load Data of CASE38

Node	Load (kW)	a_p	b_p	c_p	α_p	β_p
1	0	0	0	0	1	0
2	0.1	0	0	0	1	0.92
3	0.09	0	0	0	1	0.18
4	0.12	0	0	0	1	1.51
5	0.06	0	0	0	1	0.92
6	0.06	0	0	0	1	0.18
7	0.2	0	0	0	1	1.51
8	0.2	0	0	0	1	1.51
9	0.06	0	0	0	1	0.18
10	0.06	0	0	0	1	1.51
11	0.045	0	0	0	1	1.51
12	0.06	0	0	0	1	0.92
13	0.06	0	0	0	1	1.51
14	0.12	0	0	0	1	0.92
15	0.06	0	0	0	1	1.51
16	0.06	0	0	0	1	0.18
17	0.06	0	0	0	1	1.51
18	0.09	0	0	0	1	0.18
19	0.09	0	0	0	1	0.92
20	0.09	0	0	0	1	1.51
21	0.09	0	0	0	1	0.18
22	0.09	0	0	0	1	0.92
23	0.09	0	0	0	1	1.51
24	0.42	0	0	0	1	1.51
25	0.42	0	0	0	1	1.51
26	0.06	0	0	0	1	1.51
27	0.06	0	0	0	1	0.18
28	0.06	0	0	0	1	1.51
29	0.12	0	0	0	1	1.51
30	0.2	0	0	0	1	1.51
31	0.15	0	0	0	1	0.92
32	0.21	0	0	0	1	0.92
33	0.06	0	0	0	1	1.51
34	0	0	0	0	1	0
35	0	0	0	0	1	0
36	0	0	0	0	1	0
37	0	0	0	0	1	0
38	0	0	0	0	1	0

Table II.11: Reactive Load Data of CASE38

Node	Load (kVar)	a_q	b_q	c_q	α_q	β_q
1	0	0	0	0	1	0
2	0.06	0	0	0	1	4.04
3	0.04	0	0	0	1	6
4	0.08	0	0	0	1	3.4
5	0.03	0	0	0	1	4.04
6	0.02	0	0	0	1	6
7	0.1	0	0	0	1	3.4
8	0.1	0	0	0	1	3.4
9	0.02	0	0	0	1	6
10	0.02	0	0	0	1	3.4
11	0.03	0	0	0	1	3.4
12	0.035	0	0	0	1	4.04
13	0.035	0	0	0	1	3.4
14	0.08	0	0	0	1	4.04
15	0.01	0	0	0	1	3.4
16	0.02	0	0	0	1	6
17	0.02	0	0	0	1	3.4
18	0.04	0	0	0	1	6
19	0.04	0	0	0	1	4.04
20	0.04	0	0	0	1	3.4
21	0.04	0	0	0	1	6
22	0.04	0	0	0	1	4.04
23	0.05	0	0	0	1	3.4
24	0.2	0	0	0	1	3.4
25	0.2	0	0	0	1	3.4
26	0.025	0	0	0	1	3.4
27	0.025	0	0	0	1	6
28	0.02	0	0	0	1	3.4
29	0.07	0	0	0	1	3.4
30	0.6	0	0	0	1	3.4
31	0.07	0	0	0	1	4.04
32	0.1	0	0	0	1	4.04
33	0.04	0	0	0	1	3.4
34	0	0	0	0	1	0
35	0	0	0	0	1	0
36	0	0	0	0	1	0
37	0	0	0	0	1	0
38	0	0	0	0	1	0

Table II.12: DG's Data of CASE38

Node	m_p	n_q
34	0.005102	0.05
35	0.001502	0.03
36	0.004506	0.05
37	0.002253	0.01
38	0.002253	0.1

Table II.13: Line Data of CASE33

Node A	Node B	R	X
1	2	0.000288	0.000147
2	3	0.001538	0.000783
3	4	0.001142	0.000581
4	5	0.001189	0.000606
5	6	0.002555	0.002206
6	7	0.000584	0.00193
7	8	0.002219	0.000733
8	9	0.003213	0.002309
9	10	0.003257	0.002309
10	11	0.000613	0.000203
11	12	0.001168	0.000386
12	13	0.00458	0.003603
13	14	0.00169	0.002224
14	15	0.001844	0.001641
15	16	0.002328	0.0017
16	17	0.004021	0.005369
17	18	0.002284	0.001791
2	19	0.000512	0.000488
19	20	0.004693	0.004228
20	21	0.001277	0.001492
21	22	0.002212	0.002924
3	23	0.001408	0.000962
23	24	0.002801	0.002212
24	25	0.002795	0.002187
6	26	0.000633	0.000323
26	27	0.000887	0.000451
27	28	0.003304	0.002913
28	29	0.002509	0.002186
29	30	0.001583	0.000806
30	31	0.00304	0.003004
31	32	0.000969	0.001129
32	33	0.001064	0.001654

Table II.14: Active Load Data of CASE33

Node	Load (kW)	a_p	b_p	c_p	α_p	β_p
1	0	0	0	0	1	0
2	0.2	0	0	0	1	0
3	0.18	0	0	0	1	0
4	0.24	0	0	0	1	0
5	0.12	0	0	0	1	0
6	0.78	0	0	0	1	0
7	0.4	0	0	0	1	0
8	0.4	0	0	0	1	0
9	0.12	0	0	0	1	0
10	0.12	0	0	0	1	0
11	0.09	0	0	0	1	0
12	0.12	0	0	0	1	0
13	0.78	0	0	0	1	0
14	0.24	0	0	0	1	0
15	0.12	0	0	0	1	0
16	0.12	0	0	0	1	0
17	0.12	0	0	0	1	0
18	0.18	0	0	0	1	0
19	0.18	0	0	0	1	0
20	0.18	0	0	0	1	0
21	0.18	0	0	0	1	0
22	0.18	0	0	0	1	0
23	0.18	0	0	0	1	0
24	0.84	0	0	0	1	0
25	0.06	0	0	0	1	0
26	0.12	0	0	0	1	0
27	0.12	0	0	0	1	0
28	0.12	0	0	0	1	0
29	0.24	0	0	0	1	0
30	0.4	0	0	0	1	0
31	0.3	0	0	0	1	0
32	0.42	0	0	0	1	0
33	0.78	0	0	0	1	0

Table II.15: Reactive Load Data of CASE33

Node	Load (kVar)	a_q	b_q	c_q	α_q	β_q
1	0	0	0	0	1	0
2	0.08	0	0	0	1	0
3	0.16	0	0	0	1	0
4	0.06	0	0	0	1	0
5	0.86	0	0	0	1	0
6	0.2	0	0	0	1	0
7	0.2	0	0	0	1	0
8	0.04	0	0	0	1	0
9	0.04	0	0	0	1	0
10	0.06	0	0	0	1	0
11	0.07	0	0	0	1	0
12	0.83	0	0	0	1	0
13	0.16	0	0	0	1	0
14	0.02	0	0	0	1	0
15	0.04	0	0	0	1	0
16	0.04	0	0	0	1	0
17	0.08	0	0	0	1	0
18	0.08	0	0	0	1	0
19	0.08	0	0	0	1	0
20	0.08	0	0	0	1	0
21	0.08	0	0	0	1	0
22	0.1	0	0	0	1	0
23	0.4	0	0	0	1	0
24	0.5	0	0	0	1	0
25	0.05	0	0	0	1	0
26	0.05	0	0	0	1	0
27	0.04	0	0	0	1	0
28	0.14	0	0	0	1	0
29	1.2	0	0	0	1	0
30	0.14	0	0	0	1	0
31	0.2	0	0	0	1	0
32	0.82	0	0	0	1	0
33	0.78	0	0	0	1	0

Table II.16: DG's Data of CASE33

Node	m_p	n_q
1	0.005	0.005
6	0.1	0.1
13	0.01	0.01
25	0.1	0.1
33	0.02	0.02

Appendix III

A. Performance of ϵDE-GN on Benchmark Problems

Table III.1: Experimental Results of ϵDE-GN on CEC-2006 Benchmark Suite.

Prob	Min	Median	Mean	Std	Worst	FR	SR
1	32686	34385	34297	681	35362	100	100
2	107160	132320	130334	9273	144980	100	100
3	54670	87320	86264	11455	103030	100	100
4	20195	24075	23881	1559	26020	100	100
5	16712	18984	18818	751	19848	100	100
6	20022	22580	22424	1151	23932	100	100
7	124390	140200	138878	5626	145270	100	100
8	550	2350	2279	582	3030	100	100
9	50593	55988	55477	2450	58959	100	100
10	121256	132416	132164	5970	142152	100	100
11	2398	4074	3845	671	4710	100	100
12	120	123	124	2	126	100	100
13	9405	29160	28606	9632	42460	100	100
14	64010	70630	70660	3671	75390	100	100
15	7714	11589	11313	1109	12419	100	100
16	18190	22570	22409	1896	26865	100	100
17	46050	67258	69648	16313	95702	100	100
18	95624	110575	110915	6279	119776	100	100
19	181220	199515	200888	9800	217365	100	100
21	46468	50736	50655	2229	53847	100	100
23	145855	198620	199828	26450	253102	100	100
24	1244	3538	3362	617	4148	100	100

Table III.2: Comparison of algorithms on CEC-2006 benchmark problems

Algorithms	mean	FR	SR	SP	overall	rank
ϵDE-GN	1	1	1	3	6	1
DE	8	5	9	5	27	8
DMS	4	1	4	6	15	3
e-DE	2	1	1	7	11	2
GDE	11	11	10	9	41	10
jDE-2	9	5	8	10	32	9
MDE	5	5	5	1	16	4
MPDE	6	10	5	4	25	7
PCX	3	5	3	8	19	6
PESO+	10	9	11	11	41	10
SaDE	7	1	7	2	17	5

B. Performance of υMAESlm on Benchmark Problems

Table III.3: Experimental results of υMA-ESbm over 25 independent run on 18 test problems with 10D of IEEE CEC 2010.

Prob	1	2	3	4	5	6	7	8	9
best	-7.47E-01	-2.28E+00	0.00E+00	-2.00E-05	-4.84E+02	-5.79E+02	0.00E+00	0.00E+00	0.00E+00
median	-7.47E-01	-2.28E+00	0.00E+00	-2.00E-05	-4.75E+02	-5.79E+02	0.00E+00	7.65E+00	0.00E+00
c_1	0.00E+00	0.00E+00	0.00E+00	0.00E+00	0.00E+00	0.00E+00	0.00E+00	0.00E+00	0.00E+00
c_2	0.00E+00	0.00E+00	0.00E+00	0.00E+00	0.00E+00	0.00E+00	0.00E+00	0.00E+00	0.00E+00
c_3	0.00E+00	0.00E+00	0.00E+00	0.00E+00	0.00E+00	0.00E+00	0.00E+00	0.00E+00	0.00E+00
$\bar{\nu}$	0.00E+00	0.00E+00	0.00E+00	0.00E+00	0.00E+00	0.00E+00	0.00E+00	0.00E+00	0.00E+00
mean	-7.46E-01	-2.26E+00	0.00E+00	-2.00E-05	-4.84E+02	-5.70E+02	0.00E+00	3.27E+00	0.00E+00
std	5.90E-03	1.91E-02	0.00E+00	9.65E-09	2.46E-02	4.14E+01	0.00E+00	4.81E+00	0.00E+00
worst	-7.29E-01	-2.21E+00	0.00E+00	-2.00E-05	-4.26E+02	-3.71E+02	0.00E+00	1.09E+01	0.00E+00
FR	1.00E+00	1.00E+00	1.00E+00	1.00E+00	1.00E+00	1.00E+00	1.00E+00	1.00E+00	1.00E+00
vio	0.00E+00	0.00E+00	0.00E+00	0.00E+00	0.00E+00	0.00E+00	0.00E+00	0.00E+00	0.00E+00

Prob	10	11	12	13	14	15	16	17	18
best	0.00E+00	-2.15E-03	-1.16E+02	-6.35E+01	0.00E+00	0.00E+00	0.00E+00	4.90E-11	0.00E+00
median	0.00E+00	-2.15E-03	-2.03E-01	-6.16E+01	0.00E+00	0.00E+00	0.00E+00	4.53E-02	6.16E-33
c_1	0.00E+00	0.00E+00	0.00E+00	0.00E+00	0.00E+00	0.00E+00	0.00E+00	0.00E+00	0.00E+00
c_2	0.00E+00	0.00E+00	0.00E+00	0.00E+00	0.00E+00	0.00E+00	0.00E+00	0.00E+00	0.00E+00
c_3	0.00E+00	0.00E+00	0.00E+00	0.00E+00	0.00E+00	0.00E+00	0.00E+00	0.00E+00	0.00E+00
$\bar{\nu}$	0.00E+00	0.00E+00	0.00E+00	0.00E+00	0.00E+00	0.00E+00	0.00E+00	0.00E+00	0.00E+00
mean	0.00E+00	-2.15E-03	-4.84E+00	-6.01E+01	0.00E+00	0.00E+00	0.00E+00	3.10E-02	7.87E-31
std	0.00E+00	0.00E+00	2.32E+01	3.26E+00	0.00E+00	0.00E+00	0.00E+00	5.21E-01	3.89E-30
worst	0.00E+00	-2.15E-03	-2.03E-01	-5.41E+01	0.00E+00	0.00E+00	0.00E+00	6.43E-01	1.94E-29
FR	1.00E+00	1.00E+00	1.00E+00	1.00E+00	1.00E+00	1.00E+00	1.00E+00	1.00E+00	1.00E+00
vio	0.00E+00	0.00E+00	0.00E+00	0.00E+00	0.00E+00	0.00E+00	0.00E+00	0.00E+00	0.00E+00

Table III.4: Experimental results of υMA-ESbm over 25 independent run on 18 test problems with 30D of IEEE CEC 2010.

Prob	1	2	3	4	5	6	7	8	9
best	-8.22E-01	-2.28E+00	2.14E-19	-6.67E-06	-4.84E+02	-5.31E+02	1.78E-18	5.03E-22	3.01E-26
median	-8.20E-01	-2.28E+00	1.52E-17	-6.67E-06	-4.84E+02	-2.47E+02	3.00E-17	9.77E-14	2.10E-07
c_1	0.00E+00	0.00E+00	0.00E+00	0.00E+00	0.00E+00	0.00E+00	0.00E+00	0.00E+00	0.00E+00
c_2	0.00E+00	0.00E+00	0.00E+00	0.00E+00	0.00E+00	0.00E+00	0.00E+00	0.00E+00	0.00E+00
c_3	0.00E+00	0.00E+00	0.00E+00	0.00E+00	0.00E+00	0.00E+00	0.00E+00	0.00E+00	0.00E+00
$\bar{\nu}$	0.00E+00	0.00E+00	0.00E+00	0.00E+00	0.00E+00	0.00E+00	0.00E+00	0.00E+00	0.00E+00
mean	-8.17E-01	-2.27E+00	2.06E-17	-6.50E-06	-4.02E+02	-5.14E+02	2.81E-17	1.36E-14	1.16E+00
std	7.87E-03	1.31E-02	3.07E-17	7.20E-07	1.23E+02	2.08E+02	1.60E-17	1.24E-13	1.04E+00
worst	-7.89E-01	-2.23E+00	1.53E-16	-3.06E-06	-2.64E+01	-2.30E+01	5.71E-17	4.74E-13	1.18E+00
FR	1.00E+00	1.00E+00	1.00E+00	1.00E+00	1.00E+00	1.00E+00	1.00E+00	1.00E+00	1.00E+00
vio	0.00E+00	0.00E+00	0.00E+00	0.00E+00	0.00E+00	0.00E+00	0.00E+00	0.00E+00	0.00E+00

Prob	10	11	12	13	14	15	16	17	18
best	4.00E-28	-5.54E-04	-2.03E-01	-6.23E+01	6.73E-26	7.03E-22	0.00E+00	2.27E-07	7.67E-31
median	4.49E-10	-5.54E-04	-2.03E-01	-6.05E+01	5.81E-22	1.73E-19	0.00E+00	8.19E-06	8.81E-25
c_1	0.00E+00	0.00E+00	0.00E+00	0.00E+00	0.00E+00	0.00E+00	0.00E+00	0.00E+00	0.00E+00
c_2	0.00E+00	0.00E+00	0.00E+00	0.00E+00	0.00E+00	0.00E+00	0.00E+00	0.00E+00	0.00E+00
c_3	0.00E+00	0.00E+00	0.00E+00	0.00E+00	0.00E+00	0.00E+00	0.00E+00	0.00E+00	0.00E+00
$\bar{\nu}$	0.00E+00	0.00E+00	0.00E+00	0.00E+00	0.00E+00	0.00E+00	0.00E+00	0.00E+00	0.00E+00
mean	1.31E+00	-5.54E-04	-2.03E-01	-5.93E+01	5.66E-18	4.72E-18	0.00E+00	3.35E-04	2.76E-24
std	2.67E+00	9.88E-09	1.36E-08	2.59E+00	6.13E-18	2.11E-17	0.00E+00	1.08E-03	1.06E-23
worst	6.55E+00	-5.54E-04	-2.03E-01	-5.33E+01	2.53E-17	1.06E-17	0.00E+00	5.35E-03	5.10E-23
FR	1.00E+00	1.00E+00	1.00E+00	1.00E+00	1.00E+00	1.00E+00	1.00E+00	1.00E+00	1.00E+00
vio	0.00E+00	0.00E+00	0.00E+00	0.00E+00	0.00E+00	0.00E+00	0.00E+00	0.00E+00	0.00E+00

Table III.5: Experimental results of υMA-ESbm, CMODE, ϵDEag, ECHT-DE, ITLBO, AIS-IRP, FROFI, Co-CLPSO, and C^{2}oDE over 25 independent runs on 18 test problems with $10D$ of IEEE CEC 2010. (Mean and SD represent the average and standard deviation of the objective function values obtained in 25 runs, respectively. t-test at 0.05 significance level is performed between υMA-ESbm and other contenders. '***' indicates that feasible solutions cannot be consistently found by the corresponding algorithms in all runs.)

Prob	υMA-ESbm		CMODE			ϵDEag			ECHT-DE			ITLBO		
	Mean	SD	Mean	SD	t	Mean	SD	t	Mean	SD	t	Mean	SD	t
c01	-7.46E-01	5.90E-03	-7.47E-01	2.35E-13	=	**-7.47E-01**	**1.32E-03**	=	**-7.47E-01**	**1.40E-03**	=	**-7.47E-01**	**1.87E-03**	=
c02	-2.26E+00	3.14E-02	***	***	+	-2.26E+00	2.39E-02	=	**-2.27E+00**	**6.70E-03**	=	-2.03E+00	8.14E-02	+
c03	**0.00E+00**	**0.00E+00**	2.84E+00	4.23E+00	+	**0.00E+00**	**0.00E+00**	=	**0.00E+00**	**0.00E+00**	=	**0.00E+00**	**0.00E+00**	=
c04	**-2.00E-05**	**9.65E-09**	-9.99E-06	2.90E-08	+	-9.92E-06	1.55E-07	+	-1.00E-05	0.00E+00	+	-1.00E-05	3.39E-15	+
c05	-4.84E+02	2.46E-02	***	***	+	**-4.84E+02**	**3.89E-13**	=	-4.11E+02	7.63E+01	+	**-4.84E+02**	**1.11E-11**	=
c06	-5.70E+02	4.14E+01	-5.78E+02	1.60E-02	=	**-5.79E+02**	**3.63E-03**	=	-5.62E+02	4.51E+01	+	-5.79E+02	2.39E-04	-
c07	**0.00E+00**	**0.00E+00**	6.69E-15	8.95E-15	+	**0.00E+00**	**0.00E+00**	=	1.33E-01	7.28E-01	+	**0.00E+00**	**0.00E+00**	=
c08	3.27E+00	4.81E+00	8.94E+00	3.98E+00	+	6.73E+00	5.56E+00	+	6.16E+00	6.45E+00	=	8.47E+00	4.09E+00	+
c09	**0.00E+00**	**0.00E+00**	***	***	+	**0.00E+00**	**0.00E+00**	-	1.47E-01	8.05E-01	+	**0.00E+00**	**0.00E+00**	=
c10	**0.00E+00**	**0.00E+00**	***	***	+	**0.00E+00**	**0.00E+00**	=	1.71E+00	7.66E+00	+	1.92E-01	9.62E-01	+
c11	**-2.15E-03**	**0.00E+00**	***	***	+	-1.52E-03	6.34E-11	+	***	***	+	-1.51E-03	1.30E-05	+
c12	-4.84E+00	2.32E+01	***	***	+	-3.37E+02	1.78E+02	-	***	***	+	-2.39E+01	1.14E+02	=
c13	-6.01E+01	3.26E+00	-5.79E+01	4.09E+00	=	**-6.84E+01**	**1.03E-06**	-	-6.51E+01	2.38E+00	-	-6.52E+01	1.78E+00	-
c14	**0.00E+00**	**0.00E+00**	8.18E-09	1.64E-08	+	**0.00E+00**	**0.00E+00**	=	7.02E+05	3.19E+06	+	**0.00E+00**	**0.00E+00**	=
c15	**0.00E+00**	**0.00E+00**	1.20E+02	3.48E+02	+	1.80E-01	8.81E-01	+	2.34E+13	5.30E+13	+	3.84E+00	4.97E+00	+
c16	**0.00E+00**	**0.00E+00**	6.82E-05	1.49E-04	+	3.70E-01	3.71E-01	+	3.93E-02	4.28E-02	+	2.27E-01	3.11E-01	+
c17	3.10E-02	5.21E-01	4.37E-02	1.12E-01	-	1.25E-01	1.94E-01	+	1.12E-01	3.32E-01	=	3.91E-01	6.71E-01	+
c18	1.73E-28	8.53E-28	5.75E+00	2.64E+02	+	9.68E-19	1.81E-18	+	**0.00E+00**	**0.00E+00**	=	**0.00E+00**	**0.00E+00**	=
+/=/-			14/3/1			7/8/3			11/5/2			8/8/2		

Table III.6: Experimental results of υMA-ESbm, CMODE, ϵDEag, ECHT-DE, ITLBO, AIS-IRP, FROFI, Co-CLPSO, and C^{2}oDE over 25 independent runs on 18 test problems with $30D$ of IEEE CEC 2010. (Mean and SD represent the average and standard deviation of the objective function values obtained in 25 runs, respectively. t-test at 0.05 significance level is performed between υMA-ESbm and other contenders. '***' indicates that feasible solutions cannot be consistently found by the corresponding algorithms in all runs.)

Prob	υMA-ESbm		CMODE			ϵDEag			ECHT-DE			ITLBO		
	Mean	SD	Mean	SD	t	Mean	SD	t	Mean	SD	t	Mean	SD	t
c01	-8.17E-01	7.87E-03	-8.20E-01	8.95E-04	=	**-8.21E-01**	**7.10E-04**	=	-8.00E-01	1.79E-02	+	-8.20E-01	9.95E-04	=
c02	**-2.27E+00**	**4.95E-02**	9.75E-01	6.25E+01	+	-2.15E+00	1.20E-02	+	-1.99E+00	2.10E-01	+	-2.03E+00	7.64E-02	+
c03	**3.44E-05**	**9.51E-04**	2.18E+01	1.25E+01	+	2.88E+01	8.05E-01	+	9.89E+01	6.26E+01	+	7.84E+01	6.31E+01	+
c04	**-5.27E-06**	**1.76E-06**	6.72E-04	4.24E-04	+	8.16E-03	3.07E-03	+	-1.03E-06	9.01E-03	+	1.69E-03	1.14E-03	+
c05	-4.02E+02	1.23E+02	***	***	+	-4.50E+02	2.90E+00	-	-1.06E+02	1.67E+02	+	**-4.82E+01**	**1.73E+00**	+
c06	-5.14E+02	2.08E+02	***	***	+	-5.28E+02	4.75E-01	=	-1.38E+02	9.89E+01	+	**-5.30E+02**	**4.80E-01**	-
c07	2.05E-17	3.63E-16	5.24E-05	5.89E-05	+	2.60E-15	1.23E-15	=	1.33E-01	7.28E-01	+	1.59E-01	7.97E-01	+
c08	1.36E-14	1.24E-13	3.68E-01	2.62E-01	+	7.83E-14	4.86E-14	=	3.36E+01	1.11E+02	+	1.14E+01	2.79E+01	+
c09	**1.16E+00**	**3.04E+00**	***	***	+	1.07E+01	2.82E+01	+	4.24E+01	1.38E+02	+	2.86E+00	1.43E+01	+
c10	**1.31E+00**	**2.67E+00**	***	***	+	3.33E+01	4.55E-01	+	5.34E+01	8.83E+01	+	3.29E+01	1.41E+01	+
c11	-5.54E-04	9.88E-09	***	***	+	-2.86E-04	2.71E-05	+	***	***	+	-3.86E-04	1.14E-05	+
c12	**-2.03E-01**	**1.36E-08**	***	***	+	***	***	+	***	***	+	-1.98E-01	2.39E-03	+
c13	-5.77E+01	4.36E+00	-3.89E+01	2.17E+00	+	-6.54E+01	5.73E-01	-	-6.46E+01	1.67E+00	-	-5.05E+01	1.18E+00	+
c14	5.66E-18	6.13E-18	9.31E+00	2.46E+00	+	3.09E+13	5.61E-13	+	1.24E+05	6.77E+05	+	4.78E-01	1.32E+00	+
c15	**4.72E-18**	**2.11E-17**	1.51E+13	8.26E+12	+	2.16E+01	1.10E-04	+	1.94E+11	4.35E+11	+	2.38E+01	2.51E+01	+
c16	**0.00E+00**	**0.00E+00**	6.30E-02	2.72E-02	+	2.17E-21	1.06E-20	=	**0.00E+00**	**0.00E+00**	=	**0.00E+00**	**0.00E+00**	=
c17	**3.35E-04**	**1.08E-03**	**3.12E+02**	**2.75E+02**	+	6.33E+00	4.99E+00	+	2.75E-01	3.78E-01	+	9.65E-01	1.73E+00	+
c18	2.76E-24	1.06E-23	7.36E+03	3.12E+03	+	8.75E+01	1.66E+02	+	**0.00E+00**	**0.00E+00**	=	9.07E-17	3.18E-16	+
+/=/-			17/1/0			11/5/2			15/2/1			15/2/1		

C. Performance of ESHADE on Standard Benchmark Problem.

Table III.7: number of trials of ESHADE in a run of 50 that found correct digits

Function	Number of correct digits											Score
	0	1	2	3	4	5	6	7	8	9	10	
1	0	0	0	0	0	0	0	0	0	0	50	10
2	0	0	0	0	0	0	0	0	0	0	50	10
3	0	0	0	0	0	0	0	0	0	0	50	10
4	0	0	0	0	0	0	0	0	0	0	50	10
5	0	0	0	0	0	0	0	0	0	0	50	10
6	0	0	0	0	0	0	0	0	0	0	50	10
7	0	0	0	0	0	0	0	0	0	0	50	10
8	0	2	48	0	0	0	0	0	0	0	0	2
9	0	0	50	13	0	0	0	0	0	0	0	2.52
10	0	0	0	0	0	0	0	0	0	0	50	10
Total												84.52

Table III.8: Score achieved by HSES, EBOwithCMAR and ESHADE for problem suite of 100-Digit Challenge.

Function	HSES	EBOwithCMAR	ESHADE
1	**10**	**10**	**10**
2	0.2	**10**	**10**
3	1.72	**10**	**10**
4	4.96	**10**	**10**
5	**10**	**10**	**10**
6	**10**	**10**	**10**
7	0.28	0.28	**10**
8	0.16	1.12	**2**
9	3	3	**2.52**
10	**10**	8.64	**10**
Total	50.32	73.04	**84.52**

Appendix IV: Power Flow results of different Systems

Chapter-4

A. CASE22

A.1. Case 1:

Table IV.1: Power Flow solution of CASE22 test system operating in conventional droop.

Bus	$\|V\|$	$\angle_V$	P	Q	$\|I\|$	$\angle_I$	Bus	$\|V\|$	$\angle_V$	P	Q	$\|I\|$	$\angle_I$
1	0.9868	0.0000	0.0000	0.0000	0.0000	0.0000	12	0.9943	0.0057	-0.0163	-0.0195	0.0256	2.2728
2	0.9868	0.0000	-0.0168	-0.0209	0.0272	2.2479	13	0.9986	0.0064	0.1720	-0.0256	0.1741	0.1543
3	0.9866	0.0001	-0.0168	-0.0209	0.0272	2.2479	14	0.9959	-0.0018	-0.0347	-0.0301	0.0461	2.4253
4	0.9893	-0.0011	-0.0338	-0.0373	0.0509	2.3059	15	0.9963	-0.0023	0.0500	0.3364	0.3414	-1.4256
5	0.9907	-0.0030	0.0602	0.1725	0.1845	-1.2381	16	0.9950	-0.0008	-0.0803	-0.0701	0.1071	2.4231
6	0.9845	0.0000	-0.0105	-0.0142	0.0179	2.2075	17	0.9927	0.0039	-0.0496	-0.0478	0.0694	2.3786
7	0.9844	0.0001	-0.0088	-0.0117	0.0149	2.2157	18	0.9921	0.0041	-0.0496	-0.0478	0.0694	2.3788
8	0.9839	0.0003	-0.0144	-0.0186	0.0239	2.2299	19	0.9957	0.0102	-0.0438	-0.0389	0.0588	2.4256
9	0.9903	0.0033	-0.0193	-0.0259	0.0326	2.2145	20	0.9971	0.0115	-0.0373	-0.0360	0.0520	2.3854
10	0.9902	0.0033	-0.0144	-0.0186	0.0238	2.2329	21	0.9987	0.0121	0.2168	0.0266	0.2187	-0.1100
11	0.9945	0.0057	-0.0163	-0.0195	0.0256	2.2727	22	0.9950	0.0121	-0.0310	-0.0294	0.0429	2.3947
w	0.9996												

A.2. Case 2:

Table IV.2: Power Flow solution of CASE22 test system operating in inverse droop.

Bus	$\|V\|$	$\angle_V$	P	Q	$\|I\|$	$\angle_I$	Bus	$\|V\|$	$\angle_V$	P	Q	$\|I\|$	$\angle_I$
1	0.9881	0.0000	0.0000	0.0000	0.0000	3.1416	12	0.9933	-0.0123	-0.0163	-0.0195	0.0256	2.2548
2	0.9881	0.0000	-0.0168	-0.0209	0.0271	2.2479	13	0.9970	-0.0166	0.0189	0.1794	0.1809	-1.4827
3	0.9880	0.0001	-0.0168	-0.0209	0.0271	2.2479	14	0.9967	-0.0132	-0.0347	-0.0301	0.0461	2.4139
4	0.9906	-0.0011	-0.0338	-0.0373	0.0508	2.3059	15	0.9972	-0.0130	0.2453	0.0536	0.2518	-0.2281
5	0.9924	-0.0005	0.1374	0.0614	0.1516	-0.4210	16	0.9957	-0.0134	-0.0803	-0.0701	0.1071	2.4105
6	0.9862	0.0025	-0.0105	-0.0142	0.0179	2.2100	17	0.9928	-0.0154	-0.0496	-0.0478	0.0694	2.3593
7	0.9861	0.0025	-0.0088	-0.0117	0.0148	2.2182	18	0.9922	-0.0152	-0.0496	-0.0478	0.0694	2.3595
8	0.9856	0.0027	-0.0144	-0.0186	0.0239	2.2324	19	0.9947	-0.0211	-0.0438	-0.0389	0.0589	2.3943
9	0.9904	-0.0062	-0.0193	-0.0259	0.0326	2.2050	20	0.9958	-0.0225	-0.0373	-0.0360	0.0521	2.3514
10	0.9903	-0.0061	-0.0144	-0.0186	0.0238	2.2235	21	0.9973	-0.0237	0.0967	0.2151	0.2365	-1.1721
11	0.9934	-0.0123	-0.0163	-0.0195	0.0256	2.2547	22	0.9938	-0.0219	-0.0310	-0.0294	0.0430	2.3608
w	1.0004												

A.3. Case 3:

Table IV.3: Power Flow solution of CASE22 test system operating in mixed droop.

Bus	$\|V\|$	$\angle_V$	P	Q	$\|I\|$	$\angle_I$	Bus	$\|V\|$	$\angle_V$	P	Q	$\|I\|$	$\angle_I$
1	0.9832	0.0000	0.0000	0.0000	0.0000	3.1416	12	0.9885	-0.0046	-0.0163	-0.0195	0.0257	2.2624
2	0.9832	0.0000	-0.0168	-0.0209	0.0273	2.2479	13	0.9921	-0.0069	0.0501	0.0582	0.0774	-0.8664
3	0.9831	0.0001	-0.0168	-0.0209	0.0273	2.2479	14	0.9945	-0.0098	-0.0347	-0.0301	0.0462	2.4173
4	0.9857	-0.0011	-0.0338	-0.0373	0.0511	2.3059	15	0.9951	-0.0100	0.2099	0.2137	0.3010	-0.8044
5	0.9875	-0.0016	0.1106	0.1120	0.1594	-0.7933	16	0.9934	-0.0095	-0.0803	-0.0701	0.1073	2.4144
6	0.9813	0.0014	-0.0105	-0.0142	0.0180	2.2089	17	0.9901	-0.0087	-0.0496	-0.0478	0.0696	2.3660
7	0.9812	0.0015	-0.0088	-0.0117	0.0149	2.2171	18	0.9895	-0.0085	-0.0496	-0.0478	0.0696	2.3662
8	0.9807	0.0017	-0.0144	-0.0186	0.0240	2.2313	19	0.9912	-0.0093	-0.0438	-0.0389	0.0591	2.4061
9	0.9856	-0.0022	-0.0193	-0.0259	0.0328	2.2090	20	0.9921	-0.0096	-0.0373	-0.0360	0.0522	2.3643
10	0.9854	-0.0021	-0.0144	-0.0186	0.0239	2.2275	21	0.9935	-0.0101	0.1257	0.1247	0.1782	-0.7913
11	0.9886	-0.0047	-0.0163	-0.0195	0.0257	2.2624	22	0.9901	-0.0090	-0.0310	-0.0294	0.0432	2.3736
w	1.0000												

A.4. Case 4:

Table IV.4: Power Flow solution of CASE22 test system operating in isochronous mode.

Bus	$\|V\|$	$\angle_V$	P	Q	$\|I\|$	$\angle_I$	Bus	$\|V\|$	$\angle_V$	P	Q	$\|I\|$	$\angle_I$
1	0.9836	0.0000	0.0000	0.0000	0.0000	0.0000	12	0.9891	-0.0062	-0.0163	-0.0195	0.0257	2.2609
2	0.9836	0.0000	-0.0168	-0.0209	0.0273	2.2479	13	0.9928	-0.0088	0.1578	-0.1243	0.2023	0.6584
3	0.9835	0.0001	-0.0168	-0.0209	0.0273	2.2479	14	0.9945	-0.0337	-0.0347	-0.0301	0.0462	2.3933
4	0.9861	-0.0011	-0.0338	-0.0373	0.0510	2.3059	15	0.9951	-0.0339	0.2200	0.2071	0.3036	-0.7890
5	0.9879	-0.0014	0.1144	0.1011	0.1545	-0.7248	16	0.9933	-0.0347	-0.0803	-0.0701	0.1073	2.3892
6	0.9816	0.0017	-0.0105	-0.0142	0.0180	2.2092	17	0.9897	-0.0409	-0.0496	-0.0478	0.0696	2.3338
7	0.9815	0.0017	-0.0088	-0.0117	0.0149	2.2174	18	0.9891	-0.0407	-0.0496	-0.0478	0.0696	2.3339
8	0.9810	0.0019	-0.0144	-0.0186	0.0240	2.2315	19	0.9905	-0.0543	-0.0438	-0.0389	0.0591	2.3611
9	0.9861	-0.0030	-0.0193	-0.0259	0.0328	2.2082	20	0.9913	-0.0574	-0.0373	-0.0360	0.0523	2.3165
10	0.9859	-0.0029	-0.0144	-0.0186	0.0239	2.2267	21	0.9927	-0.0598	0.0153	0.3305	0.3333	-1.5844
11	0.9892	-0.0062	-0.0163	-0.0195	0.0257	2.2608	22	0.9893	-0.0568	-0.0310	-0.0294	0.0432	2.3258
w	0.9999												

B. CASE38

B.1. Case 1:

Table IV.5: Power Flow solution of CASE38 test system operating in conventional mode.

Bus	$\|V\|$	$\angle_V$	P	Q	$\|I\|$	$\angle_I$	Bus	$\|V\|$	$\angle_V$	P	Q	$\|I\|$	$\angle_I$
1	0.9322	0.0000	0.0000	0.0000	0.0000	0.0000	20	0.9284	-0.0018	-0.0804	-0.0311	0.0929	2.7712
2	0.9322	0.0000	-0.0937	-0.0452	0.1116	2.6924	21	0.9278	-0.0022	-0.0888	-0.0255	0.0996	2.8597
3	0.9339	0.0002	-0.0889	-0.0265	0.0993	2.8517	22	0.9272	-0.0026	-0.0840	-0.0295	0.0960	2.8014
4	0.9353	0.0010	-0.1085	-0.0637	0.1345	2.6114	23	0.9342	-0.0005	-0.0812	-0.0397	0.0967	2.6867
5	0.9371	0.0017	-0.0565	-0.0231	0.0651	2.7557	24	0.9355	-0.0018	-0.3798	-0.1594	0.4403	2.7423
6	0.9415	0.0049	-0.0594	-0.0139	0.0648	2.9159	25	0.9398	-0.0022	-0.3824	-0.1620	0.4419	2.7388
7	0.9469	0.0109	-0.1842	-0.0831	0.2134	2.7288	26	0.9399	0.0053	-0.0546	-0.0202	0.0620	2.7920
8	0.9569	0.0094	-0.1871	-0.0861	0.2153	2.7198	27	0.9377	0.0059	-0.0593	-0.0170	0.0658	2.8684
9	0.9703	0.0151	-0.0597	-0.0167	0.0639	2.8840	28	0.9283	0.0061	-0.0536	-0.0155	0.0601	2.8658
10	0.9748	0.0171	-0.0577	-0.0183	0.0621	2.8512	29	0.9216	0.0065	-0.1061	-0.0530	0.1287	2.6845
11	0.9756	0.0172	-0.0434	-0.0276	0.0527	2.5921	30	0.9186	0.0077	-0.1759	-0.4495	0.5255	1.9515
12	0.9774	0.0174	-0.0588	-0.0319	0.0684	2.6614	31	0.9151	0.0060	-0.1382	-0.0489	0.1602	2.8076
13	0.9801	0.0207	-0.0582	-0.0327	0.0681	2.6506	32	0.9143	0.0056	-0.1934	-0.0696	0.2248	2.8016
14	0.9813	0.0228	-0.1179	-0.0741	0.1420	2.6032	33	0.9141	0.0054	-0.0524	-0.0295	0.0658	2.6346
15	0.9834	0.0245	-0.0585	-0.0094	0.0603	3.0060	34	0.9693	0.0059	0.3562	0.6131	0.7315	-1.0385
16	0.9863	0.0263	-0.0599	-0.0184	0.0635	2.8695	35	0.9897	0.0263	1.2100	0.3422	1.2705	-0.2493
17	0.9923	0.0330	-0.0593	-0.0195	0.0629	2.8572	36	0.9860	0.0190	0.4033	0.2795	0.4977	-0.5871
18	0.9958	0.0351	-0.0899	-0.0390	0.0984	2.7675	37	0.9987	0.0373	0.8067	0.1263	0.8175	-0.1181
19	0.9317	-0.0002	-0.0843	-0.0301	0.0961	2.7989	38	0.9443	-0.0013	0.8067	0.5568	1.0380	-0.6055
w	0.9982												

B.2. Case 2:

Table IV.6: Power Flow solution of CASE38 test system operating in inverse mode.

Bus	$\|V\|$	$\angle_V$	P	Q	$\|I\|$	$\angle_I$	Bus	$\|V\|$	$\angle_V$	P	Q	$\|I\|$	$\angle_I$
1	0.9183	0.0000	0.0000	0.0000	0.0000	-0.4636	20	0.9145	-0.0019	-0.0786	-0.0786	0.0918	2.7807
2	0.9183	0.0000	-0.0925	-0.0925	0.1108	2.7106	21	0.9138	-0.0023	-0.0886	-0.0886	0.1002	2.8821
3	0.9199	0.0002	-0.0887	-0.0887	0.0999	2.8749	22	0.9132	-0.0028	-0.0828	-0.0828	0.0956	2.8157
4	0.9216	0.0008	-0.1061	-0.1061	0.1326	2.6233	23	0.9198	-0.0002	-0.0793	-0.0793	0.0955	2.6985
5	0.9237	0.0013	-0.0558	-0.0558	0.0648	2.7708	24	0.9202	-0.0010	-0.3704	-0.3704	0.4346	2.7542
6	0.9289	0.0042	-0.0592	-0.0592	0.0652	2.9320	25	0.9235	-0.0009	-0.3724	-0.3724	0.4358	2.7519
7	0.9348	0.0105	-0.1806	-0.1806	0.2111	2.7374	26	0.9273	0.0046	-0.0535	-0.0535	0.0614	2.7995
8	0.9452	0.0086	-0.1837	-0.1837	0.2131	2.7278	27	0.9252	0.0051	-0.0592	-0.0592	0.0662	2.8877
9	0.9582	0.0086	-0.0595	-0.0595	0.0642	2.8959	28	0.9159	0.0052	-0.0525	-0.0525	0.0596	2.8716
10	0.9635	0.0089	-0.0567	-0.0567	0.0616	2.8493	29	0.9093	0.0055	-0.1040	-0.1040	0.1272	2.6936
11	0.9644	0.0087	-0.0426	-0.0426	0.0520	2.5935	30	0.9064	0.0066	-0.1724	-0.1724	0.5106	1.9591
12	0.9663	0.0083	-0.0581	-0.0581	0.0679	2.6671	31	0.9029	0.0048	-0.1365	-0.1365	0.1597	2.8193
13	0.9700	0.0079	-0.0573	-0.0573	0.0674	2.6462	32	0.9021	0.0044	-0.1910	-0.1910	0.2240	2.8135
14	0.9720	0.0083	-0.1169	-0.1169	0.1409	2.6020	33	0.9019	0.0043	-0.0513	-0.0513	0.0649	2.6442
15	0.9746	0.0085	-0.0577	-0.0577	0.0600	2.9926	34	0.9583	0.0176	0.8334	0.8334	0.8899	-0.1966
16	0.9779	0.0085	-0.0598	-0.0598	0.0637	2.8654	35	0.9762	0.0110	0.7944	0.7944	1.0295	-0.6483
17	0.9859	0.0113	-0.0587	-0.0587	0.0626	2.8391	36	0.9752	0.0122	0.4951	0.4951	0.5495	-0.3808
18	0.9899	0.0117	-0.0898	-0.0898	0.0984	2.7565	37	0.9933	0.0125	0.6698	0.6698	0.7908	-0.5372
19	0.9178	-0.0003	-0.0832	-0.0832	0.0957	2.8136	38	0.9273	0.0003	0.7270	0.7270	0.9002	-0.5137
w	1.0009												

B.3. Case 3:

Table IV.7: Power Flow solution of CASE38 test system operating in mixed mode.

Bus	$\|V\|$	$\angle_V$	P	Q	$\|I\|$	$\angle_I$	Bus	$\|V\|$	$\angle_V$	P	Q	$\|I\|$	$\angle_I$
1	0.9026	0.0000	0.0000	0.0000	0.0000	0.0000	20	0.8989	-0.0020	-0.0766	-0.0278	0.0907	2.7911
2	0.9026	0.0000	-0.0910	-0.0397	0.1100	2.7305	21	0.8982	-0.0024	-0.0883	-0.0210	0.1010	2.9055
3	0.9043	0.0003	-0.0884	-0.0219	0.1007	2.8992	22	0.8977	-0.0029	-0.0815	-0.0259	0.0952	2.8314
4	0.9063	0.0006	-0.1034	-0.0572	0.1304	2.6366	23	0.9037	0.0001	-0.0772	-0.0354	0.0940	2.7116
5	0.9086	0.0009	-0.0549	-0.0204	0.0645	2.7874	24	0.9032	-0.0001	-0.3601	-0.1415	0.4284	2.7672
6	0.9147	0.0034	-0.0590	-0.0117	0.0658	2.9491	25	0.9055	0.0006	-0.3615	-0.1427	0.4292	2.7663
7	0.9210	0.0098	-0.1766	-0.0756	0.2086	2.7471	26	0.9131	0.0037	-0.0523	-0.0184	0.0607	2.8078
8	0.9318	0.0076	-0.1798	-0.0786	0.2106	2.7368	27	0.9110	0.0042	-0.0590	-0.0143	0.0666	2.9082
9	0.9455	0.0103	-0.0594	-0.0143	0.0646	2.9159	28	0.9019	0.0041	-0.0513	-0.0141	0.0590	2.8781
10	0.9518	0.0107	-0.0557	-0.0169	0.0611	2.8575	29	0.8955	0.0043	-0.1016	-0.0481	0.1255	2.7037
11	0.9529	0.0104	-0.0418	-0.0255	0.0514	2.6053	30	0.8926	0.0054	-0.1685	-0.4077	0.4942	1.9680
12	0.9551	0.0099	-0.0575	-0.0291	0.0675	2.6835	31	0.8891	0.0036	-0.1346	-0.0435	0.1591	2.8324
13	0.9602	0.0105	-0.0564	-0.0305	0.0668	2.6568	32	0.8884	0.0031	-0.1883	-0.0620	0.2232	2.8267
14	0.9628	0.0115	-0.1159	-0.0686	0.1399	2.6184	33	0.8882	0.0030	-0.0502	-0.0267	0.0640	2.6550
15	0.9659	0.0121	-0.0569	-0.0089	0.0597	2.9989	34	0.9460	0.0100	0.6262	0.4541	0.8177	-0.6174
16	0.9699	0.0126	-0.0597	-0.0167	0.0639	2.8821	35	0.9619	0.0183	0.9277	0.3429	1.0282	-0.3358
17	0.9792	0.0169	-0.0581	-0.0186	0.0623	2.8485	36	0.9643	0.0125	0.4542	0.2593	0.5424	-0.5062
18	0.9839	0.0178	-0.0897	-0.0363	0.0984	2.7752	37	0.9877	0.0190	0.8079	0.4181	0.9210	-0.4585
19	0.9022	-0.0003	-0.0819	-0.0264	0.0953	2.8295	38	0.9086	0.0021	0.6518	0.2620	0.7731	-0.3800
w	0.9991												

B.4. Case 4:

Table IV.8: Power Flow solution of CASE38 test system operating in isochronous mode.

Bus	$\|V\|$	$\angle_V$	P	Q	$\|I\|$	$\angle_I$	Bus	$\|V\|$	$\angle_V$	P	Q	$\|I\|$	$\angle_I$
1	0.9244	0.0000	0.0000	0.0000	0.0000	-0.4636	20	0.9206	-0.0018	-0.0794	-0.0302	0.0923	2.7766
2	0.9244	0.0000	-0.0930	-0.0437	0.1112	2.7027	21	0.9199	-0.0023	-0.0887	-0.0242	0.0999	2.8724
3	0.9261	0.0002	-0.0888	-0.0252	0.0996	2.8649	22	0.9193	-0.0027	-0.0833	-0.0285	0.0958	2.8095
4	0.9275	0.0013	-0.1071	-0.0619	0.1334	2.6186	23	0.9263	-0.0009	-0.0802	-0.0385	0.0960	2.6926
5	0.9293	0.0025	-0.0561	-0.0223	0.0650	2.7654	24	0.9276	-0.0032	-0.3750	-0.1549	0.4374	2.7466
6	0.9336	0.0065	-0.0593	-0.0132	0.0650	2.9282	25	0.9319	-0.0045	-0.3776	-0.1574	0.4390	2.7422
7	0.9387	0.0131	-0.1818	-0.0806	0.2118	2.7371	26	0.9320	0.0069	-0.0539	-0.0197	0.0616	2.7988
8	0.9488	0.0122	-0.1848	-0.0836	0.2137	2.7287	27	0.9299	0.0075	-0.0592	-0.0162	0.0660	2.8827
9	0.9624	0.0155	-0.0596	-0.0159	0.0641	2.8964	28	0.9206	0.0076	-0.0530	-0.0151	0.0598	2.8715
10	0.9667	0.0171	-0.0570	-0.0178	0.0618	2.8557	29	0.9139	0.0080	-0.1047	-0.0515	0.1277	2.6923
11	0.9675	0.0172	-0.0428	-0.0268	0.0522	2.5992	30	0.9110	0.0091	-0.1737	-0.4370	0.5162	1.9583
12	0.9692	0.0172	-0.0583	-0.0308	0.0681	2.6721	31	0.9075	0.0074	-0.1372	-0.0473	0.1599	2.8171
13	0.9730	0.0178	-0.0576	-0.0319	0.0676	2.6535	32	0.9067	0.0070	-0.1919	-0.0673	0.2243	2.8112
14	0.9751	0.0187	-0.1172	-0.0722	0.1412	2.6081	33	0.9065	0.0068	-0.0517	-0.0286	0.0652	2.6427
15	0.9776	0.0192	-0.0580	-0.0093	0.0601	3.0024	34	0.9594	0.0166	0.5672	0.2453	0.6441	-0.3915
16	0.9810	0.0197	-0.0598	-0.0178	0.0636	2.8715	35	0.9833	0.0225	1.0936	0.5574	1.2484	-0.4489
17	0.9889	0.0236	-0.0590	-0.0193	0.0628	2.8497	36	0.9755	0.0220	0.4274	0.0629	0.4429	-0.1240
18	0.9930	0.0244	-0.0899	-0.0383	0.0984	2.7627	37	0.9964	0.0255	0.7291	0.3602	0.8162	-0.4334
19	0.9239	-0.0002	-0.0837	-0.0290	0.0959	2.8072	38	0.9365	-0.0041	0.7291	0.6353	1.0326	-0.7209
w	0.9984												

C. CASE69

C.1. Case 1:

Table IV.9: Power Flow solution of CASE69 test system operating in conventional mode.

Bus	$\|V\|$	$\angle_V$	P	Q	$\|I\|$	$\angle_I$	Bus	$\|V\|$	$\angle_V$	P	Q	$\|I\|$	$\angle_I$	Bus	$\|V\|$	$\angle_V$	P	Q	$\|I\|$	$\angle_I$
1	0.9974	0.0000	0.3745	0.2514	0.4522	-0.5913	24	0.9633	-0.0998	-0.0280	-0.0200	0.0357	2.4215	47	0.9970	-0.0001	0.0000	0.0000	0.0000	3.1416
2	0.9974	0.0000	0.0000	0.0000	0.0000	1.5708	25	0.9883	-0.1137	0.4240	0.4335	0.6136	-0.9102	48	0.9924	0.0017	-0.0790	-0.0564	0.0978	2.5233
3	0.9974	0.0000	0.0000	0.0000	0.0000	0.7854	26	0.9876	-0.1135	-0.0140	-0.0100	0.0174	2.4079	49	0.9810	0.0105	-0.3847	-0.2745	0.4817	2.5323
4	0.9972	-0.0002	0.0000	0.0000	0.0000	-2.3562	27	0.9875	-0.1134	-0.0140	-0.0100	0.0174	2.4079	50	0.9833	0.0165	0.4633	-0.0076	0.4713	0.0330
5	0.9954	-0.0016	0.0000	0.0000	0.0000	0.0000	28	0.9979	0.0004	-0.0260	-0.0186	0.0320	2.5210	51	0.9415	-0.0181	-0.0405	-0.0283	0.0525	2.5136
6	0.9718	-0.0086	-0.0026	-0.0022	0.0035	2.4307	29	1.0052	0.0062	0.8220	0.4643	0.9393	-0.5080	52	0.9414	-0.0181	-0.0036	-0.0027	0.0048	2.4800
7	0.9474	-0.0162	-0.0404	-0.0300	0.0531	2.4867	30	1.0040	0.0066	0.0000	0.0000	0.0000	-1.5708	53	0.9367	-0.0223	-0.0043	-0.0035	0.0059	2.4361
8	0.9419	-0.0182	-0.0750	-0.0540	0.0981	2.4994	31	1.0037	0.0067	0.0000	0.0000	0.0000	-0.3588	54	0.9335	-0.0259	-0.0264	-0.0190	0.0348	2.4918
9	0.9395	-0.0193	-0.0300	-0.0220	0.0396	2.4895	32	1.0027	0.0070	0.0000	0.0000	0.0000	1.5708	55	0.9298	-0.0311	-0.0240	-0.0172	0.0318	2.4887
10	0.9155	-0.0204	-0.0280	-0.0190	0.0370	2.5250	33	1.0001	0.0077	-0.0140	-0.0100	0.0172	2.5291	56	0.9268	-0.0364	0.0000	0.0000	0.0000	-1.1071
11	0.9104	-0.0208	-0.1450	-0.1040	0.1960	2.4986	34	0.9967	0.0088	-0.0195	-0.0140	0.0241	2.5277	57	0.9074	-0.0621	0.0000	0.0000	0.0000	0.4636
12	0.9022	-0.0260	-0.1450	-0.1040	0.1978	2.4933	35	0.9961	0.0090	-0.0060	-0.0040	0.0072	2.5626	58	0.8981	-0.0751	0.0000	0.0000	0.0000	2.6779
13	0.9081	-0.0398	-0.0080	-0.0055	0.0107	2.4995	36	0.9972	-0.0001	-0.0260	-0.0186	0.0321	2.5205	59	0.8946	-0.0803	-0.1000	-0.0720	0.1377	2.4373
14	0.9149	-0.0538	-0.0080	-0.0055	0.0106	2.4855	37	0.9955	-0.0013	-0.0260	-0.0186	0.0321	2.5194	60	0.8932	-0.0879	0.3745	1.1678	1.3730	-1.3484
15	0.9228	-0.0680	0.0000	0.0000	0.0000	-1.5708	38	0.9939	-0.0017	0.0000	0.0000	0.0000	-1.5708	61	0.8591	-0.0589	-1.2440	-0.8880	1.7791	2.4627
16	0.9243	-0.0706	-0.0455	-0.0300	0.0590	2.4881	39	0.9934	-0.0018	-0.0240	-0.0170	0.0296	2.5235	62	0.8646	-0.0553	-0.0320	-0.0230	0.0456	2.4631
17	0.9285	-0.0759	-0.0600	-0.0350	0.0748	2.5376	40	0.9934	-0.0018	-0.0240	-0.0170	0.0296	2.5235	63	0.8734	-0.0500	0.0000	0.0000	0.0000	-2.6779
18	0.9286	-0.0760	-0.0600	-0.0350	0.0748	2.5375	41	0.9863	-0.0038	-0.0012	-0.0010	0.0016	2.4431	64	0.9163	-0.0257	-0.2270	-0.1620	0.3043	2.4960
19	0.9355	-0.0813	0.0000	0.0000	0.0000	2.8966	42	0.9833	-0.0046	0.0000	0.0000	0.0000	0.0000	65	1.0020	0.0020	1.2130	0.2244	1.2311	-0.1809
20	0.9399	-0.0847	-0.0010	-0.0006	0.0012	2.5164	43	0.9829	-0.0047	-0.0060	-0.0043	0.0075	2.5151	66	0.9098	-0.0205	-0.0180	-0.0130	0.0244	2.4956
21	0.9471	-0.0902	-0.1140	-0.0810	0.1477	2.4337	44	0.9829	-0.0047	0.0000	0.0000	0.0000	-2.3562	67	0.9098	-0.0205	-0.0180	-0.0130	0.0244	2.4956
22	0.9476	-0.0904	-0.0053	-0.0035	0.0067	2.4675	45	0.9819	-0.0050	-0.0392	-0.0263	0.0481	2.5456	68	0.8986	-0.0248	-0.0280	-0.0200	0.0383	2.4965
23	0.9525	-0.0934	0.0000	0.0000	0.0000	0.0000	46	0.9819	-0.0050	-0.0392	-0.0263	0.0481	2.5456	69	0.8986	-0.0248	-0.0280	-0.0200	0.0383	2.4965
w	0.9981																			

C.2. Case 2:

Table IV.10: Power Flow solution of CASE69 test system operating in inverse mode.

Bus	$\|V\|$	$\angle_V$	P	Q	$\|I\|$	$\angle_I$	Bus	$\|V\|$	$\angle_V$	P	Q	$\|I\|$	$\angle_I$	Bus	$\|V\|$	$\angle_V$	P	Q	$\|I\|$	$\angle_I$
1	0.9974	0.0000	0.4210	0.2577	0.4991	-0.5492	24	0.9633	0.0123	-0.0280	-0.0200	0.0358	2.5336	47	0.9970	-0.0006	0.0000	0.0000	0.0000	1.4828
2	0.9974	0.0000	0.0000	0.0000	0.0000	1.5708	25	0.9883	0.0061	0.4700	0.2918	0.5607	-0.5495	48	0.9924	-0.0079	-0.0790	-0.0564	0.0985	2.5137
3	0.9974	0.0000	0.0000	0.0000	0.0000	1.5516	26	0.9876	0.0063	-0.0140	-0.0100	0.0175	2.5277	49	0.9810	-0.0305	-0.3847	-0.2745	0.4835	2.4913
4	0.9972	-0.0003	0.0000	0.0000	0.0000	-2.0344	27	0.9875	0.0064	-0.0140	-0.0100	0.0175	2.5277	50	0.9833	-0.0334	-0.0932	0.3090	0.3291	-1.8970
5	0.9954	-0.0006	0.0000	0.0000	0.0000	-2.7828	28	0.9979	0.0005	-0.0260	-0.0186	0.0323	2.5211	51	0.9415	0.0132	-0.0405	-0.0283	0.0529	2.5449
6	0.9718	0.0052	-0.0026	-0.0022	0.0035	2.4446	29	1.0052	0.0087	1.0837	0.5649	1.2234	-0.4719	52	0.9414	0.0132	-0.0036	-0.0027	0.0048	2.5113
7	0.9474	0.0116	-0.0404	-0.0300	0.0535	2.5144	30	1.0040	0.0090	0.0000	0.0000	0.0000	3.1416	53	0.9367	0.0154	-0.0043	-0.0035	0.0060	2.4738
8	0.9419	0.0131	-0.0750	-0.0540	0.0989	2.5307	31	1.0037	0.0091	0.0000	0.0000	0.0000	-0.1244	54	0.9335	0.0172	-0.0264	-0.0190	0.0351	2.5350
9	0.9395	0.0138	-0.0300	-0.0220	0.0399	2.5227	32	1.0027	0.0094	0.0000	0.0000	0.0000	-0.3948	55	0.9298	0.0196	-0.0240	-0.0172	0.0319	2.5394
10	0.9155	0.0222	-0.0280	-0.0190	0.0372	2.5676	33	1.0001	0.0102	-0.0140	-0.0100	0.0173	2.5316	56	0.9268	0.0220	0.0000	0.0000	0.0000	1.5708
11	0.9104	0.0240	-0.1450	-0.1040	0.1973	2.5434	34	0.9967	0.0112	-0.0195	-0.0140	0.0242	2.5302	57	0.9074	0.0361	0.0000	0.0000	0.0000	0.0000
12	0.9022	0.0273	-0.1450	-0.1040	0.1990	2.5467	35	0.9961	0.0114	-0.0060	-0.0040	0.0073	2.5650	58	0.8981	0.0432	0.0000	0.0000	0.0000	-0.2450
13	0.9081	0.0258	-0.0080	-0.0055	0.0107	2.5651	36	0.9972	-0.0001	-0.0260	-0.0186	0.0323	2.5205	59	0.8946	0.0460	-0.1000	-0.0720	0.1359	2.5636
14	0.9149	0.0241	-0.0080	-0.0055	0.0107	2.5634	37	0.9955	-0.0013	-0.0260	-0.0186	0.0324	2.5193	60	0.8932	0.0484	1.0226	0.2577	1.1617	-0.1985
15	0.9228	0.0222	0.0000	0.0000	0.0000	-1.5708	38	0.9939	-0.0017	0.0000	0.0000	0.0000	3.1416	61	0.8591	0.0415	-1.2440	-0.8880	1.7599	2.5631
16	0.9243	0.0218	-0.0455	-0.0300	0.0591	2.5805	39	0.9934	-0.0019	-0.0240	-0.0170	0.0299	2.5234	62	0.8646	0.0381	-0.0320	-0.0230	0.0452	2.5565
17	0.9285	0.0208	-0.0600	-0.0350	0.0750	2.6343	40	0.9934	-0.0019	-0.0240	-0.0170	0.0299	2.5234	63	0.8734	0.0330	0.0000	0.0000	0.0000	-0.4636
18	0.9286	0.0208	-0.0600	-0.0350	0.0750	2.6343	41	0.9863	-0.0039	-0.0012	-0.0010	0.0016	2.4430	64	0.9163	0.0092	-0.2270	-0.1620	0.3051	2.5309
19	0.9355	0.0191	0.0000	0.0000	0.0000	3.1416	42	0.9833	-0.0047	0.0000	0.0000	0.0000	0.0000	65	1.0020	-0.0252	0.6967	0.8333	1.1001	-0.8997
20	0.9399	0.0181	-0.0010	-0.0006	0.0012	2.6192	43	0.9829	-0.0048	-0.0060	-0.0043	0.0076	2.5150	66	0.9098	0.0243	-0.0180	-0.0130	0.0246	2.5404
21	0.9471	0.0164	-0.1140	-0.0810	0.1480	2.5402	44	0.9829	-0.0048	0.0000	0.0000	0.0000	-2.5536	67	0.9098	0.0243	-0.0180	-0.0130	0.0246	2.5404
22	0.9476	0.0163	-0.0053	-0.0035	0.0067	2.5742	45	0.9819	-0.0052	-0.0392	-0.0263	0.0485	2.5455	68	0.8986	0.0285	-0.0280	-0.0200	0.0385	2.5498
23	0.9525	0.0150	0.0000	0.0000	0.0000	0.2450	46	0.9819	-0.0052	-0.0392	-0.0263	0.0485	2.5455	69	0.8986	0.0285	-0.0280	-0.0200	0.0385	2.5499
w	1.0013																			

C.3. Case 3:

Table IV.11: Power Flow solution of CASE69 test system operating in mixed mode.

Bus	$\|V\|$	$\angle_V$	P	Q	$\|I\|$	$\angle_I$	Bus	$\|V\|$	$\angle_V$	P	Q	$\|I\|$	$\angle_I$	Bus	$\|V\|$	$\angle_V$	P	Q	$\|I\|$	$\angle_I$
1	0.9775	0.0000	0.3802	0.2699	0.4770	-0.6174	24	0.9450	-0.0210	-0.0280	-0.0200	0.0364	2.5003	47	0.9768	-0.0004	0.0000	0.0000	0.0000	2.4469
2	0.9775	0.0000	0.0000	0.0000	0.0000	3.1416	25	0.9706	-0.0297	0.4566	0.3317	0.5814	-0.6580	48	0.9689	-0.0036	-0.0790	-0.0564	0.1002	2.5180
3	0.9774	0.0000	0.0000	0.0000	0.0000	-1.3141	26	0.9699	-0.0295	-0.0140	-0.0100	0.0177	2.4919	49	0.9463	-0.0122	-0.3847	-0.2745	0.4994	2.5096
4	0.9771	-0.0002	0.0000	0.0000	0.0000	0.5880	27	0.9697	-0.0294	-0.0140	-0.0100	0.0177	2.4919	50	0.9456	-0.0109	0.0622	-0.0773	0.1049	0.8828
5	0.9749	-0.0010	0.0000	0.0000	0.0000	-2.5432	28	0.9782	0.0004	-0.0260	-0.0186	0.0327	2.5211	51	0.9194	0.0038	-0.0405	-0.0283	0.0537	2.5355
6	0.9507	0.0011	-0.0026	-0.0022	0.0036	2.4404	29	0.9904	0.0076	1.0796	0.8373	1.3795	-0.6521	52	0.9192	0.0039	-0.0036	-0.0027	0.0049	2.5020
7	0.9255	0.0033	-0.0404	-0.0300	0.0544	2.5061	30	0.9892	0.0080	0.0000	0.0000	0.0000	0.7854	53	0.9143	0.0041	-0.0043	-0.0035	0.0061	2.4625
8	0.9197	0.0038	-0.0750	-0.0540	0.1005	2.5213	31	0.9889	0.0080	0.0000	0.0000	0.0000	-0.3588	54	0.9110	0.0042	-0.0264	-0.0190	0.0357	2.5220
9	0.9172	0.0039	-0.0300	-0.0220	0.0406	2.5128	32	0.9878	0.0084	0.0000	0.0000	0.0000	0.1244	55	0.9071	0.0043	-0.0240	-0.0172	0.0326	2.5241
10	0.8933	0.0098	-0.0280	-0.0190	0.0379	2.5552	33	0.9852	0.0092	-0.0140	-0.0100	0.0175	2.5305	56	0.9038	0.0043	0.0000	0.0000	0.0000	-0.4636
11	0.8883	0.0111	-0.1450	-0.1040	0.2009	2.5305	34	0.9818	0.0102	-0.0195	-0.0140	0.0244	2.5291	57	0.8868	0.0070	0.0000	0.0000	0.0000	1.5708
12	0.8804	0.0119	-0.1450	-0.1040	0.2027	2.5313	35	0.9811	0.0104	-0.0060	-0.0040	0.0073	2.5640	58	0.8784	0.0084	0.0000	0.0000	0.0000	-1.5708
13	0.8872	0.0067	-0.0080	-0.0055	0.0109	2.5460	36	0.9773	-0.0001	-0.0260	-0.0186	0.0327	2.5205	59	0.8751	0.0090	-0.1000	-0.0720	0.1408	2.5265
14	0.8948	0.0013	-0.0080	-0.0055	0.0108	2.5406	37	0.9755	-0.0013	-0.0260	-0.0186	0.0328	2.5193	60	0.8744	0.0085	0.7331	0.6229	1.1002	-0.6958
15	0.9033	-0.0043	0.0000	0.0000	0.0000	0.0000	38	0.9739	-0.0018	0.0000	0.0000	0.0000	-1.5708	61	0.8355	0.0184	-1.2440	-0.8880	1.8293	2.5400
16	0.9049	-0.0053	-0.0455	-0.0300	0.0602	2.5534	39	0.9734	-0.0019	-0.0240	-0.0170	0.0302	2.5234	62	0.8404	0.0181	-0.0320	-0.0230	0.0469	2.5365
17	0.9093	-0.0077	-0.0600	-0.0350	0.0764	2.6058	40	0.9734	-0.0019	-0.0240	-0.0170	0.0302	2.5234	63	0.8481	0.0177	0.0000	0.0000	0.0000	-3.0861
18	0.9094	-0.0077	-0.0600	-0.0350	0.0764	2.6058	41	0.9661	-0.0039	-0.0012	-0.0010	0.0016	2.4429	64	0.8860	0.0157	-0.2270	-0.1620	0.3148	2.5375
19	0.9165	-0.0105	0.0000	0.0000	0.0000	-1.5708	42	0.9631	-0.0048	0.0000	0.0000	0.0000	1.5708	65	0.9643	0.0097	0.8905	0.5330	1.0763	-0.5296
20	0.9211	-0.0123	-0.0010	-0.0006	0.0013	2.5889	43	0.9627	-0.0049	-0.0060	-0.0043	0.0077	2.5149	66	0.8876	0.0113	-0.0180	-0.0130	0.0250	2.5274
21	0.9285	-0.0151	-0.1140	-0.0810	0.1506	2.5087	44	0.9626	-0.0049	0.0000	0.0000	0.0000	1.7127	67	0.8876	0.0113	-0.0180	-0.0130	0.0250	2.5274
22	0.9290	-0.0153	-0.0053	-0.0035	0.0068	2.5427	45	0.9616	-0.0053	-0.0392	-0.0263	0.0491	2.5454	68	0.8768	0.0132	-0.0280	-0.0200	0.0392	2.5346
23	0.9340	-0.0171	0.0000	0.0000	0.0000	-1.5708	46	0.9616	-0.0053	-0.0392	-0.0263	0.0491	2.5454	69	0.8767	0.0132	-0.0280	-0.0200	0.0392	2.5346
w	0.9994																			

C.4. Case 4:

Table IV.12: Power Flow solution of CASE69 test system operating in isochronous mode.

Bus	$\|V\|$	$\angle_V$	P	Q	$\|I\|$	$\angle_I$	Bus	$\|V\|$	$\angle_V$	P	Q	$\|I\|$	$\angle_I$	Bus	$\|V\|$	$\angle_V$	P	Q	$\|I\|$	$\angle_I$
1	0.9930	0.0000	0.3632	0.3396	0.5007	-0.7519	24	0.9528	0.1028	-0.0280	-0.0200	0.0361	2.6241	47	0.9925	-0.0001	0.0000	0.0000	0.0000	-1.7726
2	0.9930	0.0000	0.0000	0.0000	0.0000	3.1416	25	0.9781	0.1063	0.5250	0.1138	0.5493	-0.1072	48	0.9882	0.0012	-0.0790	-0.0564	0.0982	2.5228
3	0.9929	0.0000	0.0000	0.0000	0.0000	1.1584	26	0.9774	0.1065	-0.0140	-0.0100	0.0176	2.6279	49	0.9777	0.0083	-0.3847	-0.2745	0.4834	2.5302
4	0.9927	-0.0002	0.0000	0.0000	0.0000	1.8158	27	0.9772	0.1066	-0.0140	-0.0100	0.0176	2.6279	50	0.9803	0.0139	0.4377	0.0229	0.4471	-0.0384
5	0.9903	-0.0010	0.0000	0.0000	0.0000	-1.2315	28	0.9936	0.0003	-0.0260	-0.0186	0.0322	2.5209	51	0.9303	0.0034	-0.0405	-0.0283	0.0531	2.5351
6	0.9641	0.0009	-0.0026	-0.0022	0.0035	2.4402	29	1.0030	0.0051	0.7964	0.6855	1.0477	-0.7056	52	0.9302	0.0034	-0.0036	-0.0027	0.0048	2.5015
7	0.9369	0.0029	-0.0404	-0.0300	0.0537	2.5057	30	1.0017	0.0054	0.0000	0.0000	0.0000	2.8966	53	0.9247	0.0004	-0.0043	-0.0035	0.0060	2.4588
8	0.9307	0.0033	-0.0750	-0.0540	0.0993	2.5209	31	1.0015	0.0055	0.0000	0.0000	0.0000	-0.4636	54	0.9210	-0.0033	-0.0264	-0.0190	0.0353	2.5145
9	0.9279	0.0035	-0.0300	-0.0220	0.0401	2.5123	32	1.0005	0.0058	0.0000	0.0000	0.0000	-0.7854	55	0.9166	-0.0086	-0.0240	-0.0172	0.0322	2.5112
10	0.9033	0.0239	-0.0280	-0.0190	0.0375	2.5693	33	0.9979	0.0066	-0.0140	-0.0100	0.0172	2.5279	56	0.9129	-0.0140	0.0000	0.0000	0.0000	-1.4181
11	0.8982	0.0286	-0.1450	-0.1040	0.1987	2.5480	34	0.9945	0.0076	-0.0195	-0.0140	0.0241	2.5265	57	0.8899	-0.0400	0.0000	0.0000	0.0000	0.7854
12	0.8900	0.0427	-0.1450	-0.1040	0.2005	2.5621	35	0.9938	0.0078	-0.0060	-0.0040	0.0073	2.5614	58	0.8788	-0.0533	0.0000	0.0000	0.0000	0.0000
13	0.8962	0.0570	-0.0080	-0.0055	0.0108	2.5963	36	0.9928	-0.0001	-0.0260	-0.0186	0.0322	2.5205	59	0.8746	-0.0585	-0.1000	-0.0720	0.1409	2.4590
14	0.9034	0.0711	-0.0080	-0.0055	0.0107	2.6104	37	0.9911	-0.0013	-0.0260	-0.0186	0.0323	2.5194	60	0.8724	-0.0663	0.3632	1.3757	1.6309	-1.3790
15	0.9116	0.0848	0.0000	0.0000	0.0000	-1.5708	38	0.9894	-0.0017	0.0000	0.0000	0.0000	1.5708	61	0.8333	-0.0264	-1.2440	-0.8880	1.8342	2.4952
16	0.9132	0.0874	-0.0455	-0.0300	0.0597	2.6461	39	0.9890	-0.0018	-0.0240	-0.0170	0.0297	2.5235	62	0.8383	-0.0207	-0.0320	-0.0230	0.0470	2.4977
17	0.9176	0.0917	-0.0600	-0.0350	0.0757	2.7053	40	0.9890	-0.0018	-0.0240	-0.0170	0.0297	2.5235	63	0.8463	-0.0123	0.0000	0.0000	0.0000	-0.6435
18	0.9176	0.0918	-0.0600	-0.0350	0.0757	2.7053	41	0.9818	-0.0038	-0.0012	-0.0010	0.0016	2.4431	64	0.8861	0.0263	-0.2270	-0.1620	0.3147	2.5481
19	0.9247	0.0948	0.0000	0.0000	0.0000	0.0000	42	0.9789	-0.0046	0.0000	0.0000	0.0000	1.5708	65	0.9691	0.0722	1.2401	0.0235	1.2799	0.0533
20	0.9292	0.0968	-0.0010	-0.0006	0.0013	2.6979	43	0.9785	-0.0047	-0.0060	-0.0043	0.0075	2.5150	66	0.8976	0.0288	-0.0180	-0.0130	0.0247	2.5449
21	0.9365	0.0999	-0.1140	-0.0810	0.1493	2.6237	44	0.9784	-0.0048	0.0000	0.0000	0.0000	-0.4993	67	0.8976	0.0288	-0.0180	-0.0130	0.0247	2.5449
22	0.9370	0.0999	-0.0053	-0.0035	0.0068	2.6579	45	0.9774	-0.0051	-0.0392	-0.0263	0.0483	2.5456	68	0.8864	0.0440	-0.0280	-0.0200	0.0388	2.5653
23	0.9420	0.1008	0.0000	0.0000	0.0000	-3.0703	46	0.9774	-0.0051	-0.0392	-0.0263	0.0483	2.5456	69	0.8864	0.0440	-0.0280	-0.0200	0.0388	2.5654
w	0.9981																			

Chapter-5

A. CASE6

Table IV.13: Power Flow solution of CASE6 test system operating in islanded mode.

Bus	$\|V\|$	$\angle_V$	P	Q	$\|I\|$	$\angle_I$
1	0.9600	0.0000	-0.1487	-0.0984	0.1858	2.5570
2	0.9725	-0.0091	0.0000	0.0000	0.0000	-0.8961
3	0.9639	-0.0466	-0.1993	-0.1409	0.2532	2.4797
4	0.9872	-0.0013	0.1187	0.0587	0.1341	-0.4608
5	0.9901	-0.0078	0.1187	0.0457	0.1284	-0.3751
6	0.9693	-0.0498	0.1187	0.1411	0.1902	-0.9212
w	0.9991					

Chapter-7

A. CASE22

A.1. Without Optimization condition

Table IV.14: Power Flow solution of CASE22 test system in case of without optimization condition.

Bus	$\|V\|$	$\angle_V$	P	Q	Bus	$\|V\|$	$\angle_V$	P	Q
1	0.9868	0.0000	0.0000	0.0000	12	0.9943	0.0057	-0.0163	-0.0195
2	0.9868	0.0000	-0.0168	-0.0209	13	0.9986	0.0064	0.1720	-0.0256
3	0.9866	0.0001	-0.0168	-0.0209	14	0.9959	-0.0018	-0.0347	-0.0301
4	0.9893	-0.0011	-0.0338	-0.0373	15	0.9963	-0.0023	0.0500	0.3364
5	0.9907	-0.0030	0.0602	0.1725	16	0.9950	-0.0008	-0.0803	-0.0701
6	0.9845	0.0000	-0.0105	-0.0142	17	0.9927	0.0039	-0.0496	-0.0478
7	0.9844	0.0001	-0.0088	-0.0117	18	0.9921	0.0041	-0.0496	-0.0478
8	0.9839	0.0003	-0.0144	-0.0186	19	0.9957	0.0102	-0.0438	-0.0389
9	0.9903	0.0033	-0.0193	-0.0259	20	0.9971	0.0115	-0.0373	-0.0360
10	0.9902	0.0033	-0.0144	-0.0186	21	0.9987	0.0121	0.2168	0.0266
11	0.9945	0.0057	-0.0163	-0.0195	22	0.9950	0.0121	-0.0310	-0.0294

A.2. Min of $\mathbf{P}_{loss}$

Table IV.15: Power Flow solution of CASE22 test system in case of minimization of $\mathbf{P}_{loss}$.

Bus	$\|V\|$	$\angle_V$	P	Q	Bus	$\|V\|$	$\angle_V$	P	Q
1	0.9936	0.0000	0.0000	0.0000	12	0.9955	-0.0010	-0.0163	-0.0195
2	0.9936	0.0000	-0.0168	-0.0209	13	0.9982	-0.0022	0.0537	0.0629
3	0.9935	0.0001	-0.0168	-0.0209	14	0.9975	-0.0023	-0.0347	-0.0301
4	0.9961	-0.0011	-0.0338	-0.0373	15	0.9980	-0.0024	0.1815	0.1684
5	0.9984	-0.0020	0.1212	0.1473	16	0.9965	-0.0020	-0.0803	-0.0701
6	0.9922	0.0009	-0.0105	-0.0142	17	0.9936	-0.0011	-0.0496	-0.0478
7	0.9921	0.0010	-0.0088	-0.0117	18	0.9930	-0.0010	-0.0496	-0.0478
8	0.9916	0.0012	-0.0144	-0.0186	19	0.9955	-0.0017	-0.0438	-0.0389
9	0.9942	-0.0003	-0.0193	-0.0259	20	0.9966	-0.0020	-0.0373	-0.0360
10	0.9941	-0.0002	-0.0144	-0.0186	21	0.9981	-0.0024	0.1396	0.1298
11	0.9956	-0.0011	-0.0163	-0.0195	22	0.9946	-0.0014	-0.0310	-0.0294

A.3. Min of $\mathbf{Q}_{loss}$

Table IV.16: Power Flow solution of CASE22 test system in case of minimization of $\mathbf{Q}_{loss}$.

Bus	$\|V\|$	$\angle_V$	P	Q	Bus	$\|V\|$	$\angle_V$	P	Q
1	0.9937	0.0000	0.0000	0.0000	12	0.9956	-0.0009	-0.0163	-0.0195
2	0.9937	0.0000	-0.0168	-0.0209	13	0.9982	-0.0021	0.0532	0.0637
3	0.9936	0.0001	-0.0168	-0.0209	14	0.9975	-0.0020	-0.0347	-0.0301
4	0.9962	-0.0011	-0.0338	-0.0373	15	0.9980	-0.0021	0.1825	0.1662
5	0.9984	-0.0021	0.1207	0.1482	16	0.9965	-0.0017	-0.0803	-0.0701
6	0.9922	0.0009	-0.0105	-0.0142	17	0.9936	-0.0008	-0.0496	-0.0478
7	0.9922	0.0010	-0.0088	-0.0117	18	0.9931	-0.0006	-0.0496	-0.0478
8	0.9917	0.0012	-0.0144	-0.0186	19	0.9955	-0.0014	-0.0438	-0.0389
9	0.9943	-0.0002	-0.0193	-0.0259	20	0.9967	-0.0017	-0.0373	-0.0360
10	0.9941	-0.0002	-0.0144	-0.0186	21	0.9981	-0.0021	0.1394	0.1303
11	0.9957	-0.0009	-0.0163	-0.0195	22	0.9946	-0.0011	-0.0310	-0.0294

A.3. Min of $(0.5 * \mathbf{P}_{loss} + 0.5 * \mathbf{Q}_{loss})$

Table IV.17: Power Flow solution of CASE22 test system in case of minimization of $(0.5 * \mathbf{P}_{loss} + 0.5 * \mathbf{Q}_{loss})$.

Bus	$\|V\|$	$\angle_V$	P	Q	Bus	$\|V\|$	$\angle_V$	P	Q
1	0.9936	0.0000	0.0000	0.0000	12	0.9955	-0.0005	-0.0163	-0.0195
2	0.9936	0.0000	-0.0168	-0.0209	13	0.9982	-0.0016	0.0518	0.0649
3	0.9935	0.0001	-0.0168	-0.0209	14	0.9976	-0.0010	-0.0347	-0.0301
4	0.9961	-0.0011	-0.0338	-0.0373	15	0.9981	-0.0011	0.1849	0.1638
5	0.9983	-0.0021	0.1193	0.1507	16	0.9965	-0.0007	-0.0803	-0.0701
6	0.9921	0.0009	-0.0105	-0.0142	17	0.9936	0.0002	-0.0496	-0.0478
7	0.9921	0.0009	-0.0088	-0.0117	18	0.9931	0.0004	-0.0496	-0.0478
8	0.9915	0.0011	-0.0144	-0.0186	19	0.9955	-0.0003	-0.0438	-0.0389
9	0.9942	0.0000	-0.0193	-0.0259	20	0.9966	-0.0006	-0.0373	-0.0360
10	0.9941	0.0000	-0.0144	-0.0186	21	0.9981	-0.0010	0.1398	0.1289
11	0.9956	-0.0005	-0.0163	-0.0195	22	0.9946	0.0000	-0.0310	-0.0294

B. CASE38

B.1. Without Optimization condition

Table IV.18: Power Flow solution of CASE38 test system in without optimization condition.

Bus	$\|V\|$	$\angle_V$	P	Q	Bus	$\|V\|$	$\angle_V$	P	Q
1	0.9322	0.0000	0.0000	0.0000	20	0.9284	-0.0018	-0.0804	-0.0311
2	0.9322	0.0000	-0.0937	-0.0452	21	0.9278	-0.0022	-0.0888	-0.0255
3	0.9339	0.0002	-0.0889	-0.0265	22	0.9272	-0.0026	-0.0840	-0.0295
4	0.9353	0.0010	-0.1085	-0.0637	23	0.9342	-0.0005	-0.0812	-0.0397
5	0.9371	0.0017	-0.0565	-0.0231	24	0.9355	-0.0018	-0.3798	-0.1594
6	0.9415	0.0049	-0.0594	-0.0139	25	0.9398	-0.0022	-0.3824	-0.1620
7	0.9469	0.0109	-0.1842	-0.0831	26	0.9399	0.0053	-0.0546	-0.0202
8	0.9569	0.0094	-0.1871	-0.0861	27	0.9377	0.0059	-0.0593	-0.0170
9	0.9703	0.0151	-0.0597	-0.0167	28	0.9283	0.0061	-0.0536	-0.0155
10	0.9748	0.0171	-0.0577	-0.0183	29	0.9216	0.0065	-0.1061	-0.0530
11	0.9756	0.0172	-0.0434	-0.0276	30	0.9186	0.0077	-0.1759	-0.4495
12	0.9774	0.0174	-0.0588	-0.0319	31	0.9151	0.0060	-0.1382	-0.0489
13	0.9801	0.0207	-0.0582	-0.0327	32	0.9143	0.0056	-0.1934	-0.0696
14	0.9813	0.0228	-0.1179	-0.0741	33	0.9141	0.0054	-0.0524	-0.0295
15	0.9834	0.0245	-0.0585	-0.0094	34	0.9693	0.0059	0.3562	0.6131
16	0.9863	0.0263	-0.0599	-0.0184	35	0.9897	0.0263	1.2100	0.3422
17	0.9923	0.0330	-0.0593	-0.0195	36	0.9860	0.0190	0.4033	0.2795
18	0.9958	0.0351	-0.0899	-0.0390	37	0.9987	0.0373	0.8067	0.1263
19	0.9317	-0.0002	-0.0843	-0.0301	38	0.9443	-0.0013	0.8067	0.5568

B.2. Min of $\mathbf{P}_{loss}$

Table IV.19: Power Flow solution of CASE38 test system in case of minimization of $\mathbf{P}_{loss}$.

Bus	$\|V\|$	$\angle_V$	P	Q	Bus	$\|V\|$	$\angle_V$	P	Q
1	0.9434	0.0000	0.0000	0.0000	20	0.9396	-0.0016	-0.0819	-0.0324
2	0.9434	0.0000	-0.0948	-0.0474	21	0.9389	-0.0021	-0.0890	-0.0274
3	0.9451	0.0002	-0.0891	-0.0285	22	0.9383	-0.0024	-0.0849	-0.0309
4	0.9448	0.0004	-0.1101	-0.0659	23	0.9475	0.0004	-0.0830	-0.0416
5	0.9448	0.0006	-0.0569	-0.0239	24	0.9532	0.0014	-0.3907	-0.1699
6	0.9452	0.0013	-0.0594	-0.0143	25	0.9619	0.0031	-0.3961	-0.1753
7	0.9492	0.0046	-0.1849	-0.0838	26	0.9435	0.0017	-0.0550	-0.0205
8	0.9560	0.0026	-0.1869	-0.0858	27	0.9414	0.0023	-0.0594	-0.0174
9	0.9625	0.0024	-0.0596	-0.0159	28	0.9320	0.0027	-0.0539	-0.0157
10	0.9649	0.0018	-0.0568	-0.0177	29	0.9253	0.0032	-0.1067	-0.0538
11	0.9653	0.0016	-0.0427	-0.0266	30	0.9224	0.0045	-0.1770	-0.4558
12	0.9662	0.0011	-0.0581	-0.0305	31	0.9188	0.0029	-0.1388	-0.0497
13	0.9662	0.0004	-0.0570	-0.0311	32	0.9181	0.0024	-0.1941	-0.0708
14	0.9666	0.0002	-0.1163	-0.0697	33	0.9179	0.0023	-0.0527	-0.0299
15	0.9676	0.0001	-0.0571	-0.0089	34	0.9713	0.0073	0.7831	0.4193
16	0.9691	0.0000	-0.0597	-0.0166	35	0.9724	0.0053	0.5042	0.2758
17	0.9730	0.0014	-0.0576	-0.0182	36	0.9744	0.0028	0.3889	0.2564
18	0.9752	0.0016	-0.0896	-0.0344	37	0.9772	0.0021	0.4033	0.2280
19	0.9429	-0.0002	-0.0853	-0.0315	38	0.9690	0.0055	1.4894	0.7325

B.3. Min of $\mathbf{Q}_{loss}$

Table IV.20: Power Flow solution of CASE38 test system in case of minimization of $\mathbf{Q}_{loss}$.

Bus	$\|V\|$	$\angle_V$	P	Q	Bus	$\|V\|$	$\angle_V$	P	Q
1	0.9428	0.0000	0.0000	0.0000	20	0.9390	-0.0016	-0.0818	-0.0323
2	0.9428	0.0000	-0.0947	-0.0473	21	0.9384	-0.0020	-0.0890	-0.0273
3	0.9445	0.0001	-0.0891	-0.0284	22	0.9378	-0.0024	-0.0848	-0.0309
4	0.9441	0.0004	-0.1100	-0.0658	23	0.9470	0.0003	-0.0829	-0.0416
5	0.9441	0.0007	-0.0569	-0.0238	24	0.9530	0.0011	-0.3905	-0.1698
6	0.9442	0.0015	-0.0594	-0.0142	25	0.9619	0.0026	-0.3961	-0.1752
7	0.9480	0.0047	-0.1845	-0.0834	26	0.9426	0.0019	-0.0549	-0.0204
8	0.9547	0.0028	-0.1865	-0.0854	27	0.9404	0.0025	-0.0593	-0.0173
9	0.9614	0.0027	-0.0596	-0.0158	28	0.9312	0.0030	-0.0539	-0.0157
10	0.9643	0.0026	-0.0568	-0.0177	29	0.9246	0.0036	-0.1066	-0.0536
11	0.9648	0.0024	-0.0426	-0.0266	30	0.9216	0.0048	-0.1768	-0.4546
12	0.9660	0.0021	-0.0581	-0.0304	31	0.9181	0.0033	-0.1387	-0.0496
13	0.9663	0.0018	-0.0570	-0.0311	32	0.9174	0.0029	-0.1940	-0.0706
14	0.9668	0.0018	-0.1163	-0.0698	33	0.9171	0.0028	-0.0527	-0.0298
15	0.9679	0.0018	-0.0571	-0.0090	34	0.9686	0.0070	0.7203	0.3785
16	0.9695	0.0019	-0.0597	-0.0166	35	0.9707	0.0045	0.4478	0.2926
17	0.9737	0.0037	-0.0576	-0.0183	36	0.9747	0.0044	0.4451	0.2526
18	0.9760	0.0041	-0.0896	-0.0346	37	0.9781	0.0048	0.4451	0.2191
19	0.9423	-0.0002	-0.0852	-0.0315	38	0.9691	0.0048	1.5089	0.7639

B.4. Min of $(0.5 * \mathbf{P}_{loss} + 0.5 * \mathbf{Q}_{loss})$

Table IV.21: Power Flow solution of CASE38 test system in case of minimization of $(0.5 * \mathbf{P}_{loss} + 0.5 * \mathbf{Q}_{loss})$.

Bus	$\|V\|$	$\angle_V$	P	Q	Bus	$\|V\|$	$\angle_V$	P	Q
1	0.9428	0.0000	0.0000	0.0000	20	0.9390	-0.0016	-0.0818	-0.0323
2	0.9428	0.0000	-0.0947	-0.0473	21	0.9383	-0.0020	-0.0890	-0.0273
3	0.9445	0.0001	-0.0891	-0.0284	22	0.9377	-0.0024	-0.0848	-0.0309
4	0.9441	0.0004	-0.1100	-0.0658	23	0.9469	0.0003	-0.0829	-0.0415
5	0.9441	0.0006	-0.0569	-0.0238	24	0.9527	0.0012	-0.3904	-0.1696
6	0.9444	0.0013	-0.0594	-0.0142	25	0.9615	0.0028	-0.3958	-0.1750
7	0.9483	0.0046	-0.1846	-0.0835	26	0.9428	0.0018	-0.0549	-0.0205
8	0.9550	0.0026	-0.1866	-0.0855	27	0.9406	0.0024	-0.0593	-0.0173
9	0.9617	0.0024	-0.0596	-0.0158	28	0.9313	0.0029	-0.0539	-0.0157
10	0.9644	0.0020	-0.0568	-0.0177	29	0.9247	0.0035	-0.1066	-0.0536
11	0.9648	0.0018	-0.0426	-0.0266	30	0.9218	0.0047	-0.1769	-0.4548
12	0.9659	0.0014	-0.0581	-0.0304	31	0.9183	0.0031	-0.1387	-0.0496
13	0.9660	0.0008	-0.0569	-0.0311	32	0.9175	0.0027	-0.1940	-0.0706
14	0.9665	0.0007	-0.1163	-0.0697	33	0.9173	0.0026	-0.0527	-0.0298
15	0.9675	0.0007	-0.0571	-0.0089	34	0.9694	0.0068	0.7402	0.3948
16	0.9691	0.0007	-0.0597	-0.0166	35	0.9714	0.0048	0.4852	0.2856
17	0.9731	0.0022	-0.0576	-0.0182	36	0.9744	0.0034	0.4212	0.2562
18	0.9753	0.0024	-0.0896	-0.0344	37	0.9774	0.0030	0.4212	0.2262
19	0.9423	-0.0002	-0.0852	-0.0315	38	0.9686	0.0051	1.4989	0.7438

References

[1] M. Hellwig and H. Beyer, "A matrix adaptation evolution strategy for constrained real-parameter optimization," in *2018 IEEE Congress on Evolutionary Computation (CEC)*, July 2018, pp. 1–8.

[2] F. Mumtaz, M. Syed, M. Al Hosani, and H. Zeineldin, "A novel approach to solve power flow for islanded microgrids using modified newton raphson with droop control of dg," *IEEE Transactions on Sustainable Energy*, vol. 7, no. 2, pp. 493–503, 2015.

[3] M.-S. Chen and W. E. Dillon, "Power system modeling," *Proceedings of the IEEE*, vol. 62, no. 7, pp. 901–915, 1974.

[4] J. Arrillaga and C. Arnold, "Computer analysis of power systems," 1990.

[5] M. Irving and A. Al-Othman, "Admittance matrix models of three-phase transformers with various neutral grounding configurations," *IEEE Transactions on Power Systems*, vol. 18, no. 3, pp. 1210–1212, 2003.

[6] W. H. Kersting, W. H. Phillips, and W. Carr, "A new approach to modeling three-phase transformer connections," *IEEE Transactions on Industry Applications*, vol. 35, no. 1, pp. 169–175, 1999.

[7] H. Ying-Yi and W. Fu-Ming, "Investigation of impacts of different three-phase transformer connections and load models on unbalance in power systems by optimization," *IEEE Transactions on Power Systems*, vol. 12, no. 2, pp. 689–697, 1997.

[8] U. Ghatak and V. Mukherjee, "An improved load flow technique based on load current injection for modern distribution system," *International Journal of Electrical Power & Energy Systems*, vol. 84, pp. 168–181, 2017.

[9] A. B. Eltantawy and M. M. Salama, "A novel zooming algorithm for distribution load flow analysis for smart grid," *IEEE Transactions on Smart Grid*, vol. 5, no. 4, pp. 1704–1711, 2014.

[10] S. Tripathy, G. D. Prasad, O. Malik, and G. Hope, "Load-flow solutions for ill-conditioned power systems by a newton-like method," *IEEE Transactions on Power Apparatus and Systems*, no. 10, pp. 3648–3657, 1982.

[11] D. Rajicic and A. Bose, "A modification to the fast decoupled power flow for networks with high r/x ratios," *IEEE Transactions on Power Systems*, vol. 3, no. 2, pp. 743–746, 1988.

[12] R. Berg, E. Hawkins, and W. Pleines, "Mechanized calculation of unbalanced load flow on radial distribution circuits," *IEEE Transactions on Power Apparatus and Systems*, no. 4, pp. 415–421, 1967.

[13] D. Shirmohammadi, H. W. Hong, A. Semlyen, and G. Luo, "A compensation-based power flow method for weakly meshed distribution and transmission networks," *IEEE Transactions on Power Systems*, vol. 3, no. 2, pp. 753–762, 1988.

[14] G.-X. Luo and A. Semlyen, "Efficient load flow for large weakly meshed networks," *IEEE Transactions on Power Systems*, vol. 5, no. 4, pp. 1309–1316, 1990.

[15] Y. Zhu and K. Tomsovic, "Adaptive power flow method for distribution systems with dispersed generation," *IEEE Transactions on Power Delivery*, vol. 17, no. 3, pp. 822–827, 2002.

[16] C. S. Cheng and D. Shirmohammadi, "A three-phase power flow method for real-time distribution system analysis," *IEEE Transactions on Power Systems*, vol. 10, no. 2, pp. 671–679, 1995.

[17] R. M. Ciric, A. P. Feltrin, and L. F. Ochoa, "Power flow in four-wire distribution networks-general approach," *IEEE Transactions on Power Systems*, vol. 18, no. 4, pp. 1283–1290, 2003.

[18] M. Haque, "Load flow solution of distribution systems with voltage dependent load models," *Electric Power Systems Research*, vol. 36, no. 3, pp. 151–156, 1996.

[19] U. Eminoglu and M. H. Hocaoglu, "Distribution systems forward/backward sweep-based power flow algorithms: a review and comparison study," *Electric Power Components and Systems*, vol. 37, no. 1, pp. 91–110, 2008.

[20] M. Baran and F. F. Wu, "Optimal sizing of capacitors placed on a radial distribution system," *IEEE Transactions on Power Delivery*, vol. 4, no. 1, pp. 735–743, 1989.

[21] H.-D. Chiang, "A decoupled load flow method for distribution power networks: algorithms, analysis and convergence study," *International Journal of Electrical Power & Energy Systems*, vol. 13, no. 3, pp. 130–138, 1991.

[22] V. M. da Costa, N. Martins, and J. L. R. Pereira, "Developments in the newton raphson power flow formulation based on current injections," *IEEE Transactions on Power Systems*, vol. 14, no. 4, pp. 1320–1326, 1999.

[23] M. L. de Oliveira, M. R. Guedes *et al.*, "Developments in the analysis of unbalanced three-phase power flow solutions," *International Journal of Electrical Power & Energy Systems*, vol. 29, no. 2, pp. 175–182, 2007.

[24] P. A. Garcia, J. L. R. Pereira, S. Carneiro, V. M. da Costa, and N. Martins, "Three-phase power flow calculations using the current injection method," *IEEE Transactions on Power Systems*, vol. 15, no. 2, pp. 508–514, 2000.

[25] L. R. de Araujo, D. R. R. Penido, S. C. Júnior, J. L. R. Pereira, and P. A. N. Garcia, "Comparisons between the three-phase current injection method and the forward/backward sweep method," *International Journal of Electrical Power & Energy Systems*, vol. 32, no. 7, pp. 825–833, 2010.

[26] J. Vieira, W. Freitas, and A. Morelato, "Phase-decoupled method for three-phase power-flow analysis of unbalanced distribution systems," *IEE Proceedings-Generation, Transmission and Distribution*, vol. 151, no. 5, pp. 568–574, 2004.

[27] T. Chen, M. Chen, K. Hwang, P. Kotas, and E. Chebli, "Distribution system power flow analysis," in *Submitted to IEEE Winter Power Meeting*, 1990.

[28] J.-H. Teng, "A modified gauss–seidel algorithm of three-phase power flow analysis in distribution networks," *International Journal of Electrical Power & Energy Systems*, vol. 24, no. 2, pp. 97–102, 2002.

[29] T.-H. Chen and N.-C. Yang, "Loop frame of reference based three-phase power flow for unbalanced radial distribution systems," *Electric Power Systems Research*, vol. 80, no. 7, pp. 799–806, 2010.

[30] R. Allan and A. L. Da Silva, "Probabilistic load flow using multilinearisations," in *IEE Proceedings C (Generation, Transmission and Distribution)*, vol. 128, no. 5. IET, 1981, pp. 280–287.

[31] M. Brucoli, F. Torelli, and R. Napoli, "Quadratic probabilistic load flow with linearly modelled dispatch," *International Journal of Electrical Power & Energy Systems*, vol. 7, no. 3, pp. 138–146, 1985.

[32] P. Zhang and S. T. Lee, "Probabilistic load flow computation using the method of combined cumulants and gram-charlier expansion," *IEEE Transactions on Power Systems*, vol. 19, no. 1, pp. 676–682, 2004.

[33] C.-L. Su, "Probabilistic load-flow computation using point estimate method," *IEEE Transactions on Power Systems*, vol. 20, no. 4, pp. 1843–1851, 2005.

[34] W. El-Khattam, Y. Hegazy, and M. Salama, "Investigating distributed generation systems performance using monte carlo simulation," *IEEE Transactions on Power Systems*, vol. 21, no. 2, pp. 524–532, 2006.

[35] P. Chen, Z. Chen, and B. Bak-Jensen, "Probabilistic load flow: A review," in *2008 Third International Conference on Electric Utility Deregulation and Restructuring and Power Technologies*. IEEE, 2008, pp. 1586–1591.

[36] M. T. Schilling, A. L. Da Silva, R. Billinton, and M. El-Kady, "Bibliography on power system probabilistic analysis (1962-88)," *IEEE Transactions on Power Systems*, vol. 5, no. 1, pp. 1–11, 1990.

[37] J. A. Martinez and J. Mahseredjian, "Load flow calculations in distribution systems with distributed resources. a review," in *2011 IEEE Power and Energy Society General Meeting*. IEEE, 2011, pp. 1–8.

[38] J. M. Morales and J. Perez-Ruiz, "Point estimate schemes to solve the probabilistic power flow," *IEEE Transactions on Power Systems*, vol. 22, no. 4, pp. 1594–1601, 2007.

[39] J. M. Morales, L. Baringo, A. J. Conejo, and R. Mínguez, "Probabilistic power flow with correlated wind sources," *IET Generation, Transmission & Distribution*, vol. 4, no. 5, pp. 641–651, 2010.

[40] J. Usaola, "Probabilistic load flow in systems with wind generation," *IET Generation, Transmission & Distribution*, vol. 3, no. 12, pp. 1031–1041, 2009.

[41] H. Hale and J. Ward, "Digital computer solution of power flow problems," *AIEE Transactions, pt. III (Power Apparatus and Systems)*, vol. 75, pp. 398–402, 1956.

[42] D. Tazumi, M. Kazuo, N. Tatsuki, F. Hisao, and K. Tokuya, "Digital computer solution of power-flow problems," *Information Processing in Japan*, vol. 2, pp. 28–31, 1962.

[43] M. Abdel-Akher, K. M. Nor, and A. A. Rashid, "Improved three-phase power-flow methods using sequence components," *IEEE Transactions on Power Systems*, vol. 20, no. 3, pp. 1389–1397, 2005.

[44] H. Brown, G. Carter, H. Happ, and C. Person, "Power flow solution by impedance matrix iterative method," *IEEE Transactions on Power Apparatus and Systems*, vol. 82, no. 65, pp. 1–10, 1963.

[45] C. W. T. N. J. Balu and D. Maratukulam, *Power system voltage stability*. McGraw-Hill, 1994.

[46] B. Stott, "Decoupled newton load flow," *IEEE Transactions on Power Apparatus and Systems*, no. 5, pp. 1955–1959, 1972.

[47] B. Stott, "Review of load-flow calculation methods," *Proceedings of the IEEE*, vol. 62, no. 7, pp. 916–929, 1974.

[48] B. Stott and O. Alsac, "Fast decoupled load flow," *IEEE Transactions on Power Apparatus and Systems*, no. 3, pp. 859–869, 1974.

[49] S. Goswami and S. Basu, "Direct solution of distribution systems," in *IEE Proceedings C (Generation, Transmission and Distribution)*, vol. 138, no. 1. IET, 1991, pp. 78–88.

[50] M. Haque, "A general load flow method for distribution systems," *Electric Power Systems Research*, vol. 54, no. 1, pp. 47–54, 2000.

[51] D. L. Mendive, "An application of ladder network theory to the solution of three-phase radial load-flow problems," Ph.D. dissertation, New Mexico State University, 1975.

[52] W. F. Tinney and C. E. Hart, "Power flow solution by newton's method," *IEEE Transactions on Power Apparatus and Systems*, no. 11, pp. 1449–1460, 1967.

[53] D. Thukaram, H. W. Banda, and J. Jerome, "A robust three phase power flow algorithm for radial distribution systems," *Electric Power Systems Research*, vol. 50, no. 3, pp. 227–236, 1999.

[54] R. Cespedes, "New method for the analysis of distribution networks," *IEEE Transactions on Power Delivery*, vol. 5, no. 1, pp. 391–396, 1990.

[55] D. Das, D. Kothari, and A. Kalam, "Simple and efficient method for load flow solution of radial distribution networks," *International Journal of Electrical Power & Energy Systems*, vol. 17, no. 5, pp. 335–346, 1995.

[56] M. M. A. Abdelaziz, H. E. Farag, E. F. El-Saadany, and Y. A.-R. I. Mohamed, "A novel and generalized three-phase power flow algorithm for islanded microgrids using a newton trust region method," *IEEE Transactions on Power Systems*, vol. 28, no. 1, pp. 190–201, 2012.

[57] C. A. Ferreira *et al.*, "A second order power flow based on current injection equations," *International Journal of Electrical Power & Energy Systems*, vol. 27, no. 4, pp. 254–263, 2005.

[58] S. Mallick, D. Rajan, S. Thakur, P. Acharjee, and S. Ghoshal, "Development of a new algorithm for power flow analysis," *International Journal of Electrical Power & Energy Systems*, vol. 33, no. 8, pp. 1479–1488, 2011.

[59] S. Y. Derakhshandeh and R. Pourbagher, "Application of high-order newton-like methods to solve power flow equations," *IET Generation, Transmission & Distribution*, vol. 10, no. 8, pp. 1853–1859, 2016.

[60] S. Iwamoto and Y. Tamura, "A load flow calculation method for ill-conditioned power systems," *IEEE Transactions on Power Apparatus and Systems*, no. 4, pp. 1736–1743, 1981.

[61] M. D. Schaffer and D. J. Tylavsky, "A nondiverging polar-form newton-based power flow," *IEEE Transactions on Industry Applications*, vol. 24, no. 5, pp. 870–877, 1988.

[62] M. El-Arini, "Decoupled power flow solution method for well-conditioned and ill-conditioned power systems," in *IEE Proceedings C (Generation, Transmission and Distribution)*, vol. 140, no. 1. IET, 1993, pp. 7–10.

[63] P. Bijwe and S. Kelapure, "Nondivergent fast power flow methods," *IEEE Transactions on Power Systems*, vol. 18, no. 2, pp. 633–638, 2003.

[64] J. F. Gutiérrez, M. F. Bedriñana, and C. A. Castro, "Critical comparison of robust load flow methods for ill-conditioned systems," in *2011 IEEE Trondheim PowerTech*. IEEE, 2011, pp. 1–6.

[65] H. Chen, X. Luo, Y. Li, X. Fu, Huaand Zheng, and X. Yuan, "Ill-conditioned load flow study based on asynchronous parallel computing in rural power distribution networks," *J. Convergence Inf. Technol.(JCIT)*, vol. 7, no. 19, pp. 261–268, 2012.

[66] X. Yang and X. Zhou, "Application of asymptotic numerical method with homotopy techniques to power flow problems," *International Journal of Electrical Power & Energy Systems*, vol. 57, pp. 375–383, 2014.

[67] A. Shahriari, H. Mokhlis, A. H. A. Bakar, and H. A. Illias, "Optimal multiplier load flow method using concavity theory," *Applied Mathematics and Computation*, vol. 245, pp. 487–503, 2014.

[68] A. Shahriari, H. Mokhlis, M. Karimi, A. Bakar, and H. Illias, "Quadratic discriminant index for optimal multiplier load flow method in ill conditioned system," *International Journal of Electrical Power & Energy Systems*, vol. 60, pp. 378–388, 2014.

[69] N. Rao and S. Tripathy, "Power system static state estimation by the levenberg-marquardt algorithm," *IEEE Transactions on Power Apparatus and Systems*, no. 2, pp. 695–702, 1980.

[70] F. Milano, "Continuous newton's method for power flow analysis," *IEEE Transactions on Power Systems*, vol. 24, no. 1, pp. 50–57, 2008.

[71] P. J. Lagacé, M.-H. Vuong, and I. Kamwa, "Improving power flow convergence by newton raphson with a levenberg-marquardt method," in *2008 IEEE Power and Energy Society General Meeting-Conversion and Delivery of Electrical Energy in the 21st Century*. IEEE, 2008, pp. 1–6.

[72] P. J. Lagacé, "Power flow methods for improving convergence," in *IECON 2012-38th Annual Conference on IEEE Industrial Electronics Society*. IEEE, 2012, pp. 1387–1392.

[73] F. Milano, "Analogy and convergence of levenberg's and lyapunov-based methods for power flow analysis," *IEEE Transactions on Power Systems*, vol. 31, no. 2, pp. 1663–1664, 2015.

[74] R. Pourbagher and S. Y. Derakhshandeh, "Application of high-order levenberg–marquardt method for solving the power flow problem in the ill-conditioned systems," *IET Generation, Transmission & Distribution*, vol. 10, no. 12, pp. 3017–3022, 2016.

[75] K. Balamurugan and D. Srinivasan, "Review of power flow studies on distribution network with distributed generation," in *2011 IEEE Ninth International Conference on Power Electronics and Drive Systems*. IEEE, 2011, pp. 411–417.

[76] L. A. Gallego, E. Carreno, and A. Padilha-Feltrin, "Distributed generation modelling for unbalanced three-phase power flow calculations in smart grids," in *2010 IEEE/PES Transmission and Distribution Conference and Exposition: Latin America (T&D-LA)*. IEEE, 2010, pp. 323–328.

[77] E. Dall'Anese, H. Zhu, and G. B. Giannakis, "Distributed optimal power flow for smart microgrids," *IEEE Transactions on Smart Grid*, vol. 4, no. 3, pp. 1464–1475, 2013.

[78] A. M. Vural, "Interior point-based slack-bus free-power flow solution for balanced islanded microgrids," *International Transactions on Electrical Energy Systems*, vol. 26, no. 5, pp. 968–992, 2016.

[79] S. Sivakumar, T. Parsons, and S. C. Sivakumar, "Modeling, analysis and control of bidirectional power flow in grid connected inverter systems," in *Proceedings of the Power Conversion Conference-Osaka 2002 (Cat. No. 02TH8579)*, vol. 3. IEEE, 2002, pp. 1015–1019.

[80] R. B. N. Pinheiro, A. R. Balbo, E. C. Baptista, and L. Nepomuceno, "Interior–exterior point method with global convergence strategy for solving the reactive optimal power flow problem," *International Journal of Electrical Power & Energy Systems*, vol. 66, pp. 235–246, 2015.

[81] E. J. Oliveira, L. W. Oliveira, J. Pereira, L. M. Honório, I. C. S. Junior, and A. Marcato, "An optimal power flow based on safety barrier interior point method," *International Journal of Electrical Power & Energy Systems*, vol. 64, pp. 977–985, 2015.

[82] F. Capitanescu and L. Wehenkel, "Experiments with the interior-point method for solving large scale optimal power flow problems," *Electric Power Systems Research*, vol. 95, pp. 276–283, 2013.

[83] H. Han, X. Hou, J. Yang, J. Wu, M. Su, and J. M. Guerrero, "Review of power sharing control strategies for islanding operation of ac microgrids," *IEEE Transactions on Smart Grid*, vol. 7, no. 1, pp. 200–215, 2015.

[84] N. Hatziargyriou, H. Asano, R. Iravani, and C. Marnay, "Microgrids," *IEEE Power and Energy Magazine*, vol. 5, no. 4, pp. 78–94, 2007.

[85] R. H. Lasseter and P. Piagi, "Microgrid: A conceptual solution," in *IEEE Power Electronics Specialists Conference*, vol. 6. Citeseer, 2004, pp. 4285–4291.

[86] P. Piagi and R. H. Lasseter, "Autonomous control of microgrids," in *2006 IEEE Power Engineering Society General Meeting*. IEEE, 2006, pp. 8–pp.

[87] M. C. Chandorkar, D. M. Divan, and R. Adapa, "Control of parallel connected inverters in standalone ac supply systems," *IEEE Transactions on Industry Applications*, vol. 29, no. 1, pp. 136–143, 1993.

[88] M. Chandrokar, D. Divan, and B. Banerjee, "Control of distributed ups systems," in *Proceedings of 1994 Power Electronics Specialist Conference-PESC'94*, vol. 1. IEEE, 1994, pp. 197–204.

[89] Y. Byun, T. Koo, K. Joe, E. Kim, J. Seo, and D. Kim, "Parallel operation of three-phase ups inverters by wireless load sharing control," in *INTELEC. Twenty-Second International Telecommunications Energy Conference (Cat. No. 00CH37131)*. IEEE, 2000, pp. 526–532.

[90] J. M. Guerrero, L. Hang, and J. Uceda Antolín, "Control of distributed uninterruptible power supply systems," *IEEE Transactions on Industrial Electronics*, vol. 55, no. 8, pp. 2845–2859, 2008.

[91] J. Hu, J. Zhu, D. G. Dorrell, and J. M. Guerrero, "Virtual flux droop method—a new control strategy of inverters in microgrids," *IEEE Transactions on Power Electronics*, vol. 29, no. 9, pp. 4704–4711, 2013.

[92] M. Ashabani, A.-R. M. Yasser, M. Mirsalim, and M. Aghashabani, "Multivariable droop control of synchronous current converters in weak grids/microgrids with decoupled dq-axes currents," *IEEE Transactions on Smart Grid*, vol. 6, no. 4, pp. 1610–1620, 2015.

[93] L.-Y. Lu and C.-C. Chu, "Consensus-based droop control synthesis for multiple dics in isolated micro-grids," *IEEE Transactions on Power Systems*, vol. 30, no. 5, pp. 2243–2256, 2014.

[94] A. Elrayyah, Y. Sozer, and M. E. Elbuluk, "A novel load-flow analysis for stable and optimized microgrid operation," *IEEE Transactions on Power Delivery*, vol. 29, no. 4, pp. 1709–1717, 2014.

[95] C. Li, S. K. Chaudhary, J. C. Vasquez, and J. M. Guerrero, "Power flow analysis algorithm for islanded lv microgrids including distributed generator units with droop control and virtual impedance loop," in *2014 IEEE Applied Power Electronics Conference and Exposition-APEC 2014*. IEEE, 2014, pp. 3181–3185.

[96] L. Rese, A. S. Costa, and A. S. e Silva, "A modified load flow algorithm for microgrids operating in islanded mode," in *2013 IEEE PES Conference on Innovative Smart Grid Technologies (ISGT Latin America)*. IEEE, 2013, pp. 1–7.

[97] Y. Levron, J. M. Guerrero, and Y. Beck, "Optimal power flow in microgrids with energy storage," *IEEE Transactions on Power Systems*, vol. 28, no. 3, pp. 3226–3234, 2013.

[98] G. Díaz, J. Gómez-Aleixandre, and J. Coto, "Direct backward/forward sweep algorithm for solving load power flows in ac droop-regulated microgrids," *IEEE Transactions on Smart Grid*, vol. 7, no. 5, pp. 2208–2217, 2016.

[99] H. Nikkhajoei and R. Iravani, "Steady-state model and power flow analysis of electronically-coupled distributed resource units," *IEEE Transactions on Power Delivery*, vol. 22, no. 1, pp. 721–728, 2007.

[100] M. Z. Kamh and R. Iravani, "Unbalanced model and power-flow analysis of microgrids and active distribution systems," *IEEE Transactions on Power Delivery*, vol. 25, no. 4, pp. 2851–2858, 2010.

[101] G. C. Kryonidis, E. O. Kontis, A. I. Chrysochos, K. O. Oureilidis, C. S. Demoulias, and G. K. Papagiannis, "Power flow of islanded ac microgrids: Revisited," *IEEE Transactions on Smart Grid*, vol. 9, no. 4, pp. 3903–3905, July 2018.

[102] M. Z. Kamh and R. Iravani, "A unified three-phase power-flow analysis model for electronically coupled distributed energy resources," *IEEE Transactions on Power Delivery*, vol. 26, no. 2, pp. 899–909, 2011.

[103] F. V. Berghen, "Levenberg-marquardt algorithms vs trust region algorithms," *IRIDIA, Université Libre de Bruxelles*, 2004.

[104] W. Yao, M. Chen, J. Matas, J. M. Guerrero, and Z.-M. Qian, "Design and analysis of the droop control method for parallel inverters considering the impact of the complex impedance on the power sharing," *IEEE Transactions on Industrial Electronics*, vol. 58, no. 2, pp. 576–588, 2011.

[105] K. De Brabandere, B. Bolsens, J. Van den Keybus, A. Woyte, J. Driesen, and R. Belmans, "A voltage and frequency droop control method for parallel inverters," *IEEE Transactions on Power Electronics*, vol. 22, no. 4, pp. 1107–1115, 2007.

[106] D. E. Goldberg and J. H. Holland, "Genetic algorithms and machine learning," *Machine learning*, vol. 3, no. 2, pp. 95–99, 1988.

[107] K. P. Wong, A. Li, and M. Law, "Development of constrained-genetic-algorithm load-flow method," *IEE Proceedings-Generation, Transmission and Distribution*, vol. 144, no. 2, pp. 91–99, 1997.

[108] K. P. Wong, A. Li, and T. Law, "Advanced, constrained, genetic algorithm load flow method," *IEE Proceedings-Generation, Transmission and Distribution*, vol. 146, no. 6, pp. 609–616, 1999.

[109] T. Ting, K. Wong, and C. Chung, "Hybrid constrained genetic algorithm/particle swarm optimisation load flow algorithm," *IET Generation, Transmission & Distribution*, vol. 2, no. 6, pp. 800–812, 2008.

[110] M. Varadarajan and K. S. Swarup, "Solving multi-objective optimal power flow using differential evolution," *IET Generation, Transmission & Distribution*, vol. 2, no. 5, pp. 720–730, 2008.

[111] A. Glimn and G. Stagg, "Automatic calculation of load flows," *Transactions of the American Institute of Electrical Engineers. Part III: Power Apparatus and Systems*, vol. 76, no. 3, pp. 817–825, 1957.

[112] P.-c. Chao, "On the solution of ill-conditioned, simultaneous, linear, algebraic equations by machine computation," University of Illinois at Urbana Champaign, College of Engineering ..., Tech. Rep., 1961.

[113] H. J. Kim, K. Choi, H. Lee, H. Jung, and S. Hahn, "A new algorithm for solving ill conditioned linear systems," *IEEE Transactions on Magnetics*, vol. 32, no. 3, pp. 1373–1376, 1996.

[114] P. Deuflhard, "A modified newton method for the solution of ill-conditioned systems of nonlinear equations with application to multiple shooting," *Numerische Mathematik*, vol. 22, no. 4, pp. 289–315, 1974.

[115] L. Wang and X. Lin, "Robust fast decoupled power flow," *IEEE Transactions on Power Systems*, vol. 15, no. 1, pp. 208–215, 2000.

[116] S. Naka, T. Genji, and Y. Fukuyama, "Practical equipment models for fast distribution power flow considering interconnection of distributed generators," in *2001 Power Engineering Society Summer Meeting. Conference Proceedings (Cat. No. 01CH37262)*, vol. 2. IEEE, 2001, pp. 1007–1012.

[117] T. Oomori, T. Genji, T. Yura, T. Watanabe, S. Takayama, and Y. Fukuyama, "Development of equipment models for fast distribution three-phase unbalanced load flow calculation," *Electrical Engineering in Japan*, vol. 142, no. 3, pp. 8–19, 2003.

[118] J.-H. Teng, "Modelling distributed generations in three-phase distribution load flow," *IET Generation, Transmission & Distribution*, vol. 2, no. 3, pp. 330–340, 2008.

[119] W. H. Kersting, "Radial distribution test feeders," *IEEE Transactions on Power Systems*, vol. 6, no. 3, pp. 975–985, 1991.

[120] X. Yang, "A higher-order levenberg–marquardt method for nonlinear equations," *Applied Mathematics and Computation*, vol. 219, no. 22, pp. 10 682–10 694, 2013.

[121] E. Mashhour and S. Moghaddas-Tafreshi, "Three-phase backward/forward power flow solution considering three-phase distribution transformers," in *2009 IEEE International Conference on Industrial Technology*. IEEE, 2009, pp. 1–5.

[122] J. Liang, B. Qu, and P. Suganthan, "Problem definitions and evaluation criteria for the cec 2014 special session and competition on single objective real-parameter numerical optimization," *Computational Intelligence Laboratory, Zhengzhou University, Zhengzhou China and Technical Report, Nanyang Technological University, Singapore*, vol. 635, 2013.

[123] J. Kennedy, "Particle swarm optimization," in *Encyclopedia of Machine Learning*. Springer, 2010, pp. 760–766.

[124] J. Kennedy, "Bare bones particle swarms," in *Swarm Intelligence Symposium, 2003. SIS'03. Proceedings of the 2003 IEEE*. IEEE, 2003, pp. 80–87.

[125] K. Mahadevan and P. Kannan, "Comprehensive learning particle swarm optimization for reactive power dispatch," *Applied Soft Computing*, vol. 10, no. 2, pp. 641–652, 2010.

[126] Z.-H. Zhan, J. Zhang, Y. Li, and H. S.-H. Chung, "Adaptive particle swarm optimization," *IEEE Transactions on Systems, Man, and Cybernetics, Part B (Cybernetics)*, vol. 39, no. 6, pp. 1362–1381, 2009.

[127] Z.-H. Zhan, J. Zhang, Y. Li, and Y.-H. Shi, "Orthogonal learning particle swarm optimization," *IEEE Transactions on Evolutionary Computation*, vol. 15, no. 6, pp. 832–847, 2011.

[128] Y. Li, J. Feng, and J. Hu, "Covariance and crossover matrix guided differential evolution for global numerical optimization," *SpringerPlus*, vol. 5, no. 1, p. 1176, 2016.

[129] Z. Li, Z. Shang, B. Y. Qu, and J.-J. Liang, "Differential evolution strategy based on the constraint of fitness values classification," in *Evolutionary Computation (CEC), 2014 IEEE Congress on*. IEEE, 2014, pp. 1454–1460.

[130] C. Xu, H. Huang, and S. Ye, "A differential evolution with replacement strategy for real-parameter numerical optimization," in *Evolutionary Computation (CEC), 2014 IEEE Congress on*. IEEE, 2014, pp. 1617–1624.

[131] Z. Hu, Y. Bao, and T. Xiong, "Partial opposition-based adaptive differential evolution algorithms: Evaluation on the cec 2014 benchmark set for real-parameter optimization," in *Evolutionary Computation (CEC), 2014 IEEE Congress on*. IEEE, 2014, pp. 2259–2265.

[132] R. Storn and K. Price, "Differential evolution–a simple and efficient heuristic for global optimization over continuous spaces," *Journal of Global Optimization*, vol. 11, no. 4, pp. 341–359, 1997.

[133] N. Hansen, "The cma evolution strategy: a comparing review," in *Towards a new evolutionary computation*. Springer, 2006, pp. 75–102.

[134] A. Auger and N. Hansen, "A restart cma evolution strategy with increasing population size," in *Evolutionary Computation, 2005. The 2005 IEEE Congress on*, vol. 2. IEEE, 2005, pp. 1769–1776.

[135] A. Auger, M. Schoenauer, and N. Vanhaecke, "Ls-cma-es: A second-order algorithm for covariance matrix adaptation," in *International Conference on Parallel Problem Solving from Nature*. Springer, 2004, pp. 182–191.

[136] G. A. Jastrebski and D. V. Arnold, "Improving evolution strategies through active covariance matrix adaptation," in *Evolutionary Computation, 2006. CEC 2006. IEEE Congress on*. IEEE, 2006, pp. 2814–2821.

[137] C. Igel, T. Suttorp, and N. Hansen, "A computational efficient covariance matrix update and a (1+ 1)-cma for evolution strategies," in *Proceedings of the 8th Annual Conference on Genetic and Evolutionary Computation*. ACM, 2006, pp. 453–460.

[138] S. Mirjalili, S. M. Mirjalili, and A. Lewis, "Grey wolf optimizer," *Advances in Engineering Software*, vol. 69, pp. 46–61, 2014.

[139] S. Saremi, S. Mirjalili, and A. Lewis, "Grasshopper optimisation algorithm: theory and application," *Advances in Engineering Software*, vol. 105, pp. 30–47, 2017.

[140] S. Mirjalili, S. M. Mirjalili, and A. Hatamlou, "Multi-verse optimizer: a nature-inspired algorithm for global optimization," *Neural Computing and Applications*, vol. 27, no. 2, pp. 495–513, 2016.

[141] S. Mirjalili, "Sca: a sine cosine algorithm for solving optimization problems," *Knowledge-Based Systems*, vol. 96, pp. 120–133, 2016.

[142] E. Cuevas, F. Fausto, and A. González, "The selfish herd optimizer," in *New Advancements in Swarm Algorithms: Operators and Applications*. Springer, 2020, pp. 69–109.

[143] S. Mirjalili, A. H. Gandomi, S. Z. Mirjalili, S. Saremi, H. Faris, and S. M. Mirjalili, "Salp swarm algorithm: A bio-inspired optimizer for engineering design problems," *Advances in Engineering Software*, vol. 114, pp. 163–191, 2017.

[144] G. Dhiman and V. Kumar, "Seagull optimization algorithm: Theory and its applications for large-scale industrial engineering problems," *Knowledge-Based Systems*, vol. 165, pp. 169–196, 2019.

[145] S. Mirjalili and A. Lewis, "The whale optimization algorithm," *Advances in Engineering Software*, vol. 95, pp. 51–67, 2016.

[146] T. Takahama and S. Sakai, "Constrained optimization by ε constrained particle swarm optimizer with ε-level control," in *Soft Computing as Transdisciplinary Science and Technology*. Springer, 2005, pp. 1019–1029.

[147] J. Liang, T. P. Runarsson, E. Mezura-Montes, M. Clerc, P. N. Suganthan, C. C. Coello, and K. Deb, "Problem definitions and evaluation criteria for the cec 2006 special session on constrained real-parameter optimization," *Journal of Applied Mechanics*, vol. 41, no. 8, pp. 8–31, 2006.

[148] S. Kukkonen and J. Lampinen, "Constrained real-parameter optimization with generalized differential evolution," in *2006 IEEE International Conference on Evolutionary Computation*. IEEE, 2006, pp. 207–214.

[149] E. Mezura-Montes, J. Velázquez-Reyes, and C. C. Coello, "Modified differential evolution for constrained optimization," in *2006 IEEE International Conference on Evolutionary Computation*. IEEE, 2006, pp. 25–32.

[150] J. Brest, V. Zumer, and M. S. Maucec, "Self-adaptive differential evolution algorithm in constrained real-parameter optimization," in *2006 IEEE International Conference on Evolutionary Computation*. IEEE, 2006, pp. 215–222.

[151] W.-F. Gao, G. G. Yen, and S.-Y. Liu, "A dual-population differential evolution with coevolution for constrained optimization," *IEEE Transactions on Cybernetics*, vol. 45, no. 5, pp. 1108–1121, 2015.

[152] G. Jia, Y. Wang, Z. Cai, and Y. Jin, "An improved (μ+ λ)-constrained differential evolution for constrained optimization," *Information Sciences*, vol. 222, pp. 302–322, 2013.

[153] Y. Wang and Z. Cai, "Constrained evolutionary optimization by means of (μ+ λ)-differential evolution and improved adaptive trade-off model," *Evolutionary Computation*, vol. 19, no. 2, pp. 249–285, 2011.

[154] A. H. Aguirre, A. M. Zavala, E. V. Diharce, and S. B. Rionda, "Copso: Constrained optimization via pso algorithm," *Center for Research in Mathematics (CIMAT). Technical report No. I-07-04/22-02-2007*, 2007.

[155] A. E. Munoz-Zavala, A. Hernandez-Aguirre, E. R. Villa-Diharce, and S. Botello-Rionda, "Peso+ for constrained optimization," in *2006 IEEE International Conference on Evolutionary Computation.* IEEE, 2006, pp. 231–238.

[156] V. V. De Melo and G. Iacca, "A modified covariance matrix adaptation evolution strategy with adaptive penalty function and restart for constrained optimization," *Expert Systems with Applications*, vol. 41, no. 16, pp. 7077–7094, 2014.

[157] T. P. Runarsson, "Approximate evolution strategy using stochastic ranking," in *2006 IEEE International Conference on Evolutionary Computation.* IEEE, 2006, pp. 745–752.

[158] A. Sinha, A. Srinivasan, and K. Deb, "A population-based, parent centric procedure for constrained real-parameter optimization," in *2006 IEEE International Conference on Evolutionary Computation.* IEEE, 2006, pp. 239–245.

[159] J. Brest, V. Zumer, and M. S. Maucec, "Self-adaptive differential evolution algorithm in constrained real-parameter optimization," in *2006 IEEE International Conference on Evolutionary Computation.* IEEE, 2006, pp. 215–222.

[160] M. Smith and D. Ton, "Key connections: The u.s. department of energy?s microgrid initiative," *IEEE Power and Energy Magazine*, vol. 11, no. 4, pp. 22–27, July 2013.

[161] E. Rokrok and M. E. H. Golshan, "Adaptive voltage droop scheme for voltage source converters in an islanded multibus microgrid," *IET Generation, Transmission & Distribution*, vol. 4, no. 5, pp. 562–578, 2010.

[162] C.-T. Lee, C.-C. Chu, and P.-T. Cheng, "A new droop control method for the autonomous operation of distributed energy resource interface converters," *IEEE Transactions on Power Electronics*, vol. 28, no. 4, pp. 1980–1993, 2013.

[163] Y. A.-R. I. Mohamed and E. F. El-Saadany, "Adaptive decentralized droop controller to preserve power sharing stability of paralleled inverters in distributed generation microgrids," *IEEE Transactions on Power Electronics*, vol. 23, no. 6, pp. 2806–2816, 2008.

[164] S. Jahdi, A. Etemadian, and L. L. Lai, "Dg modeling and compensation methods in distribution load flow analysis and voltage profile recovery," in *Electrical Power Quality and Utilisation (EPQU), 2011 11th International Conference on.* IEEE, 2011, pp. 1–6.

[165] D. Westermann and M. Kratz, "A real-time development platform for the next generation of power system control functions," *IEEE Transactions on Industrial Electronics*, vol. 57, no. 4, pp. 1159–1166, April 2010.

[166] R. Majumder, G. Ledwich, A. Ghosh, S. Chakrabarti, and F. Zare, "Droop control of converter-interfaced microsources in rural distributed generation," *IEEE Transactions on Power Delivery*, vol. 25, no. 4, pp. 2768–2778, Oct 2010.

[167] O. Anaya-Lara and E. Acha, "Modeling and analysis of custom power systems by pscad/emtdc," *IEEE Transactions on Power Delivery*, vol. 17, no. 1, pp. 266–272, Jan 2002.

[168] M. Hossain, H. R. Pota, M. A. Mahmud, and M. Aldeen, "Robust control for power sharing in microgrids with low-inertia wind and pv generators," *IEEE Transactions on Sustainable Energy*, vol. 6, no. 3, pp. 1067–1077, 2014.

[169] N. Pogaku, M. Prodanovic, and T. C. Green, "Modeling, analysis and testing of autonomous operation of an inverter-based microgrid," *IEEE Transactions on Power Electronics*, vol. 22, no. 2, pp. 613–625, 2007.

[170] J. M. Guerrero, J. Matas, L. G. de Vicuna, M. Castilla, and J. Miret, "Decentralized control for parallel operation of distributed generation inverters using resistive output impedance," *IEEE Transactions on Industrial Electronics*, vol. 54, no. 2, pp. 994–1004, 2007.

[171] H. Bevrani and S. Shokoohi, "An intelligent droop control for simultaneous voltage and frequency regulation in islanded microgrids," *IEEE Transactions on Smart Grid*, vol. 4, no. 3, pp. 1505–1513, 2013.

[172] A. M. Haidar and K. M. Muttaqi, "Behavioral characterization of electric vehicle charging loads in a distribution power grid through modeling of battery chargers," *IEEE Transactions on Industry Applications*, vol. 52, no. 1, pp. 483–492, 2015.

[173] *5. Newton's Method for Nonlinear Equations and Unconstrained Minimization*, pp. 86–110. [Online]. Available: https://epubs.siam.org/doi/abs/10.1137/1.9781611971200.ch5

[174] F. Hameed, M. Al Hosani, and H. Zeineldin, "A modified backward/forward sweep load flow method for islanded radial microgrids," *IEEE Transactions on Smart Grid*, 2017.

[175] M. Abedini, "A novel algorithm for load flow analysis in island microgrids using an improved evolutionary algorithm," *International Transactions on Electrical Energy Systems*, vol. 26, no. 12, pp. 2727–2743, 2016.

[176] D. Singh and R. Misra, "Effect of load models in distributed generation planning," *IEEE Transactions on Power Systems*, vol. 22, no. 4, pp. 2204–2212, 2007.

[177] H. Wu, X. Liu, and M. Ding, "Dynamic economic dispatch of a microgrid: Mathematical models and solution algorithm," *International Journal of Electrical Power & Energy Systems*, vol. 63, pp. 336–346, 2014.

[178] M. H. Moradi, M. Abedini, and S. M. Hosseinian, "Improving operation constraints of microgrid using phevs and renewable energy sources," *Renewable Energy*, vol. 83, pp. 543–552, 2015.

[179] M. Abedini, M. H. Moradi, and S. Hosseinian, "Optimal clustering of mgs based on droop controller for improving reliability using a hybrid of harmony search and genetic algorithms," *ISA Transactions*, vol. 61, pp. 119–128, 2016.

[180] J. Rocabert, A. Luna, F. Blaabjerg, and P. Rodriguez, "Control of power converters in ac microgrids," *IEEE Transactions on Power Electronics*, vol. 27, no. 11, pp. 4734–4749, 2012.

[181] V. Chuvychin, A. Sauhatas, N. Gurov, and V. Strelkovs, "Frequency control features for increasing der penetration in power system," in *2007 IEEE Lausanne Power Tech.* IEEE, 2007, pp. 1726–1729.

[182] M. H. Moradi, M. Abedini, and S. M. Hosseinian, "A combination of evolutionary algorithm and game theory for optimal location and operation of dg from dg owner standpoints," *IEEE Transactions on Smart Grid*, vol. 7, no. 2, pp. 608–616, 2016.

[183] T. C. Green and M. Prodanović, "Control of inverter-based micro-grids," *Electric Power Systems Research*, vol. 77, no. 9, pp. 1204–1213, 2007.

[184] T. L. Vandoorn, B. Meersman, J. D. De Kooning, and L. Vandevelde, "Analogy between conventional grid control and islanded microgrid control based on a global dc-link voltage droop," *IEEE Transactions on Power Delivery*, vol. 27, no. 3, pp. 1405–1414, 2012.

[185] F. Gao and M. R. Iravani, "A control strategy for a distributed generation unit in grid-connected and autonomous modes of operation," *IEEE Transactions on Power Delivery*, vol. 23, no. 2, pp. 850–859, 2008.

[186] C. S. Cheng and D. Shirmohammadi, "A three-phase power flow method for real-time distribution system analysis," *IEEE Transactions on Power Systems*, vol. 10, no. 2, pp. 671–679, 1995.

[187] F. Zhang and C. S. Cheng, "A modified newton method for radial distribution system power flow analysis," *IEEE Transactions on Power Systems*, vol. 12, no. 1, pp. 389–397, 1997.

[188] U. Eminoglu and M. H. Hocaoglu, "A new power flow method for radial distribution systems including voltage dependent load models," *Electric Power Systems Research*, vol. 76, no. 1-3, pp. 106–114, 2005.

[189] P. Kundur, N. J. Balu, and M. G. Lauby, *Power system stability and control.* McGraw-hill New York, 1994, vol. 7.

[190] F. Katiraei and M. R. Iravani, "Power management strategies for a microgrid with multiple distributed generation units," *IEEE Transactions on Power Systems*, vol. 21, no. 4, pp. 1821–1831, 2006.

[191] M. Marei, E. El-Saadany, and M. Salama, "Flexible distributed generation:(fdg)," in *IEEE Power Engineering Society Summer Meeting,*, vol. 1. IEEE, 2002, pp. 49–53.

[192] N. Awad, M. Ali, J. Liang, B. Qu, and P. Suganthan, "Problem definitions and evaluation criteria for the cec 2017 special session and competition on single objective real-parameter numerical optimization," *Tech. Rep.*, 2016.

[193] J. E. Dennis, D. M. Gay, and R. E. Welsch, "An adaptive nonlinear least square algorithm," 1977.

[194] T. Takahama and S. Sakai, "Constrained optimization by the ε constrained differential evolution with gradient-based mutation and feasible elites," in *2006 IEEE International Conference on Evolutionary Computation.* IEEE, 2006, pp. 1–8.

[195] S. Bagheri, W. Konen, and T. Back, "Equality constraint handling for surrogate-assisted constrained optimization," in *2016 IEEE Congress on Evolutionary Computation (CEC).* IEEE, 2016, pp. 1924–1931.

[196] R. G. Regis, "Constrained optimization by radial basis function interpolation for high-dimensional expensive black-box problems with infeasible initial points," *Engineering Optimization*, vol. 46, no. 2, pp. 218–243, 2014.

[197] A. Deihimi, B. K. Zahed, and R. Iravani, "An interactive operation management of a micro-grid with multiple distributed generations using multi-objective uniform water cycle algorithm," *Energy*, vol. 106, pp. 482–509, 2016.

[198] P. Chootinan and A. Chen, "Constraint handling in genetic algorithms using a gradient-based repair method," *Computers & operations research*, vol. 33, no. 8, pp. 2263–2281, 2006.

[199] C. G. Broyden, "A class of methods for solving nonlinear simultaneous equations," *Mathematics of computation*, vol. 19, no. 92, pp. 577–593, 1965.

[200] H.-G. Beyer and B. Sendhoff, "Simplify your covariance matrix adaptation evolution strategy," *IEEE Transactions on Evolutionary Computation*, vol. 21, no. 5, pp. 746–759, 2017.

[201] K. Deb, "An efficient constraint handling method for genetic algorithms," *Computer Methods in Applied Mechanics and Engineering*, vol. 186, no. 2, pp. 311–338, 2000.

[202] G. V. Raju and P. Bijwe, "Reactive power/voltage control in distribution systems under uncertain environment," *IET Generation, Transmission & Distribution*, vol. 2, no. 5, pp. 752–763, 2008.

[203] R. Viral and D. Khatod, "An analytical approach for sizing and siting of dgs in balanced radial distribution networks for loss minimization," *International Journal of Electrical Power & Energy Systems*, vol. 67, pp. 191–201, 2015.

[204] T. Ayodele, A. Ogunjuyigbe, and O. Akinola, "Optimal location, sizing, and appropriate technology selection of distributed generators for minimizing power loss using genetic algorithm," *Journal of Renewable Energy*, vol. 2015, 2015.

[205] P. Karimyan, G. Gharehpetian, M. Abedi, and A. Gavili, "Long term scheduling for optimal allocation and sizing of dg unit considering load variations and dg type," *International Journal of Electrical Power & Energy Systems*, vol. 54, pp. 277–287, 2014.

[206] S. Kansal, V. Kumar, and B. Tyagi, "Optimal placement of different type of dg sources in distribution networks," *International Journal of Electrical Power & Energy Systems*, vol. 53, pp. 752–760, 2013.

[207] M. Aman, G. Jasmon, A. Bakar, and H. Mokhlis, "A new approach for optimum simultaneous multi-dg distributed generation units placement and sizing based on maximization of system loadability using hpso (hybrid particle swarm optimization) algorithm," *Energy*, vol. 66, pp. 202–215, 2014.

[208] M. Kefayat, A. L. Ara, and S. N. Niaki, "A hybrid of ant colony optimization and artificial bee colony algorithm for probabilistic optimal placement and sizing of distributed energy resources," *Energy Conversion and Management*, vol. 92, pp. 149–161, 2015.

[209] S. G. Naik, D. Khatod, and M. Sharma, "Optimal allocation of combined dg and capacitor for real power loss minimization in distribution networks," *International Journal of Electrical Power & Energy Systems*, vol. 53, pp. 967–973, 2013.

[210] M. Aman, G. Jasmon, K. Solangi, A. Bakar, and H. Mokhlis, "Optimum simultaneous dg and capacitor placement on the basis of minimization of power losses," *International Journal of Computer and Electrical Engineering*, vol. 5, no. 5, p. 516, 2013.

[211] K. Muthukumar and S. Jayalalitha, "Optimal placement and sizing of distributed generators and shunt capacitors for power loss minimization in radial distribution networks using hybrid heuristic search optimization technique," *International Journal of Electrical Power & Energy Systems*, vol. 78, pp. 299–319, 2016.

[212] A. Khodabakhshian and M. H. Andishgar, "Simultaneous placement and sizing of dgs and shunt capacitors in distribution systems by using imde algorithm," *International Journal of Electrical Power & Energy Systems*, vol. 82, pp. 599–607, 2016.

[213] W. Fadel, U. Kilic, and S. Taskin, "Placement of dg, cb, and tcsc in radial distribution system for power loss minimization using back-tracking search algorithm," *Electrical Engineering*, vol. 99, no. 3, pp. 791–802, 2017.

[214] I. Loshchilov, "Cma-es with restarts for solving cec 2013 benchmark problems," in *2013 IEEE Congress on Evolutionary Computation*. IEEE, 2013, pp. 369–376.

[215] R. Tanabe and A. S. Fukunaga, "Improving the search performance of shade using linear population size reduction," in *2014 IEEE congress on evolutionary computation (CEC)*. IEEE, 2014, pp. 1658–1665.

[216] N. Kanwar, N. Gupta, K. Niazi, and A. Swarnkar, "Improved meta-heuristic techniques for simultaneous capacitor and dg allocation in radial distribution networks," *International Journal of Electrical Power & Energy Systems*, vol. 73, pp. 653–664, 2015.

[217] R. Tanabe and A. Fukunaga, "Success-history based parameter adaptation for differential evolution," in *2013 IEEE Congress on Evolutionary Computation*, June 2013, pp. 71–78.

[218] A. Ipakchi and F. Albuyeh, "Grid of the future," *IEEE Power and Energy Magazine*, vol. 7, no. 2, pp. 52–62, 2009.

[219] J. P. Lopes, C. Moreira, and A. Madureira, "Defining control strategies for microgrids islanded operation," *IEEE Transactions on Power Systems*, vol. 21, no. 2, pp. 916–924, 2006.

[220] D. G. Photovoltaics and E. Storage, "Ieee guide for design, operation, and integration of distributed resource island systems with electric power systems," 2011.

[221] J. M. Guerrero, J. C. Vasquez, J. Matas, L. G. De Vicuña, and M. Castilla, "Hierarchical control of droop-controlled ac and dc microgrids—a general approach toward standardization," *IEEE Transactions on Industrial Electronics*, vol. 58, no. 1, pp. 158–172, 2010.

[222] A. Engler, "Applicability of droops in low voltage grids," *International Journal of Distributed Energy Resources*, vol. 1, no. 1, pp. 1–6, 2005.

[223] E. Barklund, N. Pogaku, M. Prodanovic, C. Hernandez-Aramburo, and T. C. Green, "Energy management in autonomous microgrid using stability-constrained droop control of inverters," *IEEE Transactions on Power Electronics*, vol. 23, no. 5, pp. 2346–2352, 2008.

[224] S. Conti, R. Nicolosi, S. Rizzo, and H. Zeineldin, "Optimal dispatching of distributed generators and storage systems for mv islanded microgrids," *IEEE Transactions on Power Delivery*, vol. 27, no. 3, pp. 1243–1251, 2012.

[225] P. H. Divshali, S. H. Hosseinian, and M. Abedi, "A novel multi-stage fuel cost minimization in a vsc-based microgrid considering stability, frequency, and voltage constraints," *IEEE Transactions on Power Systems*, vol. 28, no. 2, pp. 931–939, 2012.

[226] A. W. Mohamed and A. K. Mohamed, "Adaptive guided differential evolution algorithm with novel mutation for numerical optimization," *International Journal of Machine Learning and Cybernetics*, pp. 1–25, 2017.

[227] S. Ghosh, S. Das, S. Roy, S. M. Islam, and P. N. Suganthan, "A differential covariance matrix adaptation evolutionary algorithm for real parameter optimization," *Information Sciences*, vol. 182, no. 1, pp. 199–219, 2012.

[228] K. Price, N. Awad, M. Ali, and P. Suganthan, "Problem definitions and evaluation criteria for the 100-digit challenge special session and competition on single objective numerical optimization," in *Technical Report*. Nanyang Technological University, 2018.

List of Publications

Journals

1. **Abhishek Kumar**, Bablesh Kumar Jha, Rakesh Kumar Misra, and Devender Singh. "**A New Current Injection Based Power flow Formulation**." Electric Power Components and Systems, ***Accepted for Publication***. (ISSN: 1532-5016) (**SCI Expanded, IF-1.06**)

2. **Abhishek Kumar**, Bablesh Kumar Jha, Dharmendra Kumar Dheer, Rakesh Kumar Misra, and Devender Singh."**A Nested-Iterative Newton-Raphson based Power Flow Formulation for Droop-based Islanded Microgrids**." Electric Power Systems Research. (ISSN: 0378-7796) (**SCI Expanded, IF-3.022**)

3. **Abhishek Kumar**, Bablesh Kumar Jha, Rakesh Kumar Misra, and Devender Singh. "**Novel Current Injection based Newton-Raphson Power flow algorithm for droop-based Islanded Microgrids**." IET Generation, Transmission, & Distribution. (ISSN:1350-2360) (**SCI, IF-3.229**)

4. **Abhishek Kumar**, Rakesh Kumar Misra, Devender Singh, Sujeet Mishra, and Swagatam Das. "**The Spherical Search Algorithm for Bound-constrained Global Optimization Problems**." Applied Soft Computing. (ISSN: 1568-4946) (**SCI Expanded, IF-4.873**).

5. **Abhishek Kumar**, Bablesh Kumar Jha, Dharmendra Kumar Dheer, Rakesh Kumar Misra, and Devender Singh. "**A Nested Backward/Forward Sweep Algorithm for Power Flow Analysis of Droop Regulated Islanded Microgrids**." IET Generation, Transmission, & Distribution, 13.14(2019). (ISSN:1350-2360) (**SCI, IF-3.229**)

6. **Abhishek Kumar**, Guohua Wo, Mostafa Ali, Rammohan Mallipeddi, Ponnuthurai Suganthan and Swagatam Das."**A Test-suite of Non-Convex Constrained OptimizationProblems from the Real-World and Some Baseline Results**." Swarm and Evolutionary Computation. (ISSN: 2210-6502),(**SCI Expanded, IF:6.330**).

7. Bablesh Kumar Jha, **Abhishek Kumar**, Dharmendra Kumar Dheer, Devender Singh andRakesh Kumar Misra."**A modied current injection load flow method under differentload model of EV for distribution system**." International Transactions on ElectricalEnergy Systems,accepted for publication. (ISSN:2050-7038),(**SCI Expanded, IF: 1.314**).

8. Bablesh Kumar Jha, **Abhishek Kumar**, Devender Singh, and Rakesh Kumar Misra. "**Coordinated effect of PHEVs with DGs on distribution network**." International Transactions on Electrical Energy Systems: 2019; 29:e2800. (ISSN:2050-7038) (**SCI Expanded, IF-1.314**).

9. Tarun Maini, **Abhishek Kumar**, Rakesh Kumar Misra, and Devender Singh. "**Intelligent Fuzzy Rough Set Based Feature Selection using Swarm algorithms with improved initialization**." Journal of Intelligent and Fuzzy Systems (JIFS), Accepted for publication (in April 2019), in press. (ISSN: 1875-8967) (**SCI Expanded, IF-1.637**).

10. Bablesh Kumar Jha, Amit Singh, **Abhishek Kumar**, Dharmendra Kumar Dheer, Devender Singh and Rakesh Kumar Misra."**Day ahead scheduling of PHEVs and D-BESSs inpresence of DGs in distribution system**." IET Electrical Systems in Transportation. (ISSN:2042-9738),(**ESCI**).

11. Tarun Maini, Rakesh Kumar Misra, Devender Singh, and **Abhishek Kumar**. "**Rough Set Based Feature Selection Using Swarm Algorithms with Improved Initialization**." Journal of Computational and Theoretical Nanoscience 15, no. 6-7 (2018): 2350-2354. (ISSN 1546-1963) (**Scopus indexed**)

12. Sujeet Mishra, **Abhishek Kumar**, Rakesh Kumar Misra, and Devender Singh. "**Feeder Phase Balancing using Single Phase Distributed Generations Considering Voltage Dependency of Loads**."Journal of Advanced Research in Dynamical and Control Systems. (ISSN: 1943-023X) (**Scopus indexed**)

Book Chapters

1. Sujeet Mishra, **Abhishek Kumar**, Devender Singh, and Rakesh Kumar Misra. "**Butterfly Optimizer for Placement and Sizing of Distributed Generation for Feeder Phase Balancing**." In Computational Intelligence: Theories, Applications and Future Directions-Volume II, pp. 519-530. Advances in Intelligent Systems and Computing, vol 799. Springer, Singapore, 2019. (ISSN:978-981-13-1135-2) (**SCOPUS indexed**)

2. **Abhishek Kumar**, Tarun Maini, Rakesh Kumar Misra, and Devender Singh. "**Butterfly Constrained Optimizer for Constrained Optimization Problems**." In Computational Intelligence: Theories, Applications and Future Directions-Volume II, pp. 477-486. Advances in Intelligent Systems and Computing, vol 799.Springer, Singapore, 2019.(ISSN:978-981-13-1135-2) (**SCOPUS indexed**)

3. Tarun Maini, **Abhishek Kumar**, Rakesh Kumar Misra, and Devender Singh. "**Fuzzy Rough Set-Based Feature Selection with Improved Seed Population in PSO and IDS**." In Computational Intelligence: Theories, Applications and Future Directions-Volume II, pp. 137-149. Advances in Intelligent Systems and Computing, vol 799.Springer, Singapore, 2019. (ISSN:978-981-13-1135-2) (**SCOPUS indexed**)

International Conferences

1. **Abhishek Kumar**, Rakesh Kumar Misra, Devender Singh and Swagatam Das. "**Testing A Multi-Operator based Differential Evolution Algorithm on the 100-Digit Challenge for Single Objective Numerical Optimization**." 2019 IEEE Congress onEvolutionary Computation (CEC). IEEE, 2019,(**Fifth Rank out of 26 in competition of IEEE CEC-2019**).

2. **Abhishek Kumar**, Rakesh Kumar Misra, and Devender Singh. "**Improving the local search capability of effective butterfly optimizer using covariance matrix adapted retreat phase**." In 2017 IEEE Congress on Evolutionary Computation (CEC), pp. 1835-1842. IEEE, 2017. (**Winner of competition of IEEE CEC-2017**)

3. Tarun Maini, **Abhishek Kumar**, Rakesh Kumar Misra, and Devender Singh. "**Rough set based feature selection using swarm intelligence with distributed sampled initialization**." In 2017 6th International Conference on Computer Applications In Electrical Engineering-Recent Advances (CERA), pp. 92-97. IEEE, 2017.

4. Tarun Maini, **Abhishek Kumar**, Rakesh Kumar Misra and Devender Singh, "**Feature selection with intelligent dynamic swarm and fuzzy rough set**," 2017 International Conference on Computing, Communication and Automation (ICCCA), Greater Noida, 2017, pp. 384-388.

5. **Abhishek Kumar**, Rakesh Kumar Misra, and Devender Singh. "**Butterfly Optimizer**." In 2015 IEEE Workshop on Computational Intelligence: Theories, Applications and Future Directions (WCI), pp. 1-6. IEEE, 2015.